

Survey of Period Variations of Superhumps in SU UMa-Type Dwarf Novae. III: The Third Year (2010–2011)

Taichi KATO,^{1*} Hiroyuki MAEHARA,² Ian MILLER,³ Tomohito OHSHIMA,¹ Enrique de MIGUEL,^{4,5} Kenji TANABE,⁶
Kazuyoshi IMAMURA,⁶ Hidehiko AKAZAWA,⁶ Nanae KUNITOMI,⁶ Ryosuke TAKAGI,⁶ Mikiha NOSE,⁶
Franz-Josef HAMBSCH,^{7,8,9} Seiichiro KIYOTA,¹⁰ Elena P. PAVLENKO,¹¹ Aleksei V. BAKLANOV,¹¹
Oksana I. ANTONYUK,¹¹ Denis SAMSONOV,¹¹ Aleksei SOSNOVSKIJ,¹¹ Kirill ANTONYUK,¹¹
Maksim V. ANDREEV,^{12,13} Etienne MORELLE,¹⁴ Pavol A. DUBOVSKY,¹⁵ Igor KUDZEJ,¹⁵ Arto OKSANEN,¹⁶
Gianluca MASI,¹⁷ Thomas KRAJCI,¹⁸ Roger D. PICKARD,^{19,20} Richard SABO,²¹ Hiroshi ITOH,²² William STEIN,²³
Shawn DVORAK,²⁴ Arne HENDEN,²⁵ Shinichi NAKAGAWA,²⁶ Ryo NOGUCHI,²⁶ Eriko IINO,²⁶ Katsura MATSUMOTO,²⁶
Hiroki NISHITANI,²⁶ Tomoya AOKI,²⁶ Hiroshi KOBAYASHI,²⁶ Chihiro AKASAKA,²⁶ Greg BOLT,²⁷ Jeremy SHEARS,²⁸
Javier RUIZ,^{29,30} Sergey Yu. SHUGAROV,^{31,32} Drahomir CHOCHOL,³² Nikolai A. PARAKHIN,¹³ Berto MONARD,³³
Kazuhiko SHIOKAWA,³⁴ Kiyoshi KASAI,³⁵ Bart STAELS,^{25,36} Atsushi MIYASHITA,³⁷ Donn R. STARKEY,³⁸
Yenal ÖGMEN,³⁹ Colin LITTLEFIELD,⁴⁰ Natalia KATYSHEVA,³¹ Ivan M. SERGEY,⁴¹ Denis DENISENKO,⁴²
Tamas TORDAI,⁴³ Robert FIDRICH,⁴³ Vitaly P. GORANSKIJ,³¹ Jani VIRTANEN,⁴⁴ Tim CRAWFORD,⁴⁵
Jochen PIETZ,⁴⁶ Robert A. KOFF,⁴⁷ David BOYD,⁴⁸ Steve BRADY,⁴⁹ Nick JAMES,⁵⁰ William N. GOFF,⁵¹
Koh-ichi ITAGAKI,⁵² Hideo NISHIMURA,⁵³ Youichirou NAKASHIMA,⁵⁴ Seiichi YOSHIDA,⁵⁵ Rod STUBBINGS,⁵⁶
Gary POYNER,⁵⁷ Yutaka MAEDA,⁵⁸ Stanislav A. KOROTKIY,⁵⁹ Kirill V. SOKOLOVSKY,^{60,61} Seiji UEDA,⁶²

¹ Department of Astronomy, Kyoto University, Kyoto 606-8502

*tkato@kusastro.kyoto-u.ac.jp

² Kwasan and Hida Observatories, Kyoto University, Yamashina, Kyoto 607-8471

³ Furzehill House, Ilston, Swansea, SA2 7LE, UK

⁴ Departamento de Física Aplicada, Facultad de Ciencias Experimentales, Universidad de Huelva, 21071 Huelva, Spain

⁵ Center for Backyard Astrophysics, Observatorio del CIECEM, Parque Dunar, Matalascañas, 21760 Almonte, Huelva, Spain

⁶ Department of Biosphere-Geosphere System Science, Faculty of Informatics, Okayama University of Science, 1-1 Ridai-cho, Okayama, Okayama 700-0005

⁷ Groupe Européen d'Observations Stellaires (GEOS), 23 Parc de Levesville, 28300 Bailleau l'Evêque, France

⁸ Bundesdeutsche Arbeitsgemeinschaft für Veränderliche Sterne (BAV), Munsterdamm 90, 12169 Berlin, Germany

⁹ Vereniging Voor Sterrenkunde (VVS), Oude Bleken 12, 2400 Mol, Belgium

¹⁰ Variable Star Observers League in Japan (VSOLJ), 405-1003 Matsushiro, Tsukuba, Ibaraki 305-0035

¹¹ Crimean Astrophysical Observatory, 98409, Nauchny, Crimea, Ukraine

¹² Institute of Astronomy, Russian Academy of Sciences, 361605 Peak Terskol, Kabardino-Balkaria, Russia

¹³ International Center for Astronomical, Medical and Ecological Research of NASU, Ukraine 27 Akademika Zabolotnoho Str. 03680 Kyiv, Ukraine

¹⁴ 9 rue Vasco de GAMA, 59553 Lauwin Planque, France

¹⁵ Vihorlat Observatory, Mierova 4, Humenne, Slovakia

¹⁶ Nyrola observatory, Jyvaskylan Sirius ry, Vertaalantie 419, FI-40270 Palokka, Finland

¹⁷ The Virtual Telescope Project, Via Madonna del Loco 47, 03023 Ceccano (FR), Italy

¹⁸ Astrokolhoz Observatory, Center for Backyard Astrophysics New Mexico, PO Box 1351 Cloudcroft, New Mexico 83117, USA

¹⁹ The British Astronomical Association, Variable Star Section (BAA VSS), Burlington House, Piccadilly, London, W1J 0DU, UK

²⁰ 3 The Birches, Shobdon, Leominster, Herefordshire, HR6 9NG, UK

²¹ 2336 Trailcrest Dr., Bozeman, Montana 59718, USA

²² VSOLJ, 1001-105 Nishiterakata, Hachioji, Tokyo 192-0153

²³ 6025 Calle Paraiso, Las Cruces, New Mexico 88012, USA

²⁴ Rolling Hills Observatory, 1643 Nightfall Drive, Clermont, Florida 34711, USA

²⁵ American Association of Variable Star Observers, 49 Bay State Rd., Cambridge, MA 02138, USA

²⁶ Osaka Kyoiku University, 4-698-1 Asahigaoka, Osaka 582-8582

²⁷ Camberwarra Drive, Craigie, Western Australia 6025, Australia

²⁸ "Pemberton", School Lane, Bunbury, Tarporley, Cheshire, CW6 9NR, UK

²⁹ Observatorio de Cantabria, Ctra. de Rocamundo s/n, Valderredible, Cantabria, Spain

³⁰ Agrupación Astronómica Cantabria, Apartado 573, 39080-Santander, Spain

³¹ Sternberg Astronomical Institute, Moscow University, Universitetsky Ave., 13, Moscow 119992, Russia

³² Astronomical Institute of the Slovak Academy of Sciences, 05960, Tatranska Lomnica, the Slovak Republic

³³ Bronberg Observatory, Center for Backyard Astronomy Pretoria, PO Box 11426, Tiegterpoort 0056, South Africa

- ³⁴ *Moriyama 810, Komoro, Nagano 384-0085*
- ³⁵ *Baselstrasse 133D, CH-4132 Muttenz, Switzerland*
- ³⁶ *Center for Backyard Astrophysics (Flanders), American Association of Variable Star Observers (AAVSO), Alan Guth Observatory, Koningshofbaan 51, Hofstade, Aalst, Belgium*
- ³⁷ *Seikei Meteorological Observatory, Seikei High School, 3-3-1, Kichijoji-Kitamachi, Musashino-shi, Tokyo 180-8633*
- ³⁸ *DeKalb Observatory, H63, 2507 County Road 60, Auburn, Indiana 46706, USA*
- ³⁹ *Green Island Observatory, Geçitkale, Magosa, via Mersin, North Cyprus*
- ⁴⁰ *Department of Physics, University of Notre Dame, Notre Dame, Indiana 46556, USA*
- ⁴¹ *Group Betelgeuse, Republic Center of Technical Creativity of Pupils, Minsk, Belarus*
- ⁴² *Space Research Institute (IKI), Russian Academy of Sciences, Moscow, Russia*
- ⁴³ *Polaris Observatory, Hungarian Astronomical Association, Laborc utca 2/c, 1037 Budapest, Hungary*
- ⁴⁴ *Ollilantie 98, 84880 Ylivieska, Finland*
- ⁴⁵ *Arch Cape Observatory, 79916 W. Beach Road, Arch Cape, Oregon 97102, USA*
- ⁴⁶ *Nollenweg 6, 65510 Idstein, Germany*
- ⁴⁷ *Antelope Hills Observatory, 980 Antelope Drive West Bennett, CO 80102, USA*
- ⁴⁸ *Silver Lane, West Challow, Wantage, OX12 9TX, UK*
- ⁴⁹ *5 Melba Drive, Hudson, New Hampshire 03051, USA*
- ⁵⁰ *11 Tavistock Road, Chelmsford, Essex CM1 6JL, UK*
- ⁵¹ *13508 Monitor Ln., Sutter Creek, California 95685, USA*
- ⁵² *Itagaki Astronomical Observatory, Teppo-cho, Yamagata 990-2492*
- ⁵³ *Miyawaki 302-6, Kakegawa, Shizuoka 436-0086*
- ⁵⁴ *968-4 Yamadanoshou, Oku-cho, Setouchi-City, Okayama 701-4246*
- ⁵⁵ *2-4-10-708 Tsunashima-nishi, Kohoku-ku, Yokohama-City, Kanagawa 223-0053*
- ⁵⁶ *Tetoora Observatory, Tetoora Road, Victoria, Australia*
- ⁵⁷ *BAA Variable Star Section, 67 Ellerton Road, Kingstanding, Birmingham B44 0QE, UK*
- ⁵⁸ *Kaminishiyamamachi 12-14, Nagasaki, Nagasaki 850-0006*
- ⁵⁹ *Ka-Dar Scientific Center and Public Observatory, Neopalimovskij 1-j per. d. 16/13, 119121 Moscow, Russia*
- ⁶⁰ *Max-Planck-Institute für Radioastronomie, Auf dem Hügel 69, 53121 Bonn, Germany*
- ⁶¹ *Astro-Space Center, Lebedev Physical Institute of Russian Academy of Sciences, Profsoyuznaya 84/32, 117997 Moscow, Russia*
- ⁶² *6-23-9 Syowa-Minami, Kushiro City, Hokkaido 084-0909*

(Received 201 0; accepted 201 0)

Abstract

Continuing the project described by Kato et al. (2009a), we collected times of superhump maxima for 51 SU UMa-type dwarf novae mainly observed during the 2010–2011 season. Although most of the new data for systems with short superhump periods basically confirmed the findings by Kato et al. (2009a) and Kato et al. (2010), the long-period system GX Cas showed an exceptionally large positive period derivative. An analysis of public Kepler data of V344 Lyr and V1504 Cyg yielded less striking stage transitions. In V344 Lyr, there was prominent secondary component growing during the late stage of superoutbursts, and the component persisted at least for two more cycles of successive normal outbursts. We also investigated the superoutbursts of two conspicuous eclipsing objects: HT Cas and the WZ Sge-type object SDSS J080434.20+510349.2. Strong beat phenomena were detected in both objects, and late-stage superhumps in the latter object had an almost constant luminosity during the repeated rebrightenings. The WZ Sge-type object SDSS J133941.11+484727.5 showed a phase reversal around the rapid fading from the superoutburst. The object showed a prominent beat phenomenon even after the end of the superoutburst. A pilot study of superhump amplitudes indicated that the amplitudes of superhumps are strongly correlated with orbital periods, and the dependence on the inclination is weak in systems with inclinations smaller than 80°.

Key words: accretion, accretion disks — stars: novae, cataclysmic variables — stars: dwarf novae

1. Introduction

In papers Kato et al. (2009a) and Kato et al. (2010), we systematically surveyed period variations of superhumps in SU UMa-type dwarf novae (for general information of SU UMa-type dwarf novae and superhumps, see Warner

1995). These works indicated that evolution of superhump period (P_{SH}) is generally composed of three distinct stages: early evolutionary stage with a longer superhump period (stage A), middle stage with systematically varying periods (stage B), final stage with a shorter, stable superhump period (stage C). In short- P_{SH} systems, these

Table 1. Types of late-stage superhumps.

Superhump type	Usage in this paper
traditional late superhumps	Superhumps with a ~ 0.5 phase shift seen during the very late or post-superoutburst stages. At least some of these traditional late superhumps reported in past literature may have been mis-identification of stage C superhumps. We used this term only if ~ 0.5 phase shift is confirmed.
post-superoutburst superhumps	Superhumps during the post-superoutburst stages (persisting superhumps). This term is mostly used in WZ Sge-type dwarf novae and related systems, in which clear stage B-C transitions are often missing or continuity of the phase becomes unclear during the rapid fading stage, making it difficult to assign our stage-based classification.
late-stage superhumps	General term referring to superhumps seen during the late stage of superoutbursts.
stage C superhumps	Superhumps after stage B-C transition based on our staging scheme. No ~ 0.5 phase shift is recognized.

stages are often observed as distinct segments (e.g. see a representative example in figure 24: $E \leq 25$ in this figure corresponds to stage A, $25 < E < 140$ with a parabolic $O - C$ curve corresponds to stage B with an increasing period, and $E \geq 140$ corresponds to stage C). Although systems with longer P_{SH} tend to show less distinct stages, there is often a systematic “break” in the $O - C$ diagram, which we attribute to a stage B-C transition based on the knowledge in the systematic variation of the $O - C$ diagrams against P_{SH} (cf. subsection 3.2 and figure 4 in Kato et al. 2009a). It was also shown that the period derivatives ($P_{\text{dot}} = \dot{P}/P$) during stage B is correlated with P_{SH} , or binary mass-ratios ($q = M_2/M_1$).

We used similar, but either phenomenologically or conceptually different, terminologies referring the superhumps observed during the late stages of superoutbursts or post-superoutburst stages. For reader’s convenience, we summarized them in table 1. Note that the use of the terminology is not the same between different authors. Although some authors use the term “late superhumps” for our stage C superhumps, we restrict the usage of (traditional) late superhumps to superhumps with an ~ 0.5 phase shift.

In the present study, we extended the survey to newly

recorded objects and superoutbursts since the publication of Kato et al. (2010). Some of new observations have led to revisions of analysis in the previous studies. We also include a few past superoutbursts not analyzed in the previous studies.

The present study is particularly featured with extensively observed rare phenomena, including a superoutburst of the eclipsing dwarf nova HT Cas, first ever since 1985, the eclipsing WZ Sge-type dwarf nova SDSS J080434.20+510349.2, and the bright WZ Sge-type dwarf nova with a long-lasting post-superoutburst state SDSS J133941.11+484727.5, all of which provided a significant contribution to our knowledge in the evolution of superhumps.

Two new topics will be discussed: comparison of Kepler observations with ground-based observations, and a pilot study of superhump amplitudes, the latter having been motivated by a recent work by Smak (2010).

The structure of the paper follows the scheme in Kato et al. (2009a), in which we mostly restricted ourselves to superhump timing analysis. We also include some more details (evidence for an SU UMa-type dwarf nova by presenting period analysis and averaged superhump profile) if the paper provides the first solid presentation of individual objects.

2. Observation and Analysis

The data were obtained under campaigns led by the VSNET Collaboration (Kato et al. 2004b). In some objects, we used archival data for published papers, and the public data from the AAVSO International Database¹. The majority of the data were acquired by time-resolved CCD photometry by using 30 cm-class telescopes, whose observational details on individual objects will be presented in future papers dealing with analysis and discussion on individual objects. The list of outbursts and observers is summarized in table 2. The data analysis was performed just in the same way described in Kato et al. (2009a). The times of all observations are expressed in Barycentric Julian Dates (BJD). We also use the same abbreviations P_{orb} for the orbital period and $\epsilon = P_{\text{SH}}/P_{\text{orb}} - 1$ for the fractional superhump excess.

The derived P_{SH} , P_{dot} and other parameters are listed in table 3 in same format as in Kato et al. (2009a). The definitions of parameters P_1, P_2, E_1, E_2 and P_{dot} are the same as in Kato et al. (2009a). We also present comparisons of $O - C$ diagrams between different superoutbursts since this has been one of the motivations of these surveys (cf. Uemura et al. 2005).

While most of the analyses were performed using the same technique as in Kato et al. (2009a), we introduced a variety of bootstrapping in estimating the robustness of the result of Phase Dispersion Minimization (PDM; Stellingwerf 1978). We typically analyzed 100 samples which randomly contain 50 % of observations, and performed PDM analysis for these samples. The bootstrap

¹ <<http://www.aavso.org/data-download>>.

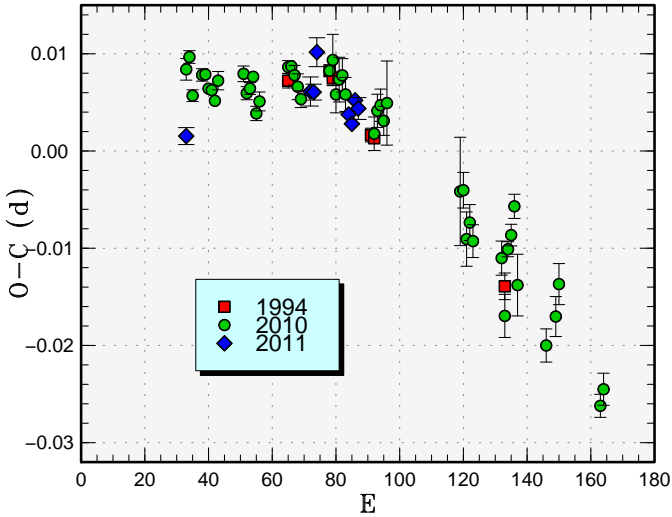


Fig. 1. Comparison of $O - C$ diagrams of FO And between different superoutbursts. A period of 0.07451 d was used to draw this figure. Approximate cycle counts (E) after the start of the superoutburst were used. Since the starts of the 1994 and 2011 superoutbursts were not well constrained, we shifted the $O - C$ diagrams to best fit the best-recorded 2010 one.

result is shown as a form of 90 % confidence intervals in the resultant θ statistics.

We also employed locally-weighted polynomial regression (LOWESS, Cleveland 1979) in removing trends resulting from outbursts for highly structured and uninterrupted light curves like Kepler observations.

3. Individual Objects

3.1. FO Andromedae

We observed two superoutbursts of this object in 2010 and 2011. The 2010 superoutburst was well-observed except for the initial part (table 4). The 2011 superoutburst was only partly observed (table 5). The 2010 observation confirmed the presence of a stage B-C transition. The later part of the 2011 observation probably caught a part of stage C, and we listed values based on this interpretation (figure 1).

FO And has a short supercycle of 100–140 d and has similar outburst properties to V503 Cyg, V344 Lyr (Kato et al. 2002) and MN Dra (Pavlenko et al. 2010b), all of which are known to show distinct negative superhumps in quiescence (Harvey et al. 1995; Still et al. 2010; Pavlenko et al. 2010c). The recent discovery of long-persisting negative superhumps in ER UMa (Ohshima et al. 2011a) and its unusual development of superhumps (Kato et al. 2003a) has led to a question whether these system show unusual behavior similar to ER UMa. In the case of FO And, the $O - C$ behavior and variation of the superhump profile (figure 2) of the 2010 superoutburst looked relatively normal for an ordinary SU UMa-type dwarf nova.

Table 4. Superhump Maxima of FO And (2010).

E	max*	error	$O - C^\dagger$	N^\ddagger
0	55486.9737	0.0011	-0.0041	108
1	55487.0494	0.0006	-0.0026	108
2	55487.1200	0.0006	-0.0064	107
5	55487.3456	0.0006	-0.0036	77
6	55487.4202	0.0005	-0.0033	74
7	55487.4933	0.0006	-0.0045	71
8	55487.5676	0.0005	-0.0044	73
9	55487.6410	0.0006	-0.0053	74
10	55487.7176	0.0009	-0.0030	45
18	55488.3144	0.0008	-0.0005	64
19	55488.3869	0.0007	-0.0022	76
20	55488.4619	0.0006	-0.0015	77
21	55488.5376	0.0005	-0.0001	77
22	55488.6084	0.0007	-0.0036	77
23	55488.6841	0.0010	-0.0022	73
32	55489.3582	0.0007	0.0034	158
33	55489.4328	0.0005	0.0037	153
34	55489.5064	0.0010	0.0030	102
35	55489.5797	0.0013	0.0021	77
36	55489.6530	0.0009	0.0010	77
45	55490.3265	0.0005	0.0060	113
46	55490.4021	0.0026	0.0073	37
47	55490.4731	0.0019	0.0040	34
48	55490.5491	0.0023	0.0057	38
49	55490.6240	0.0017	0.0064	38
50	55490.6966	0.0018	0.0047	31
59	55491.3631	0.0017	0.0027	35
60	55491.4400	0.0017	0.0053	34
61	55491.5151	0.0017	0.0061	37
62	55491.5880	0.0015	0.0047	39
63	55491.6643	0.0043	0.0067	28
86	55493.3690	0.0056	0.0029	23
87	55493.4436	0.0018	0.0032	25
88	55493.5131	0.0028	-0.0016	25
89	55493.5893	0.0018	0.0004	25
90	55493.6619	0.0017	-0.0013	25
99	55494.3307	0.0018	-0.0010	27
100	55494.3993	0.0022	-0.0067	34
101	55494.4807	0.0008	0.0003	70
102	55494.5566	0.0011	0.0020	91
103	55494.6341	0.0012	0.0052	59
104	55494.7005	0.0032	-0.0027	19
113	55495.3649	0.0017	-0.0068	33
116	55495.5914	0.0021	-0.0032	25
117	55495.6692	0.0021	0.0004	26
130	55496.6254	0.0012	-0.0092	38
131	55496.7016	0.0017	-0.0072	21

*BJD-2400000.

† Against max = 2455486.9778 + 0.074283 E .

‡ Number of points used to determine the maximum.

Table 2. List of Superoutbursts.

Subsection	Object	Year	Observers or references*	ID†
3.1	FO And	2010	deM, IMi, OUS, HMB	
	FO And	2011	PXR, deM, Ogm	
3.2	V402 And	2011	IMi, MEV, PXR, SRI	
3.3	BG Ari	2010	SRI, IMi, MEV, Boy, JSh	
3.4	V496 Aur	2010	IMi, KU	
3.5	TT Boo	2007	Mhh	
	TT Boo	2010	Ioh, Mhh	
3.6	GX Cas	2010	OUS, DPV	
3.7	HT Cas	2010	OKU, Mhh, KU, OUS, AAVSO, Ioh, deM, CRI, Mas, IMi, MEV, Rui, Tze, SRI, DPV, Ter, HMB, Pol, Kai, NDJ, Nyr, PXR, LCO, Ogm, DRS, Kis, SAc	
3.8	V1504 Cyg	2007	CRI	
	V1504 Cyg	2009b	Kepler	
3.9	AW Gem	2011	OUS	
3.10	V844 Her	2010b	DPV, deM	
3.11	MM Hya	2011	GBo, OUS, Mhh, IMi	
3.12	V406 Hya	2010	Ter, Kis, Mhh	
3.13	V344 Lyr	2009	Kepler	
	V344 Lyr	2009b	Kepler	
3.14	V1195 Oph	2011	SWI, Mhh	
3.15	V1212 Tau	2011	deM, Mhh, Kra, MEV, IMi, KU, SRI, SWI	
3.16	SW UMa	2010	OUS, Rui, DPV	
3.17	CI UMa	2011	IMi, DPV, HMB	
3.18	DV UMa	2011	Mhh, LCO, IMi	
3.19	1RXS J0038	2010	PIE, KU, CRI	
3.20	2QZ J2224	2010	MLF, Mhh	
3.21	ASAS J0918	2010	KU, Kis, DKS, OUS	
3.22	ASAS J1025	2011	DKS, Kis, Mas	
3.23	MisV 1443	2011	OUS, Ioh, deM, Mhh, Kis, PXR	
3.24	RX J1715	2010	IMi, KU	
3.25	SDSS J0732	2011	Kra, KU, IMi	
3.26	SDSS J0803	2011	Mhh, IMi, Mas	Wils et al. (2010)
3.27	SDSS J0804	2010	Ter, KU, deM, IMi, OKU, OUS, Mhh, AKz, KRV, NKa, HMB, CRI, Nyr, DPV, MEV, Shu, Den, Ser, SRI, Vir, AAVSO	
3.28	SDSS J0812	2008	Kato et al. (2009a)	
	SDSS J0812	2011	OUS, Mhh, IMi	
3.29	SDSS J0932	2011	OKU, deM, CRI, MEV, Nyr, SRI, DKS	
3.30	SDSS J1120	2011	SWI, JSh	Wils et al. (2010)
3.31	SDSS J1146	2011	KU, Mhh, BSt, IMi, HMB, JSh, Nyr, deM, BXS, DRS, AAVSO	
3.32	SDSS J1227	2007	Kato et al. (2009a), Gor	
	SDSS J1227	2011	Nyr, Ter, CRI, deM	
3.33	SDSS J1250	2011	Rui, Mhh, IMi	
3.34	SDSS J1339	2011	Ter, Mhh, OUS, Nyr, HMB, KU, SRI, AAVSO, IMi, Mas, DPV, GFB, DKS, PXR, CTX, BSt, JSh, MEV	
3.35	SDSS J1605	2010	KU, Mhh, Kis	Itagaki (vsnet-alert 12414)

*Key to observers: AKz (Astrokolkozhov Obs.), Boy[‡](D. Boyd), BSt (B. Staels), BXS[‡](S. Brady), CRI (Crimean Astrophys. Obs.), CTX[‡](T. Crawford), Den (D. Denisenko), deM (E. de Miguel), DKS[‡](S. Dvorak), DPV (P. Dubovsky), DRS[‡](D. Starkey), GBo (G. Bolt), GFB[‡](W. Goff), Gor (V. Goranskij), HMB (F.-J. Hambsch), IMi[‡](I. Miller), Ioh (H. Itoh), JSh[‡](J. Shears), Kai (K. Kasai), Kis (S. Kiyota), Kra (T. Krajci), KRV[‡](R. Koff), KU (Kyoto U., campus obs.), LCO[‡](C. Littlefield), Mas (G. Masi), MEV[‡](E. Morelle), Mhh (H. Maehara), MLF (B. Monard), NDJ (N. James), NKa (N. Katysheva), Nyr (Nyrola and Hankasalmi Obs.), Ogm[‡](Y. Ogmen), OKU (Osaya Kyoiku U.), OUS (Okayama U. of Science), PIE (J. Pietz), Pol (Polaris Obs.), PXR[‡](R. Pickard), Rui (J. Ruiz), SAc (Seikei High School), Ser (I. Sergey), Shu (S. Shugarov), SRI[‡](R. Sabo), SWI[‡](W. Stein), Ter (Terskol Obs.), Tze (Tzec Maun Obs., remotely operated by HMB), Vir[‡](J. Virtanen), AAVSO (AAVSO database)

†Original identifications or discoverers.

Table 2. List of Superoutbursts (continued).

Subsection	Object	Year	Observers or references*	ID [†]
3.36	SDSS J2100	2010	IMi	
3.37	OT J0009	2010	GBo, KU, Mhh	CSS101007:000938–121017
3.38	OT J0120	2010	Ter, Mhh, OUS, KU, Ioh, Siz, CRI, AAVSO, deM, MEV, IMi, DKS, Shu, Nyr, SAc, PXR, SWI, Kai	Itagaki (vsnet-alert 12431)
3.39	OT J0141	2010	Mhh, Kis	CSS101127:014150+090822
3.40	OT J0413	2011	Kra, Mhh	CSS110125:041350+094515
3.41	OT J0431	2011	SWI, Mas, KU, Kis, Kra, Mhh	CSS110113:043112–031452
3.42	OT J0442	2011	Mas	CSS071115:044216–002334
3.43	OT J0648	2011	Mhh, Kra, deM, Ter	CSS091026:064805+414702
3.44	OT J0754	2011	deM, HMB	CSS110414:075414+313216
3.45	OT J102616	2010	Ter, KU, Mhh	CSS101130:102616+192045
3.46	OT J1027	2011	GBo	SSS110314:102706–434341
3.47	OT J1200	2011	Mas	CSS110205:120053–152620
3.48	OT J1329	2011	MLF	SSS110403:132901–365859
3.49	OT J1545	2011	OKU, HMB	CSS110428:154545+442830
3.50	OT J2234	2009	Mhh	CSS090910:223418–035530
	OT J2234	2010	GBo	
3.51	OT J2304	2011	Siz, Ioh, Mhh, CRI	Nishimura (Nakano et al. 2011)

*Key to observers.

[†]Original identifications or discoverers.[‡]Inclusive of observations from the AAVSO database.**Table 5.** Superhump Maxima of FO And (2011).

E	max*	error	$O - C$ [†]	N [‡]
0	55578.4067	0.0009	−0.0017	77
39	55581.3172	0.0015	0.0012	81
40	55581.3916	0.0008	0.0011	158
41	55581.4702	0.0015	0.0052	61
51	55582.2089	0.0006	−0.0017	55
52	55582.2825	0.0004	−0.0027	89
53	55582.3594	0.0006	−0.0003	40
54	55582.4331	0.0011	−0.0012	32

*BJD−2400000.

[†]Against max = 245578.4084 + 0.074553*E*.[‡]Number of points used to determine the maximum.**Table 6.** Superhump maxima of V402 And (2011).

E	max*	error	$O - C$ [†]	N [‡]
0	55582.3645	0.0004	0.0037	49
14	55583.2496	0.0009	0.0005	38
15	55583.3127	0.0003	0.0002	116
16	55583.3781	0.0006	0.0021	63
35	55584.5783	0.0004	−0.0031	46
36	55584.6425	0.0007	−0.0024	37
46	55585.2761	0.0005	−0.0032	59
47	55585.3392	0.0012	−0.0035	52
78	55587.3085	0.0006	−0.0011	58
94	55588.3279	0.0008	0.0032	78
125	55590.3008	0.0027	0.0093	17
141	55591.3067	0.0009	0.0001	65
142	55591.3704	0.0008	0.0004	39
156	55592.2548	0.0033	−0.0035	39
157	55592.3208	0.0012	−0.0009	126
158	55592.3831	0.0032	−0.0020	37

*BJD−2400000.

[†]Against max = 245582.3608 + 0.063445*E*.[‡]Number of points used to determine the maximum.

3.2. V402 Andromedae

We observed the 2011 superoutburst (table 6). The data demonstrated stage B with a positive P_{dot} of $+7.7(0.8) \times 10^{-5}$ and stage C first time for this object. A comparison of $O - C$ diagrams for different superoutbursts is shown in figure 3.

3.3. BG Arietis

We observed the 2010 superoutburst of this object (=PG 0149+138, SDSS J015151.87+140047.2). The outburst was well-observed since its earliest stage. The times of superhump maxima are listed in table 7. All A–C stages are clearly present. There was a marginal hint of positive P_{dot} during stage B, as in the 2009 superoutburst (Kato et al. 2010).

Table 3. Superhump Periods and Period Derivatives

Object	Year	P_1 (d)	err	E_1^*	P_{dot}^\dagger	err †	P_2 (d)	err	E_2^*	P_{orb} (d)	Q ‡		
FO And	2010	0.074512	0.000017	0	50	4.6	3.5	0.074117	0.000030	59	131	0.07161	B
FO And	2011	–	–	–	–	–	–	0.074266	0.000114	39	54	0.07161	C
V402 And	2011	0.063489	0.000030	0	125	7.7	0.8	0.063128	0.000071	125	158	–	B
BG Ari	2010	0.084897	0.000025	32	91	4.9	3.0	0.084683	0.000081	102	221	–	B
V496 Aur	2010	0.061162	0.000076	0	20	–	–	–	–	–	–	–	C
TT Boo	2007	0.077876	0.000116	0	26	–	–	–	–	–	–	–	C2
TT Boo	2010	0.078115	0.000025	0	104	5.4	1.4	–	–	–	–	–	B
GX Cas	2010	0.092998	0.000054	0	60	25.0	4.6	–	–	–	–	–	B
HT Cas	2010	0.076349	0.000016	12	58	3.0	3.6	0.075900	0.000011	57	126	0.073647	A
V1504 Cyg	2007	0.072323	0.000146	0	55	–	–	0.071865	0.000040	55	139	0.069549	C
V1504 Cyg	2009b	0.072221	0.000009	21	89	–1.0	1.4	0.071883	0.000009	89	163	0.069549	A
AW Gem	2011	0.079376	0.000037	0	27	–	–	0.078627	0.000013	38	102	0.07621	B
V844 Her	2010b	0.056115	0.000041	0	72	8.9	5.8	0.055906	0.000044	70	107	0.054643	C
MM Hya	2011	0.058855	0.000017	16	120	7.2	0.9	–	–	–	–	0.057590	B
V344 Lyr	2009	0.091583	0.000009	26	79	–0.3	1.3	0.091277	0.000016	80	156	–	A
V344 Lyr	2009b	0.091614	0.000012	30	72	–1.4	2.3	0.091259	0.000010	73	170	–	A
V1195 Oph	2011	0.067038	0.000070	0	25	–	–	–	–	–	–	–	C2
V1212 Tau	2011	0.070115	0.000018	20	90	7.0	2.7	0.069778	0.000032	89	167	–	B
SW UMa	2010	0.058208	0.000034	52	174	12.9	0.9	0.057978	0.000035	171	277	0.056815	B
CI UMa	2011	0.062690	0.000029	0	66	16.8	3.2	–	–	–	–	–	B
DV UMa	2011	0.088933	0.000045	0	52	14.6	6.6	–	–	–	–	0.085853	C
1RXS J0038	2010	0.097080	0.000080	0	42	–	–	–	–	–	–	–	CG
2QZ J2224	2010	–	–	–	–	–	–	0.058243	0.000011	0	106	–	C
ASAS J0918	2010	–	–	–	–	–	–	0.062618	0.000036	20	86	–	C
ASAS J1025	2011	0.063538	0.000023	0	72	9.9	2.4	0.063271	0.000083	72	103	0.06136	CE
MisV 1443	2011	0.056725	0.000014	19	110	5.5	1.5	–	–	–	–	–	B
RX J1715	2010	–	–	–	–	–	–	0.070752	0.000102	0	30	0.0683	C
SDSS J0732	2011	–	–	–	–	–	–	0.079325	0.000042	0	72	–	C
SDSS J0803	2011	0.075100	0.000033	0	50	13.6	4.2	–	–	–	–	–	C
SDSS J0804	2010	0.059630	0.000016	31	159	9.6	1.1	–	–	–	–	0.059005	A
SDSS J0812	2008	0.077559	0.000148	0	103	–24.8	6.2	–	–	–	–	–	BG
SDSS J0812	2011	0.077892	0.000029	13	53	–7.6	6.3	0.077337	0.000072	77	131	–	B
SDSS J0932	2011	–	–	–	–	–	–	0.068110	0.000016	0	161	0.066304	B
SDSS J1120	2011	0.070550	0.000054	0	22	–	–	–	–	–	–	–	C
SDSS J1146	2011	0.063326	0.000017	9	83	10.9	3.0	0.063055	0.000086	83	105	–	BG
SDSS J1227	2007	0.064604	0.000029	33	129	10.5	2.4	0.064399	0.000046	126	216	0.062950	B
SDSS J1227	2011	0.064883	0.000032	0	29	–	–	0.064494	0.000021	43	184	0.062950	C
SDSS J1250	2011	0.060261	0.000057	0	59	–	–	–	–	–	–	0.058736	CGM
SDSS J1339	2011	0.058094	0.000007	34	205	5.4	0.2	–	–	–	–	0.057289	A
SDSS J2100	2010	0.087295	0.000186	0	69	–34.1	2.2	–	–	–	–	–	CG
OT J0009	2010	0.090005	0.000055	0	14	–	–	0.088851	0.000049	12	48	–	C
OT J0120	2010	0.057833	0.000009	0	174	4.3	0.5	–	–	–	–	0.057157	AE
OT J0141	2010	0.062488	0.000040	0	115	10.1	1.6	0.062060	0.000086	114	131	–	B
OT J0413	2011	0.054830	0.000007	0	76	4.2	0.8	–	–	–	–	–	B
OT J0431	2011	0.067583	0.000026	0	112	8.4	1.2	0.067309	0.000043	125	200	0.066050	B
OT J0442	2011	0.076761	0.000037	0	27	–	–	–	–	–	–	–	CG
OT J0648	2011	0.066324	0.000033	0	70	14.5	2.9	–	–	–	–	–	B
OT J0754	2011	0.063080	0.000081	0	33	–	–	0.062682	0.000044	31	96	–	C
OT J102616	2010	0.082830	0.000013	13	36	–	–	0.082526	0.000017	36	107	–	B
OT J1027	2011	0.080887	0.000034	0	15	–	–	–	–	–	–	–	C

*Interval used for calculating the period (corresponding to E in section 3).

† Unit 10^{-5} .

‡ Data quality and comments. A: excellent, B: partial coverage or slightly low quality, C: insufficient coverage or observations with large scatter, G: P_{dot} denotes global P_{dot} , M: observational gap in middle stage, 2: late-stage coverage, the listed period may refer to P_2 , E: P_{orb} refers to the period of early superhumps.

Table 3. Superhump Periods and Period Derivatives (continued)

Object	Year	P_1	err	E_1	$P_{\dot{}}$	err	P_2	err	E_2	P_{orb}	Q		
OT J1200	2011	0.097710	0.000058	0	11	–	–	–	–	–	CG		
OT J1329	2011	0.070999	0.000066	0	16	–	–	–	–	–	C		
OT J1545	2011	–	–	–	–	–	0.076930	0.000022	0	45	–	C	
OT J2234	2009	0.092192	0.000020	0	109	–	–	–	–	–	CG		
OT J2234	2010	0.092000	0.000400	0	2	–	–	–	–	–	C		
OT J2304	2010	0.067194	0.000030	0	123	–3.9	2.4	0.066281	0.000063	118	254	–	C

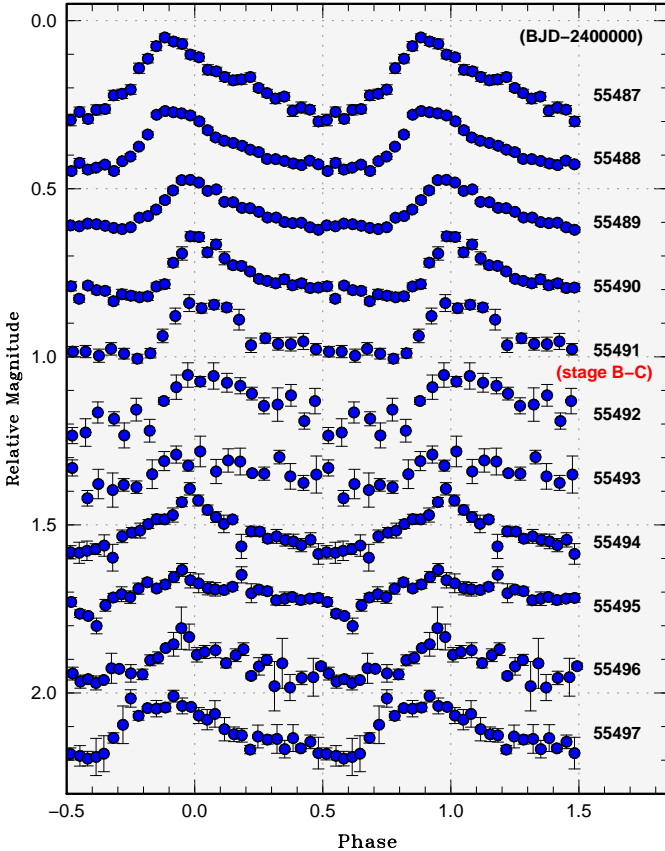


Fig. 2. Superhump profiles of FO And (2010). There was no apparent growth of secondary maxima as in ER UMa (Kato et al. 2003a). The apparent regrowth of the amplitudes of superhump at BJD 2455494 corresponds to 3 d after the stage B–C transition. The figure was drawn against a mean period of 0.074283 d.

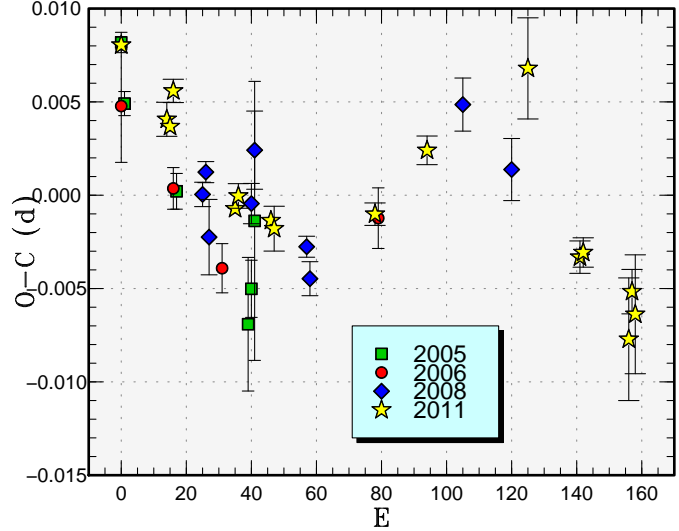


Fig. 3. Comparison of $O - C$ diagrams of V402 And between different superoutbursts. A period of 0.06350 d was used to draw this figure. Approximate cycle counts (E) after the start of the superoutburst were used.

A comparison of $O - C$ diagrams is shown in figure 4.

3.4. V496 Aurigae

V496 Aur is a dwarf nova discovered by Qiu et al. (1997), reporting the maximum unfiltered CCD magnitude of 15.7, and the absence of the quiescent counterpart on the Palomar Observatory Sky Survey plates. Based on spectroscopy during outburst, they confirmed the dwarf nova-type classification. Wei et al. (1998) reported another outburst in 1998. Unpublished photometry by one of the authors (T. Kato) during this 1998 outburst did not yield significant superhumps.

The 2010 outburst of this object was by chance detected by the Catalina Real-time Transient Survey (CRTS, Drake et al. 2009).² Subsequent observations confirmed the presence of superhumps (vsnet-alert 12430, 12439; figure 5). The times of superhump maxima are listed in table 8. The relatively small amplitudes might suggest that the object had already entered the late stage (possibly stage C) of the superoutburst. Observations taken four days later (December 5) did not detect significant superhump sig-

² <<http://nessi.cacr.caltech.edu/catalina/>>. For the information of the individual Catalina CVs, see <<http://nessi.cacr.caltech.edu/catalina/AllCV.html>>.

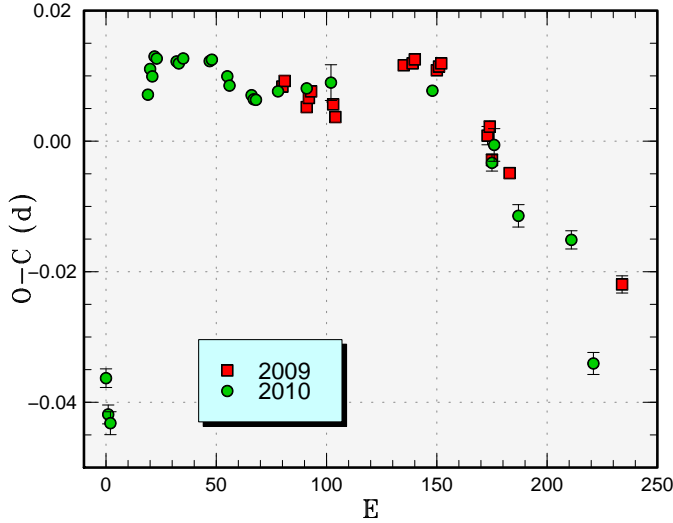


Fig. 4. Comparison of $O - C$ diagrams of BG Ari between different superoutbursts. A period of 0.08501 d was used to draw this figure. Approximate cycle counts (E) after the start of the superoutburst were used, assuming that the 2010 outburst was detected in its earliest stage. Since the start of the 2009 superoutburst was not well constrained, we shifted the $O - C$ diagram to best fit [in this and many other cases involving shifting $O - C$ diagrams, we adjusted the location of the “break” (stage B–C transition) in the $O - C$ diagram] the best-recorded 2010 one.

nals, and were excluded from this analysis. The improved astrometry by the CRTS is $07^{\text{h}}27^{\text{m}}52^{\text{s}}23$, $+40^{\circ}46'52''.5$ (J2000.0).

3.5. *TT Bootis*

We report on two more superoutbursts in 2007 and 2010 (tables 9 and 10). The 2007 observations were performed during the middle stage of the superoutburst. The 2010 observations fairly well covered the superoutburst except the final stage. The resultant P_{dot} of $+5.4(1.4) \times 10^{-5}$ confirms the rather large positive P_{dot} for this P_{SH} or P_{orb} (Kato et al. 2009a). A comparison of $O - C$ diagrams is presented in figure 6. The figure might suggest that a stage B–C transition already occurred before the 2007 observation.

3.6. *GX Cassiopeiae*

Although GX Cas was observed in multiple instances (Kato et al. 2009a), no significant variation of period was recorded, mostly due to the short baseline of observations.

During the 2010 superoutburst, we finally obtained a relatively dense set of observations during the later half of the superoutburst. The times of superhump maxima are listed in table 11. Surprisingly, they suggest a positive P_{dot} of $+25(5) \times 10^{-5}$ for $E \leq 60$ (see also figure 7; the conclusion is unchanged even using a rather discrepant point at $E = 62$; $E = 71$ corresponds to a point during the rapid decline phase). A combined $O - C$ diagram (figure 8) also seems to support a general trend of a positive P_{dot} .

As discussed in Kato et al. (2009a) (subsection 4.10),

Table 7. Superhump maxima of BG Ari (2010).

E	max*	error	$O - C^{\dagger}$	N^{\ddagger}
0	55536.6520	0.0014	-0.0391	79
1	55536.7314	0.0014	-0.0446	70
2	55536.8151	0.0018	-0.0459	64
19	55538.3106	0.0005	0.0051	87
20	55538.3996	0.0007	0.0090	89
21	55538.4834	0.0005	0.0079	87
22	55538.5715	0.0004	0.0110	134
23	55538.6562	0.0004	0.0107	69
32	55539.4208	0.0003	0.0106	92
33	55539.5055	0.0003	0.0104	80
35	55539.6763	0.0003	0.0112	69
47	55540.6960	0.0006	0.0112	76
48	55540.7813	0.0007	0.0115	58
55	55541.3738	0.0002	0.0092	91
56	55541.4574	0.0002	0.0078	56
66	55542.3060	0.0004	0.0067	54
67	55542.3904	0.0005	0.0061	53
68	55542.4753	0.0004	0.0061	56
78	55543.3267	0.0006	0.0078	83
91	55544.4323	0.0004	0.0087	56
102	55545.3683	0.0027	0.0100	29
148	55549.2775	0.0007	0.0105	48
175	55551.5617	0.0013	0.0004	52
176	55551.6495	0.0025	0.0032	41
187	55552.5737	0.0017	-0.0072	54
211	55554.6103	0.0014	-0.0100	51
221	55555.4415	0.0017	-0.0286	82

*BJD–2400000.

\dagger Against max = $2455536.6911 + 0.084973E$.

\ddagger Number of points used to determine the maximum.

Table 8. Superhump maxima of V496 Aur (2010).

E	max*	error	$O - C^{\dagger}$	N^{\ddagger}
0	55530.4937	0.0011	0.0007	60
1	55530.5521	0.0012	-0.0021	67
2	55530.6167	0.0012	0.0014	52
19	55531.6556	0.0012	0.0005	48
20	55531.7158	0.0015	-0.0005	61

*BJD–2400000.

\dagger Against max = $2455530.4930 + 0.061162E$.

\ddagger Number of points used to determine the maximum.

Table 9. Superhump maxima of TT Boo (2007).

E	max*	error	$O - C^{\dagger}$	N^{\ddagger}
0	54200.1584	0.0006	0.0013	168
1	54200.2326	0.0006	-0.0024	98
13	54201.1714	0.0005	0.0019	167
26	54202.1810	0.0005	-0.0009	168

*BJD–2400000.

\dagger Against max = $2454200.1571 + 0.077876E$.

\ddagger Number of points used to determine the maximum.

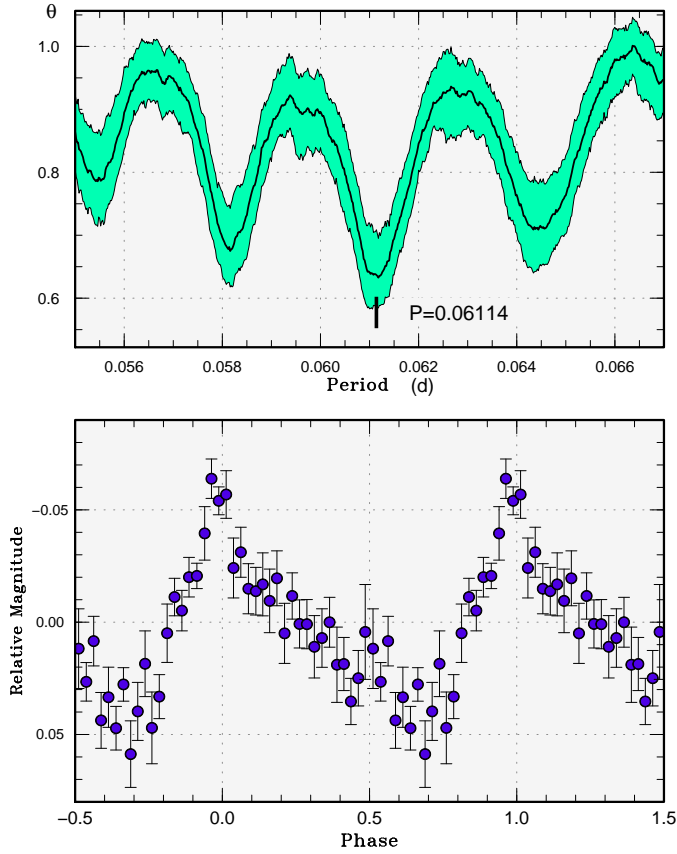


Fig. 5. Superhumps in V496 Aur (2010). (Upper): PDM analysis. (Lower): Phase-averaged profile.

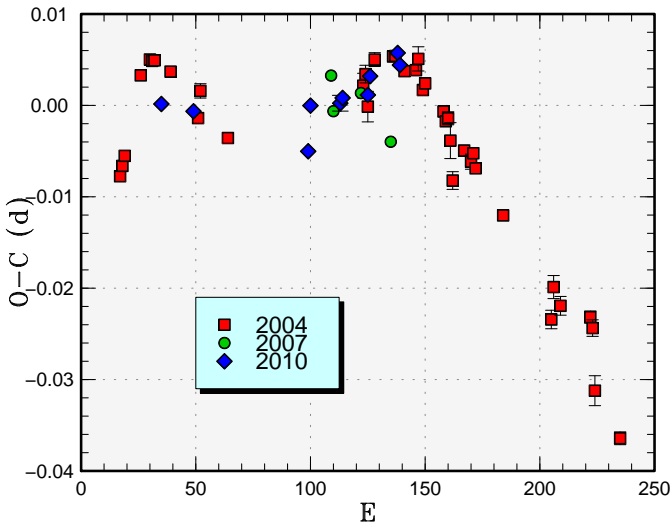


Fig. 6. Comparison of $O - C$ diagrams of TT Boo between different superoutbursts. A period of 0.07807 d was used to draw this figure. Approximate cycle counts (E) after the start of the superoutburst were used. Since the starts of the 2010 superoutburst was not well constrained, we shifted the $O - C$ diagrams to best fit the best-recorded 2004 one.

Table 10. Superhump maxima of TT Boo (2010).

E	max*	error	$O - C^\dagger$	N^\ddagger
0	55311.0879	0.0001	0.0022	232
14	55312.1801	0.0003	0.0008	161
64	55316.0792	0.0008	-0.0058	140
65	55316.1623	0.0007	-0.0009	163
78	55317.1774	0.0009	-0.0012	146
79	55317.2561	0.0006	-0.0006	152
90	55318.1152	0.0006	-0.0008	152
91	55318.1953	0.0009	0.0012	154
103	55319.1347	0.0007	0.0032	148
104	55319.2114	0.0006	0.0018	156

*BJD-2400000.

† Against max = $2455311.0857 + 0.078115E$.

‡ Number of points used to determine the maximum.

most long- P_{orb} objects generally show relatively large negative P_{dot} , while some objects (mostly rarely outbursting objects) have nearly zero P_{dot} . GX Cas is clearly an exception. Although this conclusion may have been affected by the lack of observations during the early stage of the superoutburst, the object will be worth studying in more details. Being a bright object, the object would be a good target for a radial-velocity study in calibrating $P_{\text{orb}} - \epsilon$ relation in long-period systems.

3.7. HT Cassiopeiae

HT Cas is renowned for its deep eclipses and for its historical superoutburst in 1985. There were only fragmentary observations of superhumps during the 1985 superoutburst (Zhang et al. 1986; reanalyzed by Kato et al. 2009a). Although there were known normal outbursts (1987, 1989, 1995, 1997, 1998, 1999, 2002, 2008) since then, there have been no confirmed superoutburst. The 1995 normal outburst was particularly well observed (Ioannou et al. 1999).

The 2010 superoutburst was detected by T. Parsons on November 2.43 UT at a visual magnitude of 12.9 (cvnet-discussion 1404). The object further brightened, and growing superhumps were detected ~ 1.5 d later (vsnet-alert 12353, 12359; figure 9). The superhumps (figure 10) quickly developed to the full amplitude and slowly decayed.

Due to the overlapping eclipses and very strong effect of beat phenomenon (figure 11), we first subtracted the template orbital variation (cf. figure 13) scaled by fitting individual eclipses (the results were globally smoothed; cf. figure 11c) and removed the part (within 0.11 P_{orb} of eclipses) most strongly affected by eclipses, and applied the usual method of fitting maxima. The ephemeris of eclipse used in this procedure is given in equation 1, which were determined by one of the authors (H. Maehara) using published and newly obtained eclipse timings since 2009 January 1.³

³ Since the orbital period of HT Cas is known to vary significantly (e.g. Borges et al. 2008), we only used recent timing data for

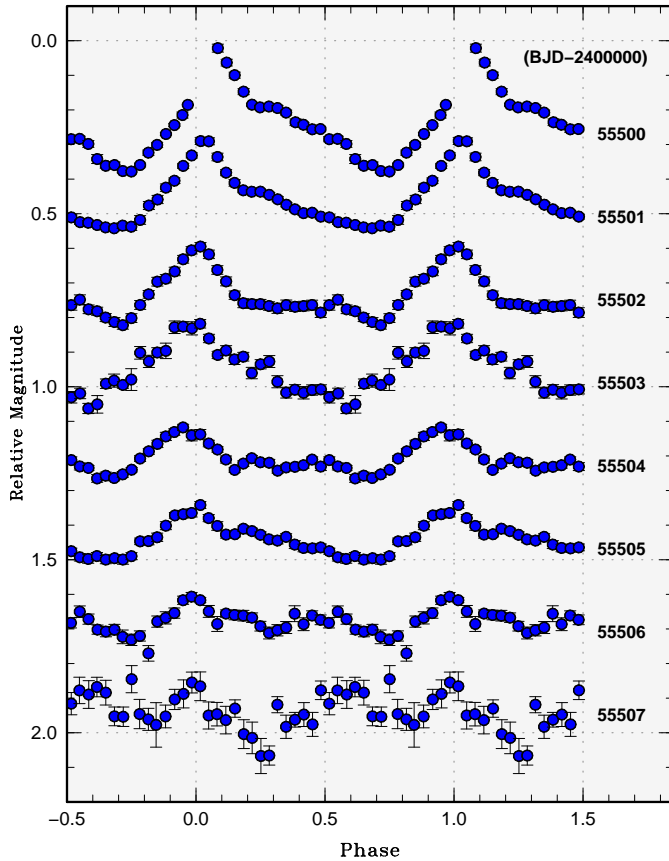


Fig. 7. Superhump profiles of GX Cas (2010). The positive P_{dot} is also evident from these phase-averaged nightly light curves except for the final night during the rapid fading stage. The figure was drawn against a mean period of 0.092959 d.

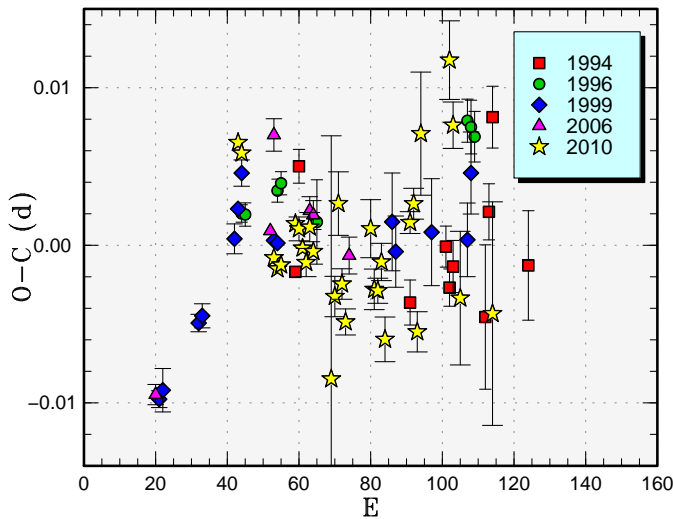


Fig. 8. Comparison of $O - C$ diagrams of GX Cas between different superoutbursts. A period of 0.092959 d was used to draw this figure. Approximate cycle counts (E) after the start of the superoutburst were used. Since the starts of the 1994 and 2011 superoutbursts was not well constrained, we shifted the $O - C$ diagrams to best fit the best-recorded 2010 one.

Table 11. Superhump maxima of GX Cas (2010).

E	max*	error	$O - C^\dagger$	N^\ddagger
0	55500.5225	0.0004	0.0065	154
1	55500.6148	0.0003	0.0058	196
10	55501.4448	0.0003	-0.0008	203
11	55501.5370	0.0003	-0.0015	202
12	55501.6303	0.0005	-0.0013	206
16	55502.0047	0.0005	0.0014	285
17	55502.0973	0.0008	0.0010	250
18	55502.1891	0.0006	-0.0002	217
19	55502.2811	0.0009	-0.0011	230
20	55502.3763	0.0009	0.0011	208
21	55502.4677	0.0004	-0.0004	207
26	55502.9245	0.0154	-0.0085	59
27	55503.0226	0.0013	-0.0033	158
28	55503.1215	0.0020	0.0026	234
29	55503.2094	0.0010	-0.0025	112
30	55503.2999	0.0008	-0.0049	135
37	55503.9565	0.0018	0.0011	181
38	55504.0456	0.0013	-0.0028	273
39	55504.1385	0.0008	-0.0029	271
40	55504.2333	0.0012	-0.0011	130
41	55504.3213	0.0014	-0.0060	108
48	55504.9795	0.0007	0.0014	205
49	55505.0736	0.0010	0.0026	219
50	55505.1585	0.0013	-0.0055	141
51	55505.2640	0.0039	0.0071	99
59	55506.0123	0.0025	0.0118	209
60	55506.1012	0.0015	0.0076	206
62	55506.2761	0.0042	-0.0033	100
71	55507.1118	0.0071	-0.0043	119

*BJD-2400000.

\dagger Against max = 245500.5160 + 0.092959 E .

\ddagger Number of points used to determine the maximum.

$$\text{Min(BJD)} = 2443727.93823(20) + 0.0736471875(13)E. (1)$$

Although this procedure lacks the detailed treatment of variations in eclipse profiles, it will be sufficient for the present purpose of measuring the global behavior of superhumps. The times of superhump maxima are listed in table 12. Three stages of A–C are apparently present (figure 12). Stage A and the middle of stage B were very strongly affected by overlapping eclipses. By rejecting the most severely affected maxima ($26 \leq E \leq 28$), we obtained an almost zero $+3.0(3.6) \times 10^{-5}$ period derivative for stage B ($12 \leq E \leq 58$). The other values are listed in table 3. As judged from the recorded period, Zhang et al. (1986) seems to have observed stage C superhumps.

The resultant period variation was generally normal for an SU UMa-type dwarf nova with P_{orb} of 0.07365 d, despite the long lack of superoutbursts. There were no detectable features of early superhumps, which likely excludes the WZ Sge-like phenomenon suggested for the 1985 superoutburst (cf. Kato et al. 2001). The very large

calculating the orbital phase. This ephemeris is not designed for long-term prediction of eclipses.

amplitude of the outburst reported during the 1985 outburst may have resulted from an old AAVSO scale of comparison stars, combined with strong orbital/superhump modulations.

Even after the superoutburst, superhumps with slightly shorter periods persisted at least for 16 d (table 13; maxima were measured in the same way as in the superoutburst). There was no phase jump following the stage C superhumps (figure 12a,c), and these superhumps are not considered to be “traditional” late superhumps (see a discussion in Kato et al. 2009a, subsection 4.2).

Before superhumps appeared, there was likely an indication of orbital humps (figure 13a). The orbital humps were not evident during the plateau phase of the superoutburst, and there was a slight bump around orbital phase 0.5, which might look like a reflection effect on the secondary (figure 13b). The post-superoutburst phase was dominated by double-wave modulations, which probably arise from ellipsoidal variation of the secondary (figure 13c). No evident orbital humps were detected during this phase.

Figure 14 shows a more detailed dependence of orbital profiles during the plateau phase on the superhump phase (ϕ_{SH}). The superhump phases were defined so that $\phi_{\text{SH}} = 0$ corresponds to superhump maxima. Although there was a feature resembling orbital humps for $0 \leq \phi_{\text{SH}} \leq 0.4$, this feature was not persistently present at other ϕ_{SH} . The phase 0.5 bump was not clearly present independent of ϕ_{SH} , and this bump (in averaged profile) appears to have originated from complex features outside the eclipses for $0.7 \leq \phi_{\text{SH}} \leq 1.0$. Since these features have different profiles and times of maxima for different ϕ_{SH} , we regard it less likely that they arise from the reflection effect on the secondary (cf. Smak 2011). These features more likely represent the geometrical effect arising from the non-axisymmetrically extended vertical structure resulting from the heating by the superhump source. Figure 15 illustrate the same dependence after the rapid decline from the superoutburst (BJD 2455514–2455522). Although the general tendency of variations outside the eclipses were similar to those during the plateau phase, eclipses became sharper for $0.8 \leq \phi_{\text{SH}} \leq 1.0$ and a reflection-like effect became prominent.

3.8. *V1504 Cygni*

We report additional superoutburst in 2007 (table 14). Although the data were not abundant, stages B and C can be recognized. The determined periods are in good agreement with the following Kepler observations. The times of maxima derived from Kepler observations discussed in subsection 4.5.1 are presented in table 15.

3.9. *AW Geminorum*

We observed the middle-to-late stage of the 2011 superoutburst. The stage B–C transition was well-recorded (table 16). A comparison of $O - C$ diagrams between different superoutbursts is shown in figure 16.

Table 12. Superhump maxima of HT Cas (2010).

E	max*	error	$O - C^\dagger$	phase ‡	N^\S
0	55504.1036	0.0004	-0.0263	0.72	1374
1	55504.1706	0.0016	-0.0355	0.63	1133
2	55504.2600	0.0006	-0.0223	0.85	668
3	55504.3479	0.0004	-0.0106	0.04	587
4	55504.4346	0.0010	-0.0000	0.22	281
5	55504.5006	0.0003	-0.0101	0.11	188
6	55504.5807	0.0004	-0.0062	0.20	335
7	55504.6576	0.0002	-0.0055	0.24	465
8	55504.7358	0.0002	-0.0035	0.31	386
9	55504.8128	0.0002	-0.0026	0.35	303
10	55504.8899	0.0002	-0.0017	0.40	354
11	55504.9669	0.0001	-0.0008	0.44	1322
12	55505.0420	0.0001	-0.0019	0.46	1490
13	55505.1173	0.0001	-0.0027	0.49	1892
14	55505.1947	0.0001	-0.0015	0.54	2049
15	55505.2696	0.0001	-0.0028	0.55	1326
16	55505.3468	0.0001	-0.0018	0.60	1381
17	55505.4232	0.0001	-0.0015	0.64	569
18	55505.5014	0.0001	0.0006	0.70	406
19	55505.5764	0.0002	-0.0006	0.72	596
20	55505.6538	0.0002	0.0006	0.77	636
21	55505.7306	0.0003	0.0012	0.81	455
22	55505.8062	0.0004	0.0007	0.84	170
23	55505.8805	0.0003	-0.0011	0.85	261
24	55505.9573	0.0002	-0.0006	0.89	530
25	55506.0348	0.0002	0.0009	0.94	1360
26	55506.1157	0.0006	0.0056	0.04	1522
27	55506.1954	0.0003	0.0091	0.12	2008
28	55506.2688	0.0003	0.0063	0.12	1471
29	55506.3440	0.0004	0.0054	0.14	798
30	55506.4167	0.0003	0.0019	0.13	344
31	55506.4922	0.0003	0.0013	0.15	472
32	55506.5716	0.0002	0.0045	0.23	517
33	55506.6468	0.0003	0.0036	0.25	390
34	55506.7220	0.0003	0.0026	0.27	226
35	55506.7981	0.0004	0.0026	0.31	169
36	55506.8741	0.0003	0.0023	0.34	138
37	55506.9508	0.0002	0.0029	0.38	747
38	55507.0267	0.0001	0.0026	0.41	1334
39	55507.1023	0.0001	0.0021	0.44	1960
40	55507.1789	0.0001	0.0026	0.48	1149
41	55507.2528	0.0002	0.0002	0.48	710
42	55507.3294	0.0001	0.0008	0.52	805
43	55507.4056	0.0002	0.0007	0.56	583
44	55507.4835	0.0002	0.0025	0.61	434
45	55507.5611	0.0002	0.0039	0.67	466
46	55507.6365	0.0002	0.0032	0.69	493
47	55507.7141	0.0003	0.0047	0.75	233
48	55507.7915	0.0003	0.0058	0.80	202
49	55507.8659	0.0008	0.0041	0.81	102
50	55507.9428	0.0003	0.0049	0.85	170
51	55508.0197	0.0003	0.0055	0.89	269
52	55508.0963	0.0008	0.0060	0.93	273

*BJD–2400000.

† Against max = 2455504.1300 + 0.076160E.

‡ Orbital phase.

§ Number of points used to determine the maximum.

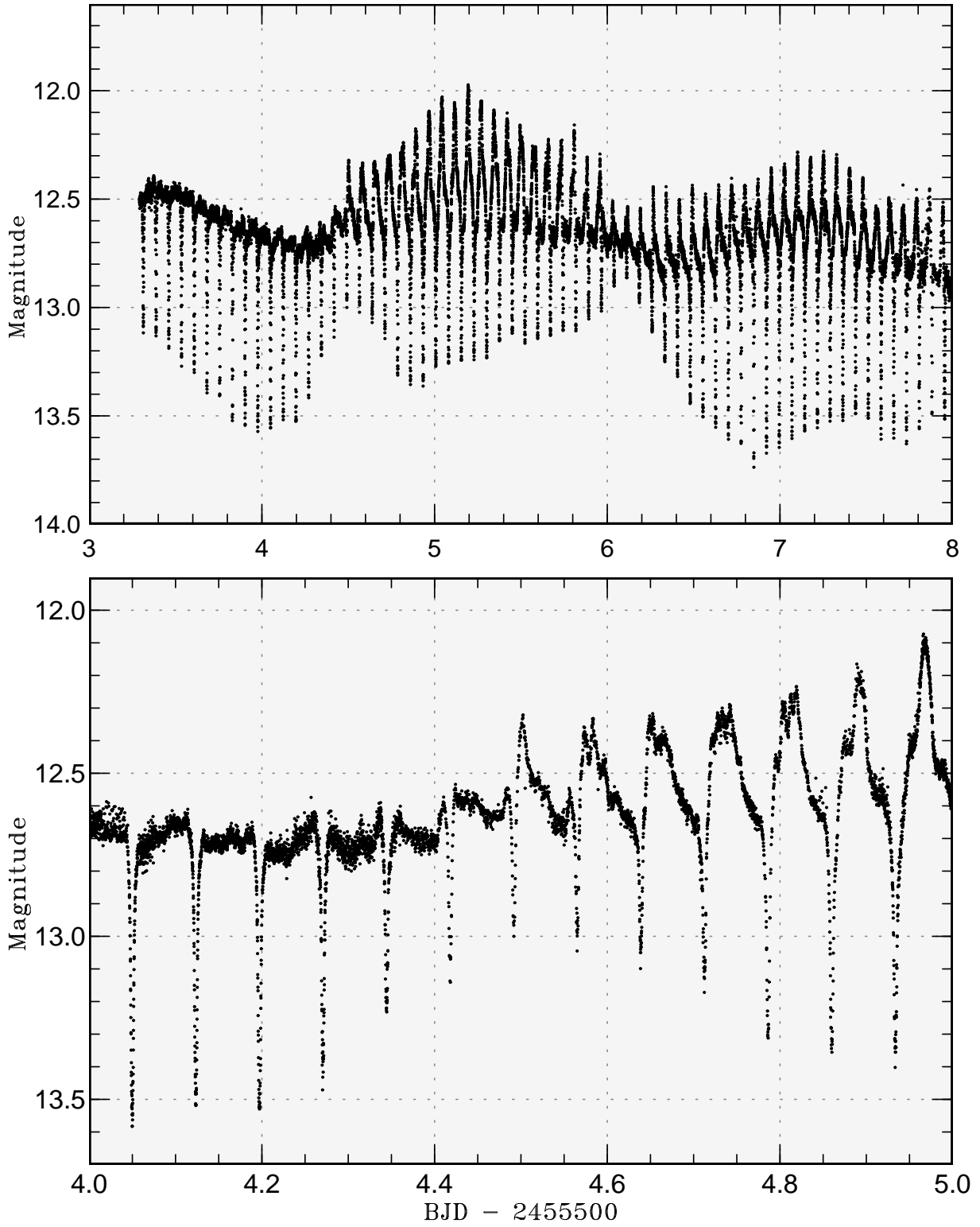


Fig. 9. Superhumps in HT Cas (2010) at the early stage. (Upper): Evolution of superhumps and beat phenomenon. (Lower): Enlargement of the evolutionary phase of superhumps.

Table 12. Superhump maxima of HT Cas (2010) (continued).

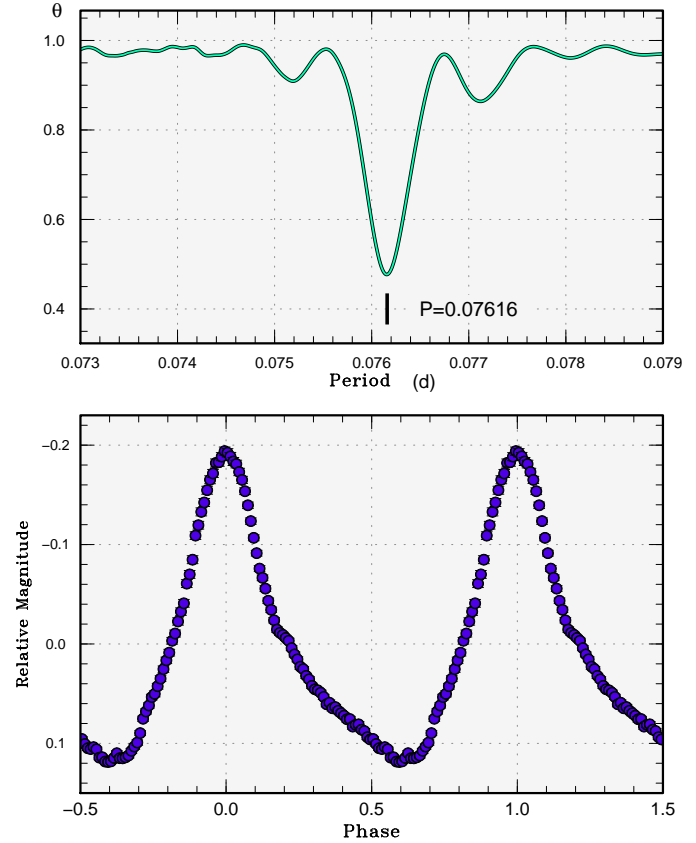
E	max*	error	$O - C^\dagger$	phase‡	N^\S
53	55508.1744	0.0004	0.0079	1.00	238
54	55508.2503	0.0006	0.0077	0.03	359
55	55508.3260	0.0003	0.0072	0.05	541
56	55508.4000	0.0002	0.0050	0.06	535
57	55508.4803	0.0004	0.0092	0.15	528
58	55508.5544	0.0003	0.0071	0.16	634
59	55508.6278	0.0003	0.0044	0.15	504
60	55508.7072	0.0009	0.0076	0.23	134
61	55508.7797	0.0007	0.0039	0.21	123
62	55508.8588	0.0005	0.0069	0.29	252
63	55508.9342	0.0004	0.0062	0.31	406
64	55509.0109	0.0003	0.0067	0.35	379
65	55509.0867	0.0002	0.0063	0.38	393
66	55509.1609	0.0003	0.0044	0.39	305
67	55509.2384	0.0002	0.0057	0.44	458
68	55509.3143	0.0002	0.0054	0.47	410
69	55509.3903	0.0002	0.0053	0.51	462
70	55509.4659	0.0002	0.0047	0.53	259
72	55509.6182	0.0005	0.0047	0.60	44
73	55509.6946	0.0003	0.0050	0.64	174
74	55509.7712	0.0003	0.0054	0.68	196
75	55509.8460	0.0006	0.0040	0.69	100
76	55509.9231	0.0002	0.0050	0.74	787
77	55509.9995	0.0002	0.0052	0.78	963
78	55510.0749	0.0001	0.0045	0.80	1396
79	55510.1502	0.0001	0.0036	0.82	1539
80	55510.2259	0.0003	0.0031	0.85	690
81	55510.2996	0.0005	0.0006	0.85	151
82	55510.3788	0.0005	0.0037	0.93	356
84	55510.5317	0.0005	0.0043	0.00	215
85	55510.6084	0.0003	0.0048	0.05	413
86	55510.6822	0.0004	0.0024	0.05	379
87	55510.7569	0.0005	0.0010	0.06	121
88	55510.8314	0.0006	-0.0006	0.07	117
89	55510.9072	0.0002	-0.0010	0.10	947
90	55510.9844	0.0001	0.0000	0.15	1719
91	55511.0601	0.0001	-0.0005	0.18	1678
92	55511.1369	0.0001	0.0002	0.22	2165
93	55511.2096	0.0001	-0.0032	0.21	2175
94	55511.2865	0.0002	-0.0025	0.25	1316
95	55511.3644	0.0003	-0.0008	0.31	413
96	55511.4395	0.0004	-0.0018	0.33	265
97	55511.5132	0.0004	-0.0043	0.33	221
98	55511.5889	0.0004	-0.0048	0.36	209
99	55511.6654	0.0002	-0.0044	0.40	379
100	55511.7413	0.0003	-0.0046	0.43	286
101	55511.8178	0.0004	-0.0043	0.47	153
102	55511.8963	0.0004	-0.0020	0.53	1033
103	55511.9714	0.0002	-0.0030	0.55	1612
104	55512.0496	0.0002	-0.0010	0.61	1866
105	55512.1239	0.0001	-0.0028	0.62	2033
106	55512.1982	0.0001	-0.0047	0.63	1734
107	55512.2749	0.0002	-0.0042	0.67	505

*BJD-2400000.

†Against max = 2455504.1300 + 0.076160E.

‡Orbital phase.

§Number of points used to determine the maximum.

**Fig. 10.** Superhumps in HT Cas (2010) during the superoutburst plateau. The averaged profile outside eclipses is shown. (Upper): PDM analysis. (Lower): Phase-averaged profile.**Table 12.** Superhump maxima of HT Cas (2010) (continued).

E	max*	error	$O - C^\dagger$	phase‡	N^\S
108	55512.3512	0.0003	-0.0040	0.71	427
109	55512.4261	0.0002	-0.0053	0.73	275
113	55512.7334	0.0009	-0.0026	0.90	37
114	55512.8057	0.0008	-0.0065	0.88	54
115	55512.8824	0.0003	-0.0059	0.92	470
116	55512.9568	0.0005	-0.0077	0.93	802
117	55513.0338	0.0012	-0.0069	0.98	582
118	55513.1057	0.0013	-0.0112	0.95	425
124	55513.5610	0.0022	-0.0128	0.14	130
125	55513.6407	0.0007	-0.0092	0.22	163
126	55513.7174	0.0007	-0.0087	0.26	94

*BJD-2400000.

†Against max = 2455504.1300 + 0.076160E.

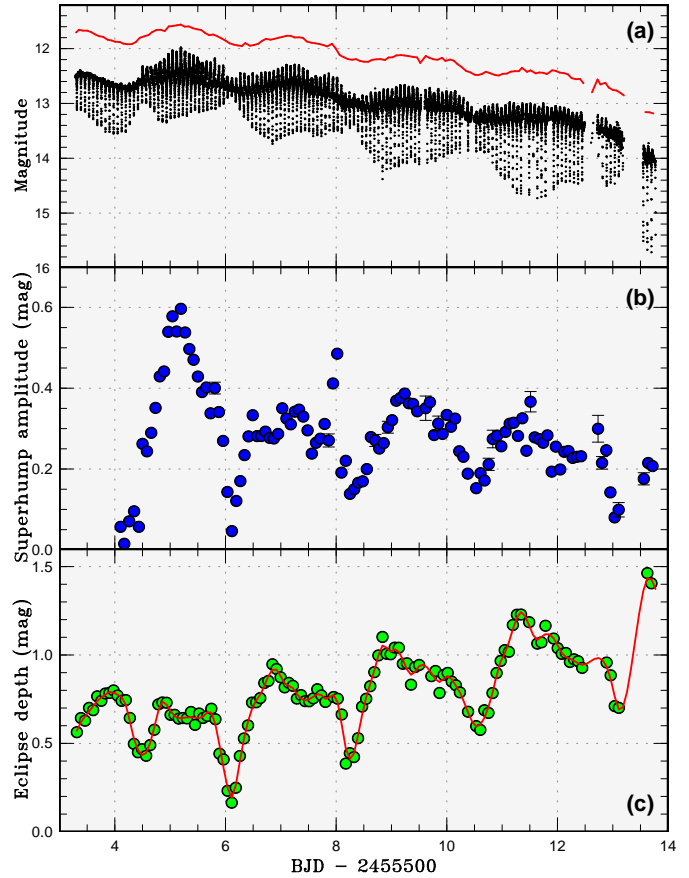
‡Orbital phase.

§Number of points used to determine the maximum.

Table 13. Superhump maxima of HT Cas (2010) (post-superoutburst).

E	max*	error	$O - C^\dagger$	N^\ddagger
0	55514.2505	0.0009	-0.0074	51
1	55514.3298	0.0012	-0.0036	92
2	55514.4019	0.0011	-0.0070	138
5	55514.6296	0.0016	-0.0058	73
10	55515.0057	0.0008	-0.0071	116
11	55515.0804	0.0011	-0.0080	235
12	55515.1653	0.0006	0.0014	511
13	55515.2314	0.0037	-0.0080	235
14	55515.3072	0.0011	-0.0077	375
15	55515.3817	0.0011	-0.0087	326
16	55515.4665	0.0015	0.0007	396
17	55515.5356	0.0007	-0.0057	303
18	55515.6051	0.0017	-0.0118	313
19	55515.7035	0.0011	0.0112	285
22	55515.9092	0.0013	-0.0096	288
23	55515.9823	0.0010	-0.0120	576
24	55516.0672	0.0012	-0.0025	691
25	55516.1419	0.0022	-0.0034	508
26	55516.2248	0.0008	0.0041	743
28	55516.3773	0.0014	0.0055	158
30	55516.5220	0.0027	-0.0008	101
38	55517.1286	0.0003	0.0019	468
39	55517.2157	0.0014	0.0135	216
50	55518.0345	0.0008	0.0019	585
56	55518.4799	0.0015	-0.0056	52
61	55518.8810	0.0011	0.0180	87
62	55518.9501	0.0005	0.0116	50
64	55519.1068	0.0004	0.0173	907
65	55519.1772	0.0003	0.0122	1225
67	55519.3260	0.0017	0.0100	122
70	55519.5551	0.0010	0.0126	30
71	55519.6294	0.0043	0.0114	33
72	55519.7060	0.0092	0.0125	19
73	55519.7864	0.0013	0.0175	31
81	55520.3829	0.0016	0.0100	60
85	55520.6823	0.0025	0.0074	69
89	55520.9690	0.0012	-0.0078	226
92	55521.2005	0.0027	-0.0028	406
93	55521.2736	0.0017	-0.0052	309
94	55521.3474	0.0009	-0.0069	102
131	55524.1552	0.0047	0.0077	117
141	55524.8969	0.0013	-0.0056	193
142	55524.9816	0.0018	0.0037	322
145	55525.1885	0.0019	-0.0159	473
165	55526.7035	0.0020	-0.0108	26
169	55527.0147	0.0031	-0.0016	212
170	55527.0888	0.0021	-0.0030	206
171	55527.1650	0.0010	-0.0023	507
172	55527.2378	0.0087	-0.0050	290
177	55527.6099	0.0035	-0.0104	84
178	55527.6894	0.0016	-0.0063	118
179	55527.7626	0.0031	-0.0087	26
183	55528.0823	0.0011	0.0091	394
214	55530.4193	0.0016	0.0058	161

*BJD-2400000.

 † Against max = 245514.2579 + 0.075493E. ‡ Number of points used to determine the maximum.**Fig. 11.** Beat phenomenon in HT Cas (2010). (a) Light curve. The solid curve represent averaged magnitudes outside eclipses (offset by 0.8 mag). (b) Amplitude of superhumps. (c) Depth of eclipses. The curve represent the globally smoothed depths of eclipses used in subtracting the orbital variation.

3.10. V844 Herculis

We reported on the 2010 April–May superoutburst of this object in Kato et al. (2010). The object underwent another superoutburst in 2010 October–November. The interval since the April–May superoutburst was only 179 d. The current state with frequent superoutbursts started in 2009, in contrast to earlier state with relatively infrequent superoutbursts (Kato, Uemura 2000; Oizumi et al. 2007).

Since the present observations were obtained at high airmasses, we corrected observations by using a second-order atmospheric extinction whose coefficients were experimentally determined. The times of superhump maxima are listed in table 17. Despite rather unfavorable seasonal conditions, we have succeeded in obtaining good timing data of superhumps. The $O - C$ diagram indicates the presence of a stage B–C transition at late epochs.

Figure 17 illustrates a comparison of $O - C$ diagrams in different superoutbursts. It is noteworthy that the stage B–C transition in this small-scale (faint and short) superoutburst occurred much earlier than in past large-

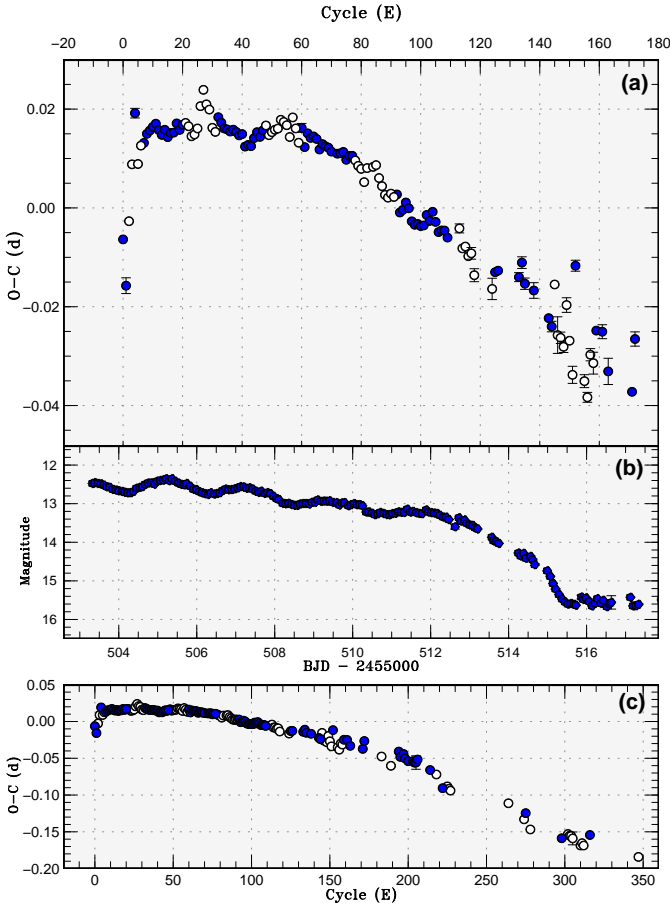


Fig. 12. $O-C$ diagram of superhumps in HT Cas (2010). (a) $O-C$ diagram indicating stage A–C evolution. Open circle indicate humps within 0.2 orbital phase of eclipses. Filled circles are humps outside the phase of eclipses. We used a period of 0.07635 d for calculating the $O-C$'s. (b) Light curve. Each point represents an orbital average of magnitudes outside the eclipses. Strong beat modulations are present. (c) $O-C$ diagram of the entire observation. Superhumps with a slightly shorter period persisted even after panel (a). There was no phase jump as expected for “traditional” late superhumps.

scale superoutbursts. The period of stage B superhumps appears to be noticeably longer than in other superoutbursts. Although this may have been a result of the lack of the early stage observations, this result suggests that the evolution of small-scale superoutbursts can be much faster than in large-scale ones.

3.11. *MM Hydrae*

In Kato et al. (2009a), we reported on rather fragmentary observations of MM Hya during the 1998 and 2001 superoutbursts. Since MM Hya was initially suggested to be related to WZ Sge-type dwarf novae (Misselt, Shafter 1995), more detailed observations were needed to examine this possibility. There has been no report on measurement of P_{dot} for stage B superhumps, which is expected to be useful in characterizing the object (cf. Kato et al. 2009a,

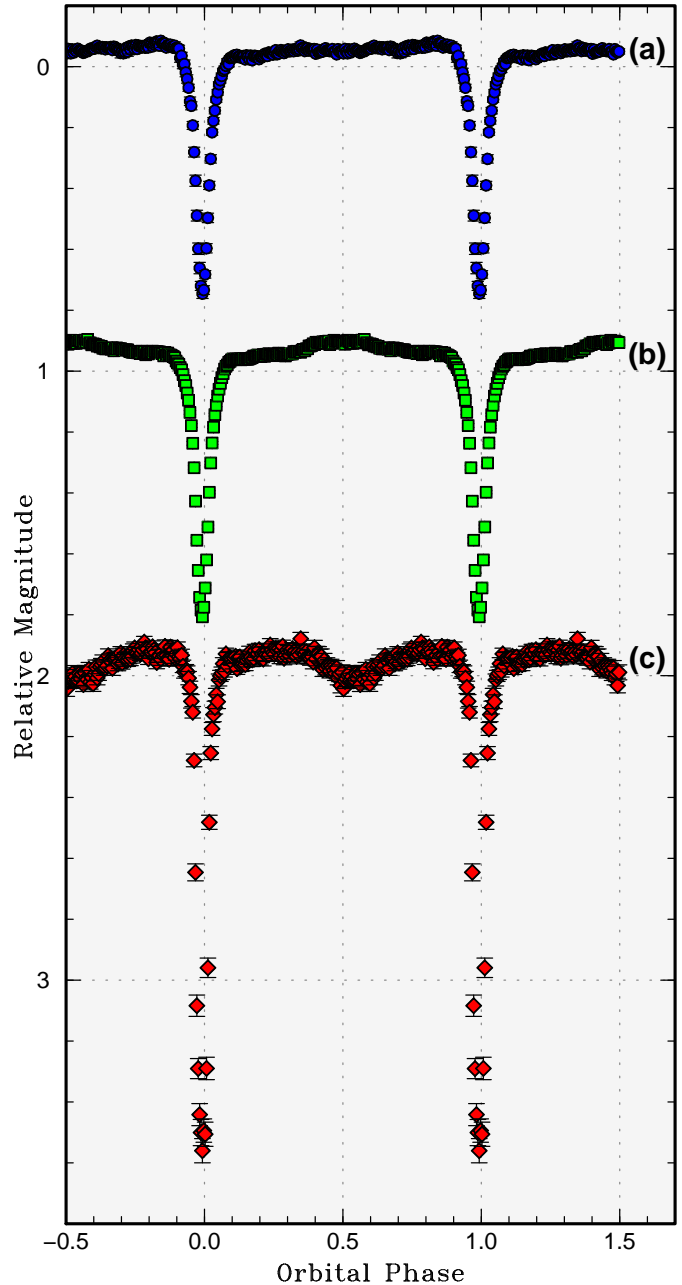


Fig. 13. Variation of orbital profile HT Cas (2010). The phases were defined against equation 1. (a) Before superhumps appeared. Although likely orbital humps were present, no indication of early superhump was present. (b) During the superoutburst plateau. There was a slight bump around phase 0.5 (see text for details). (c) Post-superoutburst. Eclipses became deeper and double-wave modulations were present.

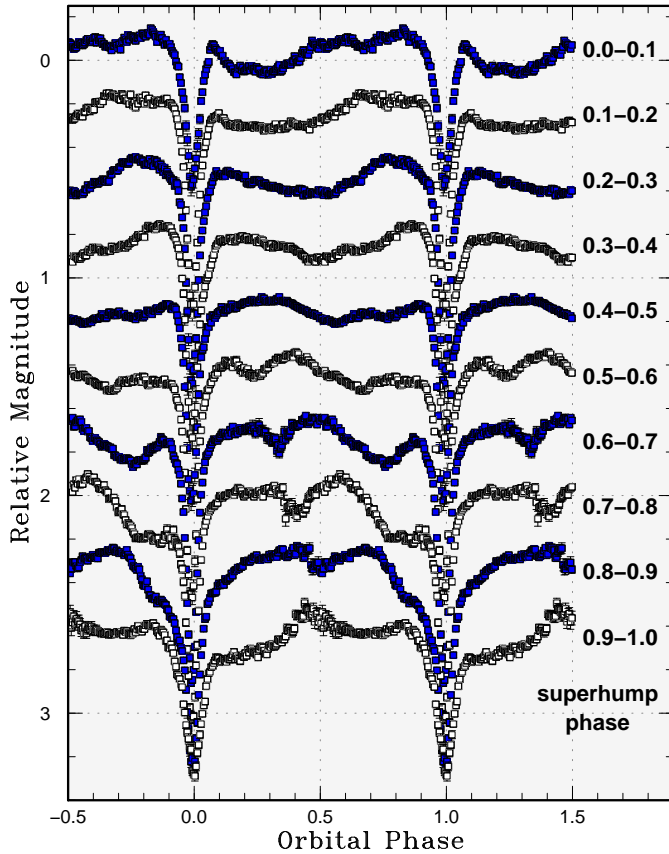


Fig. 14. Dependence of orbital profile HT Cas on superhump phase during the plateau phase of the superoutburst (2010). The data approximately covered three beat periods. There is no strong indication of persistent orbital humps nor reflection effect. The profiles outside the eclipses are highly dependent on superhump phase and highly structured.

subsection 5.3).

The 2011 superoutburst was fortunately detected during its rising stage (R. Stubbings, vsnet-alert 13113). This was the first recorded superoutburst since the last one in 2006 March. Early observations detected long-period superhumps (vsnet-alert 13130, 13131), rather than early superhumps in WZ Sge-type dwarf novae, which further developed into full superhumps within 1 d (vsnet-alert 12132).

The times of superhump maxima are listed in table 18. Due to a short gap in observation between the first and second nights, the cycle count is somewhat ambiguous in the earliest phase. We identified the cycle numbers given in the table since observations on the first night apparently recorded the growing stage (stage A) of superhumps and there must have been a large period change before the system started showing fully developed stage B superhumps. The adopted cycle counts gives a mean period of 0.0629(2) d for $E \leq 16$, which is close to the period [0.0617(3) d] obtained from the observations on the first night. The fractional excess (7 %) of the period of stage A superhumps to that of stage B superhumps is exception-

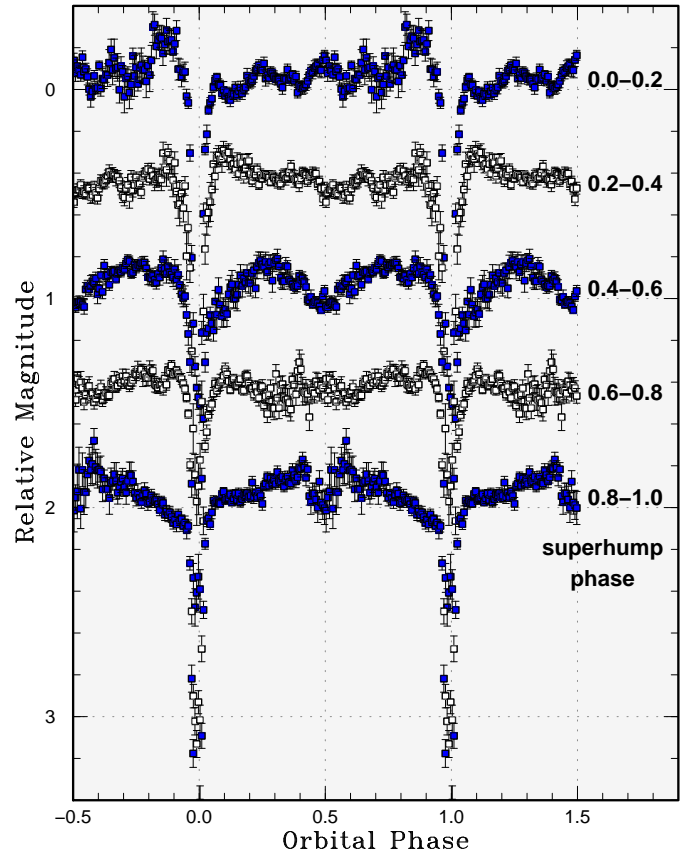


Fig. 15. Dependence of orbital profile HT Cas on superhump phase after the rapid fading of the superoutburst (2010). The features outside the eclipses have a similar tendency to figure 14.

Table 14. Superhump maxima of V1504 Cyg (2007).

E	max*	error	$O - C^\dagger$	N^\ddagger
0	54324.4787	0.0018	-0.0061	13
27	54326.4283	0.0013	-0.0019	29
41	54327.4339	0.0026	-0.0049	32
42	54327.5122	0.0016	0.0013	33
55	54328.4608	0.0039	0.0133	19
84	54330.5368	0.0017	-0.0002	15
96	54331.4028	0.0016	0.0013	18
97	54331.4754	0.0039	0.0018	19
98	54331.5491	0.0023	0.0034	18
110	54332.4129	0.0020	0.0026	13
111	54332.4855	0.0032	0.0032	13
112	54332.5530	0.0018	-0.0014	11
124	54333.4125	0.0053	-0.0064	13
125	54333.4911	0.0020	0.0000	12
126	54333.5634	0.0025	0.0004	11
139	54334.4933	0.0022	-0.0064	12

*BJD-2400000.

† Against max = 2454324.4848 + 0.072050 E .

‡ Number of points used to determine the maximum.

Table 15. Superhump maxima of V1504 Cyg (2009b).

E	max*	error	$O - C^\dagger$	N^\ddagger
0	55076.2646	0.0009	-0.0344	84
1	55076.3457	0.0014	-0.0254	84
2	55076.4227	0.0008	-0.0205	84
3	55076.4962	0.0004	-0.0192	84
4	55076.5663	0.0006	-0.0212	85
5	55076.6365	0.0003	-0.0232	85
6	55076.7075	0.0004	-0.0243	85
7	55076.7779	0.0006	-0.0260	85
8	55076.8514	0.0004	-0.0247	85
9	55076.9234	0.0005	-0.0248	84
10	55077.0023	0.0003	-0.0180	85
11	55077.0790	0.0004	-0.0135	85
12	55077.1528	0.0004	-0.0119	85
13	55077.2287	0.0003	-0.0081	84
14	55077.3023	0.0003	-0.0066	84
15	55077.3763	0.0002	-0.0048	85
16	55077.4488	0.0002	-0.0045	85
17	55077.5202	0.0002	-0.0052	84
18	55077.5922	0.0001	-0.0053	85
19	55077.6682	0.0002	-0.0014	85
20	55077.7415	0.0001	-0.0003	76
21	55077.8164	0.0002	0.0025	85
22	55077.8884	0.0001	0.0024	85
23	55077.9596	0.0001	0.0014	84
24	55078.0322	0.0001	0.0019	85
25	55078.1047	0.0002	0.0022	85
26	55078.1782	0.0002	0.0036	85
27	55078.2507	0.0002	0.0039	84
28	55078.3223	0.0002	0.0034	85
29	55078.3945	0.0003	0.0034	84
30	55078.4676	0.0002	0.0044	85
31	55078.5398	0.0002	0.0045	84
32	55078.6141	0.0002	0.0066	85
33	55078.6869	0.0003	0.0072	85
34	55078.7576	0.0002	0.0059	85
35	55078.8319	0.0002	0.0080	85
36	55078.9021	0.0003	0.0061	85
37	55078.9748	0.0003	0.0066	85
38	55079.0471	0.0003	0.0068	84
39	55079.1190	0.0003	0.0066	85
41	55079.2642	0.0003	0.0074	85
42	55079.3363	0.0002	0.0074	85
43	55079.4075	0.0004	0.0065	84
44	55079.4812	0.0003	0.0080	85
45	55079.5533	0.0003	0.0080	84
46	55079.6251	0.0002	0.0076	85
47	55079.6949	0.0003	0.0053	84
48	55079.7658	0.0003	0.0041	85
49	55079.8395	0.0004	0.0056	84
50	55079.9105	0.0004	0.0045	85
51	55079.9825	0.0003	0.0043	85

*BJD-2400000.

†Against max = 2455076.2990 + 0.072141*E*.

‡Number of points used to determine the maximum.

Table 15. Superhump maxima of V1504 Cyg (2009b) (continued).

E	max*	error	$O - C^\dagger$	N^\ddagger
52	55080.0552	0.0004	0.0049	85
53	55080.1261	0.0004	0.0036	85
54	55080.1989	0.0003	0.0043	85
55	55080.2704	0.0005	0.0037	84
56	55080.3446	0.0005	0.0058	84
57	55080.4193	0.0005	0.0083	84
58	55080.4909	0.0003	0.0078	85
59	55080.5613	0.0004	0.0060	84
60	55080.6338	0.0004	0.0064	85
61	55080.7065	0.0003	0.0069	74
62	55080.7780	0.0003	0.0063	85
63	55080.8496	0.0003	0.0058	85
64	55080.9221	0.0004	0.0061	85
65	55080.9940	0.0003	0.0059	85
66	55081.0665	0.0003	0.0062	84
67	55081.1401	0.0003	0.0077	84
68	55081.2115	0.0003	0.0070	84
69	55081.2852	0.0004	0.0085	84
70	55081.3578	0.0005	0.0089	85
71	55081.4287	0.0003	0.0077	84
72	55081.5004	0.0003	0.0073	85
73	55081.5740	0.0003	0.0087	85
74	55081.6460	0.0002	0.0086	84
75	55081.7172	0.0003	0.0077	85
76	55081.7899	0.0003	0.0082	84
77	55081.8615	0.0002	0.0077	84
78	55081.9332	0.0003	0.0073	85
79	55082.0055	0.0003	0.0074	85
80	55082.0805	0.0003	0.0102	84
81	55082.1528	0.0004	0.0104	85
82	55082.2246	0.0002	0.0101	85
83	55082.2978	0.0004	0.0112	85
84	55082.3672	0.0003	0.0084	85
85	55082.4393	0.0003	0.0083	85
86	55082.5108	0.0003	0.0077	85
87	55082.5837	0.0003	0.0085	85
88	55082.6554	0.0003	0.0080	85
89	55082.7286	0.0004	0.0091	84
90	55082.7989	0.0003	0.0073	85
91	55082.8708	0.0003	0.0070	84
92	55082.9431	0.0003	0.0072	84
93	55083.0154	0.0005	0.0073	85
94	55083.0893	0.0004	0.0091	85
95	55083.1593	0.0004	0.0069	85
96	55083.2323	0.0004	0.0078	85
97	55083.3031	0.0003	0.0064	84
98	55083.3751	0.0004	0.0063	85
99	55083.4482	0.0003	0.0073	85
100	55083.5177	0.0003	0.0047	85

*BJD-2400000.

†Against max = 2455076.2990 + 0.072141*E*.

‡Number of points used to determine the maximum.

Table 15. Superhump maxima of V1504 Cyg (2009b) (continued).

E	max*	error	$O - C^\dagger$	N^\ddagger
101	55083.5903	0.0003	0.0051	85
102	55083.6613	0.0003	0.0039	74
103	55083.7337	0.0005	0.0042	84
104	55083.8059	0.0004	0.0043	84
105	55083.8770	0.0003	0.0032	84
106	55083.9501	0.0005	0.0042	85
107	55084.0222	0.0004	0.0041	85
108	55084.0949	0.0004	0.0047	85
109	55084.1676	0.0004	0.0053	85
110	55084.2378	0.0003	0.0033	85
111	55084.3083	0.0003	0.0017	84
112	55084.3809	0.0004	0.0021	85
113	55084.4522	0.0003	0.0013	85
114	55084.5230	0.0003	0.0000	85
115	55084.5968	0.0003	0.0016	85
116	55084.6686	0.0004	0.0013	85
117	55084.7415	0.0004	0.0021	84
118	55084.8104	0.0003	-0.0012	84
119	55084.8862	0.0004	0.0024	84
120	55084.9563	0.0004	0.0004	85
121	55085.0291	0.0003	0.0011	85
122	55085.1008	0.0004	0.0006	85
123	55085.1703	0.0004	-0.0020	85
124	55085.2432	0.0004	-0.0013	84
125	55085.3143	0.0004	-0.0023	85
126	55085.3864	0.0003	-0.0024	85
127	55085.4591	0.0004	-0.0018	85
128	55085.5303	0.0004	-0.0027	85
129	55085.6038	0.0003	-0.0014	85
130	55085.6746	0.0004	-0.0027	85
131	55085.7459	0.0004	-0.0035	85
132	55085.8191	0.0004	-0.0025	85
133	55085.8938	0.0003	0.0001	85
134	55085.9637	0.0004	-0.0021	85
135	55086.0351	0.0004	-0.0029	85
136	55086.1051	0.0004	-0.0050	85
137	55086.1790	0.0004	-0.0033	85
138	55086.2495	0.0003	-0.0049	85
139	55086.3237	0.0003	-0.0028	84
140	55086.3943	0.0003	-0.0044	84
141	55086.4671	0.0003	-0.0037	85
142	55086.5397	0.0003	-0.0033	84
143	55086.6096	0.0004	-0.0055	84
144	55086.6818	0.0004	-0.0054	74
145	55086.7560	0.0003	-0.0034	85
146	55086.8282	0.0005	-0.0034	84
147	55086.8996	0.0004	-0.0041	85
148	55086.9711	0.0004	-0.0047	84
149	55087.0413	0.0005	-0.0066	85

*BJD-2400000.

 \dagger Against max = 2455076.2990 + 0.072141*E*. \ddagger Number of points used to determine the maximum.**Table 15.** Superhump maxima of V1504 Cyg (2009b) (continued).

E	max*	error	$O - C^\dagger$	N^\ddagger
150	55087.1146	0.0003	-0.0055	85
151	55087.1876	0.0004	-0.0046	84
152	55087.2567	0.0003	-0.0077	85
153	55087.3278	0.0004	-0.0087	85
154	55087.3972	0.0005	-0.0115	85
155	55087.4706	0.0006	-0.0102	84
156	55087.5428	0.0008	-0.0102	85
157	55087.6146	0.0004	-0.0105	85
158	55087.6897	0.0005	-0.0075	85
159	55087.7620	0.0010	-0.0073	84
160	55087.8269	0.0005	-0.0146	85
161	55087.9015	0.0005	-0.0122	85
162	55087.9788	0.0009	-0.0070	85
163	55088.0412	0.0012	-0.0168	85
164	55088.1033	0.0012	-0.0268	84

*BJD-2400000.

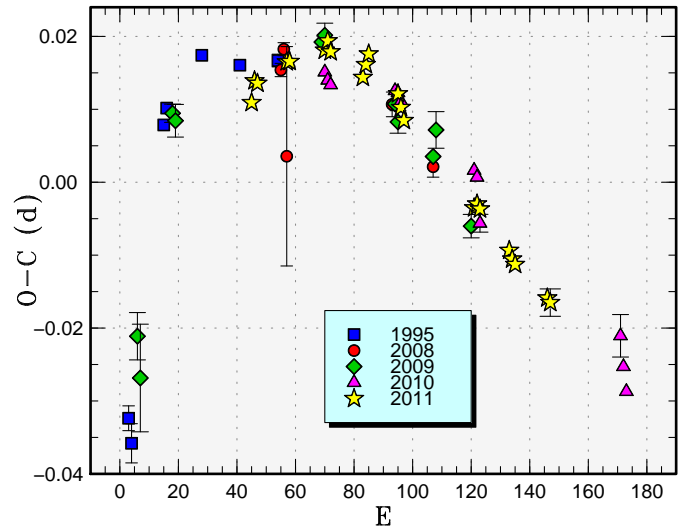
 \dagger Against max = 2455076.2990 + 0.072141*E*. \ddagger Number of points used to determine the maximum.**Fig. 16.** Comparison of $O - C$ diagrams of AW Gem between different superoutbursts. A period of 0.07915 d was used to draw this figure. Approximate cycle counts (E) after the start of the superoutburst were used. Since the start of 2008, 2010 and 2011 superoutburst were poorly constrained, we shifted the $O - C$ diagrams to best match other other superoutbursts.

Table 16. Superhump maxima of AW Gem (2011).

E	max*	error	$O - C^\dagger$	N^\ddagger
0	55571.1836	0.0002	-0.0112	112
1	55571.2657	0.0002	-0.0079	111
2	55571.3445	0.0005	-0.0079	83
12	55572.1390	0.0003	-0.0017	108
13	55572.2182	0.0003	-0.0013	112
25	55573.1695	0.0003	0.0042	108
26	55573.2500	0.0003	0.0058	111
27	55573.3276	0.0005	0.0046	84
38	55574.1947	0.0003	0.0048	165
39	55574.2757	0.0003	0.0068	168
40	55574.3563	0.0006	0.0086	84
50	55575.1423	0.0003	0.0065	112
51	55575.2196	0.0003	0.0049	112
52	55575.2969	0.0004	0.0035	111
76	55577.1845	0.0006	-0.0006	115
77	55577.2642	0.0006	0.0003	114
78	55577.3427	0.0013	-0.0001	77
88	55578.1285	0.0005	-0.0025	84
89	55578.2065	0.0007	-0.0033	87
90	55578.2849	0.0006	-0.0037	87
101	55579.1509	0.0013	-0.0047	88
102	55579.2295	0.0019	-0.0050	87

*BJD-2400000.

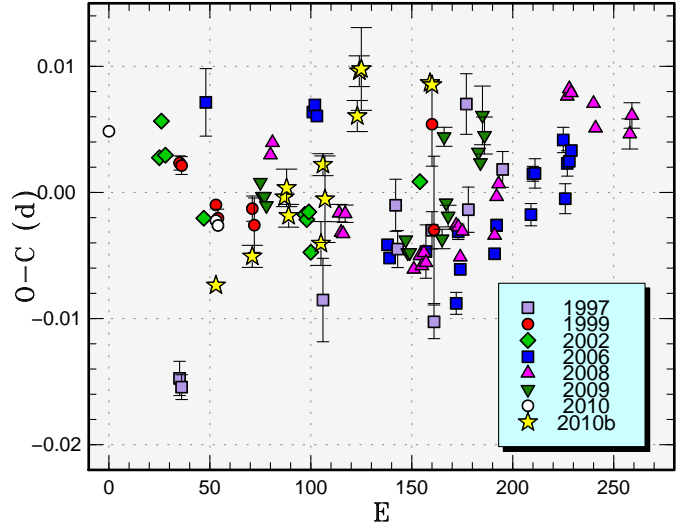
 † Against max = 245571.1948 + 0.078820*E*. ‡ Number of points used to determine the maximum.

Fig. 17. Comparison of $O - C$ diagrams of V844 Her between different superoutbursts. A period of 0.05590 d was used to draw this figure. Approximate cycle counts (E) after the start of the superoutburst were used. Since the start of the 2009 superoutburst was not well constrained, we shifted the $O - C$ diagram to best match the others. The initial superhump maximum of the 2010 superoutburst may have a one-cycle ambiguity in the cycle count, and the large $O - C$ may have been a result of the rapidly evolving stage A superhumps. There was only 2 d gap of observation before the initial detection of the 2010b superoutburst, and the cycle counts drawn in this figure has a ambiguity less than ~ 35 . The stage B-C transition in this small-scale superoutburst occurred much earlier than in past large-scale superoutbursts.

Table 17. Superhump maxima of V844 Her (2010 Oct.).

E	max*	error	$O - C^\dagger$	N^\ddagger
0	55495.2921	0.0005	-0.0003	38
18	55496.3006	0.0009	-0.0010	60
34	55497.1996	0.0008	0.0010	112
35	55497.2563	0.0015	0.0016	123
36	55497.3100	0.0009	-0.0008	124
52	55498.2022	0.0017	-0.0056	120
53	55498.2643	0.0009	0.0004	123
54	55498.3175	0.0034	-0.0025	92
70	55499.2185	0.0012	0.0015	119
71	55499.2779	0.0012	0.0049	121
72	55499.3340	0.0033	0.0049	57
106	55501.2335	0.0007	-0.0019	126
107	55501.2892	0.0008	-0.0022	122

*BJD-2400000.

 † Against max = 2455495.2923 + 0.056067*E*. ‡ Number of points used to determine the maximum.

ally large (cf. Kato et al. 2009a, subsection 3.7). If we assume an additional cycle count between the first and second nights, we get a period of 0.0590(4) d on these nights. Although this value is close to that of stage B superhumps, the $O - C$ variations within the first night become inconsistent with the later evolution. We therefore favor the former assumption of the cycle counts.

The resultant P_{dot} for stage B superhumps was $+7.2(0.9) \times 10^{-5}$, which also supports the classification as an usual SU UMa-type dwarf nova with a short P_{orb} .

3.12. V406 Hydrae

V406 Hya is an AM CVn-type CV (for a recent review, see Solheim 2010) which was initially discovered as a possible supernova (Woudt, Warner 2003 and references therein). Nogami et al. (2004) reported on the unusual behavior of its 2004 superoutburst. Roelofs et al. (2006) further reported phase-resolved spectroscopy and obtained an orbital period of 2027.8(5) s = 0.023470(6) d. A bright (~ 15.0 mag) outburst of this object in 2010 December was detected by CRTS. Superhumps with amplitudes of 0.065 mag were detected (vsnet-alert 12483). The times of superhump maxima are listed in table 19. The mean period of superhumps was 0.02365(5) d (PDM analysis), which is in agreement with previous measurements [0.023628(4) d, Woudt, Warner (2003); 0.02357(4)

Table 18. Superhump maxima of MM Hya (2011).

E	max*	error	$O - C^\dagger$	N^\ddagger
0	55660.0258	0.0018	-0.0393	113
1	55660.0952	0.0011	-0.0291	113
2	55660.1546	0.0006	-0.0289	112
3	55660.2149	0.0012	-0.0277	59
16	55661.0355	0.0003	0.0237	76
17	55661.0944	0.0002	0.0235	113
18	55661.1528	0.0002	0.0228	106
22	55661.3880	0.0004	0.0213	58
32	55661.9756	0.0013	0.0173	47
33	55662.0327	0.0014	0.0151	64
39	55662.3856	0.0005	0.0131	60
49	55662.9702	0.0012	0.0060	47
50	55663.0342	0.0010	0.0108	118
51	55663.0898	0.0009	0.0073	125
66	55663.9713	0.0008	0.0013	159
67	55664.0301	0.0008	0.0009	181
68	55664.0915	0.0022	0.0032	67
83	55664.9723	0.0015	-0.0035	101
84	55665.0337	0.0007	-0.0012	108
85	55665.0925	0.0008	-0.0016	113
86	55665.1519	0.0010	-0.0014	110
117	55666.9788	0.0010	-0.0086	113
118	55667.0397	0.0010	-0.0069	106
119	55667.0972	0.0014	-0.0085	113
120	55667.1553	0.0010	-0.0096	87

*BJD-2400000.

 † Against max = 2455660.0651 + 0.059165 E . ‡ Number of points used to determine the maximum.

d, Nogami et al. (2004)].

The known outbursts of this object are listed in table 20. Based on magnitudes and durations, all known outbursts appear to be superoutbursts, and the intervals between superoutbursts are apparently longer than the one (60 d) in KL Dra (Ramsay et al. 2010) or ~ 100 d in CP Eri based on CRTS data (vsnet-alert 11504)⁴.

3.13. V344 Lyrae

The data discussed in subsection 4.5.3 are presented. The object showed prominent double peaks during the late course of the superoutbursts. We therefore used phases -0.2 to 0.2 (instead of -0.4 to 0.4 , cf. Kato et al. 2009a) for fitting the template superhump profile in order to separate individual peaks. The times of maxima of main peaks are listed in table 21. The times of secondary maxima, which smoothly evolved into persisting superhumps during the next normal outburst and subsequent interval of quiescence, are listed in table 22. The object underwent another superoutburst in 2009 November–December. The data for this superoutburst are listed in tables 23 and 24.

Table 19. Superhump maxima of V406 Hya (2010).

E	max*	error	$O - C^\dagger$	N^\ddagger
0	55539.5314	0.0007	-0.0004	34
1	55539.5564	0.0004	0.0008	49
2	55539.5800	0.0005	0.0005	47
3	55539.6026	0.0006	-0.0007	47
4	55539.6267	0.0004	-0.0004	48
26	55540.1552	0.0038	0.0042	62
28	55540.1955	0.0011	-0.0032	43
29	55540.2201	0.0011	-0.0024	72
30	55540.2405	0.0013	-0.0059	87
31	55540.2776	0.0070	0.0074	50

*BJD-2400000.

 † Against max = 2455539.5318 + 0.023817 E . ‡ Number of points used to determine the maximum.**Table 20.** List of known outbursts of V406 Hya.

Month	max*	magnitude	source
2003 2	52677	17.8	Wood-Vasey et al. (2003)
2004 5	53143	14.7–15.2	Nogami et al. (2004)
2005 4	53465	15.2	CRTS
2006 11	54057	17.5	CRTS
2008 4	54565	15.3	CRTS
2009 12	55181	15.8	CRTS
2010 12	55536	15.0	CRTS

*JD-2400000.

3.14. V1195 Ophiuchi

Very little has been known for this dwarf nova. The object was originally selected as a recurrent nova or a Mira-type star (Plaut 1968) based on two detections at a photographic magnitude of 16.2 on 1956 June 12 and 15.8 on 1959 April 29. Duerbeck (1987) favored the latter classification based on its red color. P. Schmeer, however, noted that this object is a dwarf nova and reported an outburst on 1999 June 16 at an unfiltered CCD magnitude of 16.4 (vsnet-alert 3086). J. Kemp conducted multicolor and time-resolved photometry upon this information and reported the detection of superhumps with an amplitude ~ 0.20 mag and a period of ~ 0.068 d (vsnet-alert 3087). There have been three other known outburst detections (all observations gave unfiltered CCD magnitudes): 2004 February 8 (16.1 mag, B. Monard), 2004 September 2 (17.3, B. Monard) and 2005 April 17 (16.3, P. Schmeer).

The object was again detected in outburst by M. Simonsen at a magnitude of $V=17.54$ on 2011 April 3.390 and $V=16.00$ on April 9.374. Subsequent observations indeed detected superhumps (vsnet-alert 13144, 13151). The times of superhump maxima are listed in table 25. Since the first observations were obtained 9 d after the recorded maximum, the observation likely recorded only stage C superhumps.

⁴ <<http://nessi.cacr.caltech.edu/catalina/20090925/9092500901741>>

Table 21. Superhump maxima of V344 Lyr (2009).

E	max*	error	$O - C^\dagger$	N^\ddagger
0	55057.6071	0.0008	-0.0327	54
1	55057.7010	0.0024	-0.0303	53
2	55057.7969	0.0011	-0.0258	54
3	55057.8860	0.0006	-0.0283	54
4	55057.9779	0.0008	-0.0279	54
5	55058.0721	0.0003	-0.0253	53
6	55058.1630	0.0002	-0.0259	54
7	55058.2559	0.0002	-0.0245	54
8	55058.3535	0.0001	-0.0184	54
9	55058.4484	0.0001	-0.0150	54
10	55058.5440	0.0001	-0.0109	54
11	55058.6380	0.0001	-0.0084	53
12	55058.7317	0.0001	-0.0063	54
13	55058.8239	0.0001	-0.0056	54
14	55058.9165	0.0001	-0.0046	53
15	55059.0096	0.0001	-0.0029	54
16	55059.1027	0.0001	-0.0013	53
17	55059.1942	0.0002	-0.0014	54
18	55059.2874	0.0001	0.0003	54
19	55059.3804	0.0001	0.0017	54
20	55059.4729	0.0001	0.0028	54
21	55059.5640	0.0001	0.0023	54
22	55059.6546	0.0001	0.0014	54
23	55059.7477	0.0001	0.0030	54
24	55059.8402	0.0001	0.0040	43
25	55059.9316	0.0001	0.0038	53
26	55060.0257	0.0001	0.0064	54
27	55060.1165	0.0001	0.0057	54
28	55060.2093	0.0002	0.0070	54
29	55060.3006	0.0002	0.0068	53
30	55060.3914	0.0001	0.0060	54
31	55060.4833	0.0002	0.0064	54
32	55060.5753	0.0002	0.0069	54
33	55060.6675	0.0002	0.0076	54
34	55060.7590	0.0002	0.0076	54
35	55060.8498	0.0001	0.0069	54
36	55060.9410	0.0002	0.0065	54
37	55061.0329	0.0002	0.0069	53
38	55061.1249	0.0002	0.0074	54
39	55061.2169	0.0002	0.0079	54
40	55061.3078	0.0001	0.0072	54
41	55061.3998	0.0002	0.0077	53
42	55061.4918	0.0002	0.0082	53
43	55061.5827	0.0003	0.0075	54
44	55061.6742	0.0002	0.0075	54
45	55061.7652	0.0003	0.0070	54
46	55061.8574	0.0003	0.0076	54
47	55061.9487	0.0002	0.0075	54
48	55062.0405	0.0002	0.0077	54
49	55062.1319	0.0003	0.0076	53
50	55062.2227	0.0004	0.0069	54
51	55062.3126	0.0007	0.0053	54
52	55062.4076	0.0002	0.0087	54
53	55062.4980	0.0003	0.0076	54

*BJD-2400000.

†Against max = 2455057.6397 + 0.091522*E*.

‡Number of points used to determine the maximum.

Table 21. Superhump maxima of V344 Lyr (2009) (continued).

E	max*	error	$O - C^\dagger$	N^\ddagger
54	55062.5902	0.0003	0.0083	54
55	55062.6838	0.0002	0.0104	54
56	55062.7741	0.0004	0.0092	54
57	55062.8649	0.0003	0.0084	54
58	55062.9561	0.0002	0.0081	54
59	55063.0462	0.0003	0.0067	54
60	55063.1397	0.0002	0.0087	54
61	55063.2324	0.0002	0.0099	54
74	55064.4234	0.0003	0.0111	54
75	55064.5144	0.0003	0.0105	54
76	55064.6035	0.0003	0.0082	54
77	55064.6956	0.0002	0.0087	54
78	55064.7865	0.0002	0.0081	54
79	55064.8803	0.0002	0.0104	54
80	55064.9714	0.0003	0.0099	53
81	55065.0578	0.0003	0.0048	54
82	55065.1536	0.0003	0.0091	54
83	55065.2456	0.0003	0.0096	53
84	55065.3374	0.0002	0.0098	54
85	55065.4268	0.0002	0.0077	54
86	55065.5203	0.0003	0.0097	54
87	55065.6094	0.0003	0.0073	54
88	55065.6988	0.0003	0.0052	54
89	55065.7918	0.0006	0.0067	43
90	55065.8815	0.0003	0.0048	53
91	55065.9753	0.0003	0.0071	54
92	55066.0649	0.0004	0.0051	54
93	55066.1574	0.0003	0.0062	54
94	55066.2475	0.0003	0.0047	54
95	55066.3406	0.0006	0.0064	54
96	55066.4299	0.0005	0.0041	54
97	55066.5207	0.0004	0.0033	53
98	55066.6125	0.0004	0.0037	53
99	55066.7034	0.0003	0.0030	53
100	55066.7941	0.0007	0.0022	54
101	55066.8838	0.0004	0.0004	54
102	55066.9771	0.0007	0.0022	54
103	55067.0691	0.0007	0.0026	53
104	55067.1599	0.0007	0.0019	54
105	55067.2518	0.0013	0.0023	54
106	55067.3405	0.0006	-0.0005	54
107	55067.4333	0.0006	0.0008	54
108	55067.5243	0.0006	0.0003	54
109	55067.6156	0.0011	-0.0000	54
110	55067.7062	0.0017	-0.0009	54
111	55067.7990	0.0007	0.0004	53
112	55067.8892	0.0005	-0.0009	54
113	55067.9812	0.0003	-0.0004	54
114	55068.0719	0.0003	-0.0012	54
115	55068.1620	0.0005	-0.0028	53
116	55068.2543	0.0006	-0.0019	54
117	55068.3450	0.0006	-0.0027	54
118	55068.4376	0.0004	-0.0017	54
119	55068.5302	0.0006	-0.0006	54

*BJD-2400000.

†Against max = 2455057.6397 + 0.091522*E*.

‡Number of points used to determine the maximum.

Table 21. Superhump maxima of V344 Lyr (2009) (continued).

E	max*	error	$O - C^\dagger$	N^\ddagger
120	55068.6203	0.0006	-0.0020	54
121	55068.7128	0.0005	-0.0011	54
122	55068.8044	0.0006	-0.0009	54
123	55068.8988	0.0010	0.0019	54
124	55068.9884	0.0020	0.0000	54
125	55069.0782	0.0005	-0.0017	54
126	55069.1682	0.0006	-0.0033	53
127	55069.2614	0.0006	-0.0015	53
128	55069.3531	0.0006	-0.0014	54
129	55069.4448	0.0006	-0.0012	54
130	55069.5342	0.0006	-0.0033	54
131	55069.6271	0.0018	-0.0019	54
132	55069.7217	0.0020	0.0012	54
133	55069.8121	0.0006	0.0000	54
134	55069.9016	0.0005	-0.0021	54
135	55069.9920	0.0003	-0.0031	54
136	55070.0827	0.0004	-0.0039	53
137	55070.1752	0.0007	-0.0030	54
138	55070.2681	0.0008	-0.0016	54
139	55070.3551	0.0005	-0.0061	54
140	55070.4493	0.0007	-0.0035	54
141	55070.5393	0.0004	-0.0050	54
142	55070.6358	0.0011	0.0000	54
143	55070.7252	0.0006	-0.0021	54
144	55070.8154	0.0005	-0.0034	54
145	55070.9067	0.0004	-0.0036	54
146	55071.0009	0.0010	-0.0010	54
147	55071.0900	0.0006	-0.0034	53
148	55071.1801	0.0005	-0.0048	53
149	55071.2654	0.0010	-0.0110	54
150	55071.3573	0.0004	-0.0107	53
151	55071.4471	0.0007	-0.0124	54
152	55071.5399	0.0005	-0.0111	54
153	55071.6266	0.0007	-0.0159	54
154	55071.7156	0.0006	-0.0184	54
155	55071.8050	0.0021	-0.0206	54
156	55071.9007	0.0006	-0.0164	54

*BJD-2400000.

 † Against max = 2455057.6397 + 0.091522*E*. ‡ Number of points used to determine the maximum.**Table 22.** Secondary superhump maxima of V344 Lyr (2009).

E	max*	error	$O - C^\dagger$	N^\ddagger
0	55065.9135	0.0009	0.0029	54
1	55066.0041	0.0021	0.0018	54
3	55066.1883	0.0012	0.0028	53
4	55066.2770	0.0009	-0.0001	54
5	55066.3677	0.0011	-0.0011	53
6	55066.4627	0.0008	0.0022	54
7	55066.5528	0.0008	0.0008	54
8	55066.6498	0.0006	0.0061	53
9	55066.7347	0.0009	-0.0006	54
10	55066.8240	0.0004	-0.0029	53
11	55066.9168	0.0007	-0.0017	54
12	55067.0051	0.0012	-0.0051	54
14	55067.1914	0.0013	-0.0020	54
15	55067.2814	0.0012	-0.0037	54
16	55067.3649	0.0012	-0.0118	54
18	55067.5586	0.0010	-0.0014	54
19	55067.6466	0.0007	-0.0050	54
20	55067.7406	0.0007	-0.0026	54
21	55067.8325	0.0017	-0.0024	54
22	55067.9235	0.0007	-0.0030	54
24	55068.1060	0.0009	-0.0038	54
25	55068.1964	0.0007	-0.0050	54
26	55068.2845	0.0013	-0.0085	54
27	55068.3782	0.0009	-0.0065	53
28	55068.4739	0.0036	-0.0024	54
29	55068.5636	0.0014	-0.0043	54
30	55068.6575	0.0005	-0.0021	54
31	55068.7487	0.0008	-0.0024	44
32	55068.8392	0.0011	-0.0036	54
34	55069.0220	0.0006	-0.0040	53
35	55069.1078	0.0011	-0.0099	54
36	55069.2086	0.0005	-0.0007	54
37	55069.2964	0.0009	-0.0045	54
38	55069.3879	0.0010	-0.0046	54
39	55069.4823	0.0003	-0.0019	54
40	55069.5726	0.0008	-0.0033	54
41	55069.6618	0.0007	-0.0057	54
42	55069.7558	0.0013	-0.0033	54
43	55069.8474	0.0013	-0.0034	53
44	55069.9411	0.0008	-0.0012	54
45	55070.0317	0.0004	-0.0023	54
46	55070.1236	0.0006	-0.0020	54
47	55070.2167	0.0009	-0.0006	54
48	55070.3079	0.0006	-0.0010	54
49	55070.4011	0.0004	0.0006	54
50	55070.4931	0.0006	0.0009	54
51	55070.5853	0.0004	0.0016	54
52	55070.6749	0.0004	-0.0005	54
53	55070.7641	0.0006	-0.0029	54
54	55070.8552	0.0009	-0.0035	54
55	55070.9495	0.0003	-0.0007	54
56	55071.0371	0.0006	-0.0048	54

*BJD-2400000.

 † Against max = 2455065.9106 + 0.091629*E*. ‡ Number of points used to determine the maximum.

Table 22. Secondary superhump maxima of V344 Lyr (2009) (continued).

E	max*	error	$O - C^\dagger$	N^\ddagger
57	55071.1300	0.0006	-0.0035	54
58	55071.2262	0.0010	0.0011	54
59	55071.3175	0.0011	0.0008	54
60	55071.4121	0.0005	0.0037	54
61	55071.5063	0.0010	0.0063	54
62	55071.5987	0.0007	0.0071	54
63	55071.6912	0.0006	0.0079	54
64	55071.7831	0.0007	0.0081	54
65	55071.8731	0.0006	0.0065	54
66	55071.9745	0.0016	0.0163	54
67	55072.0668	0.0019	0.0170	53
68	55072.1560	0.0014	0.0145	54
69	55072.2488	0.0023	0.0158	54
70	55072.3349	0.0018	0.0102	54
71	55072.4267	0.0009	0.0104	54
72	55072.5160	0.0009	0.0080	54
73	55072.6119	0.0010	0.0123	54
74	55072.7007	0.0010	0.0094	54
75	55072.7964	0.0015	0.0136	54
76	55072.8855	0.0017	0.0110	53
77	55072.9814	0.0007	0.0153	54
79	55073.1619	0.0014	0.0126	53
80	55073.2460	0.0010	0.0050	54
81	55073.3395	0.0007	0.0068	52
82	55073.4322	0.0013	0.0079	54
83	55073.5232	0.0006	0.0073	54
84	55073.6162	0.0005	0.0086	54
85	55073.7047	0.0009	0.0055	54
86	55073.7978	0.0006	0.0071	54
87	55073.8886	0.0006	0.0062	54
88	55073.9830	0.0005	0.0090	53
89	55074.0743	0.0013	0.0086	54
90	55074.1639	0.0005	0.0066	54
91	55074.2569	0.0006	0.0080	54
92	55074.3490	0.0014	0.0084	54
93	55074.4350	0.0010	0.0028	53
94	55074.5247	0.0007	0.0009	54
95	55074.6157	0.0008	0.0003	53
96	55074.7047	0.0005	-0.0023	54
97	55074.7957	0.0006	-0.0030	54
98	55074.8871	0.0006	-0.0033	53
99	55074.9791	0.0005	-0.0029	54
100	55075.0703	0.0006	-0.0033	54
101	55075.1604	0.0007	-0.0048	54
102	55075.2549	0.0008	-0.0020	53
103	55075.3466	0.0005	-0.0018	54
104	55075.4349	0.0008	-0.0052	54
105	55075.5297	0.0015	-0.0020	54
106	55075.6173	0.0010	-0.0061	54
107	55075.7055	0.0009	-0.0095	54
108	55075.7982	0.0012	-0.0085	54
109	55075.8896	0.0020	-0.0087	54

*BJD-2400000.

 † Against max = 2455065.9106 + 0.091629E. ‡ Number of points used to determine the maximum.**Table 22.** Secondary superhump maxima of V344 Lyr (2009) (continued).

E	max*	error	$O - C^\dagger$	N^\ddagger
112	55076.1611	0.0008	-0.0120	54
113	55076.2642	0.0010	-0.0005	54
117	55076.6187	0.0019	-0.0126	54
118	55076.7048	0.0015	-0.0181	54
119	55076.7971	0.0007	-0.0174	53
120	55076.8900	0.0007	-0.0162	54
121	55076.9811	0.0008	-0.0168	54
122	55077.0731	0.0008	-0.0164	54
123	55077.1646	0.0015	-0.0165	54
124	55077.2577	0.0013	-0.0150	54
125	55077.3515	0.0010	-0.0128	54
126	55077.4458	0.0010	-0.0102	53
127	55077.5342	0.0011	-0.0134	54
128	55077.6270	0.0007	-0.0122	54
129	55077.7204	0.0011	-0.0105	43
130	55077.8142	0.0021	-0.0083	54
131	55077.9033	0.0007	-0.0108	54
132	55078.0032	0.0020	-0.0025	54
133	55078.0996	0.0027	0.0023	54
134	55078.1934	0.0012	0.0044	54
135	55078.2936	0.0030	0.0130	53
136	55078.3777	0.0011	0.0055	54
137	55078.4686	0.0015	0.0047	54
138	55078.5609	0.0010	0.0054	54
139	55078.6530	0.0016	0.0058	54
140	55078.7427	0.0013	0.0039	53
141	55078.8349	0.0008	0.0045	54
142	55078.9250	0.0010	0.0030	53
143	55079.0135	0.0010	-0.0001	54
144	55079.1104	0.0012	0.0052	53
146	55079.2897	0.0005	0.0011	54
146	55079.2897	0.0005	0.0011	54
147	55079.3781	0.0010	-0.0021	54
148	55079.4778	0.0008	0.0060	54
149	55079.5651	0.0007	0.0017	53
150	55079.6511	0.0029	-0.0039	54
151	55079.7558	0.0016	0.0091	53
152	55079.8427	0.0008	0.0043	53
154	55080.0151	0.0050	-0.0065	53
155	55080.1040	0.0007	-0.0092	54
156	55080.2077	0.0030	0.0029	54
157	55080.3105	0.0023	0.0140	54
158	55080.3926	0.0010	0.0045	54
160	55080.5653	0.0040	-0.0061	54
161	55080.6736	0.0021	0.0106	54
162	55080.7633	0.0015	0.0087	54
163	55080.8489	0.0009	0.0027	54
164	55080.9429	0.0034	0.0050	54
165	55081.0375	0.0025	0.0079	54
166	55081.1283	0.0021	0.0072	54
167	55081.2182	0.0023	0.0054	54
168	55081.3018	0.0020	-0.0026	54
169	55081.3934	0.0014	-0.0026	54

*BJD-2400000.

 † Against max = 2455065.9106 + 0.091629E. ‡ Number of points used to determine the maximum.

Table 22. Secondary superhump maxima of V344 Lyr (2009) (continued).

E	max*	error	$O - C^\dagger$	N^\ddagger
170	55081.5011	0.0059	0.0134	54
171	55081.5750	0.0017	-0.0043	53
172	55081.6704	0.0008	-0.0005	54
173	55081.7619	0.0013	-0.0006	54
174	55081.8498	0.0011	-0.0044	54
175	55081.9463	0.0022	0.0005	54
176	55082.0429	0.0020	0.0055	54
177	55082.1342	0.0054	0.0052	54
178	55082.2234	0.0091	0.0027	54
179	55082.3130	0.0008	0.0007	54
180	55082.4069	0.0015	0.0029	54
181	55082.4974	0.0015	0.0018	54
182	55082.5900	0.0007	0.0028	54
183	55082.6700	0.0013	-0.0088	54
184	55082.7594	0.0012	-0.0110	54
185	55082.8545	0.0009	-0.0076	54
186	55082.9446	0.0018	-0.0091	54
187	55083.0394	0.0018	-0.0059	53
188	55083.1421	0.0022	0.0051	54

*BJD-2400000.

†Against max = 2455065.9106 + 0.091629*E*.

‡Number of points used to determine the maximum.

3.15. V1212 Tauri

V1212 Tau was discovered as an eruptive object near M45 (Parsamyan et al. 1983), whose location might suggest one of Pleiades flare stars. Although the object remained unnamed for long, members of the Variable Star Observers' League in Japan (VSOLJ) suspected that the object is more likely a dwarf nova based on published observations, and continued their own monitoring since 1987. There was a visual record of a bright outburst in 1987 October, which remained unconfirmed. The object was detected in outburst in 2007 January by G. Gualdoni (vsnet-alert 9190). Although observations of this outburst was rather fragmentary, J. Patterson reported the detection of superhumps with a period of 0.075 d.⁵

The object was again detected in outburst in 2011 January (baavss-alert 2473, vsnet-alert 12718). This outburst was detected sufficiently early, and full evolution of superhumps were recorded (vsnet-alert 12727, 12730, 12736, 12743; figure 18). The time of superhump maxima are listed in table 26. Stages A–C can be well recognized. The double-wave modulations reported during the early stage were likely stage A superhumps having longer period than stage B superhumps.⁶ The evolution of superhumps is quite typical for a system with this P_{SH} .

⁵ <<http://cbastro.org/communications/news/messages/0518.html>>.

⁶ Olech et al. (2011) discussed the possibility of early superhumps in SDSS J162520.29+120308.7. The present case clearly excludes this possibility because of its long period (e.g. vsnet-alert 12727, 12730). The result and discussion by Olech et al. (2011) probably need to be re-examined in the light of the knowledge from this object.

Table 23. Superhump maxima of V344 Lyr (2009b).

E	max*	error	$O - C^\dagger$	N^\ddagger
0	55161.9728	0.0038	-0.0600	54
1	55162.0796	0.0015	-0.0448	54
2	55162.1711	0.0022	-0.0447	54
3	55162.2755	0.0011	-0.0318	53
4	55162.3654	0.0006	-0.0335	54
5	55162.4583	0.0020	-0.0321	54
6	55162.5509	0.0004	-0.0310	54
7	55162.6437	0.0009	-0.0297	54
8	55162.7356	0.0004	-0.0294	54
9	55162.8323	0.0003	-0.0242	54
10	55162.9261	0.0003	-0.0219	54
11	55163.0186	0.0002	-0.0209	54
12	55163.1135	0.0002	-0.0175	54
13	55163.2077	0.0002	-0.0148	54
14	55163.3022	0.0001	-0.0118	53
15	55163.3965	0.0001	-0.0090	54
16	55163.4910	0.0001	-0.0060	54
17	55163.5833	0.0001	-0.0053	54
18	55163.6774	0.0001	-0.0027	54
19	55163.7713	0.0001	-0.0003	53
20	55163.8634	0.0001	0.0003	53
21	55163.9565	0.0001	0.0018	54
22	55164.0483	0.0001	0.0021	53
23	55164.1404	0.0001	0.0028	54
24	55164.2318	0.0001	0.0026	53
25	55164.3240	0.0001	0.0033	54
26	55164.4170	0.0001	0.0048	54
27	55164.5094	0.0002	0.0056	54
28	55164.6011	0.0001	0.0058	54
29	55164.6930	0.0001	0.0063	54
30	55164.7856	0.0001	0.0073	54
31	55164.8771	0.0001	0.0073	54
32	55164.9702	0.0002	0.0088	54
33	55165.0609	0.0001	0.0080	53
34	55165.1531	0.0002	0.0087	54
35	55165.2456	0.0001	0.0097	54
36	55165.3359	0.0002	0.0084	54
37	55165.4286	0.0002	0.0096	54
38	55165.5203	0.0001	0.0098	54
39	55165.6117	0.0002	0.0097	54
40	55165.7044	0.0002	0.0110	54
41	55165.7946	0.0003	0.0096	54
42	55165.8860	0.0002	0.0095	53
43	55165.9772	0.0002	0.0092	54
44	55166.0699	0.0002	0.0104	54
45	55166.1612	0.0003	0.0101	54
46	55166.2528	0.0003	0.0102	54
47	55166.3447	0.0002	0.0106	54
48	55166.4352	0.0004	0.0096	53
49	55166.5268	0.0002	0.0097	53
50	55166.6205	0.0002	0.0119	54
51	55166.7106	0.0003	0.0105	54

*BJD-2400000.

†Against max = 2455162.0328 + 0.091517*E*.

‡Number of points used to determine the maximum.

Table 23. Superhump maxima of V344 Lyr (2009b) (continued).

E	max*	error	$O - C^\dagger$	N^\ddagger
52	55166.8022	0.0003	0.0105	54
53	55166.8921	0.0003	0.0089	54
54	55166.9838	0.0002	0.0091	54
55	55167.0757	0.0002	0.0094	53
56	55167.1675	0.0004	0.0098	53
57	55167.2611	0.0002	0.0118	54
58	55167.3504	0.0002	0.0096	54
59	55167.4437	0.0003	0.0114	53
60	55167.5347	0.0002	0.0109	54
61	55167.6283	0.0002	0.0130	54
62	55167.7192	0.0004	0.0124	54
63	55167.8107	0.0002	0.0123	54
64	55167.9021	0.0003	0.0122	53
65	55167.9947	0.0004	0.0133	54
66	55168.0846	0.0003	0.0117	54
67	55168.1762	0.0003	0.0118	53
68	55168.2682	0.0002	0.0122	54
69	55168.3602	0.0003	0.0128	53
70	55168.4492	0.0002	0.0103	53
71	55168.5438	0.0002	0.0134	54
72	55168.6331	0.0001	0.0111	53
73	55168.7239	0.0002	0.0104	54
74	55168.8165	0.0003	0.0114	54
75	55168.9084	0.0003	0.0118	54
76	55168.9978	0.0002	0.0097	54
77	55169.0909	0.0002	0.0113	54
78	55169.1822	0.0003	0.0111	54
79	55169.2711	0.0004	0.0085	54
80	55169.3650	0.0003	0.0109	43
81	55169.4541	0.0002	0.0084	54
82	55169.5478	0.0002	0.0106	53
83	55169.6376	0.0002	0.0089	54
84	55169.7288	0.0002	0.0086	53
85	55169.8210	0.0003	0.0092	54
86	55169.9117	0.0002	0.0084	54
87	55170.0059	0.0002	0.0111	54
88	55170.0972	0.0004	0.0109	54
89	55170.1867	0.0003	0.0089	54
90	55170.2782	0.0002	0.0089	54
91	55170.3698	0.0002	0.0090	54
92	55170.4611	0.0003	0.0087	53
93	55170.5505	0.0003	0.0066	54
94	55170.6441	0.0003	0.0087	54
95	55170.7346	0.0004	0.0077	54
96	55170.8248	0.0003	0.0064	54
97	55170.9145	0.0003	0.0046	54
98	55171.0087	0.0005	0.0072	54
99	55171.0973	0.0003	0.0043	54
100	55171.1899	0.0005	0.0055	54
101	55171.2798	0.0003	0.0038	54
102	55171.3725	0.0005	0.0050	54

*BJD-2400000.

†Against max = 2455162.0328 + 0.091517E.

‡Number of points used to determine the maximum.

Table 23. Superhump maxima of V344 Lyr (2009b) (continued).

E	max*	error	$O - C^\dagger$	N^\ddagger
103	55171.4609	0.0005	0.0018	54
104	55171.5544	0.0005	0.0039	54
105	55171.6454	0.0006	0.0033	54
106	55171.7352	0.0005	0.0017	54
107	55171.8287	0.0005	0.0036	54
108	55171.9198	0.0011	0.0032	54
109	55172.0102	0.0006	0.0021	54
110	55172.1012	0.0007	0.0015	54
111	55172.1939	0.0013	0.0027	54
112	55172.2829	0.0006	0.0002	54
113	55172.3741	0.0006	-0.0001	54
114	55172.4662	0.0006	0.0005	54
115	55172.5578	0.0013	0.0005	54
116	55172.6468	0.0011	-0.0020	53
117	55172.7399	0.0007	-0.0003	54
118	55172.8318	0.0007	0.0000	54
119	55172.9256	0.0009	0.0023	54
120	55173.0126	0.0007	-0.0022	54
121	55173.1047	0.0024	-0.0016	54
122	55173.1982	0.0017	0.0004	53
123	55173.2902	0.0023	0.0009	54
124	55173.3778	0.0023	-0.0031	54
125	55173.4699	0.0015	-0.0025	54
126	55173.5618	0.0010	-0.0021	54
127	55173.6550	0.0005	-0.0004	54
128	55173.7456	0.0004	-0.0014	53
129	55173.8366	0.0004	-0.0018	54
130	55173.9276	0.0004	-0.0023	53
131	55174.0180	0.0004	-0.0035	54
132	55174.1120	0.0003	-0.0010	54
133	55174.2027	0.0003	-0.0018	54
134	55174.2930	0.0003	-0.0031	54
135	55174.3858	0.0003	-0.0017	53
136	55174.4775	0.0003	-0.0016	54
137	55174.5685	0.0004	-0.0021	54
138	55174.6600	0.0003	-0.0021	54
139	55174.7515	0.0002	-0.0022	54
140	55174.8438	0.0004	-0.0014	53
141	55174.9362	0.0004	-0.0005	54
142	55175.0274	0.0006	-0.0008	54
143	55175.1174	0.0002	-0.0023	54
144	55175.2096	0.0004	-0.0016	54
145	55175.3010	0.0003	-0.0017	54
146	55175.3922	0.0005	-0.0020	54
147	55175.4828	0.0004	-0.0030	54
148	55175.5755	0.0006	-0.0017	54
149	55175.6669	0.0004	-0.0019	54
150	55175.7580	0.0003	-0.0023	54
151	55175.8477	0.0005	-0.0041	54
152	55175.9415	0.0003	-0.0018	54
153	55176.0329	0.0003	-0.0020	54
154	55176.1198	0.0004	-0.0066	54
155	55176.2125	0.0004	-0.0054	54
156	55176.3000	0.0006	-0.0094	54
157	55176.3901	0.0005	-0.0108	54

*BJD-2400000.

†Against max = 2455162.0328 + 0.091517E.

‡Number of points used to determine the maximum.

Table 23. Superhump maxima of V344 Lyr (2009b) (continued).

E	max*	error	$O - C^\dagger$	N^\ddagger
158	55176.4829	0.0006	-0.0096	54
159	55176.5708	0.0007	-0.0132	53
160	55176.6610	0.0009	-0.0144	54
161	55176.7532	0.0008	-0.0138	54
162	55176.8418	0.0008	-0.0167	54
163	55176.9339	0.0009	-0.0161	53
164	55177.0264	0.0005	-0.0151	54
165	55177.1167	0.0008	-0.0163	54
166	55177.2072	0.0008	-0.0174	54
167	55177.3015	0.0006	-0.0146	54
168	55177.3911	0.0006	-0.0165	54
169	55177.4827	0.0007	-0.0164	54
170	55177.5723	0.0015	-0.0184	54

*BJD-2400000.

 † Against max = 2455162.0328 + 0.091517 E . ‡ Number of points used to determine the maximum.**Table 24.** Secondary superhump maxima of V344 Lyr (2009b).

E	max*	error	$O - C^\dagger$	N^\ddagger
0	55169.2136	0.0006	0.0047	54
1	55169.2986	0.0013	-0.0018	54
2	55169.4014	0.0008	0.0094	54
3	55169.4837	0.0014	0.0001	54
4	55169.5834	0.0009	0.0083	53
5	55169.6736	0.0009	0.0070	53
6	55169.7640	0.0008	0.0058	54
7	55169.8514	0.0007	0.0017	53
8	55169.9480	0.0008	0.0067	54
9	55170.0308	0.0010	-0.0020	54
10	55170.1154	0.0020	-0.0090	54
11	55170.2167	0.0012	0.0008	54
12	55170.3006	0.0023	-0.0070	53
13	55170.3899	0.0011	-0.0092	54
14	55170.4816	0.0012	-0.0091	54
15	55170.5828	0.0011	0.0005	54
16	55170.6773	0.0007	0.0036	54
17	55170.7649	0.0010	-0.0004	54
18	55170.8598	0.0005	0.0029	54
19	55170.9441	0.0008	-0.0043	54
20	55171.0378	0.0005	-0.0022	54
21	55171.1286	0.0007	-0.0029	53
22	55171.2242	0.0005	0.0011	54
23	55171.3159	0.0006	0.0012	53
24	55171.4048	0.0009	-0.0014	53
25	55171.4959	0.0012	-0.0019	54
26	55171.5851	0.0007	-0.0043	54
27	55171.6751	0.0009	-0.0058	54
28	55171.7609	0.0017	-0.0115	54
29	55171.8578	0.0017	-0.0063	54
30	55171.9443	0.0043	-0.0113	53
31	55172.0419	0.0007	-0.0052	53
32	55172.1351	0.0006	-0.0036	54
33	55172.2252	0.0014	-0.0051	53
34	55172.3105	0.0030	-0.0114	50
35	55172.4060	0.0008	-0.0074	53
36	55172.4979	0.0006	-0.0071	54
37	55172.5903	0.0009	-0.0062	54
38	55172.6855	0.0008	-0.0026	54
39	55172.7774	0.0008	-0.0023	54
40	55172.8653	0.0008	-0.0059	54
41	55172.9539	0.0017	-0.0088	54
42	55173.0500	0.0008	-0.0043	53
43	55173.1440	0.0010	-0.0019	54
44	55173.2254	0.0015	-0.0120	54
45	55173.3170	0.0031	-0.0119	54
46	55173.4088	0.0012	-0.0117	54
47	55173.5088	0.0008	-0.0033	54
48	55173.6008	0.0009	-0.0028	54
49	55173.6908	0.0006	-0.0044	53
50	55173.7856	0.0003	-0.0012	54
51	55173.8774	0.0003	-0.0009	54

*BJD-2400000.

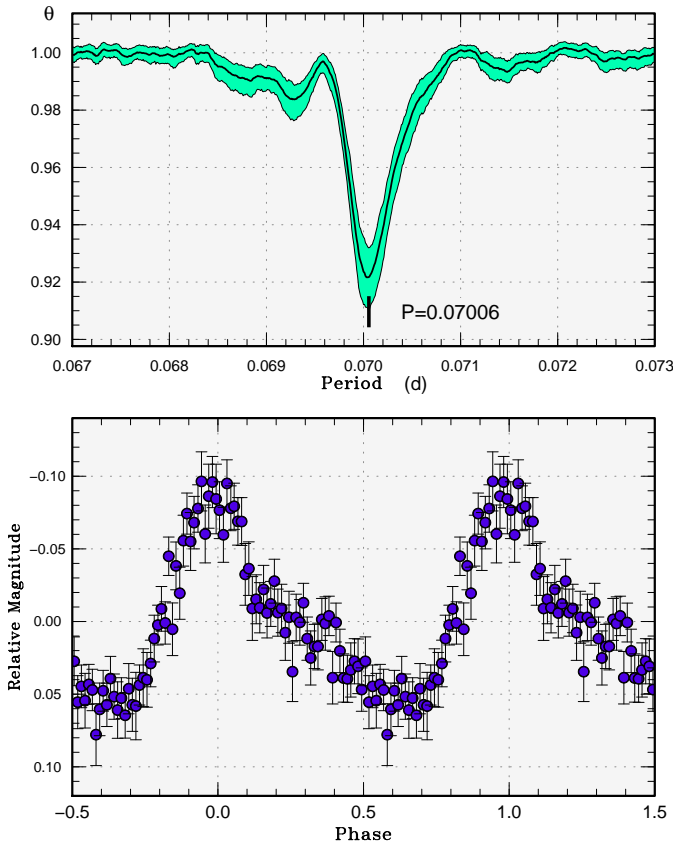
 † Against max = 2455169.2088 + 0.091558 E . ‡ Number of points used to determine the maximum.**Fig. 18.** Superhumps in V1212 Tau (2011). (Upper): PDM analysis excluding stage A (BJD 2455591–2455602). (Lower): Phase-averaged profile.

Table 24. Secondary superhump maxima of V344 Lyr (2009b) (continued).

E	max*	error	$O - C^\dagger$	N^\ddagger
52	55173.9671	0.0005	-0.0027	54
53	55174.0576	0.0007	-0.0038	54
54	55174.1508	0.0004	-0.0022	54
55	55174.2407	0.0006	-0.0038	54
56	55174.3332	0.0005	-0.0029	54
57	55174.4235	0.0006	-0.0042	54
58	55174.5187	0.0004	-0.0005	54
59	55174.6140	0.0024	0.0032	53
60	55174.6982	0.0008	-0.0041	54
61	55174.7901	0.0008	-0.0038	54
62	55174.8844	0.0004	-0.0010	54
63	55174.9743	0.0005	-0.0027	54
64	55175.0689	0.0004	0.0003	54
65	55175.1595	0.0004	-0.0006	54
66	55175.2512	0.0009	-0.0005	53
67	55175.3424	0.0004	-0.0008	43
68	55175.4344	0.0008	-0.0004	54
69	55175.5275	0.0010	0.0012	54
70	55175.6195	0.0009	0.0016	54
71	55175.7121	0.0005	0.0026	54
72	55175.8018	0.0006	0.0008	54
73	55175.8955	0.0004	0.0029	53
74	55175.9856	0.0005	0.0014	54
75	55176.0753	0.0004	-0.0004	54
76	55176.1685	0.0007	0.0012	54
77	55176.2598	0.0007	0.0010	54
78	55176.3579	0.0006	0.0075	54
79	55176.4474	0.0007	0.0055	54
80	55176.5416	0.0006	0.0081	54
81	55176.6308	0.0007	0.0057	54
82	55176.7212	0.0008	0.0046	53
83	55176.8121	0.0006	0.0039	53
84	55176.9093	0.0010	0.0096	54
85	55176.9977	0.0007	0.0064	54
86	55177.1033	0.0027	0.0205	54
87	55177.1789	0.0007	0.0045	53
88	55177.2777	0.0009	0.0118	54
89	55177.3659	0.0008	0.0084	53
90	55177.4574	0.0012	0.0083	53
91	55177.5585	0.0016	0.0179	54
92	55177.6467	0.0009	0.0145	53
93	55177.7382	0.0017	0.0145	54
94	55177.8228	0.0008	0.0075	53
95	55177.9264	0.0022	0.0196	54
96	55178.0070	0.0011	0.0086	54
97	55178.1072	0.0019	0.0172	54
98	55178.2022	0.0018	0.0207	54
99	55178.2879	0.0004	0.0148	53
100	55178.3805	0.0014	0.0159	54
101	55178.4703	0.0009	0.0141	54
102	55178.5656	0.0013	0.0179	54
103	55178.6510	0.0007	0.0117	54

*BJD-2400000.

 † Against max = 2455169.2088 + 0.091558*E*. ‡ Number of points used to determine the maximum.**Table 24.** Secondary superhump maxima of V344 Lyr (2009b) (continued).

E	max*	error	$O - C^\dagger$	N^\ddagger
104	55178.7409	0.0007	0.0100	54
105	55178.8317	0.0007	0.0092	54
106	55178.9270	0.0005	0.0130	54
107	55179.0168	0.0008	0.0113	54
108	55179.1049	0.0005	0.0078	54
109	55179.1960	0.0005	0.0074	53
110	55179.2890	0.0007	0.0088	54
111	55179.3790	0.0008	0.0073	54
112	55179.4696	0.0008	0.0063	54
113	55179.5597	0.0003	0.0048	54
114	55179.6504	0.0004	0.0040	54
115	55179.7410	0.0004	0.0030	54
116	55179.8329	0.0003	0.0033	54
117	55179.9272	0.0006	0.0061	54
118	55180.0194	0.0008	0.0067	54
119	55180.1082	0.0010	0.0040	54
120	55180.1999	0.0007	0.0041	54
121	55180.2915	0.0009	0.0041	54
122	55180.3793	0.0007	0.0004	54
123	55180.4719	0.0008	0.0014	53
124	55180.5627	0.0005	0.0007	54
125	55180.6505	0.0007	-0.0030	53
126	55180.7424	0.0004	-0.0028	54
127	55180.8324	0.0006	-0.0043	54
128	55180.9238	0.0007	-0.0044	54
129	55181.0111	0.0005	-0.0087	54
130	55181.1023	0.0008	-0.0091	54
131	55181.1919	0.0005	-0.0110	54
132	55181.2845	0.0009	-0.0100	42
133	55181.3786	0.0010	-0.0075	54
134	55181.4769	0.0027	-0.0008	54
135	55181.5639	0.0009	-0.0053	54
136	55181.6497	0.0012	-0.0110	54
137	55181.7349	0.0010	-0.0174	54
138	55181.8267	0.0005	-0.0172	54
139	55181.9202	0.0006	-0.0152	54
140	55182.0079	0.0029	-0.0191	54
141	55182.0987	0.0013	-0.0199	54
142	55182.1864	0.0010	-0.0237	54
143	55182.2850	0.0018	-0.0166	54
144	55182.3722	0.0005	-0.0210	53
145	55182.4641	0.0008	-0.0206	54

*BJD-2400000.

 † Against max = 2455169.2088 + 0.091558*E*. ‡ Number of points used to determine the maximum.

Table 25. Superhump maxima of V1195 Oph (2011).

E	max*	error	$O - C^\dagger$	N^\ddagger
0	55664.2522	0.0026	-0.0003	132
9	55664.8595	0.0006	0.0018	70
10	55664.9236	0.0009	-0.0014	69
24	55665.8666	0.0007	0.0002	69
25	55665.9334	0.0005	-0.0003	70

*BJD-2400000.

†Against max = 2455664.2525 + 0.067245 E .

‡Number of points used to determine the maximum.

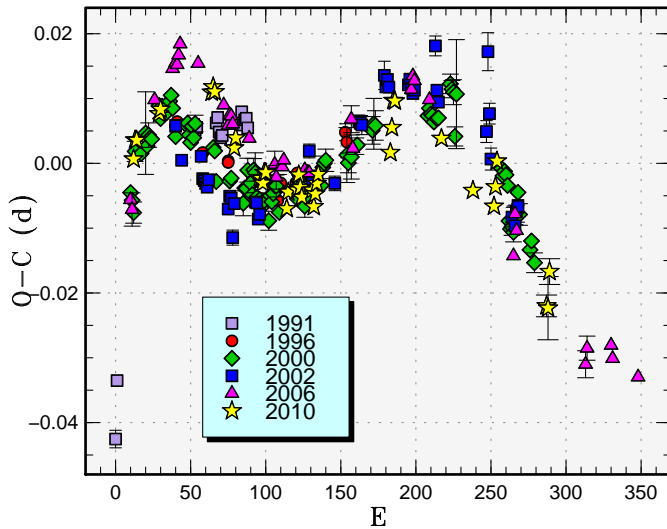


Fig. 19. Comparison of $O - C$ diagrams of SW UMa between different superoutbursts. A period of 0.05822 d was used to draw this figure. Since the delay in the appearance of superhumps is known to vary in SW UMa, we shifted individual $O - C$ diagrams to get a best match (approximately corresponds to a definition of the appearance of superhumps to be $E = 0$). Two relatively bright superoutburst in 2006 and 2010 showed a similar tendency (larger $O - C$) around the start of the stage B.

3.16. SW Ursae Majoris

We observed the 2010 superoutburst. This outburst occurred after a relatively long (~ 890 d) interval following the 2008 superoutburst. The outburst was relatively well observed despite the rather adverse seasonal conditions. Since some of the present observations were obtained at high airmasses, we used a second-order correction for atmospheric extinction as in V844 Her. The times of superhump maxima are listed in table 27. Although not all parts were observed, all stages A–C are readily identified.

A comparison of $O - C$ diagrams in different superoutbursts is shown in figure 19. The 2010 superoutburst apparently followed the similar trend to that of the 2006 superoutburst (Kato et al. 2009a), another bright superoutburst preceded by relatively long quiescence.

Table 26. Superhump maxima of V1212 Tau (2011).

E	max*	error	$O - C^\dagger$	N^\ddagger
0	55589.6637	0.0028	-0.0434	99
1	55589.7459	0.0022	-0.0313	98
11	55590.4712	0.0011	-0.0066	55
12	55590.5479	0.0010	0.0000	68
13	55590.6165	0.0003	-0.0014	97
14	55590.6863	0.0003	-0.0017	99
15	55590.7588	0.0003	0.0007	99
20	55591.1074	0.0008	-0.0010	131
24	55591.3915	0.0003	0.0028	100
25	55591.4617	0.0003	0.0030	126
26	55591.5353	0.0007	0.0066	70
27	55591.6027	0.0002	0.0039	94
28	55591.6722	0.0002	0.0033	99
29	55591.7429	0.0002	0.0040	97
33	55592.0232	0.0015	0.0039	134
37	55592.3031	0.0005	0.0036	50
38	55592.3727	0.0004	0.0032	80
39	55592.4430	0.0004	0.0034	135
42	55592.6531	0.0004	0.0033	74
43	55592.7228	0.0006	0.0029	49
46	55592.9302	0.0017	0.0002	104
47	55593.0036	0.0014	0.0035	128
52	55593.3513	0.0005	0.0009	101
53	55593.4217	0.0008	0.0012	106
54	55593.4926	0.0009	0.0020	69
56	55593.6330	0.0009	0.0023	32
57	55593.7030	0.0010	0.0023	36
66	55594.3340	0.0008	0.0027	100
67	55594.4041	0.0007	0.0027	103
68	55594.4734	0.0009	0.0020	82
71	55594.6872	0.0023	0.0055	37
72	55594.7543	0.0015	0.0026	36
76	55595.0391	0.0042	0.0071	144
80	55595.3159	0.0011	0.0036	90
81	55595.3886	0.0007	0.0063	177
82	55595.4588	0.0006	0.0064	165
84	55595.5992	0.0009	0.0067	24
85	55595.6695	0.0014	0.0070	35
89	55595.9553	0.0022	0.0124	135
90	55596.0145	0.0035	0.0016	147
95	55596.3732	0.0009	0.0100	67
96	55596.4406	0.0008	0.0074	68
109	55597.3511	0.0010	0.0070	107
110	55597.4186	0.0012	0.0044	107
111	55597.4879	0.0026	0.0036	67
118	55597.9668	0.0083	-0.0079	119
123	55598.3245	0.0019	-0.0005	66
124	55598.3951	0.0009	0.0001	104
125	55598.4645	0.0011	-0.0006	96
137	55599.3017	0.0015	-0.0042	40
138	55599.3693	0.0012	-0.0067	104
139	55599.4410	0.0012	-0.0051	97
152	55600.3453	0.0013	-0.0116	28
153	55600.4174	0.0011	-0.0096	36
166	55601.3246	0.0022	-0.0131	33
167	55601.3966	0.0019	-0.0112	27

*BJD-2400000.

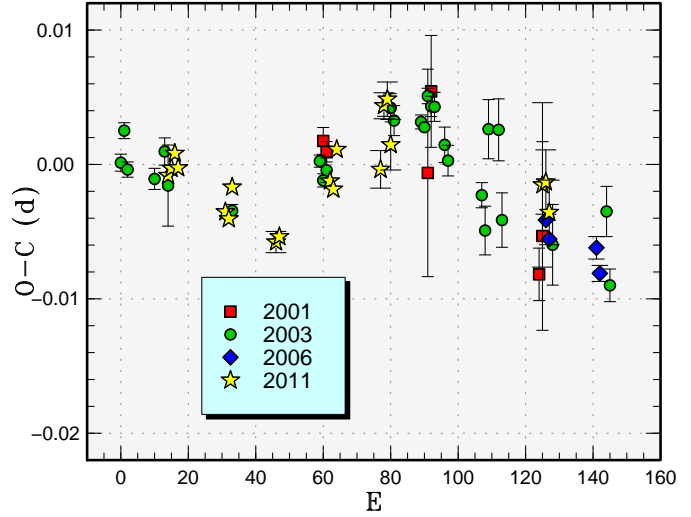
†Against max = 2455589.7071 + 0.070064 E .

‡Number of points used to determine the maximum.

Table 27. Superhump maxima of SW UMa (2010).

E	max*	error	$O - C^\dagger$	N^\ddagger
0	55535.2103	0.0004	-0.0056	234
1	55535.2715	0.0005	-0.0026	233
2	55535.3296	0.0006	-0.0025	149
17	55536.2070	0.0002	0.0024	65
18	55536.2659	0.0009	0.0032	73
52	55538.2481	0.0003	0.0078	123
53	55538.3071	0.0002	0.0087	114
54	55538.3646	0.0002	0.0080	124
67	55539.1128	0.0003	0.0001	233
68	55539.1725	0.0003	0.0017	88
84	55540.0979	0.0002	-0.0035	82
85	55540.1560	0.0002	-0.0036	358
86	55540.2135	0.0002	-0.0042	357
87	55540.2734	0.0001	-0.0025	343
88	55540.3316	0.0001	-0.0025	349
102	55541.1411	0.0006	-0.0072	127
103	55541.2019	0.0002	-0.0046	222
109	55541.5515	0.0002	-0.0039	72
110	55541.6121	0.0006	-0.0016	47
111	55541.6683	0.0003	-0.0035	82
112	55541.7251	0.0003	-0.0049	67
119	55542.1337	0.0009	-0.0034	94
120	55542.1894	0.0003	-0.0059	206
121	55542.2495	0.0002	-0.0039	303
122	55542.3094	0.0002	-0.0022	289
123	55542.3690	0.0004	-0.0007	264
171	55545.1669	0.0006	0.0055	179
172	55545.2290	0.0004	0.0094	302
173	55545.2914	0.0005	0.0136	303
174	55545.3495	0.0007	0.0136	169
205	55547.1486	0.0002	0.0096	140
226	55548.3632	0.0008	0.0028	126
240	55549.1758	0.0004	0.0012	221
241	55549.2370	0.0004	0.0043	245
242	55549.2992	0.0005	0.0083	248
275	55551.1981	0.0017	-0.0121	62
276	55551.2560	0.0049	-0.0124	82
277	55551.3199	0.0020	-0.0067	83

*BJD-2400000.

 † Against max = 2455535.2159 + 0.058161 E . ‡ Number of points used to determine the maximum.**Fig. 20.** Comparison of $O - C$ diagrams of CI UMa between different superoutbursts. The $O - C$'s were calculated against a period of 0.06264 d. Approximate cycle counts (E) after the start of the superoutburst were used.**Table 28.** Superhump maxima of CI UMa (2011).

E	max*	error	$O - C^\dagger$	N^\ddagger
0	55660.4340	0.0002	0.0005	58
1	55660.4971	0.0003	0.0011	64
2	55660.5609	0.0003	0.0022	67
3	55660.6224	0.0003	0.0011	68
17	55661.4961	0.0004	-0.0023	57
18	55661.5582	0.0005	-0.0028	68
19	55661.6232	0.0006	-0.0005	63
32	55662.4335	0.0008	-0.0047	127
33	55662.4965	0.0005	-0.0043	90
48	55663.4403	0.0007	-0.0003	66
49	55663.5023	0.0006	-0.0009	62
50	55663.5679	0.0005	0.0021	55
63	55664.3807	0.0014	0.0005	32
64	55664.4481	0.0010	0.0052	34
65	55664.5112	0.0013	0.0057	34
66	55664.5705	0.0019	0.0023	24
111	55667.3863	0.0061	-0.0010	33
112	55667.4491	0.0024	-0.0008	34
113	55667.5095	0.0024	-0.0031	23

*BJD-2400000.

 † Against max = 2455660.4334 + 0.062648 E . ‡ Number of points used to determine the maximum.

3.17. CI Ursae Majoris

We observed the 2011 superoutburst of this object (table 28). Stage B with positive P_{dot} of $+16.8(3.2) \times 10^{-5}$ and a part of stage C were observed. The behavior of $O - C$ variation is very similar between different superoutbursts (figure 20).

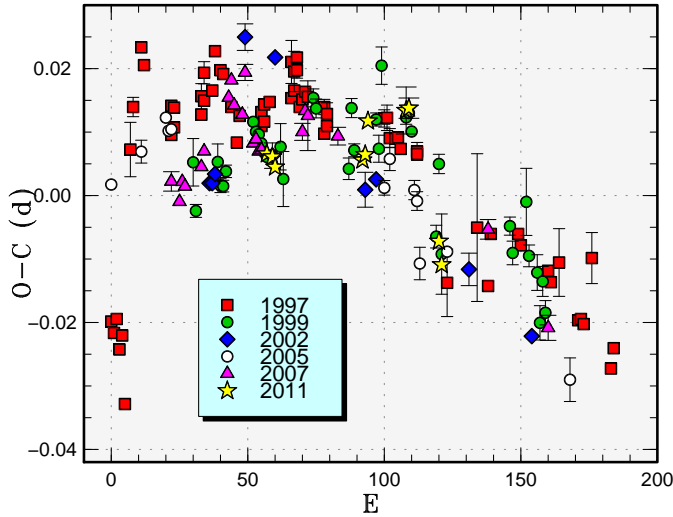


Fig. 21. Comparison of $O-C$ diagrams of DV UMa between different superoutbursts. The $O-C$'s were calculated against a period of 0.0888 d. Approximate cycle counts (E) after the start of the superoutburst were used.

Table 29. Superhump maxima of DV UMa (2011).

E	max*	error	$O-C^\dagger$	phase ‡	N^\S
0	55608.4897	0.0004	-0.0020	0.40	147
2	55608.6668	0.0004	-0.0023	0.46	138
3	55608.7540	0.0007	-0.0038	0.48	117
35	55611.5967	0.0004	0.0007	0.59	138
36	55611.6864	0.0006	0.0016	0.63	133
37	55611.7805	0.0008	0.0070	0.73	97
51	55613.0253	0.0037	0.0102	0.23	203
52	55613.1145	0.0016	0.0106	0.27	178
63	55614.0703	0.0012	-0.0092	0.40	174
64	55614.1554	0.0005	-0.0128	0.39	174

*BJD-2400000.

† Against max = 2455608.4917 + 0.088695 E .

‡ Orbital phase.

§ Number of points used to determine the maximum.

3.18. DV Ursae Majoris

We observed the 2011 superoutburst. The maxima were determined from observations outside the eclipses (table 29). The 2011 observation only recorded the final portion of stage B and partly stage C (cf. figure 21), and the resultant P_{dot} was rather unreliable.

3.19. 1RXS J003828.7+250920

This object was discovered as an eruptive object by K. Itagaki in 2007 November (vsnet-outburst 8245). The object was observed to fade by 0.3 mag in seven days. Because of the presence of a ROSAT X-ray counterpart, we call this object in its ROSAT name (hereafter 1RXS J0038).

The object was again reported to be in outburst on

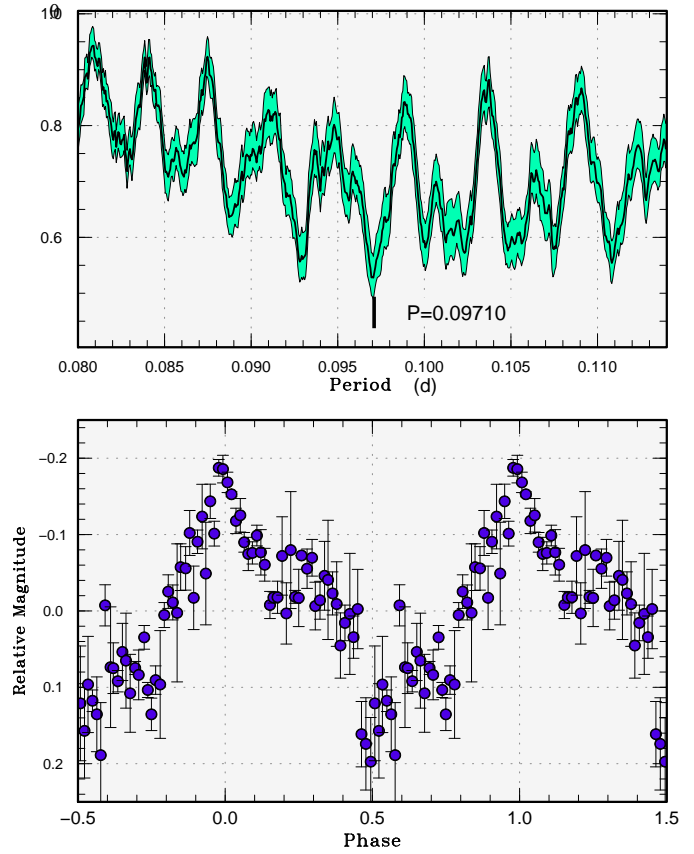


Fig. 22. Superhumps in 1RXS J0038 (2010). (Upper): PDM analysis. The rejection rate for bootstrapping was reduced to 0.2 for better visualization. (Lower): Phase-averaged profile.

Table 30. Superhump maxima of 1RXS J0038 (2010).

E	max*	error	$O-C^\dagger$	N^\ddagger
0	55495.3027	0.0008	-0.0020	94
1	55495.4040	0.0009	0.0020	97
42	55499.3928	0.0032	-0.0000	6

*BJD-2400000.

† Against max = 2455495.3046 + 0.097339 E .

‡ Number of points used to determine the maximum.

2010 October 21 at an unfiltered CCD magnitude of 14.6 (E . Muyliaert, vsnet-alert 12295). Early observations suggested the presence of superhumps (vsnet-alert 12313). The presence of long-period superhumps was finally established (vsnet-alert 12318). The long outburst in 2007 also must have been a superoutburst.

The times of superhump maxima are listed in table 30. The maximum at $E = 42$ was recorded after the rapid fading, and is not very reliable. An analysis of the single-night continuous run yielded a period of 0.0985(6) d. The PDM analysis in figure 22 used all observations, including those after the rapid fading, and yielded a mean period of 0.09708(8) d. We adopted the latter period in table 3.

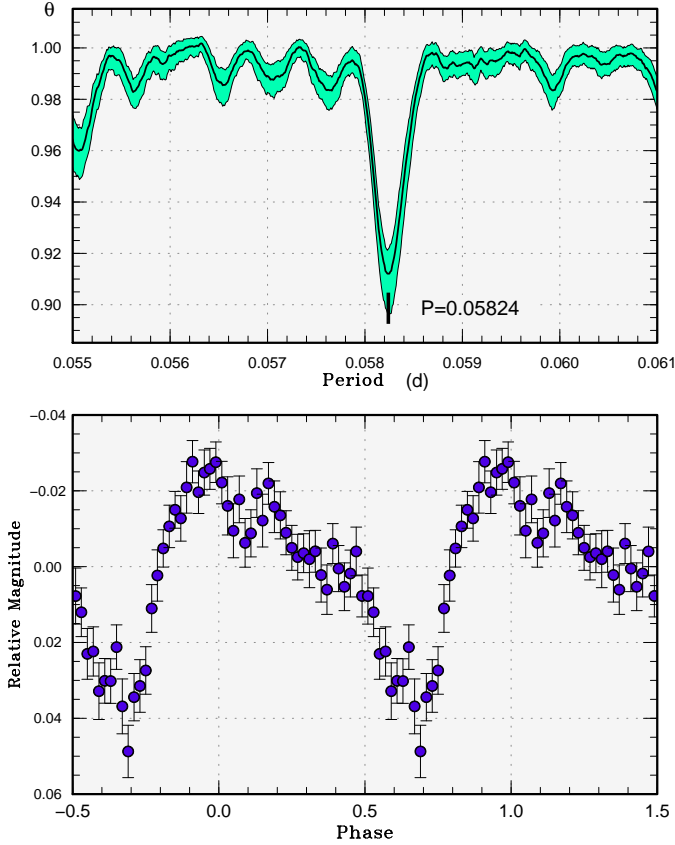


Fig. 23. Superhumps in 2QZ J2224 (2010). (Upper): PDM analysis. (Lower): Phase-averaged profile.

3.20. 2QZ J222416.2–292421

This object (hereafter 2QZ J2224) was selected as a CV during the 2dF survey for quasars (Croom et al. 2004). The spectrum was typical for a dwarf nova in quiescence with strong Balmer and HeI emission lines. There is not a strong indication of an underlying white dwarf as in many WZ Sge-type dwarf novae (see also vsnet-alert 12167). The object was for the first time detected in outburst by the CRTS Siding Spring Survey (SSS) (P. Wils, cvnet-outburst 3836). Subsequent observations confirmed the presence of superhumps (vsnet-alert 12171, 12180).

The times of superhump maxima are listed in table 31. The scatter was relatively large due to the low amplitudes of superhumps. Combined with the apparent lack of a large variation in the period, it is likely we observed the stage C superhumps during their decay phase. A PDM analysis (figure 23) has yielded a mean period of 0.05824(1) d, which is adopted in table 3.

3.21. ASAS J091858–2942.6

We observed the 2010 superoutburst of this object discovered by Pojmanski et al. (2005). The outburst, second known in its history since, was detected on 2010 December 12 at a visual magnitude of 12.8 (R. Stubbings). The first CCD observation started on December 15. Since some of

Table 31. Superhump maxima of 2QZ J2224 (2010).

E	max*	error	$O - C^\dagger$	N^\ddagger
0	55452.3543	0.0007	0.0006	127
1	55452.4112	0.0007	-0.0008	130
2	55452.4665	0.0008	-0.0037	129
3	55452.5278	0.0009	-0.0007	129
4	55452.5829	0.0010	-0.0039	115
16	55453.2838	0.0013	-0.0022	129
17	55453.3415	0.0009	-0.0027	129
18	55453.3999	0.0011	-0.0026	129
19	55453.4587	0.0013	-0.0021	129
20	55453.5170	0.0012	-0.0020	129
35	55454.4010	0.0031	0.0081	120
36	55454.4573	0.0033	0.0061	129
37	55454.5074	0.0017	-0.0021	114
52	55455.3948	0.0038	0.0115	131
53	55455.4424	0.0029	0.0007	132
54	55455.5176	0.0051	0.0177	131
55	55455.5533	0.0022	-0.0049	132
64	55456.0832	0.0014	0.0006	120
65	55456.1285	0.0025	-0.0123	121
70	55456.4307	0.0017	-0.0015	131
71	55456.4994	0.0026	0.0090	116
72	55456.5493	0.0026	0.0006	124
85	55457.3044	0.0053	-0.0017	77
86	55457.3627	0.0031	-0.0016	96
88	55457.4791	0.0021	-0.0017	56
89	55457.5396	0.0028	0.0005	89
104	55458.4094	0.0017	-0.0036	129
105	55458.4649	0.0047	-0.0063	129
106	55458.5300	0.0021	0.0004	129

*BJD–2400000.

† Against max = 2455452.3538 + 0.058262E.

‡ Number of points used to determine the maximum.

the observations were recorded at high airmasses (larger than 3), secondary corrections for atmospheric extinction were applied to these observations. The times of superhump maxima are listed in table 32. The period was relatively constant except $E = 0$. Considering that the reported magnitude was fainter than that in 2005 and the observation started relatively late, it is likely that we mostly observed stage C superhumps. The period was indeed similar to that of stage C superhumps recorded in 2005. The object underwent a rebrightening on December 30 (vsnet-alert 12544).

3.22. ASAS J102522–1542.4

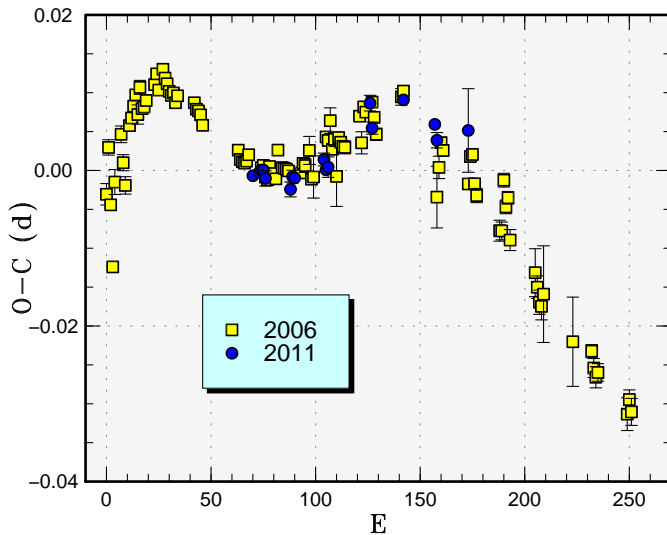
This object (hereafter ASAS J1025) is a WZ Sge-type dwarf nova discovered in 2006. The history of observations can be found in Kato et al. (2009a) and references therein.

The object was again detected in outburst in 2011 February by the CRTS (=CSS110226:102522–154222). Due to the gap in observation before the CRTS detection, the outburst detection was apparently made in a later stage than in the 2006 superoutburst. The stage of

Table 32. Superhump maxima of ASAS J0918 (2010).

E	max*	error	$O - C^\dagger$	N^\ddagger
0	55545.9210	0.0009	-0.0044	63
20	55547.1785	0.0013	-0.0001	120
21	55547.2384	0.0007	-0.0028	285
22	55547.3054	0.0007	0.0015	194
32	55547.9344	0.0010	0.0040	51
35	55548.1197	0.0015	0.0013	77
52	55549.1855	0.0007	0.0019	112
53	55549.2465	0.0008	0.0003	219
54	55549.3125	0.0005	0.0036	196
85	55551.2502	0.0014	-0.0009	171
86	55551.3094	0.0015	-0.0044	165

*BJD-2400000.

 † Against max = 2455545.9255 + 0.062655 E . ‡ Number of points used to determine the maximum.**Fig. 24.** Comparison of $O - C$ diagrams of ASAS J1025 between different superoutbursts. A period of 0.06340 d was used to draw this figure. Approximate cycle counts (E) after the appearance of the superhumps were used. Since the start of the 2011 superoutburst was not well constrained, we shifted the $O - C$ diagram to best fit the best-recorded 2006 one.

early superhumps was not recorded. The times of superhump maxima are listed in table 33, which clearly demonstrates stage B superhumps with $P_{\text{dot}} = +9.9(2.4) \times 10^{-5}$ and short segment of stage C. This value is in good agreement with the 2006 measurement (see also figure 24).

In Kato et al. (2009a), we suggested that the object would be a “borderline” long- P_{SH} WZ Sge-like dwarf nova based in the large P_{dot} and the large fractional superhump excess. The short interval of superoutbursts (5 yr or shorter) for a WZ Sge-type dwarf nova also strengthens this interpretation.

Table 33. Superhump maxima of ASAS J1025 (2011).

E	max*	error	$O - C^\dagger$	N^\ddagger
0	55619.5018	0.0003	0.0005	95
3	55619.6924	0.0006	0.0007	52
4	55619.7561	0.0005	0.0009	52
5	55619.8196	0.0006	0.0009	52
6	55619.8819	0.0010	-0.0003	50
18	55620.6413	0.0010	-0.0027	43
19	55620.7063	0.0008	-0.0012	43
20	55620.7695	0.0005	-0.0015	44
34	55621.6595	0.0008	-0.0003	51
35	55621.7216	0.0007	-0.0017	51
36	55621.7853	0.0013	-0.0014	49
56	55623.0616	0.0010	0.0051	95
57	55623.1217	0.0008	0.0018	90
72	55624.0764	0.0005	0.0042	101
87	55625.0242	0.0004	-0.0003	106
88	55625.0856	0.0010	-0.0024	91
103	55626.0378	0.0054	-0.0024	113

*BJD-2400000.

 † Against max = 2455619.5013 + 0.063485 E . ‡ Number of points used to determine the maximum.

3.23. MisV 1443

MisV 1443 was discovered as an eruptive object by Y. Nakashima at an unfiltered CCD magnitude of 14.4 mag on 2011 January 8.59707 UT. The position of the object is $06^{\text{h}}19^{\text{m}}59^{\text{s}}96$, $+19^{\circ}26'59''0$ (J2000.0) (vsnet-alert 12580; Yoshida et al. 2011). There was a 20.4-mag quiescent counterpart (vsnet-alert 12581). Soon after this discovery announcement, time-resolved photometry indicated the presence of double-wave modulations. Although this signal was initially interpreted as early superhumps, this identification requires confirmation because ordinary superhumps quickly developed (vsnet-alert 12597; figure 25). The dwarf nova nature of the object was spectroscopically confirmed by Yoshida et al. (2011) and A. Arai (vsnet-alert 12598). A retrospective analysis of survey materials revealed that the object was already in outburst at an unfiltered CCD magnitude of 12.8 on 2011 January 2.019 UT (S. Korotkiy and K. Sokolovsky, vsnet-alert 12592).

The times of superhump maxima are listed in table 34. Disregarding stage A superhumps ($E \leq 5$), evidently positive P_{dot} of $+5.5(1.5) \times 10^{-5}$ was recorded. Based on the large outburst amplitude (≥ 7.6 mag) and a long (≥ 8 d) delay before the appearance of ordinary superhumps, the object is likely a WZ Sge-type dwarf nova. The stage of early superhumps, however, was not sufficiently observed. The initial detection of double-wave modulations may be interpreted as growing stage of ordinary superhumps rather than genuine early superhumps. The maximum amplitude of superhumps (0.30 mag) was, however, rather exceptionally large for a WZ Sge-type dwarf nova (cf. subsection 4.7). MisV 1443 may bear intermediate characteristics between WZ Sge-type dwarf novae and

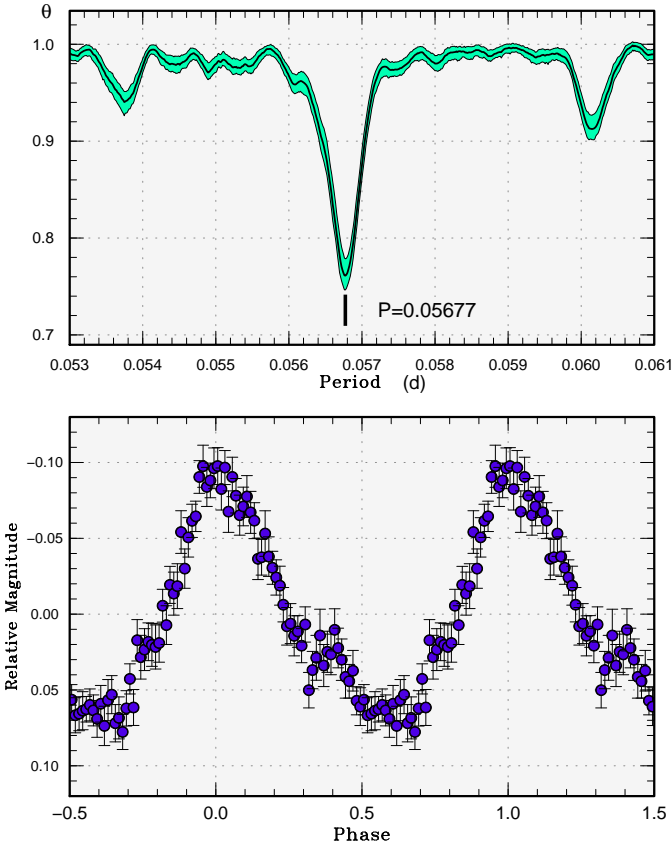
Table 34. Superhump maxima of MisV 1443 (2011).

E	max*	error	$O - C^\dagger$	N^\ddagger
0	55571.9590	0.0022	-0.0046	100
3	55572.1250	0.0005	-0.0090	146
4	55572.1842	0.0008	-0.0065	113
5	55572.2379	0.0010	-0.0096	100
19	55573.0464	0.0002	0.0038	100
20	55573.1038	0.0003	0.0045	124
21	55573.1609	0.0003	0.0048	117
22	55573.2166	0.0004	0.0037	87
23	55573.2735	0.0004	0.0038	130
26	55573.4443	0.0007	0.0043	26
27	55573.5006	0.0004	0.0038	47
28	55573.5568	0.0003	0.0032	54
29	55573.6135	0.0003	0.0031	51
35	55573.9529	0.0009	0.0017	101
37	55574.0662	0.0007	0.0015	52
38	55574.1221	0.0004	0.0006	89
39	55574.1793	0.0004	0.0010	88
40	55574.2366	0.0005	0.0015	63
41	55574.2916	0.0008	-0.0003	62
44	55574.4629	0.0004	0.0007	54
45	55574.5202	0.0004	0.0012	41
46	55574.5755	0.0007	-0.0003	52
53	55574.9743	0.0020	0.0011	61
55	55575.0868	0.0004	-0.0001	61
56	55575.1431	0.0004	-0.0006	109
57	55575.1991	0.0004	-0.0013	102
58	55575.2551	0.0006	-0.0021	59
62	55575.4849	0.0005	0.0005	49
63	55575.5408	0.0005	-0.0004	48
72	55576.0493	0.0034	-0.0030	78
73	55576.1125	0.0024	0.0035	105
74	55576.1659	0.0039	0.0001	91
75	55576.2154	0.0023	-0.0072	99
92	55577.1878	0.0008	-0.0002	63
93	55577.2434	0.0007	-0.0013	62
108	55578.0918	0.0025	-0.0048	95
109	55578.1533	0.0019	-0.0000	88
110	55578.2128	0.0017	0.0026	105

*BJD-2400000.

†Against max = 2455571.9636 + 0.056787E.

‡Number of points used to determine the maximum.

**Fig. 25.** Ordinary superhumps in MisV 1443 (2011). (Upper): PDM analysis for BJD 2455571.8–2455582 (excluding stage A superhumps) (Lower): Phase-averaged profile.

more usual SU UMa-type dwarf novae.

The final stage of the superoutburst was observed by snapshot observations. The object was recorded at 15.1 on January 27 and rapidly faded to 17.9 on January 28. The entire duration of the outburst was thus longer than 25 d. The object underwent a rebrightening at 15.3 on February 3 (vsnet-alert 12787, 12798; all observations are unfiltered CCD magnitudes). The object stayed at mag ~ 18 , 2.5 mag above quiescence, at least until March 7.

3.24. *RX J1715.6+6856*

The final stage of the 2009 superoutburst of this object (hereafter RX J1715) was reported in Shears et al. (2010a) and Kato et al. (2009a). I. Miller detected a new outburst on 2010 September 15 (baavss-alert 2386). Subsequent observations confirmed superhumps (vsnet-alert 12182, 12183). The times of superhump maxima are listed in table 35. The outburst was apparently observed in its late stage, and these superhumps can be identified as stage C superhumps.

3.25. *SDSS J073208.11+413008.7*

We observed the 2011 superoutburst of this object (hereafter SDSS J0732; the object was selected by Wils et al. 2010, see a comment in Kato et al. 2010). The times

Table 35. Superhump maxima of RX J1715 (2010).

E	max*	error	$O - C^\dagger$	N^\ddagger
0	55455.4107	0.0010	0.0005	37
14	55456.3996	0.0012	-0.0011	77
15	55456.4722	0.0007	0.0008	72
16	55456.5439	0.0011	0.0018	18
23	55457.0343	0.0051	-0.0031	127
24	55457.1051	0.0020	-0.0030	112
29	55457.4662	0.0016	0.0042	72
30	55457.5325	0.0009	-0.0001	76

*BJD-2400000.

 † Against max = 2455455.4101 + 0.070752 E . ‡ Number of points used to determine the maximum.**Table 36.** Superhump maxima of SDSS J0732 (2011).

E	max*	error	$O - C^\dagger$	N^\ddagger
0	55582.2543	0.0021	0.0037	79
12	55583.1975	0.0034	-0.0050	159
24	55584.1582	0.0022	0.0037	132
30	55584.6289	0.0011	-0.0015	153
31	55584.7073	0.0010	-0.0024	153
68	55587.6474	0.0016	0.0026	152
69	55587.7276	0.0014	0.0035	151
70	55587.8042	0.0023	0.0008	152
71	55587.8815	0.0032	-0.0012	150
72	55587.9580	0.0034	-0.0041	122

*BJD-2400000.

 † Against max = 2455582.2506 + 0.079325 E . ‡ Number of points used to determine the maximum.

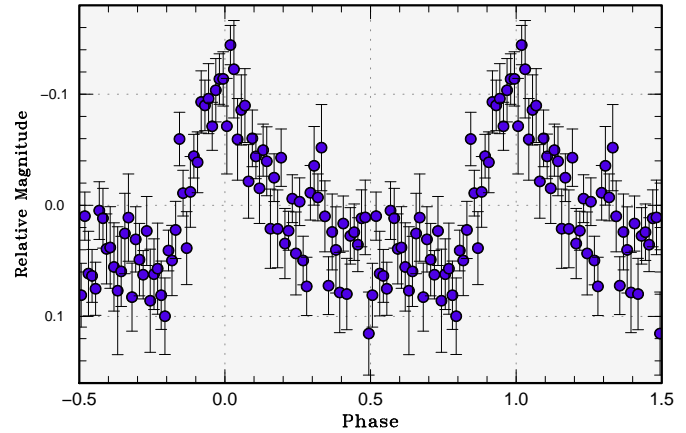
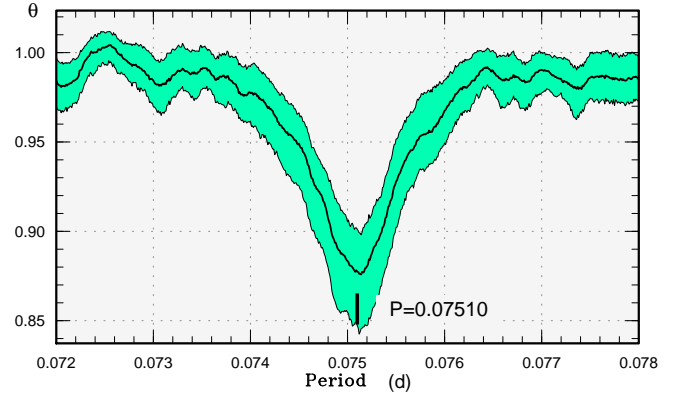
of superhump maxima are listed in table 36. The observation most likely recorded stage C superhumps, whose period is in good agreement with the value in Kato et al. (2010).

3.26. SDSS J080306.99+284855.8

This object (hereafter SDSS J0803) was selected as a CV by Wils et al. (2010). The 2011 outburst was detected by the CRTS, which was the second brightest outbursts recorded by the CRTS. Subsequent observations confirmed the presence of superhumps (vsnet-alert 13070, 13073; figure 26). The times of superhump maxima are listed in table 37. As inferred from the initial large amplitudes of superhumps, the outburst was apparently detected during its early stage (cf. vsnet-alert 13075). We therefore identified these superhumps as stage B superhumps. The large P_{dot} of $+13.6(4.2) \times 10^{-5}$ is consistent with this interpretation.

3.27. SDSS J080434.20+510349.2

SDSS J080434.20+510349.2 (hereafter SDSS J0804) is a CV selected during the course of the Sloan Digital Sky Survey (SDSS) (Szkody et al. 2006). The first-ever super-outburst was recorded in 2006 (Pavlenko et al. 2007). The

**Fig. 26.** Superhumps in SDSS J0803 (2011). (Upper): PDM analysis. (Lower): Phase-averaged profile.**Table 37.** Superhump maxima of SDSS J0803 (2011).

E	max*	error	$O - C^\dagger$	N^\ddagger
0	55654.2962	0.0004	0.0017	58
1	55654.3719	0.0005	0.0023	75
11	55655.1193	0.0036	-0.0013	133
14	55655.3437	0.0005	-0.0023	100
15	55655.4210	0.0004	-0.0000	143
16	55655.4946	0.0008	-0.0015	71
23	55656.0223	0.0012	0.0005	154
37	55657.0713	0.0025	-0.0019	150
49	55657.9750	0.0079	0.0005	125
50	55658.0516	0.0040	0.0021	153

*BJD-2400000.

 † Against max = 2455654.2945 + 0.075100 E . ‡ Number of points used to determine the maximum.

detection of the 2006 superoutburst was only made during the final stage of the plateau phase and the basic period of superhumps was not very well established (Shears et al. 2007; Pavlenko et al. 2007; see Kato et al. 2009b for a discussion of the corrected superhump period). This WZ Sge-type dwarf nova is particularly notable in its grazing eclipses (Zharikov et al. 2008; Kato et al. 2009b), in the existence of eleven rebrightenings during the 2006 superoutburst (Pavlenko et al. 2007; Kato et al. 2009b) and in the ZZ Cet-type pulsation of the white dwarf (Pavlenko 2009; Pavlenko et al. 2010a).

The object underwent an unexpected outburst in 2010 September, only 4.5 yr after the preceding superoutburst (H. Maehara, vsnet-alert 12184). This outburst was fortunately detected in its rising stage, and the presence of early superhumps and evolution of ordinary superhumps were well recorded (vsnet-alert 12186, 12192, 12196; figure 29). The analysis generally follows the method described in Kato et al. (2009b).

The mean period of early superhumps (before BJD 24455462) was 0.058973(6) d, 0.05 % shorter than P_{orb} (figure 27). The mean period of ordinary superhumps during the plateau phase (BJD 2455462–55472.5) was 0.059584(2) d, 0.98 % longer than P_{orb} (figure 28).

The times of superhump maxima, determined after excluding the phases of eclipses, during the plateau phase are listed in table 38. Since the contribution of orbital signature was small, we did not subtract the mean orbital variation. The stages A–C are clearly demonstrated. The increase in the period during the stage B was not uniform, and the major increase took place during the final part of stage B. This behavior in the period evolution would explain the relatively long P_{SH} obtained during the 2006 superoutburst (Kato et al. 2009b). In table 3 we adopted $P_{\text{dot}} = +9.6(1.1) \times 10^{-5}$ ($31 \leq E \leq 159$). This value is unusually large for a WZ Sge-type dwarf nova with multiple rebrightenings. If we neglect the final part with the major increase in the period [cf. WZ Sge (2001) in Kato et al. (2009a)], we obtain $P_{\text{dot}} = +3.5(0.9) \times 10^{-5}$ ($31 \leq E \leq 143$). We will return to this issue in subsection 4.4. In contrast to the expectation in Kato et al. (2009b), shallow eclipses were present during the entire course of the outburst. The eclipses around the superoutburst maximum, however, were only observed depending on superhump phases (figure 30). Although stage B–C was apparently recorded, we did not determine the period of stage C superhumps because the change in the $O-C$ diagram was too large to be interpreted as a typical stage B–C transition. This may have been a result of contamination of increasing signal of orbital humps or a different component of superhumps as the system faded.

During the six rebrightenings, persistent superhumps were observed (figure 31). The mean period was 0.059656(4) d, confirming the slightly longer period observed during rebrightening phase of the 2006 superoutburst (Kato et al. 2009b). The rebrightenings following the current superoutburst was less numerous than in 2006. This may have resulted from the short interval (for a WZ Sge-type dwarf nova) since the preceding superoutburst.

The amplitudes of orbital humps and depths of eclipses increased by a factor of ~ 2 as the system faded from the peak of rebrightening (figure 32). Since the typical amplitudes of rebrightenings were ~ 2 mag (~ 6 times in real scale), this increase in the amplitudes cannot be simply explained by a model assuming the orbital humps with a constant luminosity and varying contribution from the accretion disk (see also the discussion in Kato et al. 2009b), and there was no particular indication of an enhanced hot spot before the start of rebrightenings (cf. Osaki, Meyer 2003). The times of superhump maxima, determined after subtracting orbital variations and excluding eclipses, during the rebrightening phase are listed in table 39.

Even after rebrightenings, the superhump signal with a mean period of 0.05967(2) d persisted (figure 33). The times of maxima determined after subtracting the orbital signal are listed in table 40.

The $O-C$ diagram together with the light curve is shown in figure 34. The global evolution of the $O-C$ diagram is remarkably similar to those of GW Lib and V455 And (Kato et al. 2009a) except the six rebrightenings after the major disturbance in the $O-C$. The late stage (during rebrightenings and after rebrightenings) superhumps can be interpreted as an extension on the stage B superhumps.

The amplitudes of superhumps (after subtracting for the orbital variation) during the rebrightening systematically varied depending on the brightness of the system (figure 35). The amplitudes increased when the system became fainter. The tendency appears to be well explained by assuming the constant luminosity of the superhump source and assuming variable contribution from the accretion disk. The general tendency in amplitudes of superhumps is similar to what was observed in persistent negative superhumps in V503 Cyg (Harvey et al. 1995) and MN Dra (Pavlenko et al. 2010b), and superhumps during the rebrightening phase of EG Cnc (Patterson et al. 1998; Kato et al. 2004a) and WZ Sge (cf. Patterson et al. 2002; reanalysis of the data in Kato et al. 2009a is shown in figure 36). The tendency showed a deviation from this relation around and after the final rebrightening. The decreased strength of superhumps, or tidal dissipation, may have prevented further rebrightenings to occur. The phenomenon (immediately following the rebrightening phase) has been also confirmed in the 2001 superoutburst of WZ Sge (figure 36).

3.28. SDSS J081207.63+131824.4

This object (hereafter SDSS J0812) was selected as a CV by Szkody et al. (2007). The outburst detection by K. Itagaki in 2008 led to a classification as an SU UMa-type dwarf nova (Kato et al. 2009a). The object was again in outburst in 2011 March (I. Miller, baavss-alert 2561, vsnet-alert 13019). Subsequent observations detected superhumps (vsnet-alert 13024, 13025). Although Kato et al. (2009a) reported a period of 0.08432(1) d, the new observations indicated that this period was a wrong alias (vsnet-alert 13030; figure 37). The times of superhump maxima for 2008 (updated) and 2011 superoutbursts are

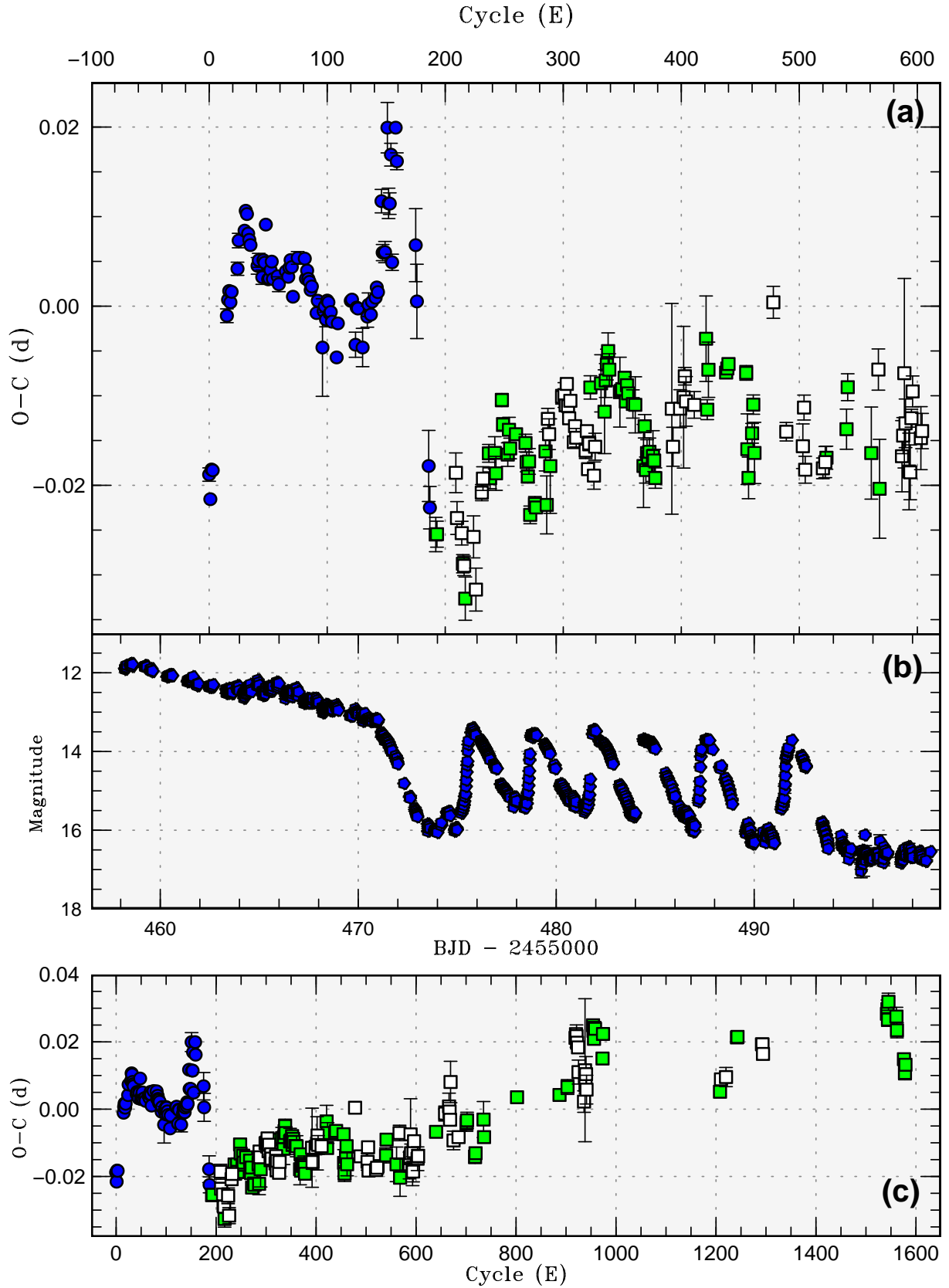
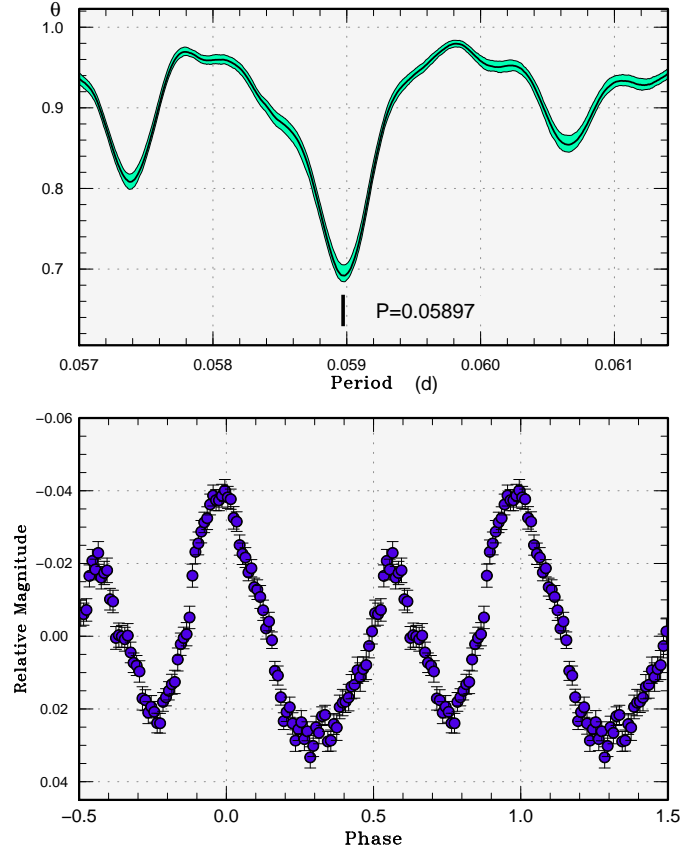


Fig. 34. $O-C$ diagram of superhumps in SDSS J0804 (2010). (a) $O-C$. Open squares indicate humps coinciding with the phase of orbital humps during the rebrightening phase. Filled squares are humps outside the phase of orbital humps and humps recorded during the plateau phase. We used a period of 0.05962 d for calculating the $O-C$'s. (b) Light curve. (c) $O-C$ diagram of the entire observation. The global evolution of the $O-C$ diagram is remarkably similar to those of GW Lib and V455 And (Kato et al. 2009a) except the six rebrightenings after the major disturbance in the $O-C$ diagram.

Table 38. Superhump maxima of SDSS J0804 (2010).

E	max*	error	$O - C^\dagger$	phase ‡	N^\S
0	55462.4512	0.0007	-0.0188	0.53	59
1	55462.5081	0.0006	-0.0216	0.49	190
2	55462.5710	0.0006	-0.0183	0.56	198
3	55462.6305	0.0006	-0.0184	0.57	129
15	55463.3632	0.0008	-0.0014	0.99	174
16	55463.4246	0.0001	0.0003	0.03	690
17	55463.4852	0.0002	0.0013	0.06	529
18	55463.5436	0.0002	0.0000	0.04	281
19	55463.6044	0.0003	0.0011	0.07	185
24	55463.9051	0.0007	0.0036	0.17	48
25	55463.9678	0.0008	0.0067	0.23	48
30	55464.2670	0.0003	0.0077	0.30	143
31	55464.3289	0.0002	0.0099	0.35	744
32	55464.3881	0.0001	0.0095	0.36	691
33	55464.4456	0.0004	0.0073	0.33	180
34	55464.5045	0.0002	0.0066	0.33	438
35	55464.5635	0.0001	0.0060	0.33	871
41	55464.9189	0.0009	0.0035	0.35	47
42	55464.9792	0.0008	0.0041	0.37	44
45	55465.1561	0.0008	0.0022	0.37	108
46	55465.2177	0.0002	0.0041	0.42	521
47	55465.2770	0.0002	0.0038	0.42	808
48	55465.3409	0.0004	0.0080	0.50	266
50	55465.4540	0.0007	0.0018	0.42	86
51	55465.5137	0.0005	0.0019	0.43	151
52	55465.5743	0.0003	0.0028	0.46	219
53	55465.6348	0.0004	0.0038	0.49	147
54	55465.6925	0.0004	0.0018	0.46	95
58	55465.9313	0.0006	0.0020	0.51	56
59	55465.9900	0.0008	0.0011	0.51	40
65	55466.3492	0.0005	0.0024	0.59	49
67	55466.4678	0.0005	0.0017	0.60	93
68	55466.5285	0.0004	0.0027	0.63	200
69	55466.5889	0.0004	0.0036	0.66	124
70	55466.6478	0.0003	0.0028	0.65	159
71	55466.7041	0.0004	-0.0006	0.61	119
75	55466.9469	0.0007	0.0037	0.72	47
81	55467.3045	0.0007	0.0035	0.78	86
82	55467.3619	0.0003	0.0012	0.76	275
83	55467.4224	0.0002	0.0021	0.78	668
84	55467.4811	0.0003	0.0011	0.78	181
85	55467.5404	0.0003	0.0008	0.78	161
86	55467.5991	0.0005	-0.0002	0.78	55
87	55467.6591	0.0003	0.0002	0.79	50
91	55467.8947	0.0005	-0.0029	0.78	64
92	55467.9557	0.0003	-0.0015	0.82	175
96	55468.1889	0.0054	-0.0068	0.77	26
97	55468.2526	0.0005	-0.0028	0.85	198
98	55468.3127	0.0004	-0.0023	0.87	681
99	55468.3709	0.0008	-0.0038	0.86	324
100	55468.4326	0.0003	-0.0017	0.90	306
101	55468.4921	0.0002	-0.0019	0.91	886
102	55468.5504	0.0003	-0.0031	0.90	289

*BJD-2400000.

 † Against max = 2455462.4700 + 0.059643*E*. ‡ Orbital phase. § Number of points used to determine the maximum.**Fig. 27.** Early superhumps in SDSS J0804 (2010). (Upper): PDM analysis. (Lower): Phase-averaged profile.

listed in tables 41 and 42, respectively.

A comparison of $O - C$ diagrams (figure 38) suggests that there is a short (~ 40 cycles or slightly longer) stage B with a relatively constant P_{SH} and subsequent stage C common to these two superoutbursts. Since these stages were identifiable in the 2011 superoutburst, we gave values for these stages in table 3. There was an apparent gap in stage B in the 2008 superoutburst and we gave a global value. The large negative P_{dot} likely referred to a stage B-C transition. The global behavior of the $O - C$ diagram is not very different from that of HT Cas (subsection 3.7) with a similar P_{SH} .

3.29. SDSS J093249.57+472523.0

This object (hereafter SDSS J0932) was selected as a short-period ($P_{orb} = 1.7$ hr) CV by Szkody et al. (2004). Homer et al. (2006) clarified its eclipsing nature and suspected that it is an intermediate polar based on X-ray observations.

This object was for the first time detected in outburst on 2011 March 18 at an unfiltered CCD magnitude of 14.9 (J. Shears, baavss-alert 2537). Subsequent observations immediately detected superhumps (vsnet-alert 13006, 13020, 13034, 13042; figure 39). The observed eclipse minima during the current outburst confirmed the shorter alias for P_{orb} given by Homer et al.

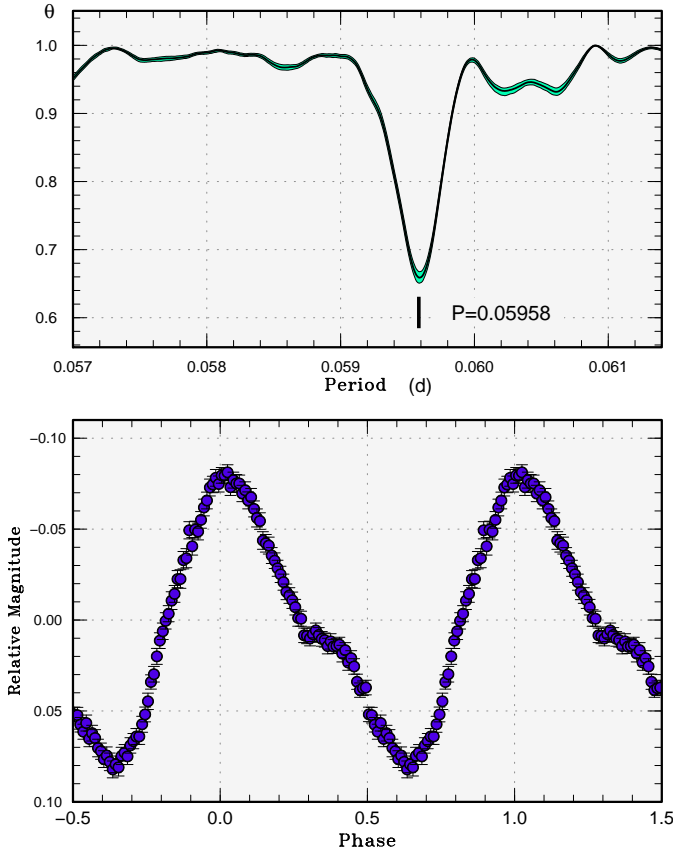


Fig. 28. Ordinary superhumps in SDSS J0804 (2010). (Upper): PDM analysis. (Lower): Phase-averaged profile.

(2006). The times of recorded eclipses, determined with the Kwee and van Woerden (KW) method (Kwee, van Woerden 1956), after removing linearly approximated trends around eclipses in order to minimize the effect of superhumps, are summarized in table 43. The resultant refined ephemeris is as follows:

$$\text{Min(BJD)} = 2453106.6834(2) + 0.066303547(6)E. \quad (2)$$

The times of superhump maxima determined from observations outside the eclipses are listed in table 44. There was no significant global trend of period variation. It is likely that we only observed stage C superhumps. The values given in table 3 follows this identification. The fractional superhump excess was 2.7 %. We also obtained post-superoutburst observations. Due to the faintness of the object and low signal of superhumps, we only obtained a mean period of 0.06814(4) d with the PDM method for the interval of BJD 2455650.3–2455656.2. This period is practically identical with the period in stage C and these superhumps are likely persistent superhumps in post-superoutburst stage of short- P_{orb} systems (e.g. Ohshima et al. 2011b).

3.30. SDSS J112003.40+663632.4

This object (hereafter SDSS J1120) was initially selected as a dwarf nova by Wils et al. (2010). The 2011

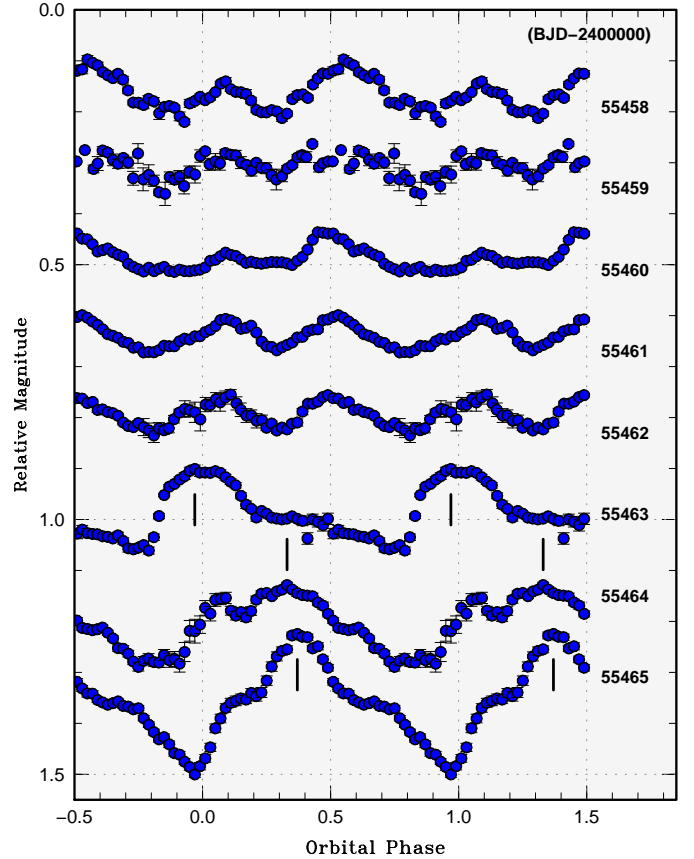


Fig. 29. Transition from early superhumps to ordinary superhumps in SDSS J0804 (2010). Early superhumps were observed on the first five nights. Ordinary superhumps (ticks) seem to grow from the first (around orbital phase 0.1) one of the double humps of early superhumps. The orbital phases were determined using the updated period of 0.05900495 d after combination of quiescent analysis in Kato et al. 2009b and post-superoutburst observations in 2010. The phase zero is defined as the expected phase of eclipses.

outburst was detected on February 14.838 UT at an unfiltered CCD magnitude of 15.7 by J. Shears (baavss-alert 2513). Superhump were detected by S. Brady (baavss-alert 2514). We analyzed the available data and obtained the times of superhump maxima (table 45). It was not possible to identify the stage of superhump evolution. The result of PDM analysis and mean profile are shown in figure 40.

3.31. SDSS J114628.80+675907.7

This object (hereafter SDSS J1146) is a CV selected during the course of the SDSS (Szkody et al. 2003). Szkody et al. (2003) reported an orbital period of 1.6 hr based on radial-velocity study. Although the spectrum suggested a dwarf nova in quiescence, no major outburst had been recorded. A small outburst was recorded on 2009 April 17 at an unfiltered CCD magnitude of 16.9 (J. Shears, cvnet-outburst 3062). J. Shears also detected an outburst on 2011 January 3 during its rising phase (baavss-alert 2459). Subsequent observations recorded

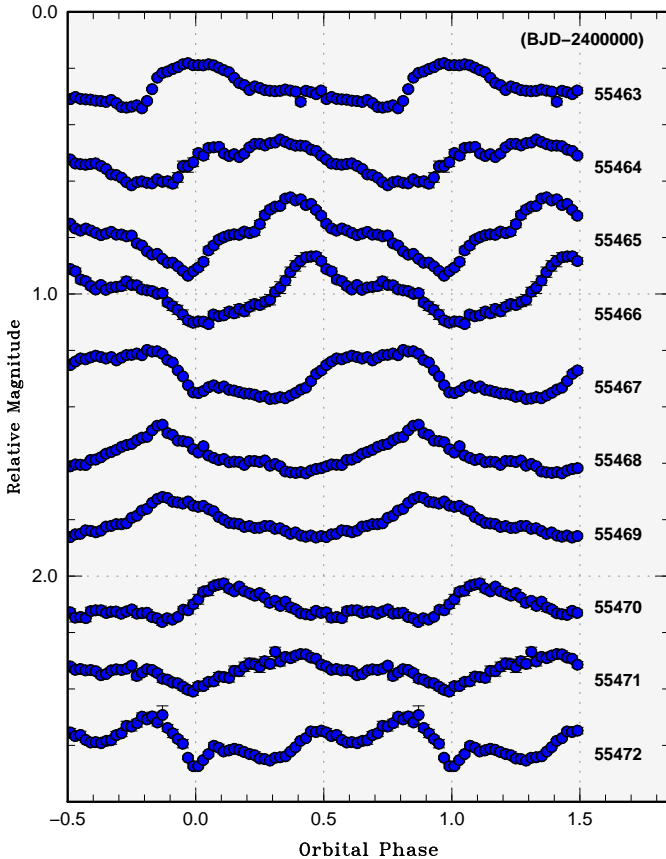


Fig. 30. Variation of profiles of ordinary superhumps in SDSS J0804 (2010). The definition of the phase is as in figure 29. Shallow eclipses were seen on BJD 2455464–2455467 and BJD 2455471–2455472.

growing superhumps (vsnet-alert 12567, 12576, 12579; figure 41).

The times of superhump maxima are listed in table 46. The values given in table 3 are somewhat uncertain because the middle of stage B was not very well observed and only the initial part of stage C was observed.

3.32. *SDSS J122740.83+513925.0*

This object (hereafter SDSS J1227) is an eclipsing SU UMa-type dwarf nova whose superoutburst was first recorded in 2007. This 2007 superoutburst was analyzed by Shears et al. (2008) and Kato et al. (2009a). Another superoutburst was observed in 2011. By using eclipses observed during the 2011 observations (table 47), it has become evident that the alias selection of the orbital ephemeris in Kato et al. (2009a) was incorrect. We have revised the eclipse ephemeris as follows:

$$\text{Min(BJD)} = 2453796.2417(6) + 0.06295041(3)E. \quad (3)$$

We have updated the results of the 2007 superoutburst because the significant addition to the data published in Kato et al. (2009a). The times of superhump maxima are listed in table 48. The data now clearly show all stages A–C and a positive P_{dot} for stage B. The updated parameters

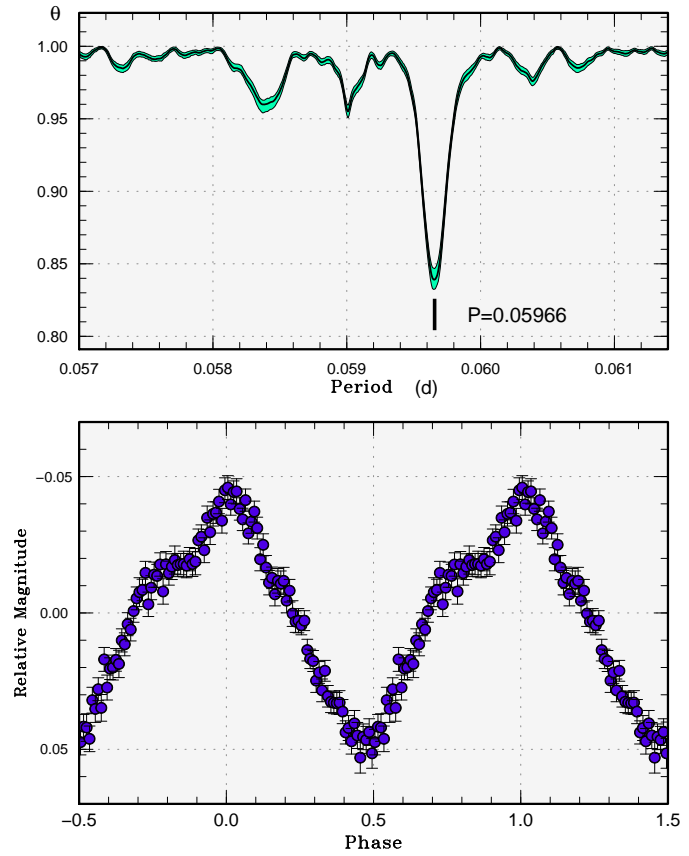


Fig. 31. Superhumps in SDSS J0804 (2010) during the re-brightening phase (BJD 2455472.5–2455494.0) after subtracting the global variations of re-brightenings, but not subtracting the orbital variations (Upper): PDM analysis. A weaker signal at $P = 0.05901$ d corresponds to the orbital period. (Lower): Phase-averaged profile.

are listed in table 3.

The 2011 outburst was detected by CRTS (= CSS110312:122741+513925). The outburst was apparently observed during its middle-to-late stage. The times of superhump maxima outside the eclipses are listed in table 49. A stage B–C transition was recorded. A combined $O-C$ diagram is shown in figure 42.

3.33. *SDSS J125023.85+665525.5*

We have observed the 2011 superoutburst of this eclipsing SU UMa-type dwarf nova (hereafter SDSS J1250). In analyzing the data, we used the refined ephemeris of eclipses (equation 4).

$$\text{Min(BJD)} = 2453407.5595(3) + 0.058735696(9)E. \quad (4)$$

The times of superhump maxima are listed in table 50. Although we likely observed stages B and C, we only measured the mean period due to the gap in the observation.

3.34. *SDSS J133941.11+484727.5*

SDSS J133941.11+484727.5 (hereafter SDSS J1339) is a CV selected during the course of the SDSS (Szkody et al.

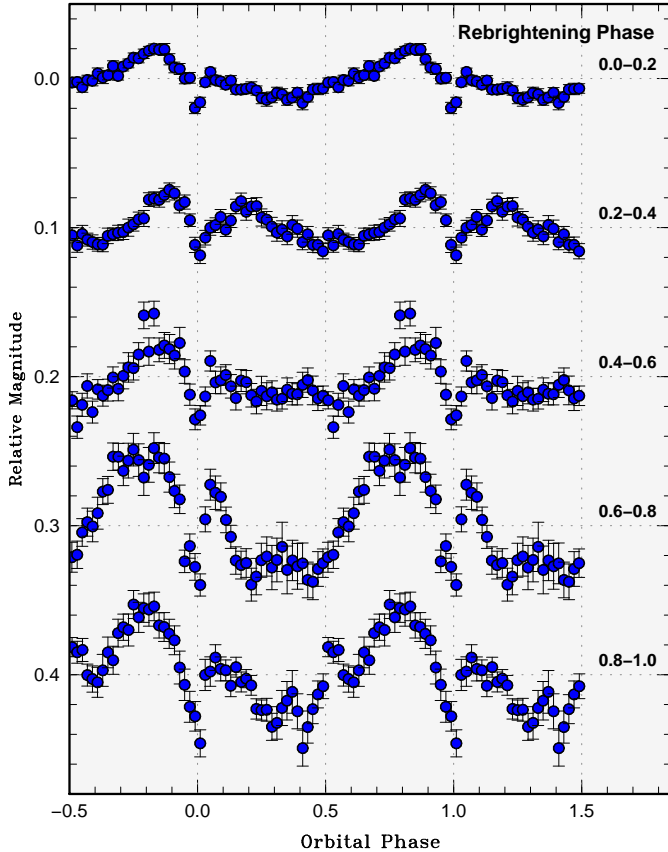


Fig. 32. Dependence of orbital variation of SDSS J0804 (2010) on the rebrightening phase. The data are the same as in figure 31. The zero phase of rebrightening is defined as the peak of each rebrightening. The amplitudes of orbital humps and depths of eclipses increased as the system faded from the peak of rebrightening.

2006). Szkody et al. (2006) reported a possible orbital period of 1.7 hr and the presence of features of a white dwarf in the spectrum, suggesting a WZ Sge-type dwarf nova. Gänsicke et al. (2006) obtained an orbital period of 0.05731(2) d and showed the presence of ZZ Cet-type pulsation of the white dwarf. Gänsicke et al. (2006) also found a long-period photometric variation, similar to the ones observed in GW Lib (Woudt, Warner 2002) and FS Aur (Neustroev 2002), whose origin is yet unknown.

The 2011 outburst, the first known outburst in its history, was detected by J. Shears on February 7.919 at a visual magnitude of 10.4 (baavss-alert 2501). P. Schmeer also made an independent detection of the outburst (vsnet-alert 12806).

Early observations detected low-amplitude (~ 0.015 – 0.025 mag) variations which can be attributed to early superhumps (vsnet-alert 12817, 12819, 12820). Early spectroscopy by A. Arai detected $H\alpha$ in emission and other Balmer lines in absorption. Although HeII emission was absent, CIII/NIII emission lines were possibly present (vsnet-alert 12822). The spectroscopic feature was less striking compared to the 2001 superoutburst of WZ Sge

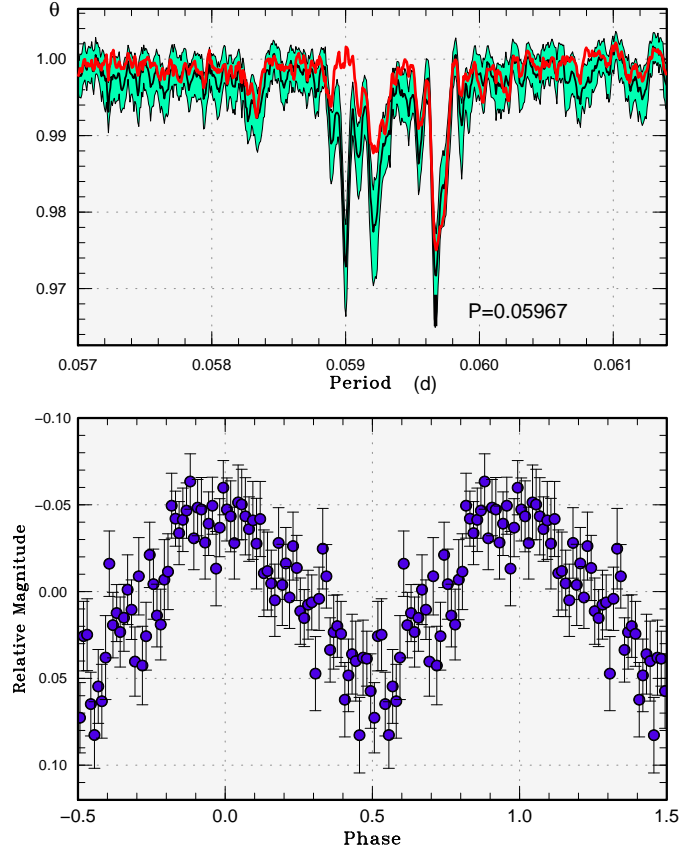


Fig. 33. Superhumps in SDSS J0804 (2010) during the post-rebrightening phase (after BJD 2455494.0) after subtracting the global variations of rebrightenings. (Upper): PDM analysis. A signal at $P = 0.05901$ d corresponds to the orbital period. The overlaid thick curve (red in the electronic version) is θ diagram after subtracting the orbital signal. (Lower): Phase-averaged profile.

(Baba et al. 2002).

Ordinary superhumps emerged four days after the outburst detection (vsnet-alert 12835, 12836, 12837). After 13 d, the object started to fade rapidly. In contrast to many WZ Sge-type dwarf novae, the object did not show post-superoutburst rebrightenings.

The times of ordinary superhumps are listed in table 51. The stages A and B are clearly recognized (cf. figure 43). During the rapid fading phase, the phase of superhumps were apparently reversed and the reversed phase continued during the entire post-superoutburst state.

During the post-superoutburst phase, a beat phenomenon between persisting superhumps and the orbital signal was strongly present (vsnet-alert 12943; figure 45). We have obtained the orbital period of 0.057289(1) d from these observations (cf. figure 44). This period is in good agreement with the period determined from radial-velocity study (Gänsicke et al. 2006). The times of superhumps during the post-superoutburst stage were determined after subtracting the averaged orbital variations (table 52). The tables includes the initial eight epochs

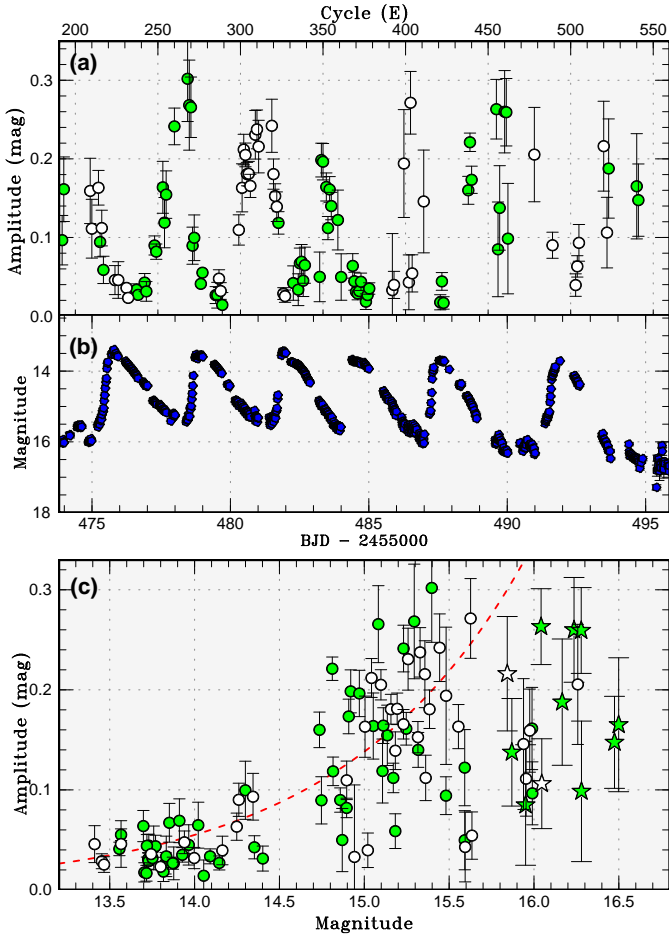


Fig. 35. Amplitudes of superhumps in SDSS J0804 (2010) during the rebrightening phase. (a) Amplitudes. Open circles indicate humps coinciding with the phase of orbital humps during the rebrightening phase. Filled circles are humps outside the phase of orbital humps and humps recorded during the plateau phase. (b) Light curve. (c) Relation between amplitudes and system brightness. The circle symbols are as in the panel (a). The star-shaped symbols represent humps during the quiescence immediately before and after the final rebrightening. The amplitudes increase when the system becomes fainter. The broken curve represents the relation assuming the constant luminosity of the superhump source and variable contribution from the accretion disk.

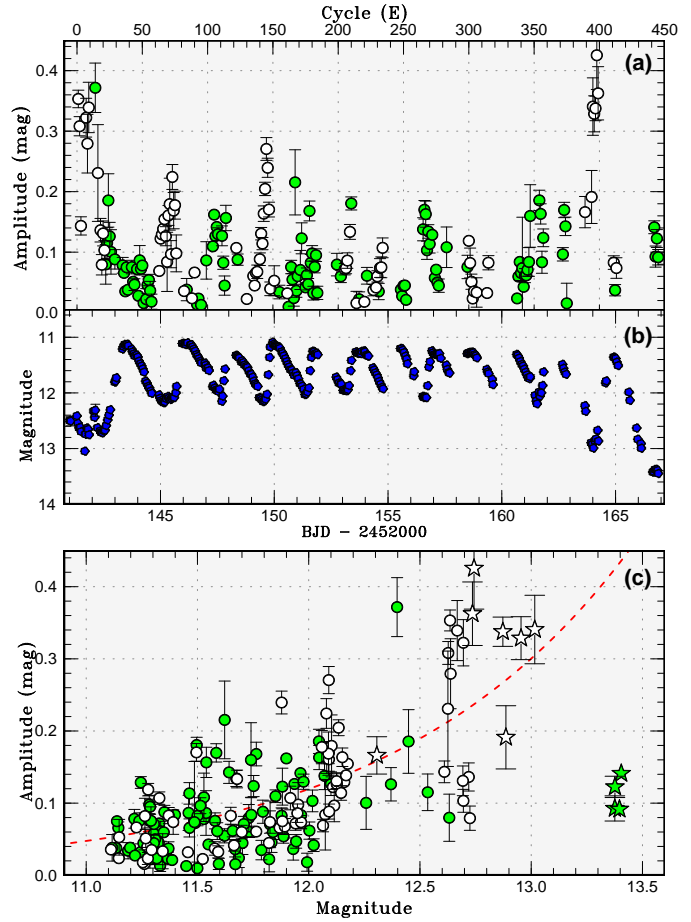


Fig. 36. Amplitudes of superhumps in WZ Sge (2001) during the rebrightening phase. (a) Amplitudes. Open circles indicate humps coinciding with the phase of orbital humps during the rebrightening phase. Filled circles are humps outside the phase of orbital humps and humps recorded during the plateau phase. (b) Light curve. (c) Relation between amplitudes and system brightness. The circle symbols are as in the panel (a). The star-shaped symbols represent humps during the quiescence immediately before and after the final rebrightening. The amplitudes increase when the system becomes fainter. The broken curve represents the relation assuming the constant luminosity of the superhump source and variable contribution from the accretion disk. The amplitude of humps immediately preceding the final rebrightening may have been affected by the overlapping orbital humps.

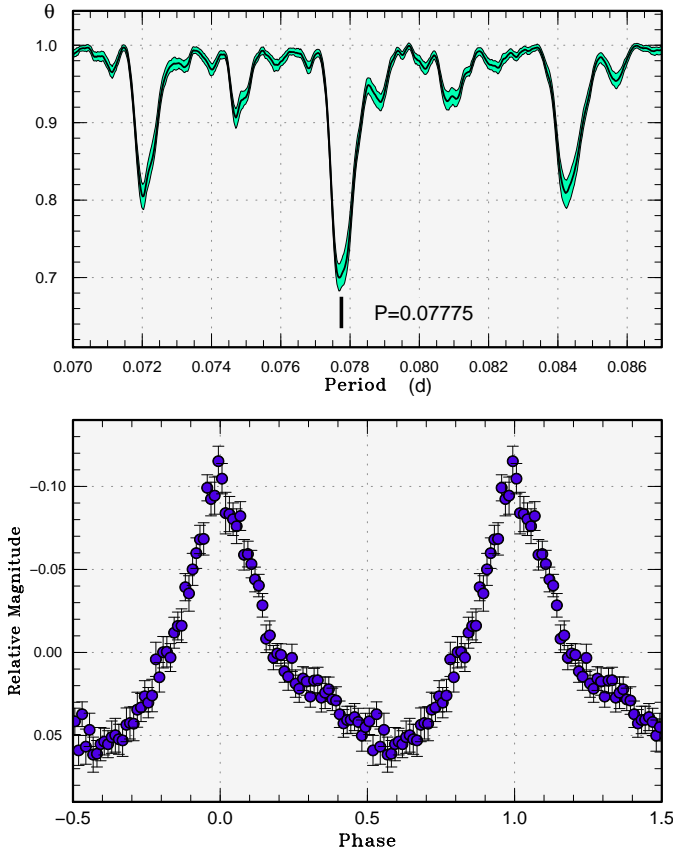


Fig. 37. Superhumps in SDSS J0812 (2011). (Upper): PDM analysis. (Lower): Phase-averaged profile.

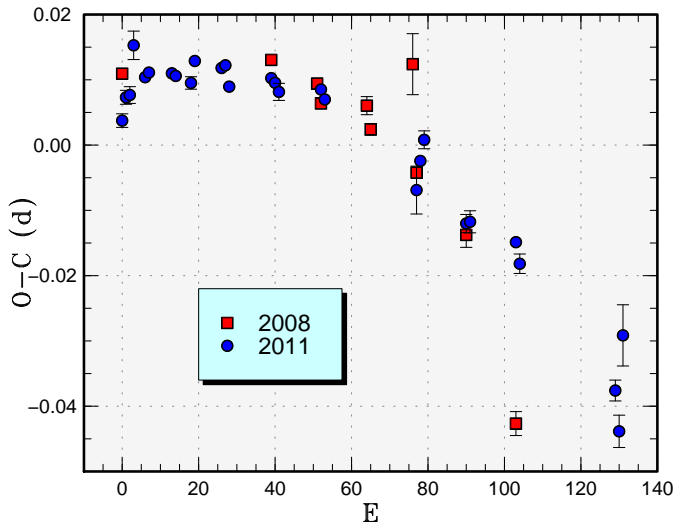


Fig. 38. Comparison of $O-C$ diagrams of SDSS J0812 between different superoutbursts. A period of 0.07798 d was used to draw this figure. Cycle counts (E) after the detection of the outburst were used. The true epochs of the starts of outbursts were unknown.

Table 38. Superhump maxima of SDSS J0804 (2010) (continued).

E	max*	error	$O-C^\dagger$	phase ‡	N^\S
103	55468.6102	0.0003	-0.0030	0.91	275
104	55468.6687	0.0004	-0.0041	0.90	90
108	55468.9032	0.0006	-0.0082	0.88	110
109	55468.9667	0.0005	-0.0044	0.95	174
120	55469.6250	0.0004	-0.0021	0.11	91
121	55469.6848	0.0004	-0.0020	0.12	92
124	55469.8586	0.0014	-0.0071	0.07	31
125	55469.9223	0.0005	-0.0030	0.15	169
126	55469.9819	0.0005	-0.0031	0.16	159
130	55470.2160	0.0021	-0.0076	0.13	62
134	55470.4579	0.0012	-0.0042	0.23	46
135	55470.5189	0.0013	-0.0029	0.26	31
137	55470.6370	0.0004	-0.0041	0.26	91
138	55470.6981	0.0003	-0.0027	0.30	89
141	55470.8774	0.0004	-0.0023	0.33	98
142	55470.9381	0.0002	-0.0011	0.36	218
143	55470.9972	0.0003	-0.0017	0.37	131
146	55471.1862	0.0013	0.0084	0.57	189
147	55471.2401	0.0009	0.0026	0.48	435
148	55471.2997	0.0004	0.0026	0.49	479
149	55471.3594	0.0012	0.0026	0.50	162
151	55471.4925	0.0028	0.0165	0.76	26
152	55471.5437	0.0017	0.0080	0.63	28
153	55471.6033	0.0012	0.0080	0.64	111
154	55471.6684	0.0013	0.0134	0.74	90
155	55471.7160	0.0009	0.0014	0.55	70
158	55471.9099	0.0006	0.0163	0.83	142
159	55471.9658	0.0009	0.0126	0.78	175
175	55472.9103	0.0041	0.0028	0.79	45
176	55472.9637	0.0042	-0.0035	0.69	45
186	55473.5415	0.0040	-0.0221	0.49	16
187	55473.5964	0.0024	-0.0268	0.42	16

*BJD-2400000.

† Against max = 2455462.4701 + 0.059636E.

‡ Orbital phase.

§ Number of points used to determine the maximum.

which were observed as the secondary maxima during the final stage of the plateau (cf. subsection 4.5.3). These maxima were measured using phases -0.2 to 0.2 of the humps in order to reduce the contamination from the primary maxima. The mean periods of late-stage superhumps were 0.058175(3) d ($18 \leq E \leq 428$) and 0.058183(5) d ($495 \leq E \leq 985$).

Since the amplitudes of early superhumps were very low, and since some of observations were made under non-ideal conditions (due to the sparse field, the comparison star was much fainter than the variable in some observations), we have analyzed a selected high-quality subset selected from the data before BJD 2455604.2. A PDM analysis of the data yielded a signal of 0.05689(2) d in addition to the likely signal of emerging ordinary superhumps (signals around 0.059–0.062 d, upper panel of figure 46). Since this signal is very weak and the baseline

Table 39. Superhump maxima of J0804 (2010) during the rebrightening phase.

E	max*	error	$O - C^\dagger$	phase [‡]	N^\S
0	55473.8915	0.0019	-0.0057	0.42	24
1	55473.9512	0.0015	-0.0056	0.43	23
17	55474.9120	0.0022	0.0007	0.71	12
18	55474.9665	0.0018	-0.0044	0.64	23
22	55475.2033	0.0013	-0.0063	0.65	79
23	55475.2595	0.0010	-0.0097	0.60	126
24	55475.3189	0.0011	-0.0100	0.61	133
25	55475.3749	0.0024	-0.0137	0.56	46
32	55475.7991	0.0023	-0.0070	0.75	32
34	55475.9125	0.0024	-0.0130	0.67	21
39	55476.2214	0.0009	-0.0023	0.90	283
40	55476.2826	0.0013	-0.0008	0.94	342
45	55476.5835	0.0010	0.0019	0.04	128
46	55476.6403	0.0012	-0.0010	0.00	140
50	55476.8817	0.0018	0.0017	0.09	75
51	55476.9390	0.0019	-0.0006	0.07	90
56	55477.2453	0.0007	0.0074	0.26	235
57	55477.3022	0.0008	0.0047	0.22	269
61	55477.5373	0.0013	0.0012	0.21	18
62	55477.5997	0.0014	0.0039	0.26	20
63	55477.6572	0.0012	0.0018	0.24	18
68	55477.9569	0.0005	0.0032	0.32	77
76	55478.4329	0.0010	0.0019	0.38	24
77	55478.4904	0.0011	-0.0002	0.36	22
78	55478.5484	0.0007	-0.0019	0.34	56
79	55478.6097	0.0014	-0.0002	0.38	60
80	55478.6633	0.0010	-0.0062	0.29	27
84	55478.9030	0.0008	-0.0051	0.35	81
85	55478.9623	0.0005	-0.0056	0.36	83
93	55479.4455	0.0022	0.0004	0.55	23
94	55479.4991	0.0032	-0.0056	0.45	23
95	55479.5684	0.0012	0.0040	0.63	22
96	55479.6263	0.0017	0.0022	0.61	23
97	55479.6823	0.0053	-0.0014	0.56	15
107	55480.2863	0.0008	0.0060	0.79	199
109	55480.4057	0.0014	0.0061	0.82	14
110	55480.4642	0.0005	0.0050	0.81	34
111	55480.5262	0.0005	0.0073	0.86	84
112	55480.5833	0.0005	0.0048	0.83	99
113	55480.6416	0.0005	0.0034	0.82	102
114	55480.7032	0.0006	0.0053	0.86	74
117	55480.8774	0.0007	0.0006	0.81	45
118	55480.9388	0.0007	0.0024	0.85	65
119	55480.9971	0.0010	0.0010	0.84	55
127	55481.4726	0.0009	-0.0007	0.90	40
128	55481.5345	0.0005	0.0015	0.95	126
129	55481.5898	0.0007	-0.0028	0.89	128
130	55481.6523	0.0008	0.0000	0.95	108
131	55481.7182	0.0013	0.0062	0.06	37
134	55481.8872	0.0015	-0.0037	0.93	66
135	55481.9500	0.0015	-0.0005	0.99	65

*BJD-2400000.

†Against max = 2455473.8972 + 0.059655*E*.

‡Orbital phase.

§Number of points used to determine the maximum.

Table 39. Superhump maxima of J0804 (2010) during the rebrightening phase (continued).

E	max*	error	$O - C^\dagger$	phase [‡]	N^\S
140	55482.2552	0.0032	0.0064	0.16	30
143	55482.4309	0.0047	0.0031	0.14	62
144	55482.4940	0.0019	0.0066	0.21	153
145	55482.5554	0.0017	0.0083	0.25	198
146	55482.6165	0.0020	0.0098	0.29	193
147	55482.6741	0.0018	0.0077	0.26	149
156	55483.2082	0.0039	0.0048	0.31	102
157	55483.2680	0.0005	0.0050	0.33	170
158	55483.3277	0.0006	0.0051	0.34	142
160	55483.4483	0.0006	0.0063	0.38	152
161	55483.5052	0.0007	0.0036	0.35	173
162	55483.5667	0.0006	0.0054	0.39	178
163	55483.6254	0.0007	0.0045	0.38	87
167	55483.8627	0.0016	0.0031	0.41	34
169	55483.9818	0.0031	0.0030	0.43	29
176	55484.3923	0.0046	-0.0041	0.38	11
177	55484.4564	0.0013	0.0003	0.47	68
178	55484.5111	0.0015	-0.0046	0.40	88
179	55484.5726	0.0015	-0.0028	0.44	197
180	55484.6318	0.0010	-0.0032	0.44	195
181	55484.6920	0.0015	-0.0027	0.46	89
184	55484.8704	0.0028	-0.0033	0.48	124
185	55484.9295	0.0012	-0.0038	0.49	135
186	55484.9872	0.0011	-0.0058	0.46	139
200	55485.8296	0.0118	0.0015	0.74	18
201	55485.8850	0.0022	-0.0028	0.68	38
207	55486.2469	0.0021	0.0012	0.81	37
210	55486.4271	0.0079	0.0024	0.87	17
211	55486.4890	0.0010	0.0047	0.92	60
212	55486.5459	0.0028	0.0019	0.88	96
219	55486.9628	0.0015	0.0012	0.95	13
229	55487.5664	0.0048	0.0083	0.18	64
230	55487.6181	0.0011	0.0003	0.05	65
231	55487.6822	0.0031	0.0047	0.14	63
246	55488.5761	0.0005	0.0039	0.29	107
247	55488.6362	0.0003	0.0043	0.31	111
248	55488.6963	0.0005	0.0048	0.33	77
263	55489.5897	0.0008	0.0033	0.47	64
264	55489.6408	0.0039	-0.0053	0.33	43
265	55489.6972	0.0023	-0.0085	0.29	43
268	55489.8810	0.0011	-0.0036	0.40	27
269	55489.9438	0.0011	-0.0005	0.47	23
270	55489.9981	0.0034	-0.0059	0.39	21
286	55490.9688	0.0018	0.0104	0.84	18
297	55491.6102	0.0010	-0.0045	0.71	56
311	55492.4432	0.0025	-0.0066	0.83	74
312	55492.5072	0.0014	-0.0023	0.91	76
313	55492.5598	0.0015	-0.0093	0.80	37
328	55493.4543	0.0012	-0.0096	0.96	18
330	55493.5742	0.0017	-0.0090	1.00	71
331	55493.6343	0.0013	-0.0085	0.01	51

*BJD-2400000.

†Against max = 2455473.8972 + 0.059655*E*.

‡Orbital phase.

§Number of points used to determine the maximum.

Table 40. Superhump maxima of SDSS J0804 (2010) during the post-rebrightening phase.

E	max*	error	$O - C^\dagger$	phase ‡	N^\S
0	55494.6511	0.0022	-0.0052	0.25	39
1	55494.7154	0.0015	-0.0005	0.34	73
21	55495.9004	0.0051	-0.0086	0.42	21
27	55496.2675	0.0023	0.0005	0.64	70
28	55496.3138	0.0055	-0.0128	0.42	94
47	55497.4502	0.0040	-0.0099	0.68	17
48	55497.5121	0.0020	-0.0076	0.73	17
49	55497.5787	0.0106	-0.0007	0.86	16
50	55497.6327	0.0027	-0.0063	0.78	17
53	55497.8062	0.0043	-0.0118	0.72	15
54	55497.8657	0.0031	-0.0120	0.73	23
55	55497.9314	0.0010	-0.0060	0.84	22
56	55497.9940	0.0017	-0.0030	0.90	21
63	55498.4061	0.0035	-0.0085	0.88	15
64	55498.4665	0.0020	-0.0077	0.91	16
100	55500.6201	0.0009	-0.0018	0.41	17
118	55501.6987	0.0022	0.0029	0.69	28
126	55502.1777	0.0039	0.0047	0.81	100
127	55502.2358	0.0014	0.0032	0.79	228
128	55502.2930	0.0014	0.0007	0.76	180
129	55502.3639	0.0061	0.0119	0.96	116
135	55502.7042	0.0028	-0.0057	0.73	31
145	55503.3014	0.0014	-0.0051	0.85	86
161	55504.2593	0.0023	-0.0017	0.08	138
162	55504.3199	0.0024	-0.0007	0.11	102
178	55505.2630	0.0020	-0.0122	0.09	85
179	55505.3237	0.0010	-0.0111	0.12	132
195	55506.2876	0.0054	-0.0017	0.46	80
196	55506.3420	0.0013	-0.0070	0.38	87
262	55510.2888	0.0015	0.0025	0.27	74
347	55515.3572	0.0014	0.0000	0.17	60
363	55516.3134	0.0022	0.0018	0.37	125
379	55517.2820	0.0018	0.0158	0.79	25
380	55517.3427	0.0015	0.0169	0.82	25
381	55517.4017	0.0033	0.0162	0.82	25
382	55517.4594	0.0013	0.0143	0.79	26
384	55517.5772	0.0016	0.0128	0.79	26
385	55517.6295	0.0036	0.0054	0.68	15
396	55518.2766	0.0032	-0.0038	0.64	57
398	55518.4051	0.0213	0.0055	0.82	25
399	55518.4603	0.0024	0.0010	0.76	25
400	55518.5232	0.0052	0.0042	0.82	24
401	55518.5782	0.0043	-0.0004	0.76	26
414	55519.3724	0.0015	0.0182	0.22	35
415	55519.4303	0.0015	0.0165	0.20	25
416	55519.4876	0.0008	0.0141	0.17	26
417	55519.5505	0.0007	0.0174	0.23	26
418	55519.6098	0.0008	0.0170	0.24	26
433	55520.4953	0.0008	0.0077	0.25	26

*BJD-2400000.

 † Against max = 2455494.6562 + 0.059657*E*. ‡ Orbital phase. § Number of points used to determine the maximum.**Table 40.** Superhump maxima of SDSS J0804 (2010) during the post-rebrightening phase (continued).

E	max*	error	$O - C^\dagger$	phase ‡	N^\S
434	55520.5622	0.0017	0.0149	0.38	24
668	55534.4961	0.0006	-0.0109	0.53	100
670	55534.6191	0.0004	-0.0073	0.61	142
680	55535.2159	0.0029	-0.0070	0.73	69
702	55536.5394	0.0010	0.0040	0.16	15
703	55536.5991	0.0008	0.0041	0.17	21
752	55539.5183	0.0012	0.0001	0.64	19
753	55539.5779	0.0013	0.0001	0.65	20
754	55539.6347	0.0006	-0.0028	0.62	19
1002	55554.4324	0.0018	-0.0001	0.40	15
1003	55554.4934	0.0027	0.0013	0.44	20
1004	55554.5499	0.0020	-0.0018	0.39	20
1005	55554.6148	0.0025	0.0034	0.49	21
1021	55555.5644	0.0027	-0.0016	0.59	21
1022	55555.6199	0.0023	-0.0057	0.53	21
1036	55556.4460	0.0015	-0.0148	0.53	20
1038	55556.5611	0.0020	-0.0189	0.48	21
1039	55556.6232	0.0010	-0.0166	0.53	18

*BJD-2400000.

 † Against max = 2455494.6562 + 0.059657*E*. ‡ Orbital phase. § Number of points used to determine the maximum.**Table 41.** Superhump maxima of SDSS J0812 (2008).

E	max*	error	$O - C^\dagger$	N^\ddagger
0	54751.2796	0.0002	-0.0150	310
39	54754.3230	0.0006	0.0035	148
51	54755.2551	0.0004	0.0049	274
52	54755.3300	0.0007	0.0023	179
64	54756.2654	0.0014	0.0070	198
65	54756.3398	0.0009	0.0038	113
76	54757.2076	0.0047	0.0184	177
77	54757.2689	0.0008	0.0022	295
90	54758.2731	0.0019	-0.0019	84
103	54759.2580	0.0018	-0.0253	102

*BJD-2400000.

 † Against max = 2454751.2946 + 0.077559*E*. ‡ Number of points used to determine the maximum.

Table 42. Superhump maxima of SDSS J0812 (2011).

E	max*	error	$O - C^\dagger$	N^\ddagger
0	55644.9450	0.0010	-0.0130	144
1	55645.0265	0.0011	-0.0091	212
2	55645.1049	0.0013	-0.0084	111
3	55645.1905	0.0022	-0.0005	45
6	55645.4195	0.0003	-0.0044	83
7	55645.4982	0.0003	-0.0033	73
13	55645.9660	0.0003	-0.0014	96
14	55646.0435	0.0003	-0.0015	102
18	55646.3544	0.0010	-0.0012	46
19	55646.4357	0.0005	0.0025	48
26	55646.9805	0.0002	0.0038	405
27	55647.0589	0.0003	0.0045	350
28	55647.1336	0.0008	0.0016	85
39	55647.9927	0.0004	0.0066	307
40	55648.0700	0.0006	0.0062	178
41	55648.1466	0.0013	0.0051	68
52	55649.0047	0.0004	0.0092	164
53	55649.0812	0.0005	0.0080	165
77	55650.9388	0.0037	0.0021	118
78	55651.0212	0.0006	0.0069	363
79	55651.1025	0.0014	0.0105	200
90	55651.9474	0.0014	0.0014	59
91	55652.0257	0.0017	0.0020	83
103	55652.9583	0.0008	0.0029	303
104	55653.0330	0.0015	-0.0001	264
129	55654.9630	0.0016	-0.0111	110
130	55655.0348	0.0025	-0.0170	112
131	55655.1275	0.0047	-0.0020	86

*BJD-2400000.

 \dagger Against max = 2455644.9580 + 0.077645*E*. \ddagger Number of points used to determine the maximum.**Table 43.** Eclipse minima of SDSS J0932.

E	Minimum*	error	$O - C^\dagger$	Source ‡
0	53106.68364	0.00045	0.00023	1
1	53106.74963	0.00020	-0.00008	1
2	53106.81609	0.00028	0.00008	1
467	53137.64733	0.00016	0.00017	1
468	53137.71340	0.00014	-0.00007	1
469	53137.77931	0.00023	-0.00046	1
470	53137.84620	0.00030	0.00013	1
38202	55639.61176	0.00005	0.00026	2
38203	55639.67801	0.00006	0.00020	2
38209	55640.07542	0.00007	-0.00021	2
38210	55640.14193	0.00006	0.00000	2
38211	55640.20853	0.00007	0.00029	2
38214	55640.40617	0.00010	-0.00097	2
38215	55640.47469	0.00011	0.00124	2
38216	55640.53892	0.00006	-0.00083	2
38217	55640.60456	0.00006	-0.00149	2
38218	55640.67125	0.00005	-0.00111	2
38220	55640.80509	0.00017	0.00013	2
38227	55641.26942	0.00007	0.00033	2
38228	55641.33602	0.00010	0.00063	2
38229	55641.40250	0.00005	0.00080	2
38232	55641.60086	0.00004	0.00025	2
38244	55642.39646	0.00007	0.00022	2
38304	55646.37486	0.00005	0.00039	2
38305	55646.44106	0.00004	0.00030	2
38314	55647.03754	0.00009	0.00004	2
38315	55647.10351	0.00007	-0.00029	2
38319	55647.36886	0.00004	-0.00015	2
38320	55647.43547	0.00005	0.00015	2
38328	55647.96488	0.00006	-0.00087	2
38329	55648.03180	0.00008	-0.00025	2
38330	55648.09873	0.00007	0.00038	2
38364	55650.35295	0.00006	0.00028	2
38365	55650.41921	0.00004	0.00023	2
38366	55650.48497	0.00006	-0.00031	2
38367	55650.55199	0.00008	0.00041	2
38410	55653.40198	0.00005	-0.00066	2
38440	55655.39143	0.00010	-0.00032	2
38442	55655.52489	0.00005	0.00054	2

*BJD-2400000.

 \dagger Against equation 2. \ddagger 1: Homer et al. (2006), 2: this work.

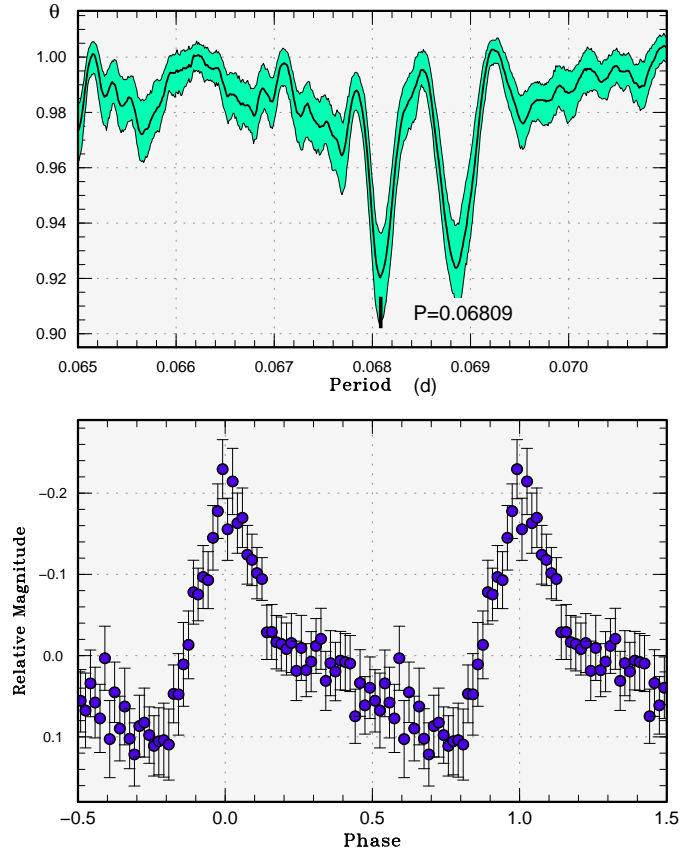
of the observation was not sufficiently long, we used the orbital period as an approximation of the period of early superhumps and extracted the averaged profile. The resultant profile had double-wave modulations characteristic to early superhumps (Kato 2002a), although the full amplitude was only 0.014 mag (lower panel of figure 46).

The relatively large P_{dot} of $+5.4(0.2) \times 10^{-5}$ during stage B in combination with the lack of post-superoutburst rebrightenings is compatible with the type-D classification of WZ Sge-type outbursts (Kato et al. 2009a, subsection 5.3). The delay times of appearance of ordinary superhumps in these type-D outbursts, however, tend to be around ~ 10 d. This delay, corresponding to the phase with early superhumps, was observed only for 4 d in SDSS J1339. Although this short duration more resembled those of type-B outbursts (outbursts with multiple rebrightenings), it may have been a result of the lack of observations around the true maximum. Indeed, S. Ueda reported retrospective positive detections 1.7 d before Miller's detection at unfiltered CCD magnitudes of 9.9 (vsnet-alert 12859). The last negative observations by S. Ueda were reported on January 29, 9 d before detection

Table 44. Superhump maxima of SDSS J0932 (2011).

E	max*	error	$O - C^\dagger$	phase ‡	N^\S
0	55639.5874	0.0013	-0.0089	0.64	42
1	55639.6605	0.0007	-0.0038	0.74	55
7	55640.0662	0.0016	-0.0068	0.86	56
8	55640.1376	0.0016	-0.0035	0.94	66
9	55640.2064	0.0008	-0.0028	0.97	43
11	55640.3556	0.0017	0.0101	0.22	41
12	55640.4179	0.0014	0.0044	0.16	56
13	55640.4874	0.0019	0.0058	0.21	57
14	55640.5540	0.0012	0.0042	0.22	57
16	55640.6848	0.0034	-0.0012	0.19	49
15	55640.6167	0.0018	-0.0012	0.16	64
17	55640.7487	0.0027	-0.0054	0.15	52
18	55640.8208	0.0044	-0.0014	0.24	50
19	55640.8884	0.0036	-0.0019	0.26	28
20	55640.9532	0.0068	-0.0053	0.24	29
25	55641.2991	0.0007	0.0001	0.45	72
26	55641.3651	0.0008	-0.0020	0.45	139
30	55641.6353	0.0015	-0.0043	0.52	71
41	55642.3853	0.0019	-0.0034	0.83	56
56	55643.4156	0.0043	0.0052	0.37	33
70	55644.3637	0.0007	-0.0002	0.67	29
71	55644.4333	0.0008	0.0013	0.72	30
72	55644.5006	0.0020	0.0005	0.74	35
81	55645.1174	0.0032	0.0043	0.04	22
85	55645.3914	0.0019	0.0058	0.17	31
86	55645.4577	0.0016	0.0040	0.17	35
87	55645.5217	0.0024	-0.0001	0.14	35
88	55645.5918	0.0017	0.0019	0.20	35
99	55646.3441	0.0012	0.0050	0.54	90
100	55646.4122	0.0008	0.0050	0.57	110
101	55646.4783	0.0006	0.0030	0.57	61
102	55646.5480	0.0011	0.0046	0.62	37
103	55646.6142	0.0008	0.0027	0.62	34
109	55647.0182	0.0022	-0.0020	0.71	23
110	55647.0894	0.0027	0.0011	0.78	37
111	55647.1597	0.0027	0.0033	0.84	43
114	55647.3625	0.0009	0.0018	0.90	61
115	55647.4297	0.0009	0.0008	0.92	72
123	55647.9826	0.0018	0.0088	0.25	47
124	55648.0505	0.0019	0.0087	0.28	53
158	55650.3542	0.0024	-0.0034	0.02	36
159	55650.4175	0.0016	-0.0082	0.98	36
160	55650.4818	0.0015	-0.0120	0.95	37
161	55650.5473	0.0022	-0.0146	0.94	36

*BJD-2400000.

 † Against max = 2455639.5962 + 0.068110 E . ‡ Orbital phase. § Number of points used to determine the maximum.**Fig. 39.** Superhumps in SDSS J0932 (2011). (Upper): PDM analysis outside the eclipses. (Lower): Phase-averaged profile.**Table 45.** Superhump maxima of SDSS J1120.

E	max*	error	$O - C^\dagger$	N^\ddagger
0	55607.4060	0.0008	-0.0016	95
1	55607.4797	0.0011	0.0016	94
7	55607.9019	0.0004	0.0005	73
8	55607.9716	0.0004	-0.0004	73
21	55608.8893	0.0005	0.0001	72
22	55608.9594	0.0005	-0.0002	73

*BJD-2400000.

 † Against max = 2455607.4076 + 0.070550 E . ‡ Number of points used to determine the maximum.

Table 46. Superhump maxima of SDSS J1146 (2011).

E	max*	error	$O - C^\dagger$	N^\ddagger
0	55565.6927	0.0043	-0.0242	30
1	55565.7744	0.0016	-0.0060	29
2	55565.8387	0.0015	-0.0051	32
3	55565.9048	0.0016	-0.0024	19
9	55566.2962	0.0018	0.0085	111
10	55566.3593	0.0015	0.0081	126
14	55566.6131	0.0004	0.0082	65
15	55566.6766	0.0005	0.0083	51
16	55566.7379	0.0004	0.0063	32
42	55568.3795	0.0006	-0.0011	123
43	55568.4464	0.0005	0.0024	105
72	55570.2859	0.0010	0.0026	249
73	55570.3475	0.0009	0.0009	180
75	55570.4714	0.0012	-0.0021	42
76	55570.5387	0.0010	0.0018	66
77	55570.6011	0.0007	0.0008	68
78	55570.6651	0.0010	0.0014	68
79	55570.7292	0.0008	0.0021	46
80	55570.7937	0.0016	0.0032	23
81	55570.8526	0.0008	-0.0014	46
82	55570.9195	0.0007	0.0021	49
83	55570.9829	0.0013	0.0021	39
88	55571.2960	0.0018	-0.0020	38
89	55571.3605	0.0007	-0.0009	100
90	55571.4255	0.0009	0.0007	96
91	55571.4889	0.0008	0.0007	94
92	55571.5482	0.0019	-0.0035	96
93	55571.6120	0.0009	-0.0031	99
94	55571.6763	0.0012	-0.0022	72
105	55572.3698	0.0009	-0.0063	33

*BJD-2400000.

†Against max = 2455565.7170 + 0.063420*E*.

‡Number of points used to determine the maximum.

Table 47. Eclipse Minima of SDSS J1227 (2011).

E	Minimum*	error	$O - C^\dagger$
29202	55634.51978	0.00002	0.00014
29203	55634.58272	0.00002	0.00012
29215	55635.33819	0.00004	0.00019
29216	55635.40145	0.00014	0.00050
29217	55635.46423	0.00002	0.00033
29218	55635.52706	0.00003	0.00021
29230	55636.28281	0.00009	0.00056
29231	55636.34561	0.00007	0.00040
29232	55636.40864	0.00005	0.00048
29246	55637.28967	0.00005	0.00021
29247	55637.35270	0.00003	0.00028
29248	55637.41573	0.00007	0.00036
29284	55639.68236	0.00008	0.00078
29300	55640.68954	0.00003	0.00075
29391	55646.41865	0.00008	0.00138

*BJD-2400000.

†Against equation 3.

Table 48. Superhump maxima of SDSS J1227 (2007).

E	max*	error	$O - C^\dagger$	phase‡	N^\S
0	54256.4379	0.0004	-0.0286	0.45	-
1	54256.5069	0.0006	-0.0242	0.55	-
33	54258.6069	0.0003	0.0073	0.91	122
34	54258.6736	0.0002	0.0094	0.97	120
35	54258.7360	0.0005	0.0071	0.96	118
40	54259.0627	0.0014	0.0107	0.15	107
61	54260.4136	0.0035	0.0041	0.61	106
63	54260.5428	0.0003	0.0040	0.66	192
75	54261.3100	0.0019	-0.0045	0.85	9
76	54261.3722	0.0019	-0.0069	0.84	18
77	54261.4411	0.0008	-0.0026	0.93	206
78	54261.5108	0.0006	0.0024	0.04	196
80	54261.6413	0.0006	0.0036	0.11	31
81	54261.7049	0.0010	0.0026	0.13	35
82	54261.7706	0.0011	0.0036	0.17	35
86	54262.0321	0.0009	0.0066	0.32	49
91	54262.3468	0.0005	-0.0020	0.32	15
101	54262.9967	0.0009	0.0015	0.64	82
102	54263.0615	0.0012	0.0017	0.67	114
106	54263.3175	0.0014	-0.0008	0.74	15
107	54263.3773	0.0019	-0.0057	0.69	28
111	54263.6418	0.0017	0.0003	0.89	35
112	54263.7040	0.0015	-0.0022	0.88	35
113	54263.7683	0.0025	-0.0026	0.90	35
114	54263.8312	0.0034	-0.0043	0.90	35
122	54264.3573	0.0014	0.0048	0.26	28
123	54264.4203	0.0008	0.0031	0.26	157
124	54264.4892	0.0005	0.0073	0.35	140
126	54264.6180	0.0010	0.0068	0.40	41
127	54264.6821	0.0013	0.0063	0.42	39
128	54264.7453	0.0010	0.0048	0.42	40
129	54264.8122	0.0032	0.0072	0.49	39
137	54265.3267	0.0015	0.0045	0.66	28
138	54265.3906	0.0014	0.0038	0.67	29
153	54266.3706	0.0026	0.0141	0.24	29
168	54267.3243	0.0014	-0.0017	0.39	24
169	54267.3903	0.0012	-0.0004	0.44	23
184	54268.3527	0.0025	-0.0076	0.73	29
199	54269.3141	0.0069	-0.0158	0.00	18
216	54270.4171	0.0015	-0.0117	0.52	17
262	54273.3961	0.0018	-0.0062	0.85	25

*BJD-2400000.

†Against max = 2454256.4664 + 0.064641*E*.

‡Orbital phase.

§Number of points used to determine the maximum.

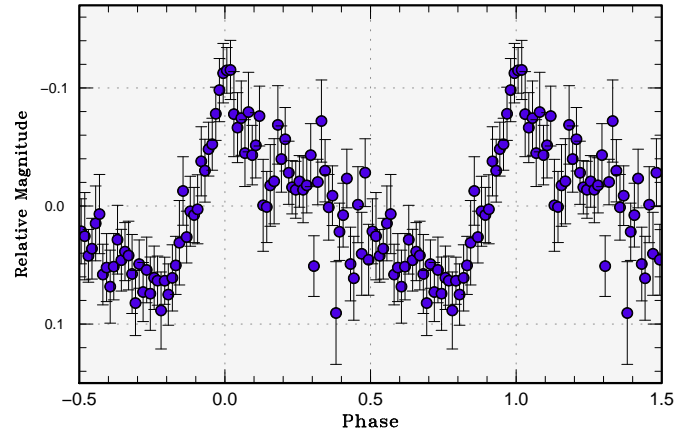
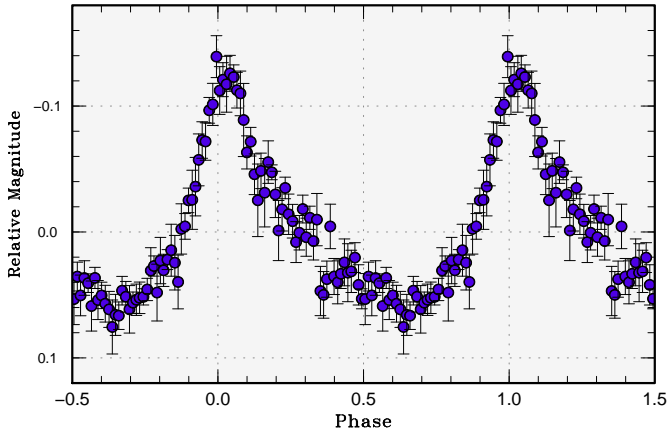
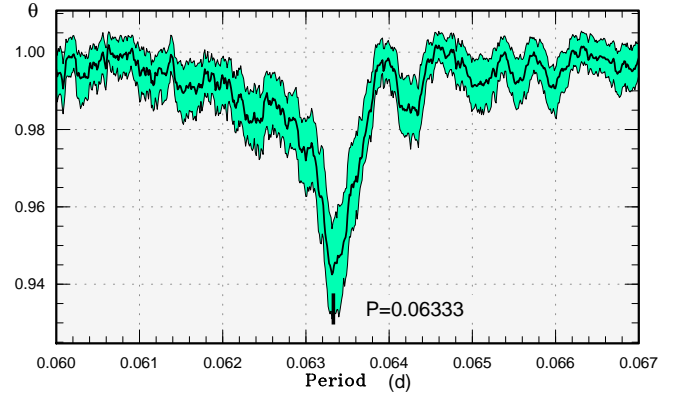
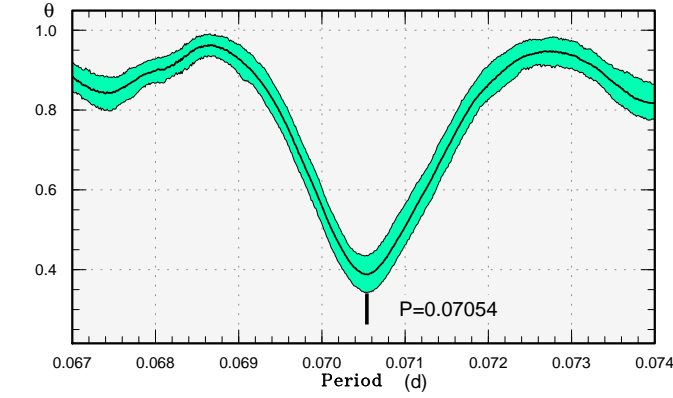


Fig. 40. Superhumps in SDSS J1120 (2011). (Upper): PDM analysis. (Lower): Phase-averaged profile.

Fig. 41. Superhumps in SDSS J1146 (2011). (Upper): PDM analysis. (Lower): Phase-averaged profile.

Table 49. Superhump maxima of SDSS J1227 (2011).

E	max*	error	$O - C^\dagger$	phase ‡	N^\S
0	55634.5319	0.0003	-0.0056	0.20	88
1	55634.5973	0.0005	-0.0048	0.24	63
13	55635.3749	0.0006	-0.0017	0.59	56
14	55635.4394	0.0004	-0.0018	0.61	190
15	55635.5029	0.0004	-0.0028	0.62	121
27	55636.2833	0.0018	0.0030	0.02	41
28	55636.3485	0.0008	0.0037	0.06	50
29	55636.4141	0.0014	0.0047	0.10	30
43	55637.3181	0.0007	0.0051	0.46	63
44	55637.3826	0.0007	0.0050	0.48	65
80	55639.6999	0.0013	-0.0014	0.29	53
96	55640.7334	0.0051	-0.0006	0.71	38
184	55646.4115	0.0010	-0.0027	0.91	59

*BJD-2400000.

† Against max = 2455634.537 + 0.064547 E .

‡ Orbital phase.

§ Number of points used to determine the maximum.

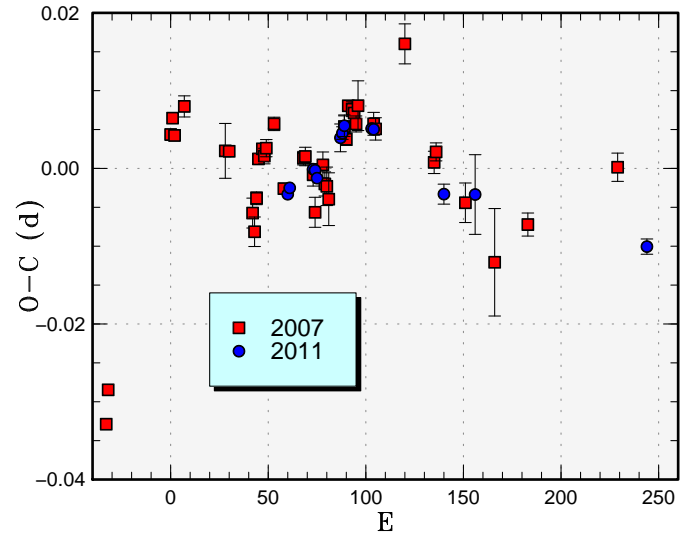


Fig. 42. Comparison of $O - C$ diagrams of SDSS J1227 between different superoutbursts. A period of 0.06460 d was used to draw this figure. Approximate cycle counts (E) after the start of the stage B were used. Since the start of the 2011 superoutburst was not well constrained, we shifted the $O - C$ diagrams to best fit the best-recorded 2007 one.

Table 50. Superhump maxima of SDSS J1250 (2011).

E	max*	error	$O - C^\dagger$	phase ‡	N^\S
0	55665.0937	0.0005	0.0003	0.47	124
40	55667.5096	0.0044	0.0058	0.60	62
41	55667.5603	0.0005	-0.0038	0.47	133
42	55667.6206	0.0006	-0.0038	0.49	134
52	55668.2272	0.0013	0.0003	0.82	106
53	55668.2868	0.0015	-0.0005	0.84	104
55	55668.4099	0.0012	0.0022	0.93	48
56	55668.4674	0.0014	-0.0006	0.91	55
58	55668.5902	0.0014	0.0017	0.00	112
59	55668.6474	0.0023	-0.0014	0.98	71

*BJD-2400000.

 † Against max = 2455665.0934 + 0.060261*E*. ‡ Orbital phase. § Number of points used to determine the maximum.

of the outburst. This possible failure to record the earliest stage of the outburst might explain the lack of highly excited emission lines in the spectrum and low amplitudes of early superhumps. If the true maximum was 6 d earlier (assuming a typical delay time of 10 d), the object should have reached a magnitude of 9.5 or brighter, giving an outburst amplitude of ~ 8.0 mag. The object is thus one of the brightest members of WZ Sge-type dwarf novae and deserves further detailed investigation.

3.35. SDSS J160501.35+203056.9

This transient was detected by K. Itagaki on 2010 November 21.36782 UT at an unfiltered CCD magnitude of 12.0 (vsnet-alert 12414). A. Drake informed that this object was spectroscopically recorded as an evident CV in SDSS and there was a possible faint outburst in 2005 (vsnet-alert 12413). Based on this information, we refer to this object by the SDSS designation (hereafter SDSS J1605). Although the outburst of the amplitude was sufficiently suggestive of an outburst of a WZ Sge-type dwarf nova, the short visibility in the evening and morning sky made observations very difficult. The rapid fading from the main superoutburst took place on December 24 (vsnet-alert 12525), 33 d after the initial detection. The object still remained bright on 2011 January 21 (61 d after the initial detection).

Since the later stage of the outburst was poorly observed and the state of the object (either continuation of the plateau phase or some kind of rebrightening phenomenon) was unknown, we restrict our analysis to the earlier part of the observation. Since some of the observations were recorded at high airmasses (larger than 3), secondary corrections for atmospheric extinction were applied to these observations. The early data showed some hint of double-wave modulations, which are possibly early superhumps (figure 47). Due to the short visibility, it was impossible to uniquely determine the period, we selected the most likely period based on our knowledge in periods of known WZ Sge-type dwarf novae with long plateau

Table 51. Superhump maxima of SDSS J1339 (2011).

E	max*	error	$O - C^\dagger$	N^\ddagger
0	55604.4595	0.0005	-0.0113	152
1	55604.5148	0.0009	-0.0141	83
2	55604.5782	0.0006	-0.0088	66
6	55604.8123	0.0008	-0.0071	72
7	55604.8699	0.0006	-0.0077	71
8	55604.9274	0.0008	-0.0083	71
11	55605.1082	0.0004	-0.0018	64
12	55605.1640	0.0005	-0.0042	70
13	55605.2208	0.0003	-0.0054	70
14	55605.2810	0.0003	-0.0033	139
15	55605.3399	0.0002	-0.0026	285
16	55605.3983	0.0004	-0.0023	82
17	55605.4572	0.0002	-0.0015	89
18	55605.5189	0.0003	0.0021	89
19	55605.5758	0.0002	0.0009	87
20	55605.6343	0.0003	0.0013	86
21	55605.6943	0.0002	0.0032	74
23	55605.8084	0.0027	0.0011	47
24	55605.8662	0.0033	0.0007	13
27	55606.0457	0.0006	0.0059	67
29	55606.1636	0.0002	0.0075	168
30	55606.2223	0.0003	0.0081	135
32	55606.3388	0.0005	0.0085	185
33	55606.3962	0.0001	0.0077	109
34	55606.4562	0.0002	0.0096	177
35	55606.5136	0.0002	0.0089	176
36	55606.5699	0.0002	0.0071	102
37	55606.6286	0.0001	0.0076	90
38	55606.6861	0.0002	0.0071	148
39	55606.7443	0.0003	0.0071	112
40	55606.8016	0.0002	0.0064	124
41	55606.8593	0.0005	0.0059	72
42	55606.9187	0.0005	0.0072	96
43	55606.9767	0.0003	0.0071	122
44	55607.0335	0.0001	0.0058	117
51	55607.4358	0.0003	0.0013	98
52	55607.4964	0.0001	0.0038	244
57	55607.7861	0.0003	0.0029	47
58	55607.8439	0.0002	0.0026	120
59	55607.9020	0.0001	0.0026	253
60	55607.9604	0.0001	0.0029	256
62	55608.0780	0.0003	0.0042	45
64	55608.1917	0.0003	0.0017	180
65	55608.2503	0.0003	0.0022	180
66	55608.3074	0.0003	0.0012	180
67	55608.3656	0.0004	0.0013	116
68	55608.4228	0.0002	0.0004	74
69	55608.4825	0.0002	0.0020	75
70	55608.5387	0.0003	0.0001	70
71	55608.5972	0.0002	0.0004	64
72	55608.6555	0.0003	0.0006	72
73	55608.7137	0.0013	0.0007	29
80	55609.1199	0.0002	0.0001	175

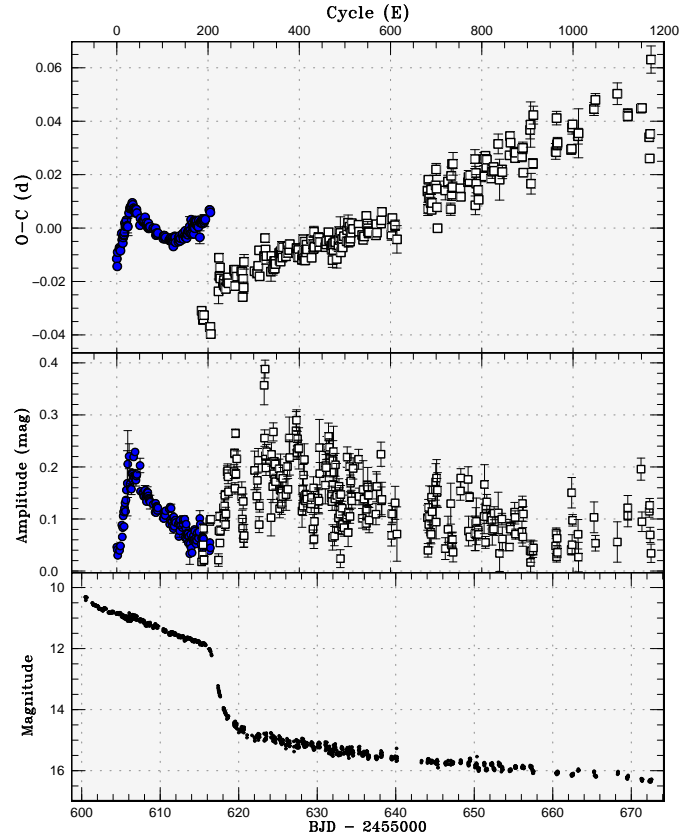
*BJD-2400000.

 † Against max = 2455604.4708 + 0.058112*E*. ‡ Number of points used to determine the maximum.

Table 51. Superhump maxima of SDSS J1339 (2011) (continued).

E	max*	error	$O - C^\dagger$	N^\ddagger
84	55609.3521	0.0003	-0.0001	361
85	55609.4104	0.0003	0.0001	536
86	55609.4660	0.0002	-0.0024	480
87	55609.5248	0.0003	-0.0017	538
88	55609.5829	0.0003	-0.0017	170
89	55609.6405	0.0003	-0.0022	67
90	55609.6992	0.0004	-0.0017	45
102	55610.3944	0.0003	-0.0038	87
103	55610.4537	0.0003	-0.0026	90
104	55610.5118	0.0002	-0.0026	88
105	55610.5698	0.0003	-0.0027	82
106	55610.6268	0.0003	-0.0038	88
107	55610.6855	0.0002	-0.0032	79
115	55611.1494	0.0002	-0.0042	241
116	55611.2073	0.0004	-0.0045	163
117	55611.2658	0.0003	-0.0041	198
118	55611.3245	0.0005	-0.0035	259
119	55611.3820	0.0005	-0.0041	68
120	55611.4395	0.0003	-0.0048	53
121	55611.4975	0.0004	-0.0048	52
122	55611.5555	0.0005	-0.0049	52
123	55611.6153	0.0003	-0.0033	58
124	55611.6700	0.0008	-0.0067	52
125	55611.7302	0.0003	-0.0046	164
126	55611.7894	0.0003	-0.0035	184
127	55611.8481	0.0003	-0.0029	235
128	55611.9059	0.0003	-0.0032	204
129	55611.9621	0.0005	-0.0051	84
135	55612.3110	0.0005	-0.0049	76
136	55612.3708	0.0007	-0.0032	188
137	55612.4279	0.0004	-0.0043	62
138	55612.4875	0.0012	-0.0027	61
139	55612.5438	0.0003	-0.0046	61
140	55612.6029	0.0004	-0.0036	56
144	55612.8365	0.0006	-0.0024	30
145	55612.8952	0.0007	-0.0018	31
146	55612.9513	0.0006	-0.0038	31
149	55613.1268	0.0005	-0.0026	64
150	55613.1868	0.0006	-0.0008	157
151	55613.2425	0.0003	-0.0032	241
152	55613.3004	0.0003	-0.0033	240
153	55613.3584	0.0009	-0.0035	107
154	55613.4180	0.0004	-0.0020	63
155	55613.4766	0.0004	-0.0015	63
156	55613.5340	0.0004	-0.0023	64
157	55613.5936	0.0009	-0.0007	58
158	55613.6515	0.0005	-0.0009	63
160	55613.7696	0.0036	0.0009	27
161	55613.8261	0.0011	-0.0007	30
162	55613.8831	0.0008	-0.0018	31
163	55613.9464	0.0012	0.0034	30
165	55614.0574	0.0014	-0.0019	42

*BJD-2400000.

 † Against max = 2455604.4708 + 0.058112 E . ‡ Number of points used to determine the maximum.**Fig. 43.** $O - C$ diagram of superhumps in SDSS J1339 (2011). (Upper): $O - C$. Filled circles and open squares represent superhumps during the plateau phase and post-superoutburst superhumps, respectively. We used a period of 0.058112 d for calculating the $O - C$'s. (Middle): Amplitudes. The symbols are common to the upper panel. (Lower): Light curve.

phases (Kato et al. 2009a, subsection 5.3). This period should be tested by future observations.

During the later stage of the outburst, there was a signal around 0.05718 d (0.9 % longer than the period of possible early superhumps) attributable to ordinary superhumps, but we did not adopt this value due to very poor statistics.

3.36. SDSS J210014.12+004446.0

We reported on the 2007 superoutburst of this object (hereafter SDSS J2100) in Kato et al. (2009a). We further obtained observations on three consecutive nights during the 2010 superoutburst (table 53). The $O - C$ values suggest that this object is either a long- P_{SH} system with a large negative P_{dot} or we incidentally spotted an epoch of stage transition. The global period with the PDM method was 0.08743(2) d, close to the value of 0.08746(8) d in Trampusch et al. (2005).

3.37. OT J000938.3-121017

This object (= CSS101007:000938-121017, hereafter OT J0009) was discovered by the CRTS on 2010 October 10. The object has a blue counterpart on the Digitized Sky

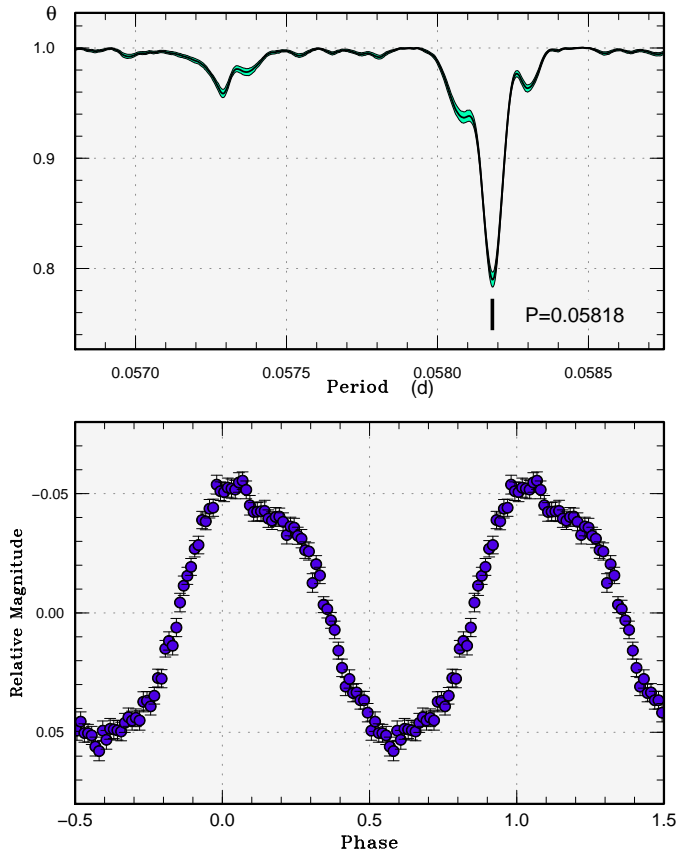


Fig. 44. Superhumps during the post-superoutburst stage in SDSS J1339 (2011). (Upper): PDM analysis. The signal at 0.057289(1) d is the orbital period. The tick is located at the orbital period. (Lower): Phase-averaged profile.

Survey (DSS). Following the initial detection, an inspection of the backlog by the CRTS team clarified another outburst in 2005 (cf. vsnet-alert 12235). Subsequent observations confirmed superhumps (vsnet-alert 12234, figure 48), identifying the object a dwarf nova near the period gap (vsnet-alert 12238, 12241, 12244). There was a distinct shortening of the superhump period after $E = 14$, which we attribute to a stage B-C transition (table 54). Although we list our tentative identifications of periods in table 3, this variation in the period may be interpreted as a continuous change with a global P_{dot} of $-51(4) \times 10^{-5}$ (see also figure 49). Although the object resembles EF Peg in its long P_{SH} , large outburst amplitude and rare outbursts, the large variation in the superhump period resembles those of more frequently outbursting SU UMa-type dwarf novae (cf. Kato et al. 2009a, subsection 4.10). As proposed for V342 Cam (=1RXS J042332.8+745300) (Shears et al. 2010b), the appearance of orbital signature in some stage of the outburst may have contributed this change of the period. Further detailed observations during future superoutbursts and in quiescence are desired.

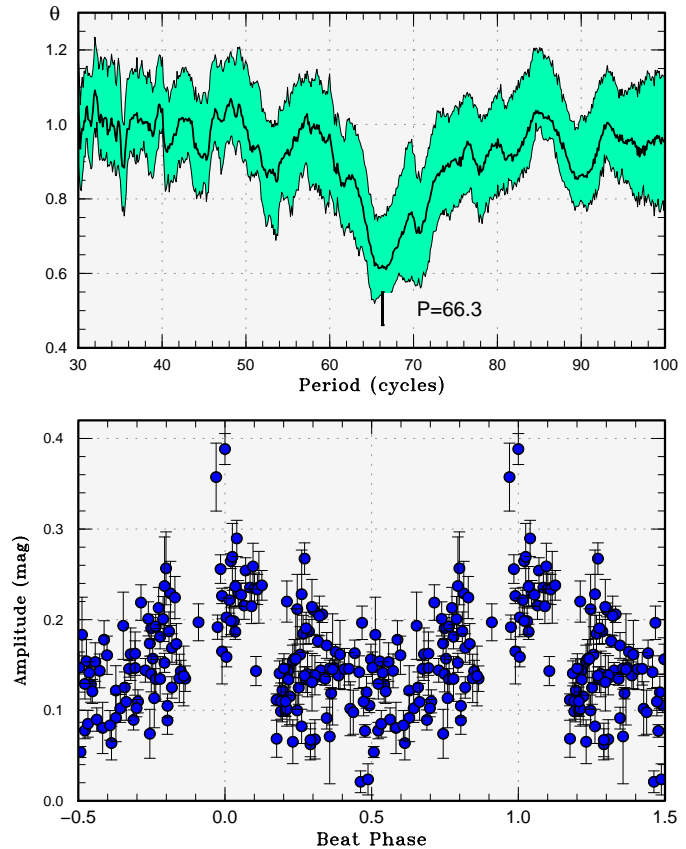


Fig. 45. Beat phenomenon during the post-superoutburst phase in SDSS J1339 (2011). (Upper): PDM analysis. Superhump maxima for $18 \leq E \leq 428$ were used. The obtained beat period of 66.3(3) cycles is close to the expected beat period of 64.7 cycles based on the orbital and superhump periods. (Lower): Phase-averaged profile using the measured beat period.

3.38. OT J012059.6+325545

This object (hereafter OT J0120) was discovered as a large-amplitude transient by K. Itagaki on 2010 November 30.50663 at an unfiltered CCD magnitude of 12.3 (vsnet-alert 12431). Immediate follow-up observations clearly indicated the presence of early superhumps (vsnet-alert 12436; figure 50). The object started to show ordinary superhumps 11 d after the discovery (vsnet-alert 12491, 12496; figure 51). Since some of the observations were recorded at high airmasses (larger than 3), secondary corrections for atmospheric extinction were applied to these observations.

The times of superhump maxima are listed in table 55. Due to the gap in the observations, stage A superhumps were not recorded. Following the stage B with a significant increase in the period [$P_{\text{dot}} = +4.3(0.5) \times 10^{-5}$], the period quickly shortened. The mean period for the interval BJD 2455554.4–2455556.3 was 0.05672(8) d (PDM method), which is 0.8 % shorter than the period of early superhumps (close to P_{orb}). This rapid excursion to a shorter period is similar to the case in SDSS J0804 (sub-

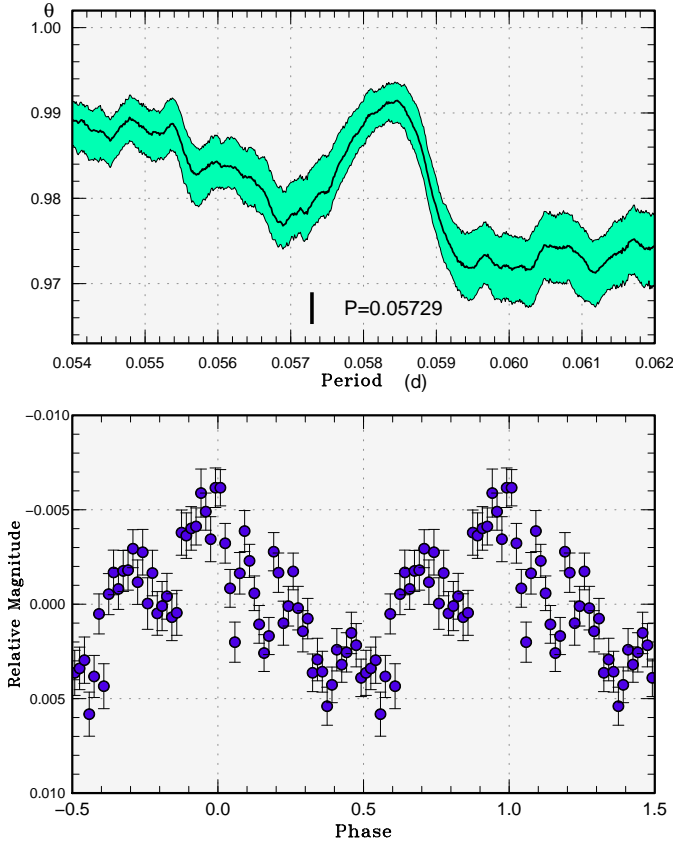


Fig. 46. Possible early superhumps in SDSS J1339 (2011). (Upper): PDM analysis. The tick is located at the orbital period. (Lower): Phase-averaged profile using the orbital period.

section 3.27), and it might be a common property in WZ Sge-type dwarf novae. Whether this period is related to negative superhumps or not requires further detailed examination.

The object underwent multiple rebrightenings (vsnet-alert 12538, 12562, 12577, 12596, 12602, 12610, 12674). Although the exact number of rebrightenings was unclear, the shortest intervals of rebrightenings were ~ 2 d, close to those of WZ Sge (2001; Patterson et al. 2002; Ishioka et al. 2002; Kato et al. 2009a) and AL Com (2007; Uemura et al. 2008), a group of rebrightening classified as type-A WZ Sge-type superoutbursts in Imada et al. (2006) and Kato et al. (2009a). A comparison with WZ Sge (2001) (figure 52) suggests at least nine rebrightenings during the observable period. An analysis of selected high signal-to-noise observations during the rebrightening phase supports the presence of persistent superhumps with a period of 0.05787(3) d, which is close to P_{SH} during the main superoutburst 53. The observed amplitude of these modulations were small because the observations were relatively restricted to maxima of rebrightening (see a discussion in SDSS J0804, subsection 3.27). These modulations apparently persisted, even with larger amplitudes, 18 d after the final observation of the rebrightening phase (vsnet-

Table 51. Superhump maxima of SDSS J1339 (2011) (continued).

E	max*	error	$O - C^\dagger$	N^\ddagger
166	55614.1193	0.0005	0.0020	63
167	55614.1762	0.0005	0.0007	61
168	55614.2339	0.0004	0.0003	231
169	55614.2897	0.0004	-0.0020	239
170	55614.3529	0.0004	0.0031	153
171	55614.4081	0.0004	0.0002	140
172	55614.4680	0.0005	0.0020	172
173	55614.5272	0.0006	0.0031	132
174	55614.5842	0.0004	0.0019	115
175	55614.6433	0.0004	0.0029	116
176	55614.6996	0.0003	0.0011	87
178	55614.8163	0.0014	0.0016	17
179	55614.8735	0.0007	0.0007	29
180	55614.9341	0.0010	0.0032	16
182	55615.0439	0.0024	-0.0032	47
183	55615.1075	0.0007	0.0023	31
185	55615.2240	0.0004	0.0025	223
186	55615.2827	0.0003	0.0031	206
187	55615.3404	0.0007	0.0027	174
188	55615.3977	0.0007	0.0019	64
189	55615.4575	0.0005	0.0036	147
190	55615.5150	0.0005	0.0030	144
191	55615.5725	0.0006	0.0024	115
192	55615.6313	0.0023	0.0030	102
194	55615.7479	0.0007	0.0034	48
203	55616.2745	0.0008	0.0070	63
204	55616.3326	0.0005	0.0070	83
205	55616.3898	0.0009	0.0061	56

*BJD-2400000.

† Against max = 2455604.4708 + 0.058112E.

‡ Number of points used to determine the maximum.

alert 12762).

3.39. OT J014150.4+090822

This object (= CSS101127:014150+090822), hereafter OT J0141) was discovered by the CRTS on 2010 November 27. No previous outburst was known. Soon after the discovery, superhumps were detected (vsnet-alert 12422; figure 54). The times of superhump maxima are listed in table 56. Stage B with a P_{dot} of $+10.1(1.6) \times 10^{-5}$ and the subsequent stage C were apparently observed, and we listed parameters in table 3 based on this identification.

3.40. OT J041350.0+094515

This object (= CSS110125:041350+094515), hereafter OT J0413) was discovered by the CRTS on 2011 January 25. Short-period superhumps were immediately detected (vsnet-alert 12713, 12719; figure 55).

The times of superhump maxima are listed in table 57. A relatively small $P_{\text{dot}} = +4.2(0.8) \times 10^{-5}$ was detected. The superhump period resembles those of WZ Sge-type dwarf novae, such as GW Lib and UW Tri. Although the early superhumps were not observed, this object may have

Table 52. Late stage superhumps in SDSS J1339 (2011).

E	max*	error	$O - C^\dagger$	N^\ddagger
0	55615.2489	0.0014	-0.0055	120
2	55615.3635	0.0016	-0.0072	94
3	55615.4198	0.0005	-0.0091	28
4	55615.4781	0.0005	-0.0090	87
5	55615.5377	0.0016	-0.0075	56
18	55616.2883	0.0005	-0.0134	30
19	55616.3470	0.0006	-0.0129	28
20	55616.4024	0.0007	-0.0157	29
37	55617.4063	0.0046	-0.0009	93
38	55617.4770	0.0008	0.0116	117
39	55617.5281	0.0006	0.0045	118
40	55617.5896	0.0010	0.0078	114
41	55617.6436	0.0009	0.0036	62
48	55618.0483	0.0020	0.0010	39
49	55618.1078	0.0011	0.0024	62
50	55618.1638	0.0010	0.0002	63
51	55618.2227	0.0005	0.0009	175
52	55618.2795	0.0009	-0.0005	168
53	55618.3370	0.0009	-0.0012	64
56	55618.5140	0.0004	0.0012	44
57	55618.5728	0.0005	0.0019	46
58	55618.6319	0.0006	0.0027	42
59	55618.6878	0.0007	0.0005	29
71	55619.3902	0.0005	0.0046	134
72	55619.4477	0.0003	0.0040	237
73	55619.5003	0.0005	-0.0016	223
74	55619.5631	0.0002	0.0031	258
75	55619.6226	0.0003	0.0043	242
77	55619.7363	0.0004	0.0016	28
87	55620.3194	0.0007	0.0029	62
88	55620.3757	0.0009	0.0010	62
89	55620.4355	0.0012	0.0026	80
90	55620.4841	0.0016	-0.0070	55
91	55620.5490	0.0008	-0.0003	53
92	55620.6038	0.0021	-0.0036	62
93	55620.6716	0.0027	0.0060	57
116	55622.0047	0.0011	0.0007	36
121	55622.2944	0.0007	-0.0005	64
122	55622.3527	0.0007	-0.0004	40
124	55622.4716	0.0009	0.0022	36
126	55622.5936	0.0012	0.0079	66
127	55622.6420	0.0007	-0.0020	61
137	55623.2307	0.0010	0.0049	42
138	55623.2886	0.0004	0.0046	64
139	55623.3536	0.0004	0.0115	41
140	55623.4075	0.0005	0.0071	65
141	55623.4617	0.0005	0.0032	87
142	55623.5213	0.0005	0.0045	68
152	55624.0958	0.0032	-0.0029	31
153	55624.1598	0.0007	0.0030	55

*BJD-2400000.

 \dagger Against max = 2455615.2543 + 0.058186*E*. \ddagger Number of points used to determine the maximum.**Table 52.** Late stage superhumps in SDSS J1339 (2011)
(continued).

E	max*	error	$O - C^\dagger$	N^\ddagger
156	55624.3306	0.0029	-0.0008	41
157	55624.3881	0.0005	-0.0015	147
158	55624.4474	0.0005	-0.0003	163
159	55624.5073	0.0003	0.0014	284
160	55624.5626	0.0003	-0.0015	274
161	55624.6236	0.0003	0.0013	271
162	55624.6805	0.0008	0.0001	134
170	55625.1496	0.0007	0.0036	62
171	55625.2048	0.0012	0.0007	62
172	55625.2661	0.0008	0.0037	63
173	55625.3206	0.0016	0.0001	100
174	55625.3826	0.0012	0.0039	121
175	55625.4409	0.0011	0.0040	103
176	55625.5009	0.0010	0.0058	101
177	55625.5546	0.0011	0.0013	107
178	55625.6166	0.0009	0.0051	67
185	55626.0200	0.0016	0.0012	35
188	55626.1980	0.0006	0.0047	119
189	55626.2537	0.0009	0.0022	115
192	55626.4291	0.0011	0.0030	38
193	55626.4889	0.0011	0.0046	37
207	55627.2998	0.0010	0.0009	49
208	55627.3596	0.0005	0.0026	111
209	55627.4176	0.0004	0.0024	128
210	55627.4737	0.0004	0.0003	138
211	55627.5305	0.0005	-0.0011	118
212	55627.5914	0.0005	0.0016	126
213	55627.6468	0.0011	-0.0012	38
220	55628.0527	0.0017	-0.0026	47
221	55628.1124	0.0010	-0.0010	64
222	55628.1765	0.0012	0.0049	62
223	55628.2285	0.0008	-0.0013	62
224	55628.2888	0.0015	0.0008	72
225	55628.3429	0.0011	-0.0033	70
226	55628.4081	0.0005	0.0037	276
227	55628.4591	0.0005	-0.0034	213
228	55628.5204	0.0004	-0.0003	210
229	55628.5784	0.0005	-0.0006	264
230	55628.6394	0.0005	0.0023	240
231	55628.6957	0.0009	0.0004	93
240	55629.2226	0.0010	0.0036	122
241	55629.2737	0.0007	-0.0035	111
244	55629.4531	0.0027	0.0014	35
245	55629.5093	0.0010	-0.0006	36
246	55629.5722	0.0020	0.0041	39
247	55629.6275	0.0021	0.0012	37
255	55630.0942	0.0010	0.0024	65
256	55630.1531	0.0011	0.0032	62
257	55630.2110	0.0012	0.0029	55

*BJD-2400000.

 \dagger Against max = 2455615.2543 + 0.058186*E*. \ddagger Number of points used to determine the maximum.

Table 52. Late stage superhumps in SDSS J1339 (2011)
(continued).

E	max*	error	$O - C^\dagger$	N^\ddagger
258	55630.2657	0.0009	-0.0006	45
259	55630.3256	0.0008	0.0011	70
271	55631.0210	0.0014	-0.0017	60
272	55631.0806	0.0007	-0.0003	103
273	55631.1383	0.0005	-0.0008	181
274	55631.1976	0.0007	0.0003	46
278	55631.4334	0.0006	0.0033	42
279	55631.4884	0.0005	0.0002	59
280	55631.5466	0.0005	0.0001	62
284	55631.7769	0.0007	-0.0023	40
285	55631.8336	0.0008	-0.0038	40
286	55631.8935	0.0010	-0.0020	40
287	55631.9461	0.0027	-0.0076	51
288	55632.0103	0.0014	-0.0016	40
289	55632.0660	0.0013	-0.0041	46
290	55632.1262	0.0007	-0.0020	64
291	55632.1851	0.0022	-0.0013	65
292	55632.2425	0.0010	-0.0022	55
293	55632.3014	0.0008	-0.0015	64
296	55632.4694	0.0034	-0.0080	24
300	55632.7070	0.0023	-0.0032	30
301	55632.7704	0.0007	0.0021	48
302	55632.8252	0.0010	-0.0013	47
303	55632.8841	0.0011	-0.0006	48
304	55632.9441	0.0060	0.0012	59
305	55632.9949	0.0009	-0.0062	48
307	55633.1131	0.0013	-0.0043	122
308	55633.1743	0.0008	-0.0014	122
309	55633.2292	0.0011	-0.0046	109
312	55633.4077	0.0014	-0.0007	42
318	55633.7545	0.0007	-0.0030	59
319	55633.8168	0.0007	0.0011	25
321	55633.9358	0.0029	0.0037	30
322	55633.9867	0.0020	-0.0035	48
324	55634.1086	0.0009	0.0020	49
325	55634.1612	0.0009	-0.0036	64
326	55634.2204	0.0006	-0.0026	64
327	55634.2813	0.0009	0.0001	51
328	55634.3389	0.0006	-0.0005	79
329	55634.4005	0.0007	0.0030	71
332	55634.5727	0.0007	0.0006	62
344	55635.2716	0.0008	0.0013	49
345	55635.3271	0.0009	-0.0014	67
352	55635.7326	0.0011	-0.0032	48
354	55635.8471	0.0012	-0.0051	24
356	55635.9645	0.0006	-0.0040	45
361	55636.2628	0.0011	0.0033	98
362	55636.3178	0.0004	0.0001	155
363	55636.3762	0.0004	0.0003	99
364	55636.4325	0.0025	-0.0016	28

*BJD-2400000.

†Against max = 2455615.2543 + 0.058186E.

‡Number of points used to determine the maximum.

Table 52. Late stage superhumps in SDSS J1339 (2011)
(continued).

E	max*	error	$O - C^\dagger$	N^\ddagger
365	55636.4895	0.0012	-0.0028	40
366	55636.5468	0.0009	-0.0036	38
367	55636.6053	0.0020	-0.0033	38
382	55637.4759	0.0014	-0.0055	38
383	55637.5382	0.0011	-0.0014	38
384	55637.5931	0.0011	-0.0047	40
393	55638.1195	0.0007	-0.0019	64
394	55638.1789	0.0013	-0.0008	61
395	55638.2401	0.0013	0.0023	48
416	55639.4520	0.0021	-0.0078	55
417	55639.5127	0.0014	-0.0052	56
418	55639.5744	0.0012	-0.0017	45
424	55639.9204	0.0020	-0.0048	29
428	55640.1475	0.0051	-0.0104	65
495	55644.0591	0.0018	0.0027	64
496	55644.1106	0.0025	-0.0040	174
497	55644.1796	0.0009	0.0068	168
498	55644.2314	0.0014	0.0004	208
499	55644.2889	0.0058	-0.0003	87
502	55644.4616	0.0019	-0.0021	61
503	55644.5245	0.0018	0.0026	64
504	55644.5751	0.0010	-0.0050	63
505	55644.6358	0.0015	-0.0025	59
513	55645.1073	0.0014	0.0035	65
514	55645.1713	0.0023	0.0094	62
515	55645.2223	0.0013	0.0021	173
516	55645.2734	0.0013	-0.0049	179
517	55645.3237	0.0015	-0.0129	189
534	55646.3257	0.0035	0.0000	40
540	55646.6777	0.0024	0.0029	23
546	55647.0160	0.0023	-0.0079	64
547	55647.0867	0.0033	0.0045	104
548	55647.1377	0.0022	-0.0026	183
549	55647.2072	0.0017	0.0088	230
550	55647.2567	0.0020	0.0001	181
551	55647.3236	0.0042	0.0087	179
567	55648.2442	0.0009	-0.0016	120
568	55648.2992	0.0008	-0.0049	116
584	55649.2344	0.0009	-0.0006	120
585	55649.2944	0.0025	0.0013	114
587	55649.4091	0.0005	-0.0005	101
588	55649.4695	0.0006	0.0017	131
599	55650.1147	0.0035	0.0070	111
600	55650.1555	0.0035	-0.0104	118
601	55650.2258	0.0025	0.0016	159
602	55650.2799	0.0034	-0.0025	115
606	55650.5100	0.0010	-0.0051	63
607	55650.5644	0.0011	-0.0089	66
619	55651.2770	0.0024	0.0055	113
620	55651.3286	0.0020	-0.0011	96

*BJD-2400000.

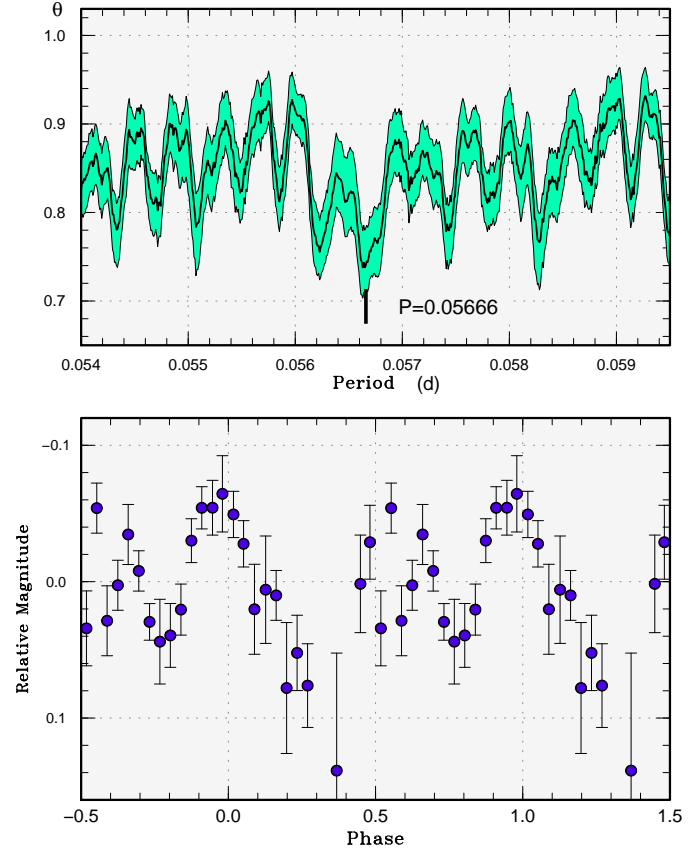
†Against max = 2455615.2543 + 0.058186E.

‡Number of points used to determine the maximum.

Table 52. Late stage superhumps in SDSS J1339 (2011) (continued).

E	max*	error	$O - C^\dagger$	N^\ddagger
622	55651.4525	0.0015	0.0065	61
623	55651.5095	0.0007	0.0053	65
624	55651.5646	0.0009	0.0022	62
625	55651.6254	0.0010	0.0048	40
634	55652.1414	0.0011	-0.0029	120
636	55652.2611	0.0012	0.0004	122
637	55652.3183	0.0025	-0.0006	109
640	55652.4943	0.0010	0.0009	31
641	55652.5509	0.0008	-0.0006	33
650	55653.0841	0.0037	0.0089	79
653	55653.2451	0.0076	-0.0047	115
658	55653.5394	0.0008	-0.0013	28
659	55653.5966	0.0025	-0.0023	28
675	55654.5327	0.0012	0.0027	87
676	55654.5980	0.0012	0.0099	52
677	55654.6536	0.0012	0.0073	29
686	55655.1733	0.0009	0.0033	53
687	55655.2290	0.0009	0.0008	241
688	55655.2891	0.0011	0.0028	300
702	55656.1012	0.0019	0.0002	123
703	55656.1623	0.0008	0.0032	186
704	55656.2207	0.0022	0.0034	142
705	55656.2695	0.0010	-0.0060	182
720	55657.1572	0.0034	0.0089	120
721	55657.2173	0.0085	0.0109	131
722	55657.2533	0.0039	-0.0114	120
726	55657.4933	0.0019	-0.0041	28
727	55657.5696	0.0034	0.0140	20
776	55660.4034	0.0030	-0.0033	55
777	55660.4613	0.0009	-0.0036	64
778	55660.5321	0.0025	0.0090	64
779	55660.5802	0.0018	-0.0011	64
780	55660.6391	0.0020	-0.0003	65
810	55662.3797	0.0017	-0.0053	32
811	55662.4383	0.0008	-0.0049	19
812	55662.5043	0.0024	0.0029	29
813	55662.5637	0.0009	0.0041	33
825	55663.2569	0.0029	-0.0009	115
826	55663.3159	0.0085	-0.0001	88
860	55665.3007	0.0024	0.0064	94
863	55665.4785	0.0023	0.0096	33
911	55668.2702	0.0041	0.0083	98
934	55669.5992	0.0019	-0.0009	27
934	55669.5983	0.0017	-0.0018	25
963	55671.2864	0.0009	-0.0011	22
965	55671.4028	0.0016	-0.0011	30
981	55672.3217	0.0007	-0.0132	31
982	55672.3719	0.0007	-0.0212	33
983	55672.4392	0.0016	-0.0121	31
985	55672.5833	0.0051	0.0157	23

*BJD-2400000.

 \dagger Against max = 2455615.2543 + 0.058186*E*. \ddagger Number of points used to determine the maximum.**Fig. 47.** Possible early superhumps in SDSS J1605 (2010). (Upper): PDM analysis. The rejection rate for bootstrapping was reduced to 0.2 for better visualization. (Lower): Phase-averaged profile.**Table 53.** Superhump maxima of SDSS J2100 (2010).

E	max*	error	$O - C^\dagger$	N^\ddagger
0	55530.2355	0.0021	-0.0030	41
1	55530.3224	0.0003	-0.0034	82
35	55533.3065	0.0009	0.0127	81
69	55536.2554	0.0012	-0.0064	77

*BJD-2400000.

 \dagger Against max = 2455530.2384 + 0.087295*E*. \ddagger Number of points used to determine the maximum.

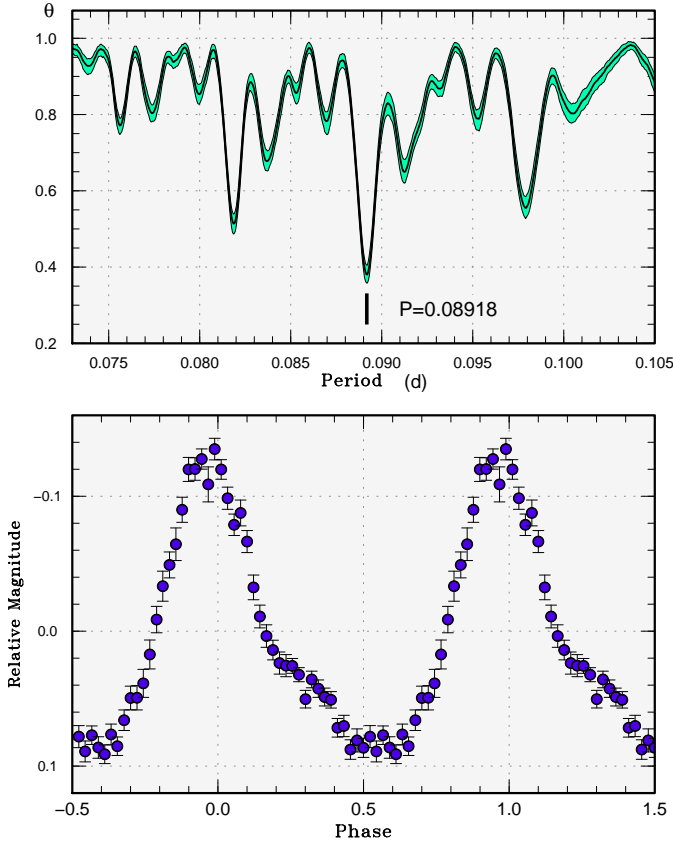


Fig. 48. Superhumps in OT J0009 (2010). (Upper): PDM analysis. (Lower): Phase-averaged profile.

Table 54. Superhump maxima of OT J0009 (2010).

E	max*	error	$O - C^\dagger$	N^\ddagger
0	55477.0085	0.0006	-0.0048	65
1	55477.0983	0.0003	-0.0041	227
2	55477.1877	0.0004	-0.0039	331
3	55477.2770	0.0004	-0.0037	94
12	55478.0893	0.0004	0.0065	93
13	55478.1778	0.0004	0.0059	94
14	55478.2674	0.0004	0.0065	94
34	55480.0493	0.0008	0.0060	111
35	55480.1349	0.0006	0.0025	222
45	55481.0229	0.0024	-0.0007	50
46	55481.1100	0.0006	-0.0028	94
47	55481.1989	0.0008	-0.0030	94
48	55481.2864	0.0009	-0.0045	94

*BJD-2400000.

† Against max = 2455477.0133 + 0.089117E.

‡ Number of points used to determine the maximum.

Table 55. Superhump maxima of OT J0120 (2010).

E	max*	error	$O - C^\dagger$	N^\ddagger
0	55544.4060	0.0003	0.0031	189
1	55544.4631	0.0005	0.0024	100
2	55544.5221	0.0003	0.0036	55
4	55544.6375	0.0004	0.0034	53
5	55544.6949	0.0006	0.0030	47
6	55544.7524	0.0004	0.0026	50
10	55544.9825	0.0006	0.0015	77
11	55545.0401	0.0004	0.0013	95
12	55545.0997	0.0005	0.0031	94
13	55545.1567	0.0006	0.0022	95
16	55545.3300	0.0004	0.0022	56
17	55545.3863	0.0003	0.0007	77
18	55545.4446	0.0004	0.0011	79
19	55545.5015	0.0005	0.0002	51
21	55545.6170	0.0006	0.0001	35
22	55545.6743	0.0008	-0.0003	48
34	55546.3688	0.0005	0.0004	86
35	55546.4252	0.0002	-0.0010	109
36	55546.4831	0.0004	-0.0009	73
44	55546.9463	0.0010	-0.0002	127
45	55547.0044	0.0010	0.0001	83
47	55547.1127	0.0010	-0.0072	216
48	55547.1743	0.0016	-0.0034	42
49	55547.2366	0.0007	0.0011	29
61	55547.9294	0.0010	0.0001	104
62	55547.9860	0.0007	-0.0010	134
72	55548.5637	0.0008	-0.0015	45
73	55548.6206	0.0008	-0.0024	47
74	55548.6773	0.0009	-0.0034	47
75	55548.7353	0.0007	-0.0032	52
78	55548.9143	0.0019	0.0023	105
79	55548.9589	0.0022	-0.0109	109
80	55549.0229	0.0020	-0.0047	108
81	55549.0815	0.0021	-0.0039	115
82	55549.1393	0.0025	-0.0039	93
88	55549.4903	0.0018	0.0003	30
89	55549.5510	0.0020	0.0031	32
101	55550.2428	0.0015	0.0012	13
102	55550.2924	0.0018	-0.0070	17
106	55550.5285	0.0008	-0.0022	46
107	55550.5858	0.0008	-0.0027	39
108	55550.6420	0.0010	-0.0043	53
109	55550.6995	0.0012	-0.0046	48
110	55550.7599	0.0060	-0.0020	28
113	55550.9334	0.0020	-0.0019	169
114	55550.9896	0.0016	-0.0035	158
115	55551.0373	0.0028	-0.0136	169
116	55551.1146	0.0028	0.0059	165
118	55551.2208	0.0008	-0.0035	31
120	55551.3335	0.0034	-0.0064	10
134	55552.1490	0.0003	-0.0002	239

*BJD-2400000.

† Against max = 2455544.4029 + 0.057809E.

‡ Number of points used to determine the maximum.

Table 55. Superhump maxima of OT J0120 (2010) (continued).

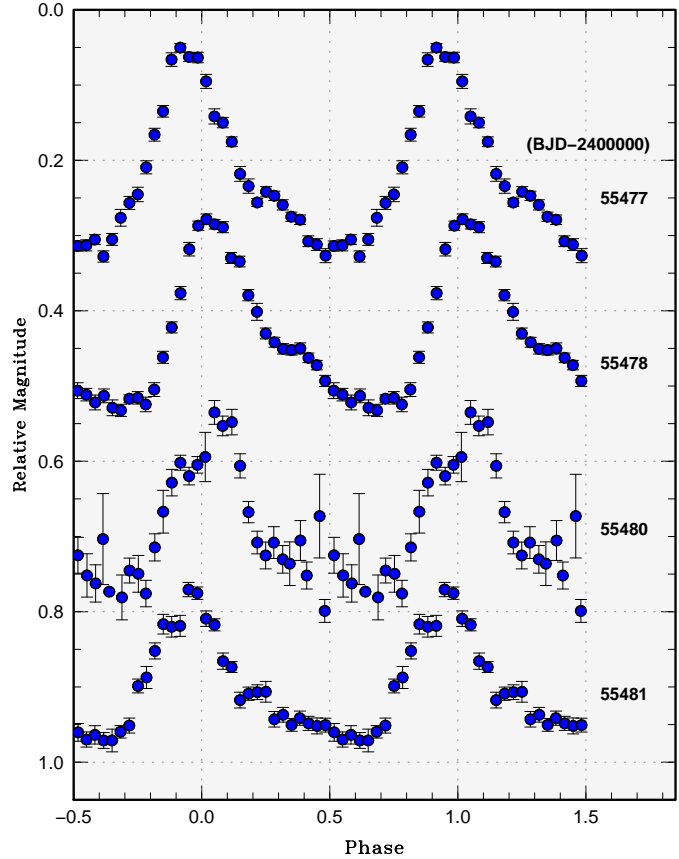
E	max*	error	$O - C^\dagger$	N^\ddagger
135	55552.2052	0.0003	-0.0019	180
136	55552.2619	0.0003	-0.0030	253
137	55552.3190	0.0005	-0.0037	204
152	55553.1998	0.0011	0.0100	255
153	55553.2536	0.0003	0.0059	118
154	55553.3109	0.0007	0.0055	253
155	55553.3626	0.0005	-0.0007	188
159	55553.6016	0.0015	0.0071	47
160	55553.6578	0.0016	0.0055	40
161	55553.7143	0.0016	0.0042	44
164	55553.8902	0.0021	0.0066	79
165	55553.9474	0.0020	0.0061	104
166	55554.0102	0.0024	0.0110	105
167	55554.0671	0.0035	0.0102	219
168	55554.1198	0.0016	0.0051	216
169	55554.1802	0.0009	0.0076	226
170	55554.2370	0.0003	0.0066	174
171	55554.2950	0.0004	0.0068	204
172	55554.3519	0.0003	0.0059	254
173	55554.4119	0.0006	0.0081	99
174	55554.4671	0.0008	0.0055	62
184	55555.0344	0.0021	-0.0053	168
185	55555.1030	0.0022	0.0055	213
186	55555.1580	0.0017	0.0026	285
187	55555.2166	0.0008	0.0035	111
188	55555.2705	0.0009	-0.0004	186
190	55555.3914	0.0012	0.0048	192
191	55555.4326	0.0024	-0.0118	136
195	55555.6597	0.0103	-0.0159	62
196	55555.7167	0.0028	-0.0167	61
197	55555.7706	0.0023	-0.0206	61

*BJD-2400000.

 † Against max = 2455544.4029 + 0.057809E. ‡ Number of points used to determine the maximum.**Table 56.** Superhump maxima of OT J0141 (2010).

E	max*	error	$O - C^\dagger$	N^\ddagger
0	55527.9421	0.0010	0.0025	126
1	55528.0072	0.0015	0.0051	125
2	55528.0677	0.0008	0.0032	128
19	55529.1230	0.0007	-0.0037	128
34	55530.0618	0.0022	-0.0021	96
35	55530.1254	0.0010	-0.0010	131
67	55532.1189	0.0027	-0.0067	79
68	55532.1811	0.0033	-0.0070	114
114	55535.0687	0.0033	0.0065	128
115	55535.1298	0.0041	0.0051	93
130	55536.0598	0.0026	-0.0020	128
131	55536.1245	0.0020	0.0001	115

*BJD-2400000.

 † Against max = 2455527.9396 + 0.062479E. ‡ Number of points used to determine the maximum.**Fig. 49.** Superhump profiles of OT J0009 (2010). The profiles of superhumps strongly varied between nights. The figure was drawn against a mean period of 0.089117 d.

been detected well after the true maximum (the last preceding CRTS negative observation was on 2011 January 9). Although the lack of past outbursts might also support the interpretation as a potential WZ Sge-type dwarf nova, the object might belong to group “X” in Uemura et al. (2010), a small group of short- P_{orb} SU UMa-type dwarf novae without noticeable WZ Sge-type characteristics. Observations of future outbursts are desired.

3.41. OT J043112.5–031452

This object (= CSS110113:043112–031452), hereafter OT J0431) was discovered by the CRTS on 2011 January 13. Subsequent observations detected both superhumps and eclipses (vsnet-alert 12612, 12613, 12615; figure 56). The times of recorded eclipses, determined with the KW method, after removing linearly approximated trends around eclipses in order to minimize the effect of superhumps, are summarized in table 58. We obtained an ephemeris of

$$\text{Min(BJD)} = 2455575.27211(6) + 0.0660495(5)E. \quad (5)$$

The times of superhump maxima outside the eclipses are listed in table 59. Well-refined stage B and C superhumps were recorded. The P_{dot} and fractional excess of stage B superhumps are $+8.4(1.2) \times 10^{-5}$ and 2.3 %, respectively.

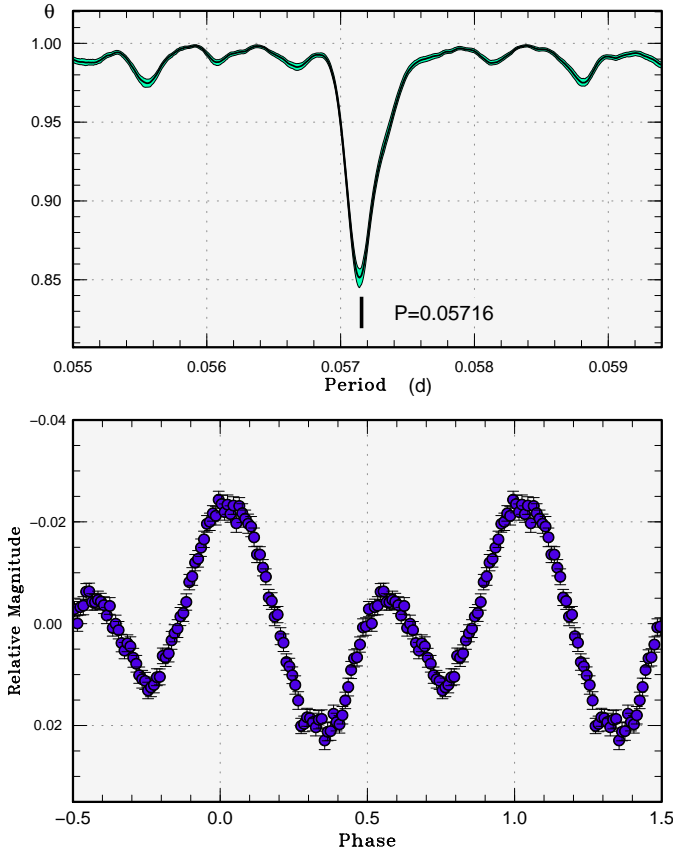


Fig. 50. Early superhumps in OT J0120 (2010). (Upper): PDM analysis. (Lower): Phase-averaged profile.

respectively, and are usual values for this P_{orb} . It is noteworthy that this object is the first eclipsing SU UMa-type dwarf nova with a very distinct positive P_{dot} and with distinct stages B and C [the best observed such an object dates back to XZ Eri (Uemura et al. 2004), with poorer statistics]. As in HT Cas (subsection 3.7), a strong beat phenomenon was observed (figure 57).

3.42. OT J044216.0–002334

This object (= CSS071115:044216–002334), hereafter OT J0442) was discovered by the CRTS in 2007 January. Three outburst have been known, and the 2011 January one was the brightest. Superhumps were subsequently detected (vsnet-alert 12784, 12785, 12786; figure 58). Since the observations were obtained at high airmasses, we corrected observations by using a second-order atmospheric extinction. The times of superhump maxima are listed in table 60.

3.43. OT J064804.5+414702

This object (= CSS091026:064805+414702, hereafter OT J0648) was discovered in outburst by the CRTS in 2009 October. During its 2011 January outburst, superhumps were detected (vsnet-alert 12735, 12737; figure 59). The times of superhump maxima are listed in table 61. The outburst was apparently already in stage B, and a

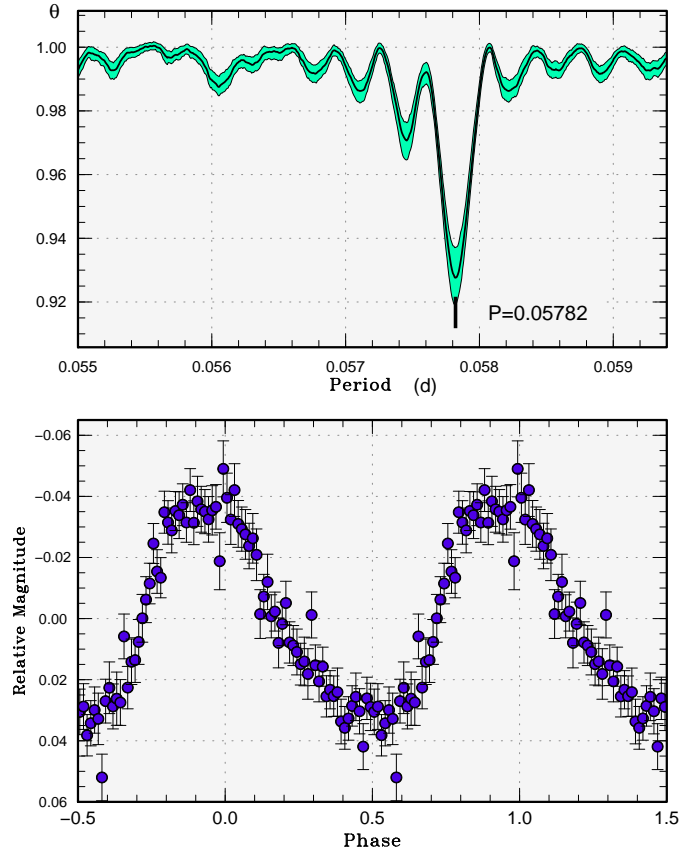


Fig. 51. Ordinary superhumps in OT J0120 (2010). (Upper): PDM analysis. (Lower): Phase-averaged profile.

transition to stage C superhumps was recorded five days later.

3.44. OT J075414.5+313216

This object (= CSS110414:075414+313216, hereafter OT J0754) was discovered by the CRTS on 2011 April 14. Two earlier outbursts (2007 February and 2008 November) were also detected by the CRTS, and the 2008 one reached a maximum of 14.2 mag. Subsequent observations detected superhumps (vsnet-alert 13166, 13186, 13202). Due to the limited nightly baselines, the possibility of one-day alias is not completely excluded (figure 60). The times of superhump maxima are listed in table 62. Although both the overall light curve and, $O-C$ variation and amplitudes of superhumps (cf. subsection 4.7) showed a typical course of a stage B–C transition (vsnet-alert 13219), the baseline was not sufficient to determine P_{dot} for stage B.

3.45. OT J102616.0+192045

This object (= CSS101130:102616+192045, hereafter OT J102616) was discovered by the CRTS on 2010 November 30. Two earlier outbursts (2006 April and 2007 April) were also detected by the CRTS. Subsequent observations immediately clarified the presence of superhumps (vsnet-alert 12447, 12452, 12459; figure 61). The

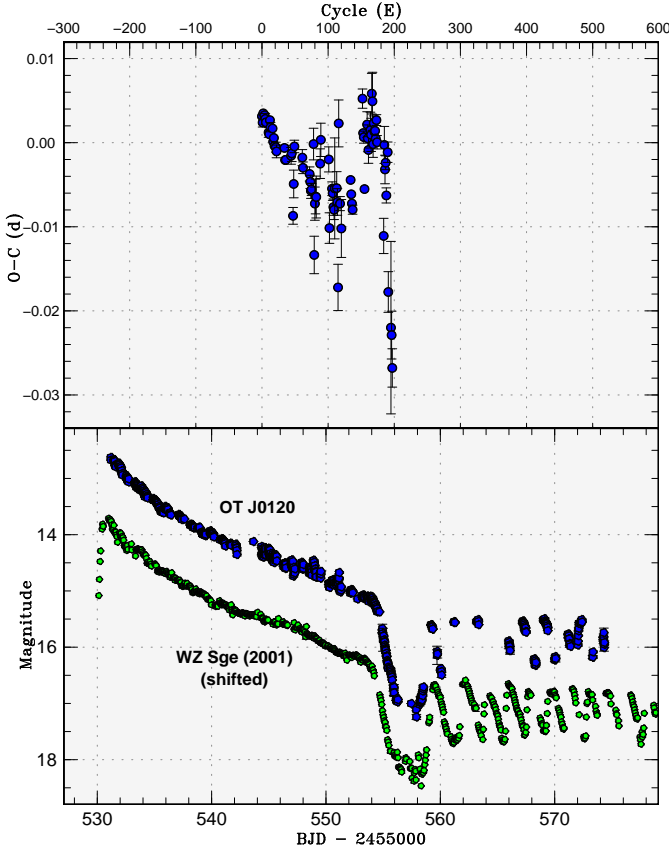


Fig. 52. $O-C$ diagram of superhumps in OT J0120 (2010). Upper: $O-C$ diagram. We used a period of 0.05784 d for calculating the $O-C$'s. Lower: Light curve and comparison with WZ Sge (2001). After a temporary “dip” following the rapid fading from the superoutburst, the object underwent multiple rebrightenings. The behavior was almost exactly same to the one in WZ Sge (2001).

large amplitudes (~ 0.3 mag) of superhumps at the start of the observation suggests that the observation succeeded in recording the relatively early stage of the superoutburst.

The times of superhump maxima are listed in table 63. There were a large systematic decrease in the superhump period, amounting to a global $P_{\text{dot}} = -8.6(1.5) \times 10^{-5}$ and a mean global $P_{\text{SH}} = 0.08267(4)$ d from timing analysis. There appeared to have been a discontinuous decrease of the period at $E = 36$ and early epochs ($E \leq 1$) may have resulted from stage A superhumps. Although we list values in table 3 based on this interpretation, there remains a possibility that the entire observation should be interpreted as stage B, as discussed in Kato et al. (2009a) (subsection 4.10). It is noteworthy that a relatively large negative P_{dot} was recorded in a system with a long- P_{orb} and with relatively infrequent outbursts. This object should require further attention.

3.46. OT J102705.8–434341

This object (= SSS110314:102706–434341, hereafter OT J1027) was discovered by the CRTS SSS on

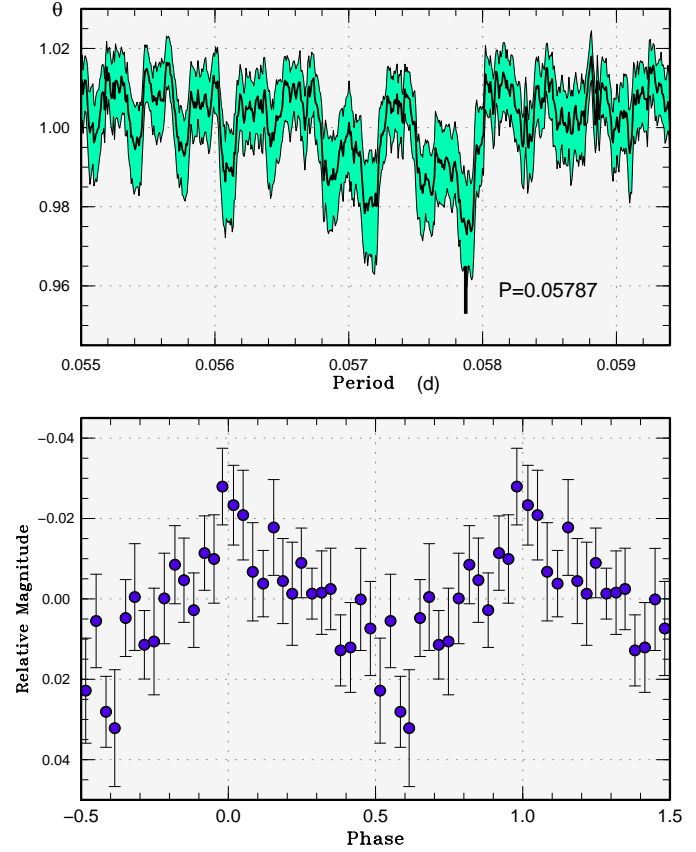


Fig. 53. Superhumps in OT J0120 during rebrightening phase (2010). (Upper): PDM analysis of the CRI and Shu data. The rejection rate for bootstrapping was reduced to 0.2 for better visualization. (Lower): Phase-averaged profile.

2011 March 14. There were four past outbursts in CRTS SSS data, and has an X-ray counterpart 1RXP J102706–4343.5. Subsequent observations detected superhumps (vsnet-alert 12997, 13009; figure 62). The times of superhump maxima are listed in table 64. The period given in table 3 was determined by the PDM method.

3.47. OT J120052.9–152620

This object (= CSS110205:120053–152620, hereafter OT J1200) was discovered by the CRTS on 2011 February 5. Both CRTS and ASAS-3 (Pojmański 2002) recorded numerous past outbursts, and the brightest outburst reaching $V = 13.39$ on 2001 February 14 recorded by ASAS-3 was indicative of a superoutburst (vsnet-alert 12792). Upon this information, follow-up observations indeed clarified the presence of superhumps (vsnet-alert 12803, 12815; figure 63). The times of superhump maxima are listed in table 65. Due to the short baseline of observations, we adopted the most likely one-day alias. Other aliases still remain viable. We adopted the period determined by the PDM method in table 3.

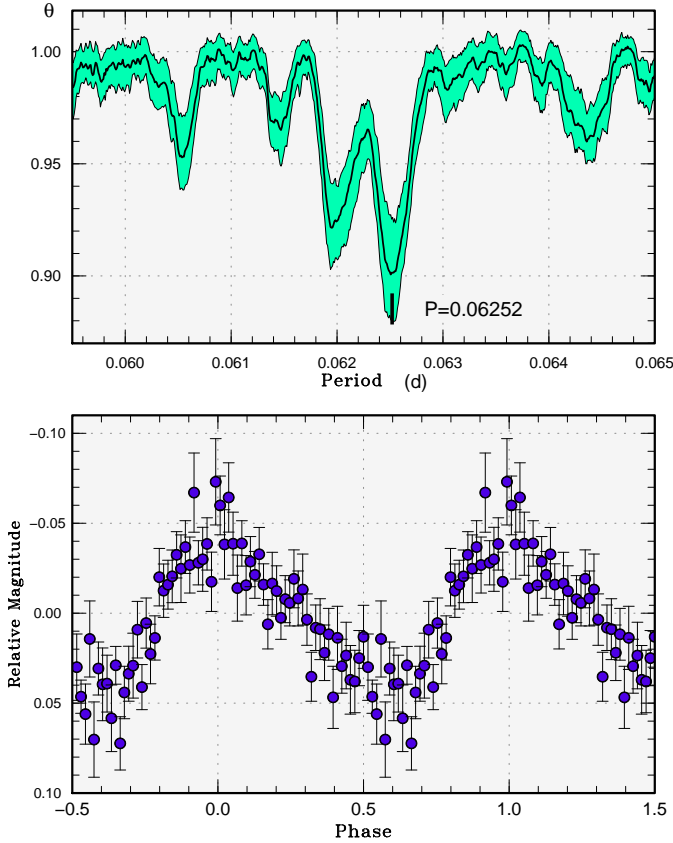


Fig. 54. Superhumps in OT J0141 (2010). (Upper): PDM analysis. (Lower): Phase-averaged profile.

3.48. OT J132900.9–365859

This object (= SSS110403:132901–365859), hereafter OT J1329) was discovered by the CRTS SSS on 2011 April 3. Subsequent observations detected apparent superhumps (vsnet-alert 13105; figure 64). The times of superhump maxima are listed in table 66. There appears to have been a stage transition between $E = 16$ and $E = 59$, and we listed a period from $E \leq 16$ for the period of stage B superhumps in table 3. Since there was no earlier record of outbursts in CRTS SSS, the object seems to have a relatively low outburst frequency.

3.49. OT J154544.9+442830

This object (= CSS110428:154545+442830), hereafter OT J1545) was discovered by the CRTS on 2011 April 28. Subsequent observations successfully detected superhumps (vsnet-alert 13275; figure 65). The times of superhump maxima are listed in table 67. The object started rapid fading only three days after the initial observation, and the outburst was observed only during its final phase. We identified the superhumps as being stage C superhumps.

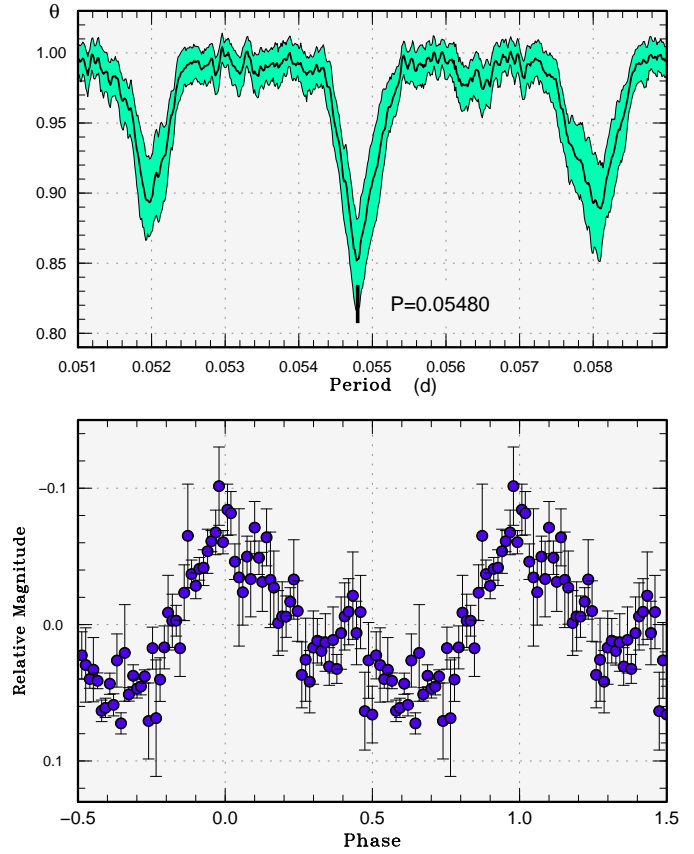


Fig. 55. Superhumps in OT J0413 (2011). (Upper): PDM analysis. (Lower): Phase-averaged profile.

3.50. OT J223418.5–035530

This object (= CSS090910:223418–035530), hereafter OT J2234) was discovered by the CRTS on 2009 September 10. We observed this object during two superoutbursts in 2009 and 2010. Although the existence of superhumps were already apparent in 2009 (cf. vsnet-alert 11480), the short observations were unable to select a unique period. Using the 2010 observations, we have selected a unique period, and the $O-C$'s referring to this period are listed in tables 68 and 69. Since the amplitudes of superhumps were low (~ 0.03 mag) and they grew to 0.18 mag six days later, the initial observations were apparently performed during the growing stage of superhumps. In table 3, we listed averaged periods for the entire runs since observations were too insufficient for determining stages and period changes. The superhumps recorded during the 2010 superoutburst is shown in figure 66.

3.51. OT J230425.8+062546

This transient was originally reported as a possible nova (Nakano et al. 2011)⁷. Soon after the announcement,

⁷ According to the information from the discoverer, the large difference in magnitudes between the discovery and confirmatory observations was probably caused by transformation of image

Table 57. Superhump maxima of OT J0413 (2011).

E	max*	error	$O - C^\dagger$	N^\ddagger
0	55587.6103	0.0005	0.0007	54
1	55587.6645	0.0006	0.0001	54
2	55587.7205	0.0004	0.0013	54
3	55587.7736	0.0006	-0.0004	54
18	55588.5962	0.0005	-0.0001	54
19	55588.6502	0.0006	-0.0008	54
20	55588.7055	0.0007	-0.0004	54
21	55588.7597	0.0006	-0.0010	53
36	55589.5831	0.0007	0.0002	54
37	55589.6360	0.0006	-0.0018	54
38	55589.6918	0.0007	-0.0008	53
39	55589.7477	0.0007	0.0003	53
54	55590.5699	0.0012	0.0002	27
55	55590.6239	0.0008	-0.0005	38
56	55590.6796	0.0007	0.0003	38
57	55590.7340	0.0008	-0.0001	37
58	55590.7890	0.0012	0.0001	22
73	55591.6125	0.0009	0.0014	36
74	55591.6676	0.0010	0.0017	38
75	55591.7226	0.0009	0.0018	37
76	55591.7766	0.0012	0.0010	29
100	55593.0881	0.0024	-0.0031	87

*BJD-2400000.

 † Against max = 245587.6096 + 0.054816*E*. ‡ Number of points used to determine the maximum.

the color of the quiescent counterpart inferred a dwarf-nova outburst (vsnet-alert 12548). Initial time-resolved photometry recorded relatively small variations (A. Arai, vsnet-alert 12558). Subsequent observations indicated the presence of superhumps with amplitude of 0.06 mag (A. Arai, vsnet-alert 12563). This finding was confirmed by subsequent observations (vsnet-alert 12564, 12578, 12633; figure 67).

Since the observations were obtained at high airmasses, we corrected observations by using a second-order atmospheric extinction. The resultant times of superhump maxima are listed in table 70. Since the observing windows were limited to the low evening sky, there remained an ambiguity in selecting the alias (cf. vsnet-alert 12578). The superhumps queerly grew since the detection until $E \sim 120$, when the period and amplitudes suddenly decreased (figure 68). Since the fractional decrease (1.4 %) is exceptionally large for a stage B-C transition (Kato et al. 2009a), we leave the interpretation of the later stage open though we tentatively assign the values in table 3. Although the results may have been affected by adverse observing conditions, the unusual development of superhumps in this system should warrant further study during future outbursts.

formats in the digital camera, and probably did not reflect true variation.

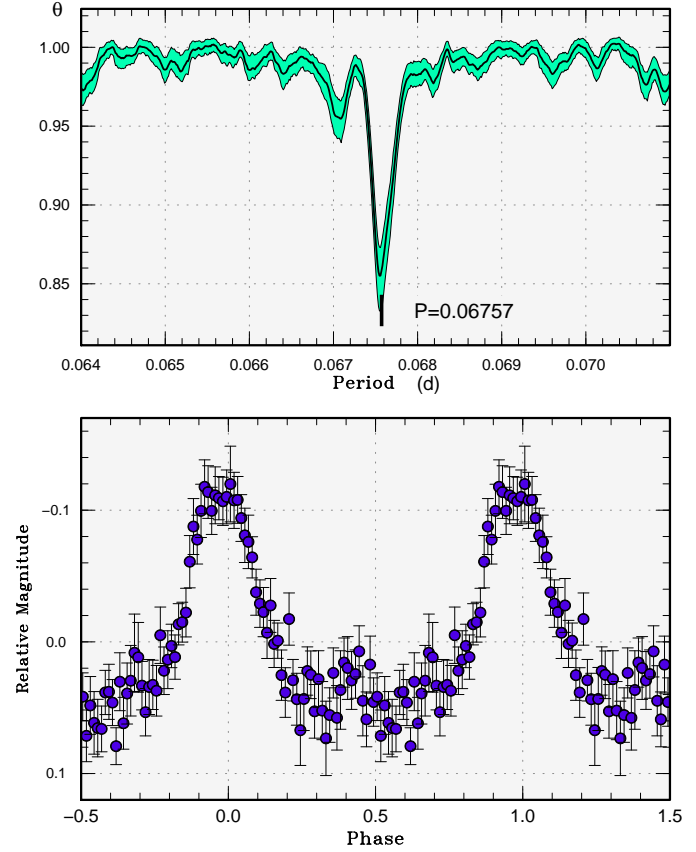


Fig. 56. Superhumps in OT J0431 (2011). (Upper): PDM analysis for the data before BJD 2455589. The data within orbital phases of 0.09 were removed before the analysis. (Lower): Phase-averaged profile.

4. Discussion

4.1. Re-calibration of $P_{\text{SH}}-P_{\text{orb}}$ Relation

The empirical relation by Stolz, Schoembs (1984) between P_{SH} and P_{orb} have been widely used in estimating P_{orb} from P_{SH} (e.g. Ritter, Kolb 2003). Since we now have a plenty of objects and know the difference between stage B and C superhumps, we provide an updated calibration. Since it was already evident that $P_{\text{orb}}-\epsilon$ relation deviates from a linear one (figure 15 in Kato et al. 2009a), we have introduced a $1/(P_{\text{orb}} - \text{const})$ -type dependence instead of the linear one in Stolz, Schoembs (1984). Using all samples with known P_{orb} and well-defined stage B superhumps (following the criteria used in Kato et al. 2009a), we have derived relations for objects below the period gap:

$$\epsilon = 0.000346(36)/(0.043 - P_{\text{orb}}) + 0.0443(21) \quad (6)$$

for the mean period of stage B superhumps, and

$$\epsilon = 0.000273(24)/(0.044 - P_{\text{orb}}) + 0.0381(13) \quad (7)$$

for the mean period of stage C superhumps.

Figure 69 represents the residuals for estimated P_{orb} from mean P_{SH} of stage B superhumps. The relation by

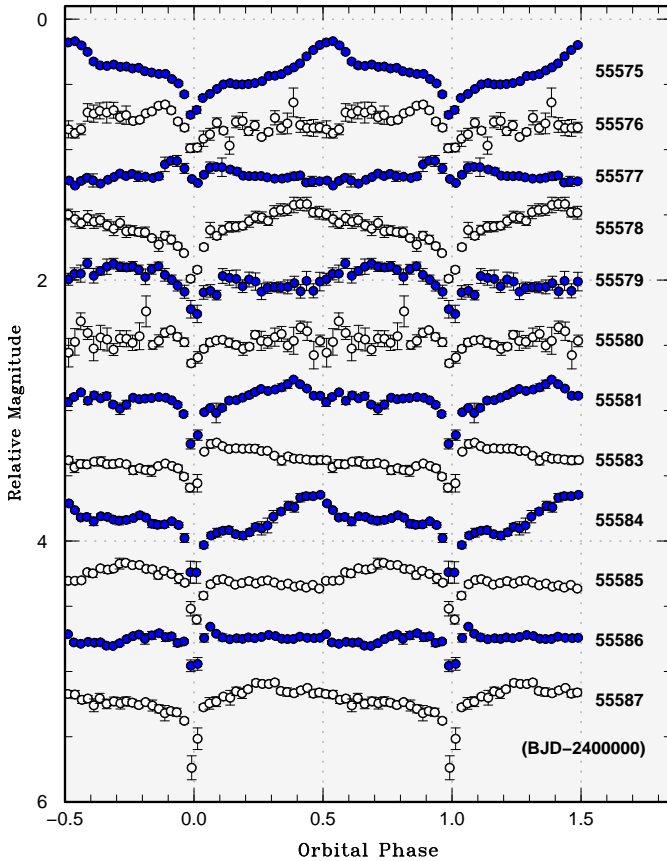


Fig. 57. Variation of superhumps and eclipses in OT J0431 (2011). The data for the first 12 d are shown. A strong beat phenomenon was observed. The symbols are interchangeably used every other day for easier visualization.

Stolz, Schoembs (1984) systematically (0.0003 d in average) gives longer P_{orb} . The $1\text{-}\sigma$ error for the estimated P_{orb} from the updated relation is 0.0003 d.

Figure 70 represents the residuals for estimated P_{orb} from mean P_{SH} of stage C superhumps. Although the relation by Stolz, Schoembs (1984) generally well reproduces the real P_{orb} , there remains a small systematic trend (shorter values for short- P_{orb} and long- P_{orb} systems and longer values for intermediate- P_{orb} systems). We conclude that the relation by Stolz, Schoembs (1984) appears to be generally useful for stage C superhumps, and suggest to use our updated relation for stage B superhumps especially when only early-stage observations and mean superhump periods are available. The $1\text{-}\sigma$ error for the estimated P_{orb} from the updated relation is 0.0003 d.

In the following subsections, orbital periods were estimated using these relations for objects without known orbital periods.

4.2. Period Derivatives during Stage B

Figure 71 represents the relation between P_{orb} and P_{dot} during stage B (note that we use P_{orb} instead of P_{SH} used in earlier papers). The enlarged figure (corresponding to figure 10 in Kato et al. 2009a) is only shown here. The

Table 58. Eclipse Minima of OT J0431 (2011).

E	Minimum*	error	$O - C^\dagger$
0	55575.27191	0.00012	-0.00020
1	55575.33844	0.00018	0.00028
2	55575.40389	0.00007	-0.00032
15	55576.26287	0.00007	0.00002
16	55576.32920	0.00030	0.00030
23	55576.79243	0.00005	0.00118
37	55577.71577	0.00006	-0.00017
38	55577.78178	0.00004	-0.00021
39	55577.84786	0.00006	-0.00018
52	55578.70661	0.00005	-0.00007
53	55578.77274	0.00005	0.00001
58	55579.10194	0.00010	-0.00103
67	55579.69737	0.00005	-0.00005
68	55579.76367	0.00009	0.00020
69	55579.82847	0.00006	-0.00106
82	55580.68795	0.00005	-0.00022
83	55580.75397	0.00005	-0.00025
84	55580.81997	0.00006	-0.00029
113	55582.73495	0.00009	-0.00075
114	55582.80158	0.00006	-0.00017
128	55583.72630	0.00005	-0.00014
129	55583.79240	0.00006	-0.00009
143	55584.71737	0.00004	0.00019
144	55584.78362	0.00006	0.00038
158	55585.70787	0.00006	-0.00005
159	55585.77401	0.00008	0.00004
173	55586.69850	0.00003	-0.00017
174	55586.76447	0.00003	-0.00024
187	55587.62349	0.00004	0.00013
188	55587.68957	0.00006	0.00016
189	55587.75559	0.00006	0.00013
203	55588.68015	0.00004	-0.00000
204	55588.74617	0.00002	-0.00003
205	55588.81211	0.00003	-0.00014

*BJD-2400000.

†Against equation 5.

new data generally confirmed the predominance of positive period derivatives during stage B in systems with orbital periods shorter than 0.07 d, in agreement with the tendency reported in Kato et al. (2009a) and Kato et al. (2010). Although longer period systems ($P_{\text{orb}} > 0.08$ d) tend to show zero or slightly negative P_{dot} , the new study suggest the presence of positive- P_{orb} systems in this period regime. The most striking example is GX Cas (2010, subsection 3.6).

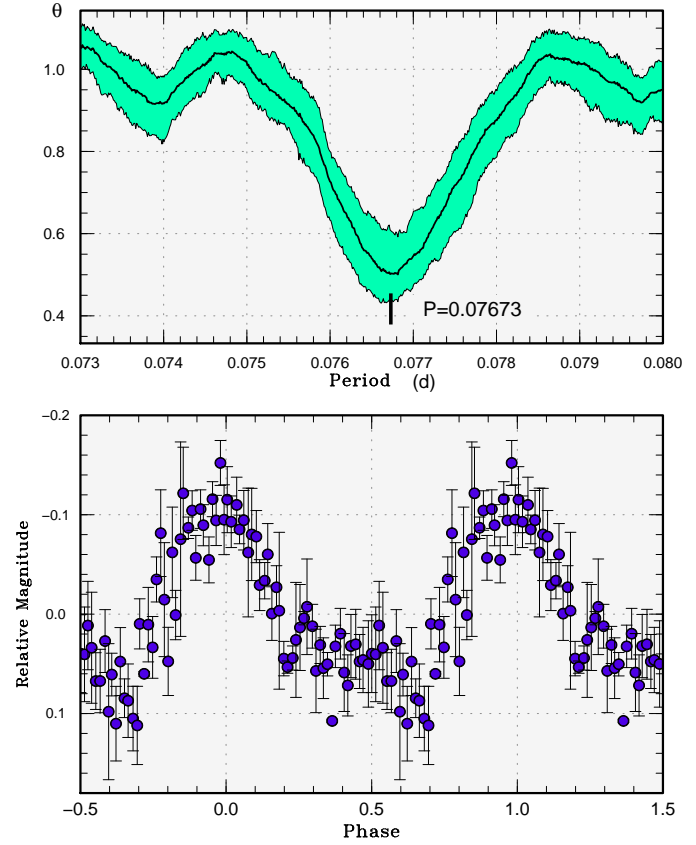
4.3. Periods of Stage A Superhumps

Since this table was missing in Kato et al. (2010), we list values for the second year and this (third) year (table 71) following the manner in Kato et al. (2009a). The combined figure is presented in figure 72. The fractional period excess (against periods of stage B superhumps) has a tendency to increase as P_{orb} increases. The result for

Table 59. Superhump maxima of OT J0431 (2011).

E	max*	error	$O - C^\dagger$	phase ‡	N^\S
0	55575.2417	0.0006	0.0021	0.54	51
1	55575.3078	0.0004	0.0007	0.54	66
2	55575.3750	0.0004	0.0004	0.56	59
3	55575.4422	0.0005	-0.0001	0.57	62
15	55576.2565	0.0011	0.0039	0.90	30
16	55576.3209	0.0009	0.0007	0.88	54
23	55576.7924	0.0011	-0.0005	0.02	50
37	55577.7350	0.0007	-0.0034	0.29	56
38	55577.8011	0.0006	-0.0048	0.29	56
40	55577.9387	0.0012	-0.0023	0.37	102
45	55578.2738	0.0006	-0.0048	0.45	45
46	55578.3437	0.0006	-0.0025	0.50	42
47	55578.4088	0.0006	-0.0050	0.49	48
52	55578.7490	0.0008	-0.0024	0.64	59
56	55579.0109	0.0028	-0.0107	0.61	26
57	55579.0860	0.0029	-0.0031	0.74	77
66	55579.6945	0.0020	-0.0023	0.96	32
67	55579.7617	0.0019	-0.0027	0.97	55
81	55580.7120	0.0006	0.0021	0.36	59
82	55580.7798	0.0006	0.0024	0.39	62
83	55580.8459	0.0011	0.0010	0.39	56
110	55582.6780	0.0024	0.0097	0.13	41
111	55582.7444	0.0014	0.0085	0.13	55
112	55582.8100	0.0012	0.0066	0.13	55
125	55583.6898	0.0011	0.0085	0.45	49
126	55583.7572	0.0005	0.0083	0.47	68
127	55583.8255	0.0009	0.0091	0.50	66
140	55584.7010	0.0005	0.0066	0.76	55
141	55584.7681	0.0007	0.0062	0.77	56
155	55585.7060	0.0008	-0.0014	0.97	57
156	55585.7705	0.0010	-0.0045	0.95	56
170	55586.7186	0.0009	-0.0018	0.30	56
171	55586.7854	0.0009	-0.0025	0.31	55
183	55587.6027	0.0026	0.0044	0.69	64
184	55587.6666	0.0012	0.0007	0.65	66
185	55587.7316	0.0010	-0.0018	0.64	70
199	55588.6665	0.0028	-0.0124	0.79	55
200	55588.7333	0.0044	-0.0131	0.80	56

*BJD-2400000.

 † Against max = 245575.2396 + 0.067534*E*. ‡ Orbital phase. § Number of points used to determine the maximum.**Fig. 58.** Superhumps in OT J0442 (2011). (Upper): PDM analysis (Lower): Phase-averaged profile.**Table 60.** Superhump maxima of OT J0442 (2011).

E	max*	error	$O - C^\dagger$	N^\ddagger
0	55596.3030	0.0030	-0.0009	23
1	55596.3821	0.0011	0.0015	41
13	55597.3014	0.0023	-0.0003	24
14	55597.3777	0.0013	-0.0008	40
26	55598.2999	0.0017	0.0002	33
27	55598.3767	0.0019	0.0003	34

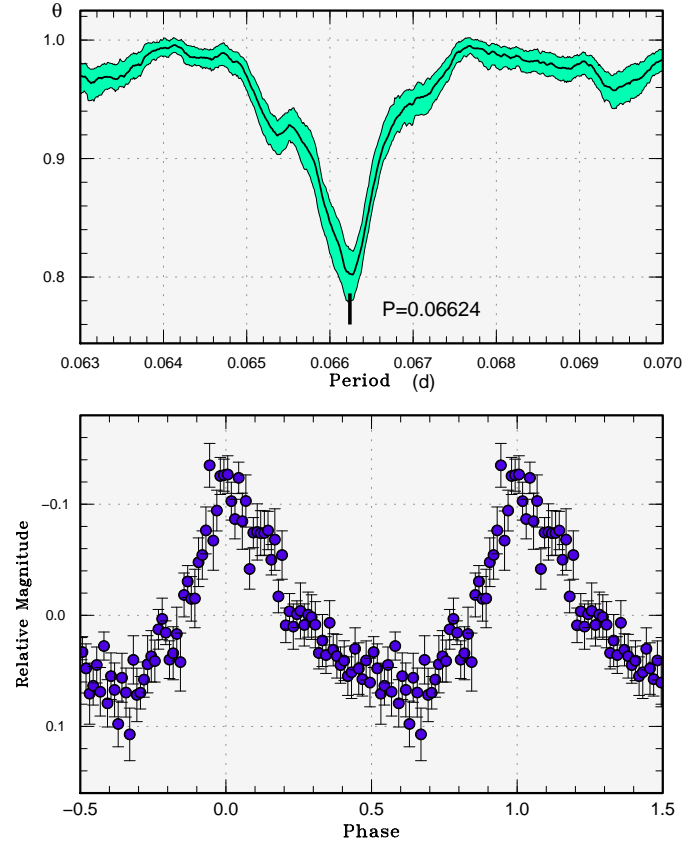
*BJD-2400000.

 † Against max = 245596.3039 + 0.076761*E*. ‡ Number of points used to determine the maximum.

Table 61. Superhump maxima of OT J0648 (2011).

E	max*	error	$O - C^\dagger$	N^\ddagger
0	55590.5903	0.0006	0.0011	67
1	55590.6583	0.0002	0.0027	126
2	55590.7236	0.0003	0.0017	126
3	55590.7902	0.0003	0.0020	126
4	55590.8552	0.0004	0.0007	126
5	55590.9218	0.0004	0.0011	125
10	55591.2531	0.0011	0.0008	133
12	55591.3849	0.0008	0.0001	76
13	55591.4514	0.0007	0.0003	88
14	55591.5168	0.0009	-0.0006	68
23	55592.1114	0.0013	-0.0026	105
24	55592.1804	0.0013	0.0001	129
25	55592.2461	0.0018	-0.0005	119
26	55592.3094	0.0021	-0.0035	82
27	55592.3749	0.0013	-0.0043	60
28	55592.4402	0.0023	-0.0053	66
29	55592.5112	0.0013	-0.0006	58
42	55593.3715	0.0022	-0.0021	63
43	55593.4412	0.0017	0.0013	23
44	55593.5072	0.0023	0.0010	68
69	55595.1644	0.0056	0.0008	134
70	55595.2399	0.0102	0.0100	81
83	55596.0875	0.0028	-0.0042	122

*BJD-2400000.

 \dagger Against max = 245590.5893 + 0.066295 E . \ddagger Number of points used to determine the maximum.**Fig. 59.** Superhumps in OT J0648 (2011). (Upper): PDM analysis. (Lower): Phase-averaged profile.**Table 62.** Superhump maxima of OT J0754 (2011).

E	max*	error	$O - C^\dagger$	N^\ddagger
0	55666.3975	0.0012	-0.0050	65
1	55666.4626	0.0015	-0.0027	55
16	55667.4058	0.0009	-0.0019	64
17	55667.4713	0.0016	0.0008	43
31	55668.3503	0.0011	0.0002	47
32	55668.4154	0.0009	0.0025	65
33	55668.4844	0.0023	0.0086	38
63	55670.3587	0.0015	-0.0018	33
64	55670.4252	0.0018	0.0019	34
65	55670.4858	0.0022	-0.0004	29
79	55671.3661	0.0015	0.0004	31
80	55671.4291	0.0026	0.0005	34
81	55671.4993	0.0038	0.0079	18
95	55672.3662	0.0050	-0.0048	34
96	55672.4276	0.0045	-0.0061	34

*BJD-2400000.

 \dagger Against max = 2455666.4025 + 0.062826 E . \ddagger Number of points used to determine the maximum.**Table 63.** Superhump maxima of OT J102616 (2010).

E	max*	error	$O - C^\dagger$	N^\ddagger
0	55533.4881	0.0006	-0.0094	131
1	55533.5744	0.0001	-0.0058	245
13	55534.5738	0.0004	0.0016	74
22	55535.3196	0.0003	0.0034	321
25	55535.5677	0.0002	0.0035	291
36	55536.4789	0.0003	0.0053	127
47	55537.3859	0.0005	0.0029	92
48	55537.4685	0.0003	0.0029	131
61	55538.5434	0.0004	0.0030	109
62	55538.6257	0.0006	0.0026	73
70	55539.2847	0.0008	0.0003	105
82	55540.2738	0.0006	-0.0026	100
95	55541.3495	0.0023	-0.0017	100
107	55542.3373	0.0012	-0.0059	185

*BJD-2400000.

 \dagger Against max = 2455533.4975 + 0.082670 E . \ddagger Number of points used to determine the maximum.

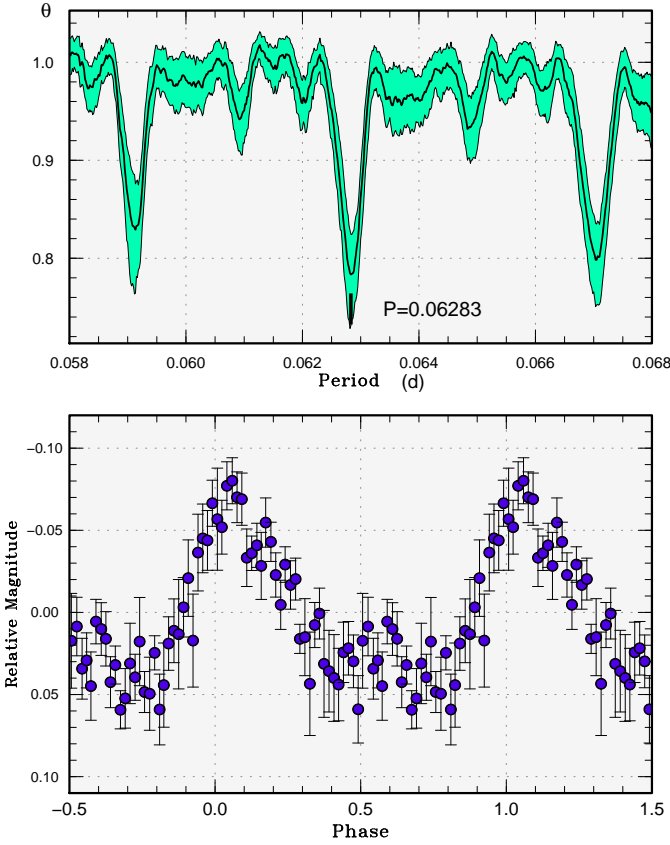


Fig. 60. Superhumps in OT J0754 (2011). (Upper): PDM analysis. (Lower): Phase-averaged profile.

Table 64. Superhump maxima of OT J1027 (2011).

E	max*	error	$O - C^\dagger$	N^\ddagger
0	55637.0723	0.0007	-0.0001	109
1	55637.1532	0.0006	-0.0001	109
2	55637.2351	0.0006	0.0009	109
3	55637.3142	0.0007	-0.0009	110
12	55638.0444	0.0008	0.0013	79
13	55638.1242	0.0009	0.0003	84
14	55638.2024	0.0010	-0.0024	84
15	55638.2867	0.0011	0.0010	85

*BJD-2400000.

†Against max = 2455637.0724 + 0.080885 E .

‡Number of points used to determine the maximum.

Table 65. Superhump maxima of OT J1200 (2011).

E	max*	error	$O - C^\dagger$	N^\ddagger
0	55599.6371	0.0005	-0.0004	87
9	55600.5242	0.0011	0.0041	62
10	55600.6145	0.0004	-0.0037	97

*BJD-2400000.

†Against max = 2455599.6375 + 0.098066 E .

‡Number of points used to determine the maximum.

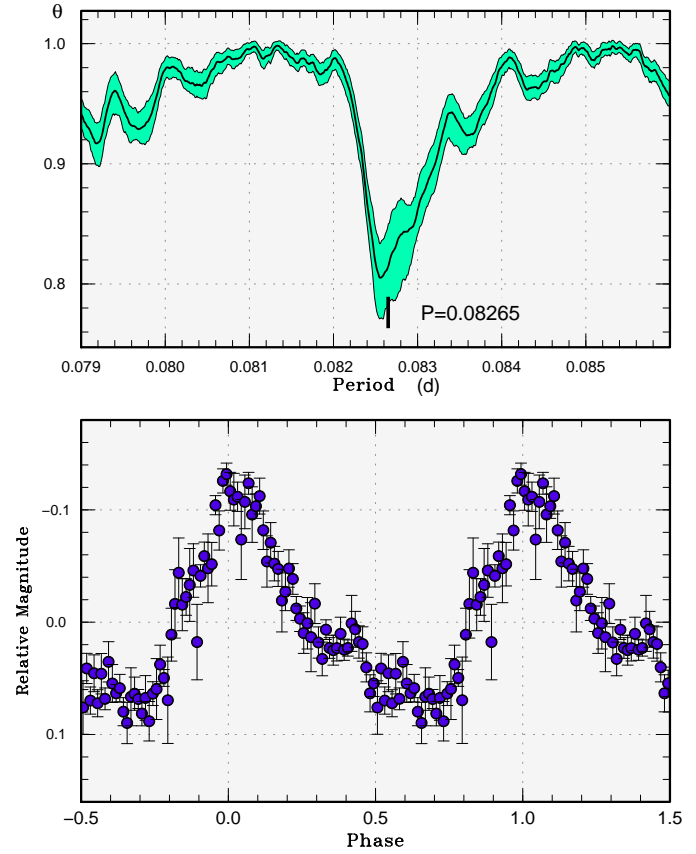


Fig. 61. Superhumps in OT J102616 (2010). (Upper): PDM analysis. The indicated period was determined from a PDM analysis of the entire data, and is slightly different from the bootstrap median. This difference probably arises from the relatively large variation in the period. (Lower): Phase-averaged profile.

Table 66. Superhump maxima of OT J1329 (2011).

E	max*	error	$O - C^\dagger$	N^\ddagger
0	55656.4074	0.0011	-0.0050	118
1	55656.4796	0.0014	-0.0033	162
13	55657.3296	0.0011	0.0007	162
14	55657.4017	0.0010	0.0023	161
15	55657.4743	0.0009	0.0045	162
16	55657.5439	0.0020	0.0035	155
59	55660.5723	0.0020	0.0007	162
60	55660.6386	0.0020	-0.0034	159

*BJD-2400000.

†Against max = 2455656.4125 + 0.070493 E .

‡Number of points used to determine the maximum.

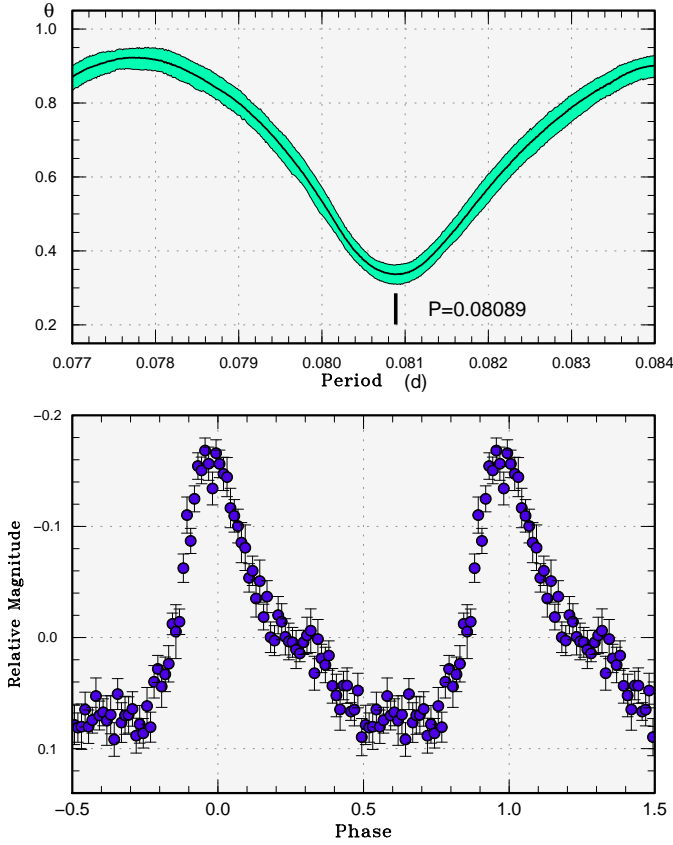


Fig. 62. Superhumps in OT J1027 (2011). (Upper): PDM analysis. (Lower): Phase-averaged profile.

Table 67. Superhump maxima of OT J1545 (2011).

E	max*	error	$O - C^\dagger$	N^\ddagger
0	55681.1443	0.0050	-0.0045	83
1	55681.2289	0.0007	0.0030	157
17	55682.4600	0.0037	0.0020	18
18	55682.5354	0.0021	0.0004	25
29	55683.3812	0.0020	-0.0008	22
30	55683.4587	0.0019	-0.0003	21
31	55683.5344	0.0017	-0.0017	22
32	55683.6176	0.0021	0.0045	14
42	55684.3821	0.0011	-0.0011	25
43	55684.4567	0.0018	-0.0035	23
44	55684.5342	0.0018	-0.0029	25
45	55684.6191	0.0040	0.0049	15

*BJD-2400000.

† Against max = 2455681.1488 + 0.077008 E .

‡ Number of points used to determine the maximum.

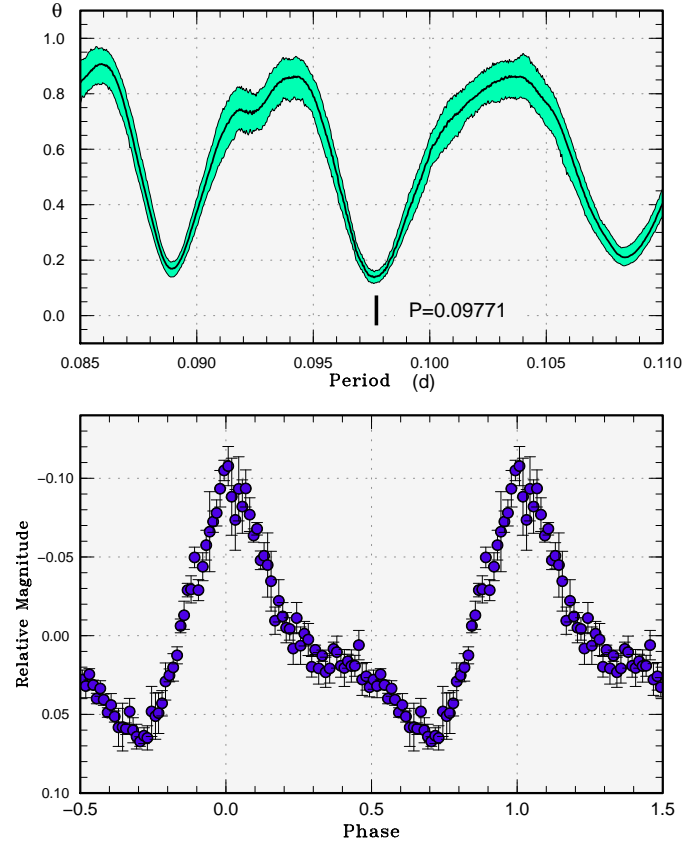


Fig. 63. Superhumps in OT J1200 (2011). (Upper): PDM analysis. (Lower): Phase-averaged profile.

Table 68. Superhump maxima of OT J2234 (2009).

E	max*	error	$O - C^\dagger$	N^\ddagger
0	55084.9749	0.0184	0.0014	134
1	55085.0638	0.0052	-0.0018	194
66	55091.0591	0.0012	0.0010	194
109	55095.0217	0.0026	-0.0006	186

*BJD-2400000.

† Against max = 2455084.9734 + 0.092192 E .

‡ Number of points used to determine the maximum.

Table 69. Superhump maxima of OT J2234 (2010).

E	max*	error	$O - C^\dagger$	N^\ddagger
0	55482.0178	0.0008	0.0001	93
1	55482.1094	0.0007	-0.0002	95
2	55482.2017	0.0011	0.0001	78

*BJD-2400000.

† Against max = 2455482.0177 + 0.091914 E .

‡ Number of points used to determine the maximum.

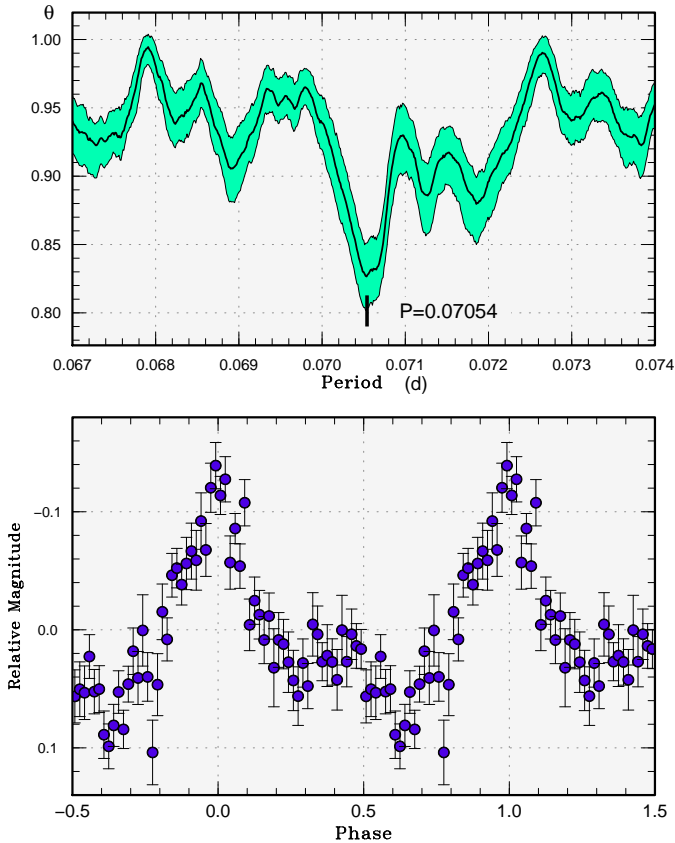


Fig. 64. Superhumps in OT J1329 (2011). (Upper): PDM analysis. (Lower): Phase-averaged profile.

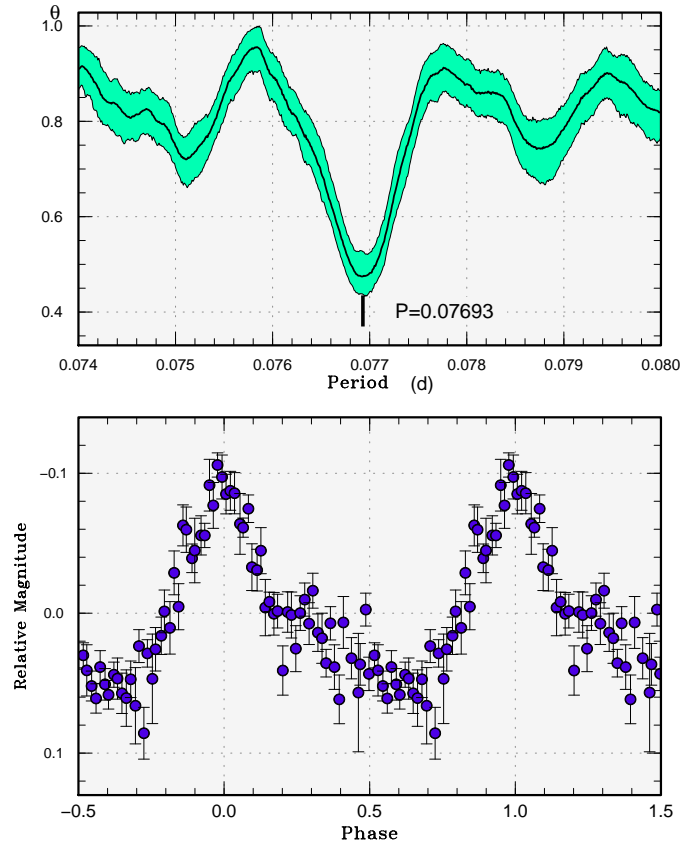


Fig. 65. Superhumps in OT J2234 (2011). (Upper): PDM analysis. (Lower): Phase-averaged profile.

high-accuracy Kepler data (subsection 4.5) agrees with other ground-based observations.

As shown in subsection 3.11, MM Hya likely had an unusually large fractional period excess for stage A superhumps. This needs to be confirmed by future observations.

We discussed the origin of stage A superhumps in Kato et al. (2009a) and presented two possibilities: larger precession rate for larger disks or longer periods during the growing stage suggested by smoothed particle hydrodynamics (SPH) simulations. There have been growing evidence favoring the latter with SPH simulations (Murray 1998; Smith et al. 2007) and most recently in Kley et al. (2008), which first successfully produced the growing eccentric mode with a grid-based simulation.

4.4. WZ Sge-Type Stars: Statistics

Table 72 summarizes the properties of new outbursts of WZ Sge-type and related objects reported in Kato et al. (2010) and this paper (the selection criteria are the same as in Kato et al. 2009a). Although many of recently discovered WZ Sge-type objects were not sufficiently observed during the earliest stages of their outbursts, the fractional superhump excesses were relatively well determined.

Figure 73 shows the relation between P_{dot} versus ϵ for WZ Sge-type dwarf novae studied in these series of pa-

pers. In Kato et al. (2010) and this paper, higher values P_{dot} were recorded for short- P_{orb} systems, and the relation described in Kato et al. (2009a) became less clear. These outbursts are V592 Her (2010), OT J2138 (2010) and SDSS J0804 (2010). As already described in subsection 3.27, the large P_{dot} in SDSS J0804 (2010) is an outlier among objects with multiple rebrightenings. The large P_{dot} in this system may have been affected by a large “disturbance” in the $O-C$ diagram near the end of the superoutburst plateau, and the P_{dot} during the earlier part of the stage B superhumps was much smaller [$P_{\text{dot}} = +3.5(0.9) \times 10^{-5}$]. The same phenomenon is sometimes obvious in other WZ Sge-type dwarf novae [V455 And (2007), figure 44 and the secondary component in WZ Sge (2001), figure 127 in Kato et al. (2009a)] and all of them are eclipsing objects. The high inclination may be somehow responsible for this phenomenon (see also a discussion in subsection 4.7), and we might better exclude the “disturbance” part of the $O-C$ diagram in determining the representative P_{dot} in such systems. The interpretation of this phenomenon needs to be investigated further.

WZ Sge-type dwarf novae show various activities during the post-superoutburst stage. In Kato et al. (2009a), we introduced a classification: type-A (long-lasting post-outburst rebrightening), type-B (multiple discrete rebrightenings), type-C (single rebrightening) and type-D

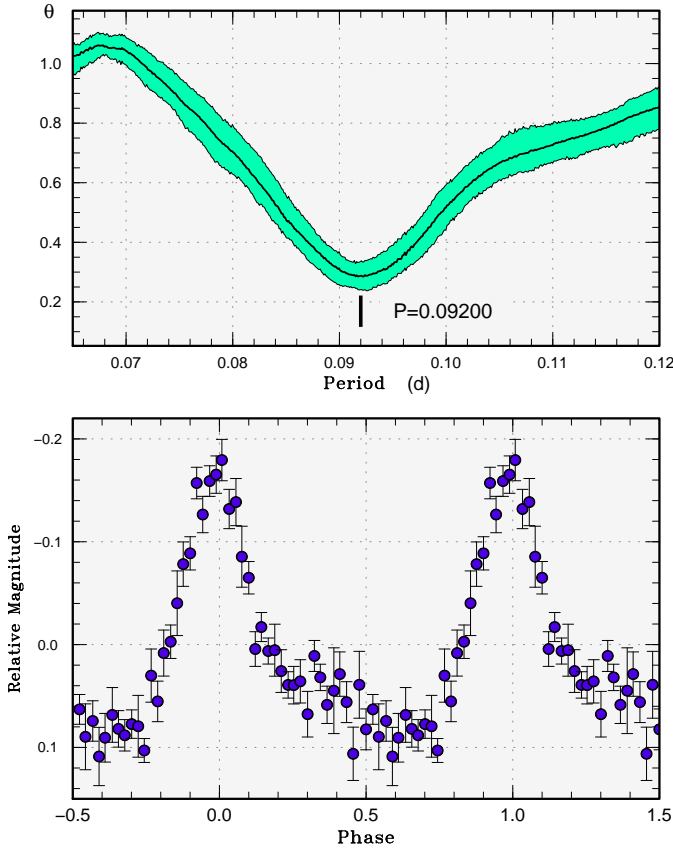


Fig. 66. Superhumps in OT J2234 (2010). (Upper): PDM analysis. (Lower): Phase-averaged profile.

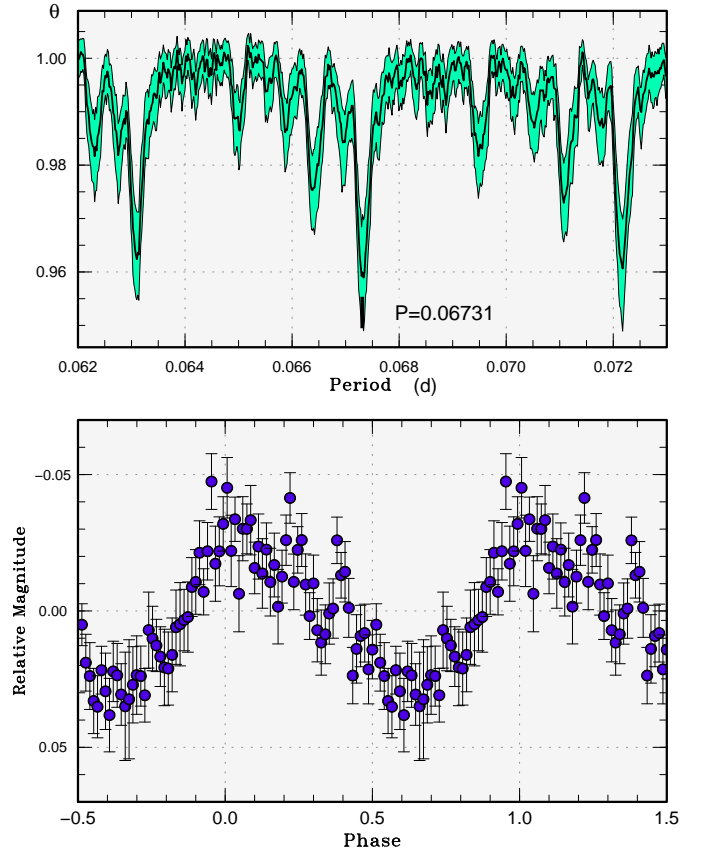


Fig. 67. Superhumps in OT J2304 (2011). (Upper): PDM analysis. (Lower): Phase-averaged profile.

(no rebrightening). It is known that there is a dependence of the types of outbursts on P_{orb} and ϵ (figure 37 in Kato et al. 2009a; note P_{SH} was instead used). The updated statistics (figure 74) basically strengthens the earlier finding: type-B objects mostly occupy low- ϵ and middle- P_{orb} region, type-A and type-D objects occupy middle- ϵ and short- P_{orb} region, and type-C objects are more scattered. The type-D outlier is SDSS J0804 as described above.

4.5. Analysis of Kepler Observations

The data for two SU UMa-type dwarf novae are available in Kepler (Koch et al. 2010) public release data. One of them (V344 Lyr) has already been published (Still et al. 2010). Cannizzo et al. (2010) compared the Kepler data with model simulations based on thermal-tidal disk instability. We examined Kepler observations from the viewpoint of the current study. The magnitudes were calculated from the corrected aperture-integrated flux obtained from the Kepler pipeline, with an arbitrary photometric zero-point.

4.5.1. Superhumps in V1504 Cygni

Kepler recorded the 2009 September superoutburst of this object (see subsection 3.8 for detailed data). This outburst was composed of a precursor outburst lasting for ~ 2 d, and superhumps started to develop around the maximum of this precursor. As the superhumps developed,

the object stopped fading and entered the plateau phase of the superoutburst (figure 75). The plateau phase lasted for ~ 9 d, followed by a steeper decline. During the entire course of the plateau phase and decline phase, ordinary superhumps were present. The amplitudes of superhumps were large around the maximum, initially decayed relatively rapidly for 3.2 d. After reaching a minimum, the amplitudes slightly increased, but again decayed in ~ 2 d.

The $O-C$ diagram indicates the presence of fine structures rather than our discrete three stages. The transitions between stages were smoother than in many objects in our present and past studies. In table 3, we assigned stage A before the epoch of maximum amplitude, and stages B and C were divided by a kink in the $O-C$ diagram. The relatively smooth variation in the $O-C$ diagram and the lack of segment with a positive P_{dot} might be attributable to the notably high frequency of outbursts in this system (Rajkov, Yushchenko 1987; Nogami, Masuda 1997), suggesting a high mass-transfer rate. Although the tendency that objects with high outburst frequencies tend to show smoother $O-C$ variation was originally proposed for long- P_{orb} systems (Kato et al. 2009a, subsection 4.10), it might also be extended to shorter- P_{orb} systems as in V1504 Cyg.

Yet another interesting feature is in the fine structure during stage A. During the first 8 superhump cycles, the

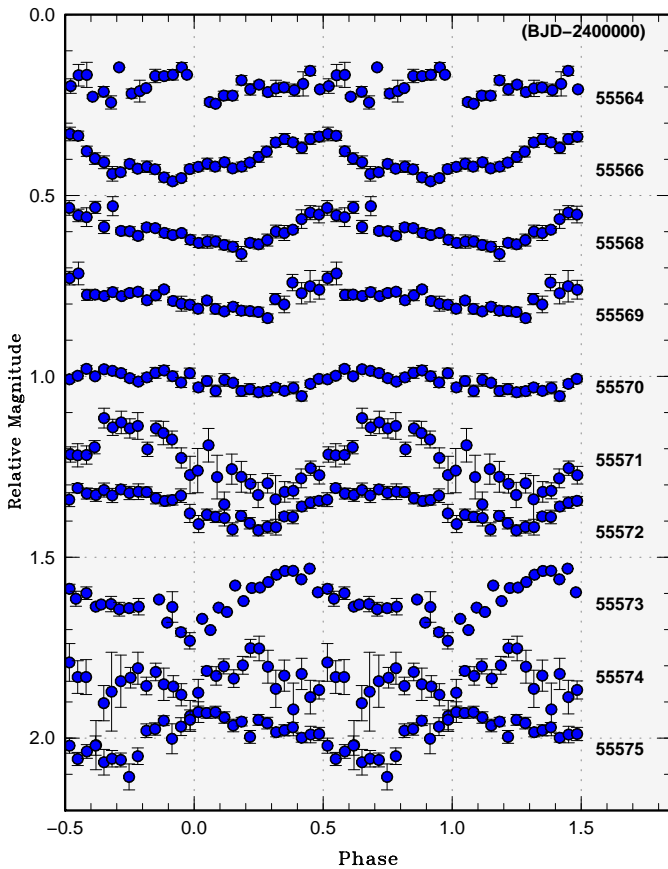
Table 72. Parameters of WZ Sge-type superoutbursts.

Object	Year	P_{SH}	P_{orb}	P_{dot}^*	err*	ϵ	Type [†]	N_{reb}^{\ddagger}	delay [§]	Max	Min
VX For	2009	0.061327	–	1.0	1.4	–	B	5	–	12.6	20.6
V592 Her	2010	0.056607	0.0561	7.4	0.6	0.009	D	0	≥ 4	14.2	21.3
BC UMa	2009	0.064553	0.06261	9.5	2.7	0.031	–	–	–	11.6	18.6
SDSS J1610	2009	0.057820	0.05695	6.8	1.4	0.015	D?	0?	≥ 2	13.9	20.1
OT J1044	2010	0.060236	0.05909	–	–	0.019	C	1	≥ 5	12.6	19.3
OT J2138	2010	0.055019	0.05450	7.9	0.7	0.010	D	0	6	8.7	[15.4
OT J2230	2009	–	0.05841	–	–	–	–	–	≥ 4	14.4	21.0
ASAS J1025	2011	0.063538	0.06136	9.9	2.4	0.035	–	–	–	12.9	19.3
MisV 1443	2011	0.056725	–	5.5	1.5	–	C?	1?	–	12.8	19.7
SDSS J0804	2010	0.059630	0.059005	9.6	1.1	0.011	B	6	4	12.0	17.8
SDSS J1339	2011	0.058094	0.057289	5.4	0.2	0.014	D	0	≥ 6	9.9	17.7
SDSS J1605	2010	–	0.05666	–	–	–	A?	?	≥ 3	12.0	19.9
OT J0120	2010	0.057833	0.057157	4.3	0.5	0.012	A	≥ 9	≥ 11	12.3	20.0

*Unit 10^{-5} .[†]A: long-lasting rebrightening; B: multiple rebrightenings; C: single rebrightening; D: no rebrightening.[‡]Number of rebrightenings.[§]Days before ordinary superhumps appeared.**Table 70.** Superhump maxima of OT J2304 (2011).

E	max*	error	$O - C^{\dagger}$	N^{\ddagger}
0	55563.9791	0.0028	-0.0354	108
29	55565.9214	0.0011	-0.0273	274
30	55565.9956	0.0023	-0.0198	64
59	55567.9479	0.0017	-0.0019	104
60	55568.0077	0.0015	-0.0087	70
74	55568.9571	0.0016	0.0069	215
88	55569.8972	0.0014	0.0132	347
89	55569.9608	0.0018	0.0101	427
103	55570.9046	0.0013	0.0201	116
104	55570.9694	0.0011	0.0182	107
118	55571.9022	0.0009	0.0172	217
119	55571.9743	0.0014	0.0226	211
122	55572.1788	0.0022	0.0271	15
123	55572.2380	0.0014	0.0195	12
137	55573.1684	0.0071	0.0162	16
149	55573.9517	0.0014	-0.0009	148
164	55574.9499	0.0013	-0.0032	107
179	55575.9383	0.0022	-0.0153	150
224	55578.9187	0.0043	-0.0364	237
254	55580.9340	0.0014	-0.0221	192

*BJD-2400000.

[†]Against max = 245564.0145 + 0.066699E.[‡]Number of points used to determine the maximum.**Fig. 68.** Superhump profiles of OT J2304 (2011) for the first 10 d. The amplitudes of superhumps gradually grew until BJD 245571. The period apparently shortened after this. The profiles of superhumps were rather irregular and the amplitudes were generally small. The figure was drawn against a period of 0.06705 d.

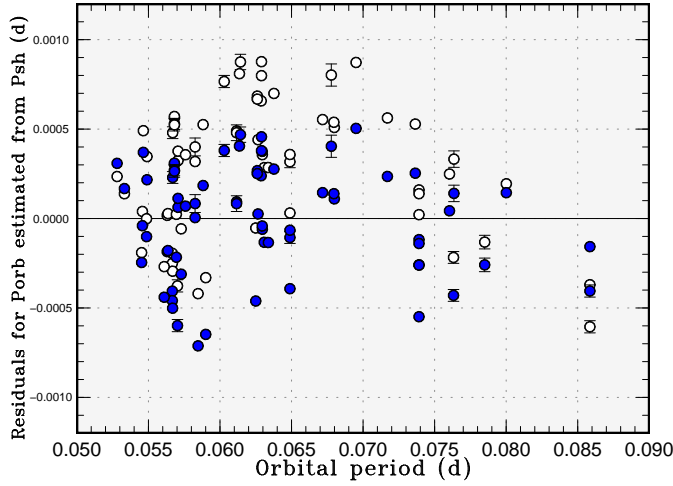


Fig. 69. Residuals for estimated P_{orb} from mean P_{SH} of stage B superhumps. Filled and open circles represent the present relation (equation 6) and Stolz, Schoembs (1984), respectively. The relation by Stolz, Schoembs (1984) systematically gives longer P_{orb} .

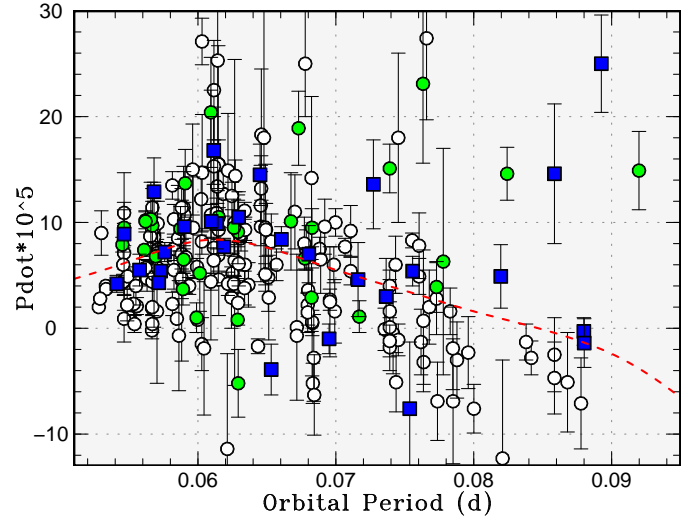


Fig. 71. P_{dot} for stage B versus P_{orb} . Open circles, filled circles and filled squares represent samples in Kato et al. (2009a), Kato et al. (2010) and this paper, respectively. The curve represents the spline-smoothed global trend.

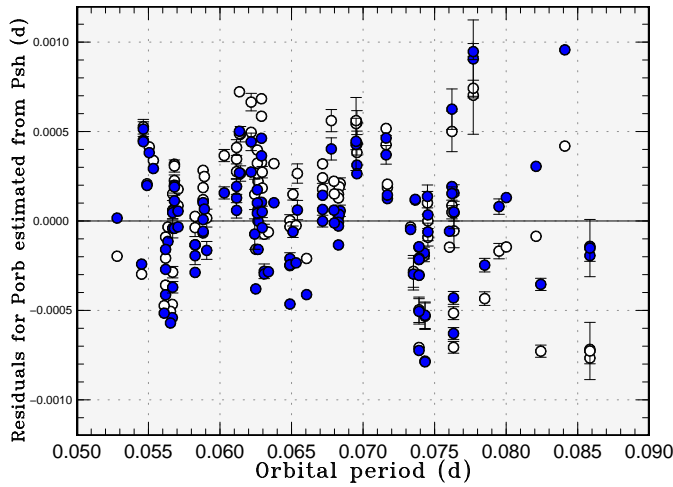


Fig. 70. Residuals for estimated P_{orb} from mean P_{SH} of stage C superhumps. Filled and open circles represent the present relation (equation 6) and Stolz, Schoembs (1984), respectively. Although the relation by Stolz, Schoembs (1984) generally well reproduces the real P_{orb} , there remains a small systematic trend.

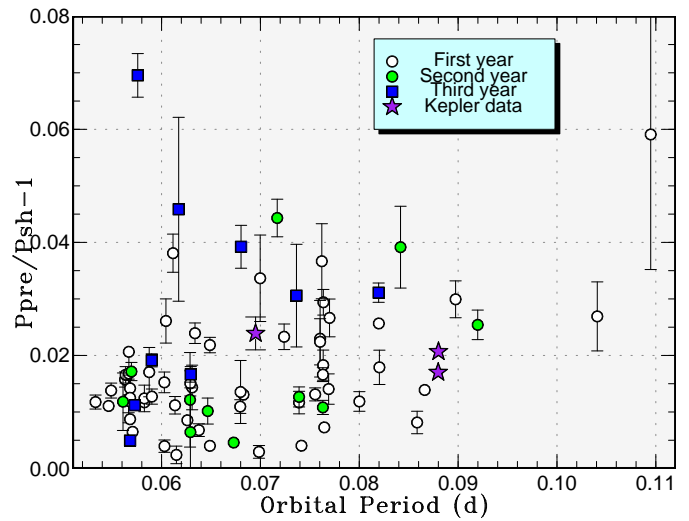


Fig. 72. Superhump periods during the stage A. Superhumps in this stage has a period typically 1.0–1.5 % longer than the one during the stage B. There is a slight tendency of increasing fractional period excess for longer- P_{orb} systems. The symbols for first, second and third years represent data in Kato et al. (2009a), Kato et al. (2010) and this paper.

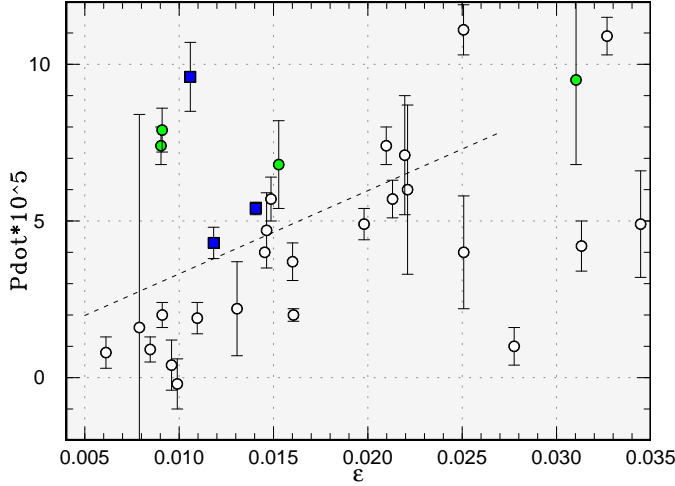


Fig. 73. P_{dot} versus ϵ for WZ Sge-type dwarf novae. Open circles, filled circles and filled squares represents outbursts reported in Kato et al. (2009a), Kato et al. (2010) and this paper, respectively. The dashed line represents a linear regression for points with $\epsilon < 0.026$ as in Kato et al. (2009a) figure 36.

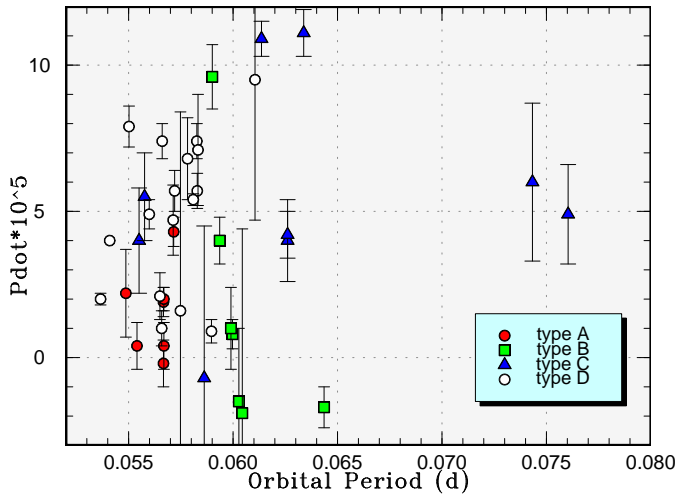


Fig. 74. P_{dot} versus P_{SH} for WZ Sge-type dwarf novae. Symbols represent the type (cf. Kato et al. 2009a) of outburst: type-A (filled circles), type-B (filled squares), type-C (filled triangles), type-D (open circles).

Table 71. Superhump Periods during Stage A

Object*	Year	period (d)	err
NN Cam	2009	0.07755	0.00025
V592 Her	2010	0.05728	0.00029
CT Hya	2010	0.06718	0.00015
EF Peg	2009	0.09077	0.00063
EK TrA	2009	0.06562	0.00054
IY UMa	2009	0.07717	0.00014
1RXS J0423	2010	0.07930	0.00010
SDSS J1610	2009	0.05881	0.00009
SDSS J1625	2010	0.09849	0.00025
OT J0506	2009	0.06964	0.00005
OT J1044	2010	0.06084	0.00003
OT J1440	2009	0.06503	0.00051
BG Ari	2010	0.08754	0.00015
HT Cas	2010	0.07868	0.00069
V1504 Cyg	2009b	0.07395	0.00021
MM Hya	2011	0.06295	0.00023
V344 Lyr	2009	0.09314	0.00009
V344 Lyr	2009b	0.09351	0.00011
V1212 Tau	2011	0.07286	0.00027
SW UMa	2010	0.05850	0.00002
SDSS J0804	2010	0.06077	0.00007
SDSS J1146	2011	0.06623	0.00103
SDSS J1227	2007	0.06568	0.00009
SDSS J1339	2011	0.05874	0.00003

*Abbreviations for Kato et al. (2010) objects:

1RXS J0423: 1RXS J042332+745300

SDSS J1610: SDSS J161027.61+090738.4

SDSS J1625: SDSS J162520.29+120308.7

OT J0506: OT J050617.4+354738

OT J1044: OT J104411.4+211307

OT J1440: OT J144011.0+494734

period of superhumps once shortened while the amplitudes stayed low. Following this stage of initial development, the amplitudes quickly grew and the period stayed at a relatively constant value. This later stage has likely been recognized as stage A superhumps in ground-based observations.

During the growing stage, small-amplitude (~ 0.01 mag) quasi-periodic oscillations (QPOs) with time-scales of ~ 10 min were superimposed on superhumps while they disappeared when superhumps quickly grew. These modulations resemble so-called “super-QPOs” in some SU UMa-type dwarf novae during the evolutionary stage of superhumps (cf. Kato et al. 1992; Kato 2002b). These QPOs must be somehow related to the evolutionary process of superhumps.

Although Antonyuk, Pavlenko (2005) reported humps with a period close to the orbital period on the first day of the superoutburst, there was no special indication of such humps in Kepler data.

Using quiescent segments of Kepler observations, we have obtained a refined orbital period of 0.069549(2) d with a mean amplitude of orbital modulation of 0.016 mag (figure 76).

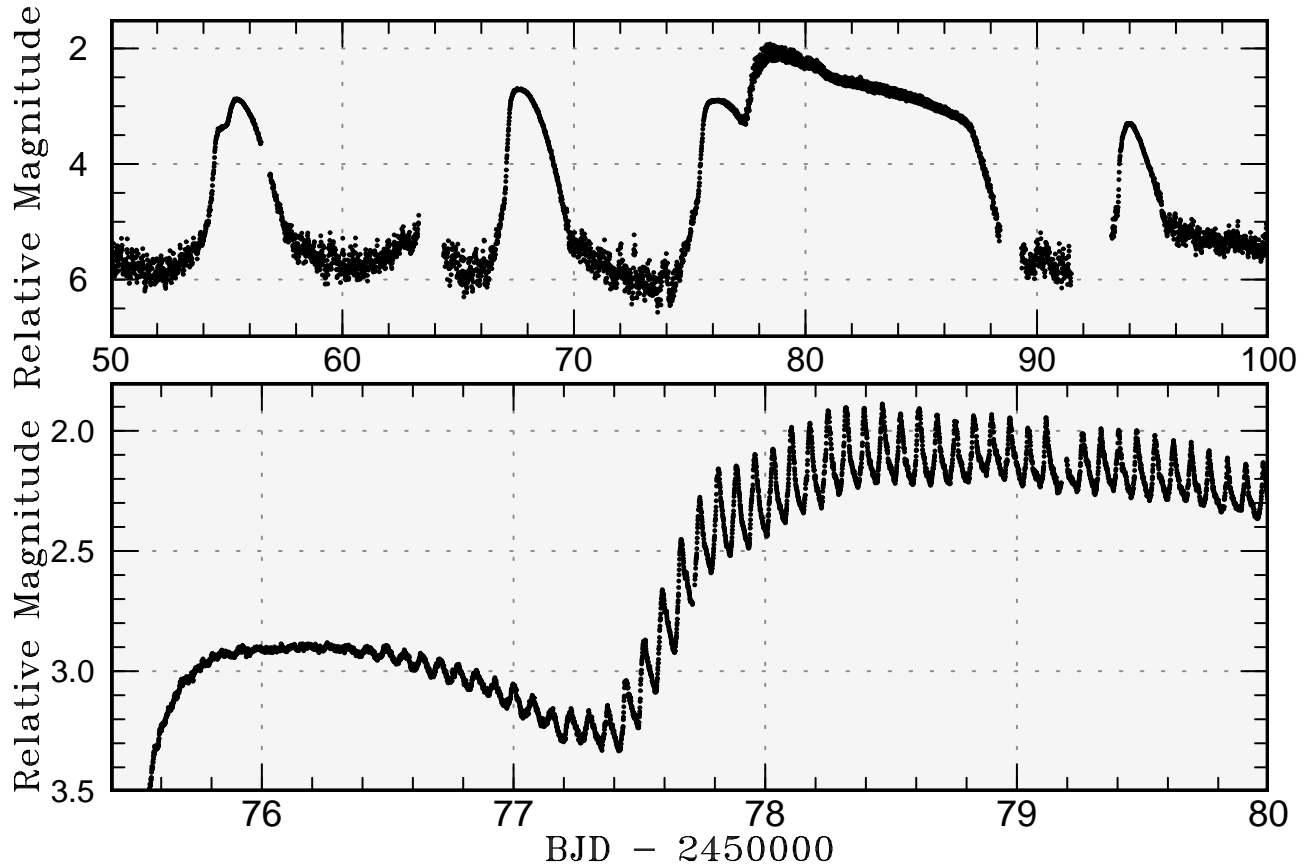


Fig. 75. Kepler light curve of V1504 Cyg (2009b). (Upper): light curve around the superoutburst in 2009 September. Note the presence of precursor outbursts (shoulders) in the first (normal) outburst and the third (super) outburst. The relative magnitudes are given against an arbitrary zero point. (Lower): enlargement of the initial part of the superoutburst. Following a distinct precursor, superhumps developed into a full superoutburst.

4.5.2. Transient Superhumps during Normal Outbursts of V1504 Cygni

During the normal outburst starting on 2009 August 10 (two outburst cycles before this superoutburst), a prominent “precursor” (or a shoulder) preceding this outburst was recorded just as in the superoutburst. During the fading stage of its second maxima, negative superhumps with a period of 0.0677(2) d [2.6(3) % shorter than P_{orb}] appeared (figure 77). This outburst may have been a failed superoutburst in which tidal instability was excited but it was not strong enough to trigger a full superoutburst. It is very suggestive that negative superhumps, instead of ordinary (positive) superhumps, were excited. This suggests that ordinary superhumps and negative superhumps can be excited under similar conditions (or have the common underlying mechanism) within a relatively short time. In ER UMa, Ohshima et al. (2011a) reported the presence of negative superhumps during its 2011 January superoutburst and the state with strong negative superhumps appeared to prevent a long-lasting superoutburst. Cannizzo et al. (2010) also discussed the prevention of disk-instability in the state with strong negative superhumps in V344 Lyr. During this normal outburst of V1504 Cyg, excitation of negative superhumps by

chance may have prevented an evolution of a full superoutburst.

During the next normal outburst starting on August 23 (outburst just prior to the superoutburst), transient low-amplitude superhumps with a period of 0.07402(7) d appeared during its fading branch (figure 78). This period is very close to the period [0.0739(2) d] of stage A superhumps, and the excitation of the superhumps apparently occurred around the maximum of this outburst. This outburst appears to be phenomenologically similar to the precursor part of the main superoutburst, but the strength of the tidal instability may have not been sufficient to trigger a full superoutburst.

Pavlenko et al. (2002) also reported the presence of short outbursts with durations of less than 1 d and maximum brightness not exceeding 15.2 mag. Pavlenko et al. (2002) referred to these outbursts as “third type” of outbursts. These outbursts are known to occur during the early phase of the supercycle. They also noted the light variations close to superhump period we detected during one normal outburst (immediately following a superoutburst). These short outbursts may be somehow related to “failed” outbursts observed by Kepler, and it is expected that further Kepler observations can detect these

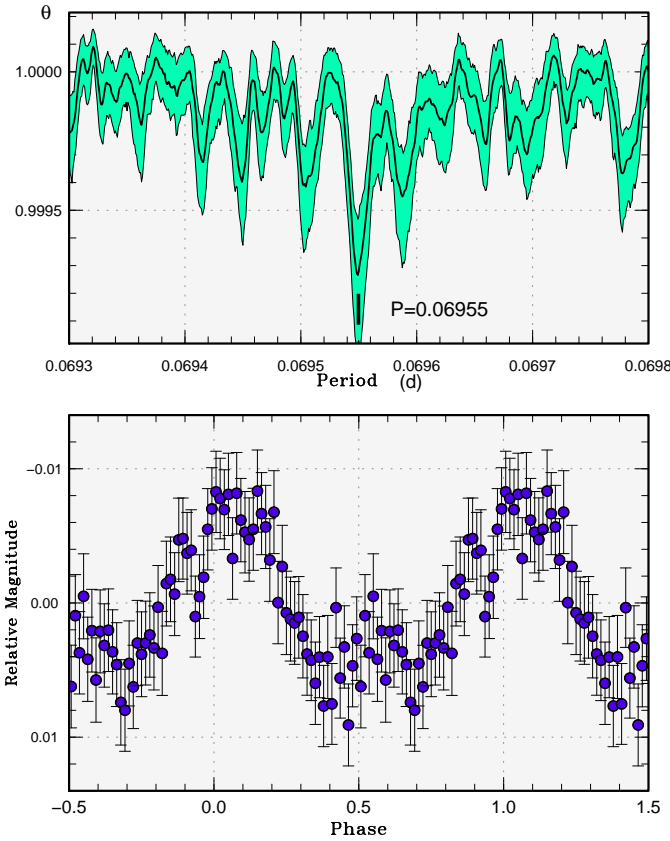


Fig. 76. Period analysis of Kepler V1504 Cyg data in quiescence. (Upper): PDM analysis. (Lower): Phase-averaged profile.

outbursts.

4.5.3. Superhumps in V344 Lyrae

The Kepler observations of V344 Lyr were analyzed by Still et al. (2010), who reported the presence of (most likely) negative superhumps in quiescence and during normal outbursts. During superoutbursts, positive superhumps were the predominant signal. We analyzed Kepler observations between 2009 June 20 and December 17. During this period, two superoutbursts were recorded (2009 August and 2009 November–December).

Both superoutbursts showed prominent precursors as in V1504 Cyg. Cannizzo et al. (2010) compared calculations based on the thermal-tidal instability model and the enhanced mass-transfer model, and indicated that the thermal-tidal instability model generally well reproduces the precursor although some differences remained between observations and model calculations.

We applied our methods to these Kepler observations. In contrast to V1504 Cyg, the superhumps had secondary maxima (a bump around superhump phase of ~ 0.4) which became stronger in later stages. The $O-C$ diagrams for these two superoutbursts are similar (figures 79 and 80). The $O-C$ diagrams of primary maxima showed stages A and B, although the transitions between them were not sharp, as in V1504 Cyg. These relatively smooth transi-

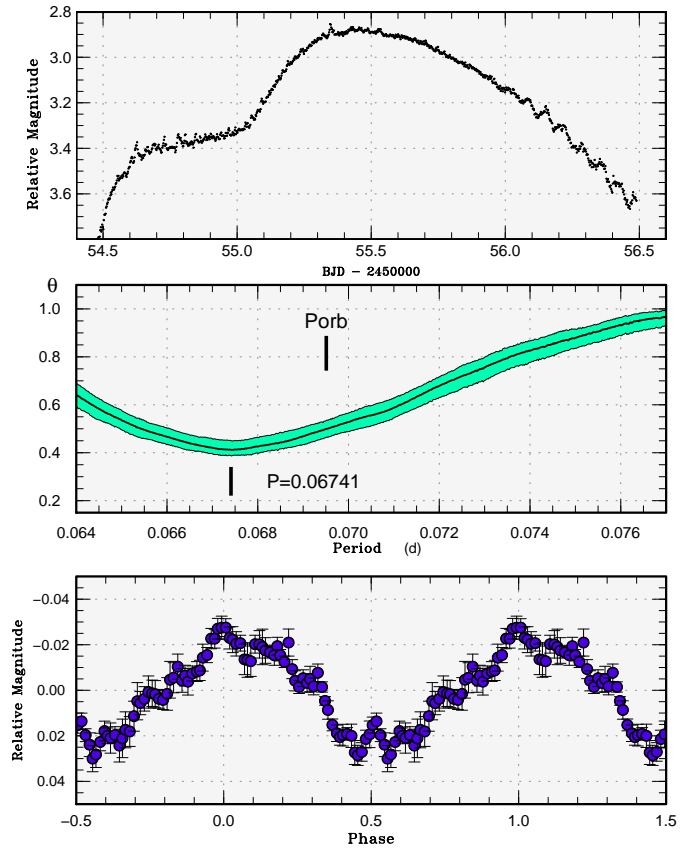


Fig. 77. Negative superhumps emerging during a normal outburst of V1504 Cyg. (Upper): Light curve. This outburst is the first outburst in figure 75. Low-amplitude modulations appeared during its fading phase. (Middle): PDM analysis. (Lower): Phase-averaged profile.

tions may have been caused by a high mass-transfer rate, as in V1504 Cyg, which enables short recurrence times of normal outbursts and superoutbursts (Kato et al. 2002; Cannizzo et al. 2010; the interval of superoutbursts was 104 d in Kepler observations).

Stages A were less structured compared to V1504 Cyg, and there were smooth variations in the periods. Stages B with relatively constant superhump periods apparently lasted for ~ 50 cycles, then the periods switched to slightly shorter ones. As in other SU UMa-type dwarf novae, this change in period can be attributed to a stage B–C transition. After this transition, the period gradually increased for approximately $120 \leq E \leq 150$, then suddenly decreased. Since the periods after $E = 150$ were similar to the periods seen in the early stage C, we interpreted that there were temporary ($120 \leq E \leq 150$) excursions to more positive $O-C$ in addition to the basic period of stage C. We therefore adopted mean periods of entire stage C in table 3.

After this stage B–C transition, the secondary maxima of superhumps became stronger, and this appearance of secondary maxima may be somehow related to the origin of stage B–C transition.

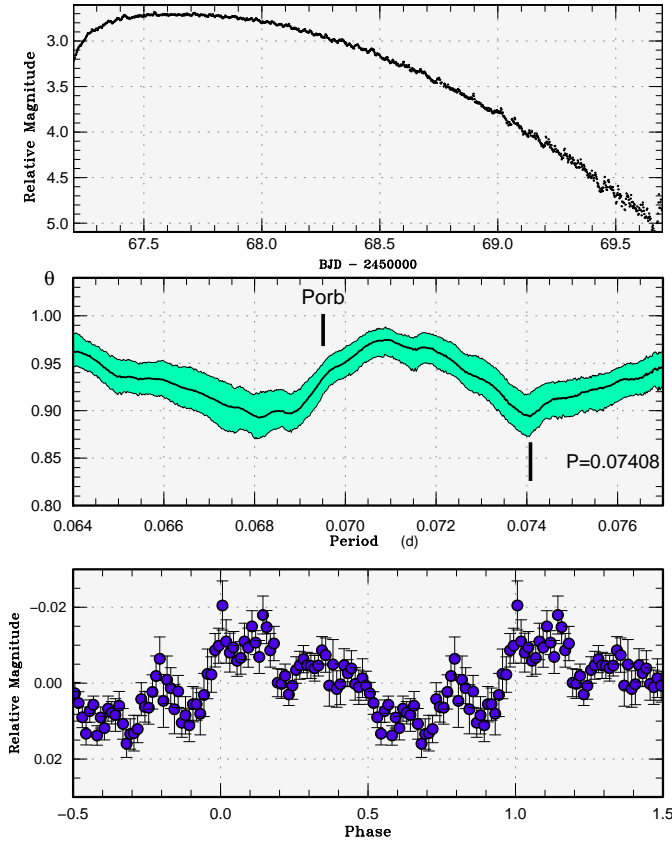


Fig. 78. Positive superhumps emerging during a normal outburst of V1504 Cyg. (Upper): Light curve. This outburst is the second outburst in figure 75. Low-amplitude modulations appeared during its fading phase. (Middle): PDM analysis. In addition to negative superhumps, there is a signal of positive superhumps. (Lower): Phase-averaged profile.

The periods derived from times of secondary maxima were initially close to superhump periods of stage B, despite that the periods of primary superhumps had already decreased after stage B–C transitions. Due to the difference in periods, the primary and secondary maxima of superhumps approached and became indistinguishable approximately after $E = 160$ – 170 . The period then suddenly shortened. The interference between these two components of superhump maxima appeared to cause temporary excursions of primary maxima toward larger $O - C$.

The merged two components of maxima then formed single-humped superhumps which lasted for two cycles of normal outbursts in 2009 August, and at least for one cycle in 2009 November–December. Although individual times of maxima became inapparent, the signal can be traced in phase-averaged light curves for one more cycle of normal outbursts.

The origin of the secondary maxima is not evident. Since the periods of the secondary component of maxima were longer than the periods of the primary component, the precession rate should be larger. Considering that the periods of the secondary component are close to those of stage B superhumps (primary maxima), it would be pos-

sible to assume that the secondary component was formed in the outermost region of the accretion disk, which had already cooled, and the hot region of the accretion disk had shrunk to a smaller radius, resulting shorter superhump periods (primary maxima). This picture would naturally explain why the secondary component was not apparent before the period of superhumps (primary maxima) shortened, i.e. stage B–C transition. The mass-transfer from the secondary might be responsible for producing a light source in the outermost region of the disk (cf. Mineshige 1988), although it will be premature to directly associate the source with an ordinary stream-impact hot spot.⁸ The behavior of amplitudes (middle panels in figures 79 and 80) was similar to those of persisting superhumps in SDSS J0804 and WZ Sge (subsection 3.27), and the luminosity from this source can be estimated to be approximately constant. It would be noteworthy that secondary maxima were temporarily present in V1504 Cyg, another high mass-transfer (\dot{M}) system, but did not evolve further as in V344 Lyr. The behavior in V1504 Cyg seems to be difficult to explain by a simple model based on stream-impact hot spot.⁹

As a possibility alternative to the emergence of stream-impact hot spot, we propose the (1,3)-mode wave (the (k, l) mode designation follows Lubow 1991a), which is a one-armed wave traveling with an angular velocity three times larger than that of the secondary. This wave meets the tidal stress of the secondary twice in a single binary rotation, and might produce observable double-wave modulations. Lubow (1991b) has shown that this (1,3)-mode wave tends to grow and persist at later epochs. It is known that short- P_{orb} systems with distinct stage B–C transitions tend to show low-amplitude double-wave modulations prior to the stage B–C transition (e.g. Uemura et al. 2010; Kato et al. 2003b; Baba et al. 2000). Such a phenomenon would be understood if the (1,0)-mode wave, the main superhump component, weakens and the other low-amplitudes modes become observable. These objects are likely low- \dot{M} systems and it would be more difficult to attribute the secondary maxima to stream-impact hot spot than in V344 Lyr. The interpretation based on the (1,3)-mode wave might have a potentiality in explaining the double-wave superhump modulations in wide range of objects, and should be further investigated.

After selecting quiescent segments without strong negative superhumps, we searched a signal of the orbital

⁸ See also a discussion in Hessman et al. (1992), who reported that the traditional model of late superhumps by Vogt (1983) did not trivially explain the observed eclipse depths in OY Car and suggested that the light source of late-stage superhumps is more extended.

⁹ During the refereeing period, Wood et al. (2011) independently reported an analysis of Kepler observations of V344 Lyr. Wood et al. (2011) interpreted that the secondary maxima are generated as the accretion stream bright spot sweeps around the rim of the non-axisymmetric disk, and attempted to reproduce the observed profile by assuming an enhanced mass-transfer from the secondary. This interpretation corresponds to the traditional interpretation of traditional late superhumps discussed in the text.

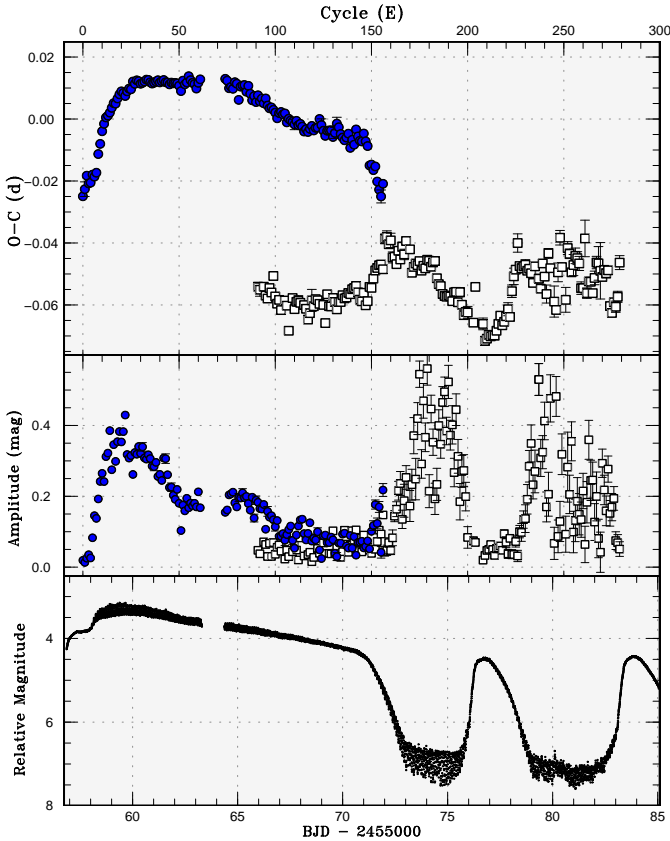


Fig. 79. $O - C$ diagram of superhumps in V344 Lyr (2009). (Upper): $O - C$ diagram. The filled circles represent primary maxima of superhumps. The open squares represent secondary maxima of superhumps and persisting superhumps. (Middle): Amplitudes of superhumps. The symbols are common to the upper panel. (Lower): Light curve.

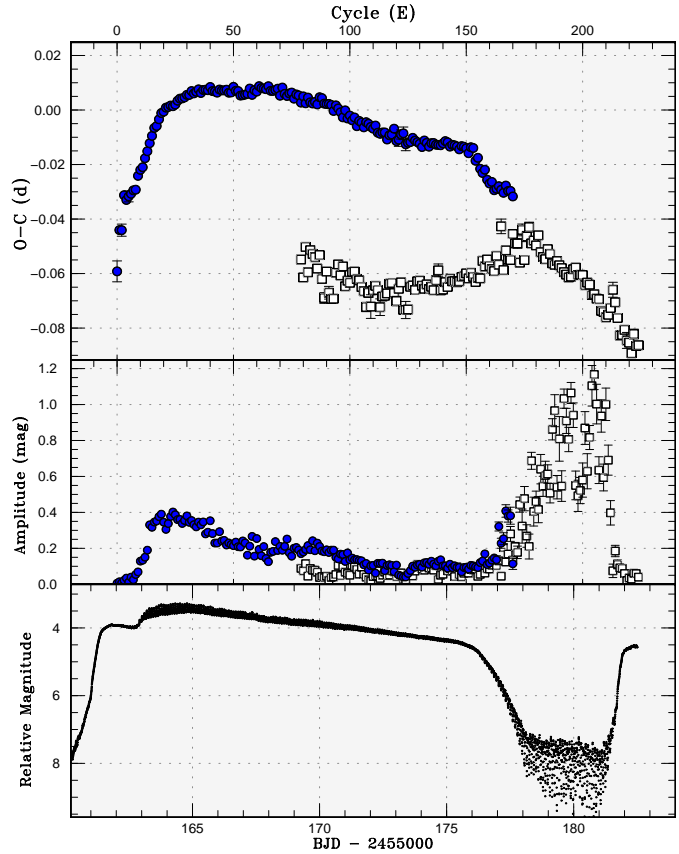


Fig. 80. $O - C$ diagram of superhumps in V344 Lyr (2009b). (Upper): $O - C$ diagram. The filled circles represent primary maxima of superhumps. The open squares represent secondary maxima of superhumps and persisting superhumps. (Middle): Amplitudes of superhumps. The symbols are common to the upper panel. (Lower): Light curve.

period with a help of estimated orbital period (0.0877–0.0880 d) from superhump periods (using the relation of Stolz, Schoembs 1984). We have found a candidate period 0.087903(2) d with a mean amplitude of 0.026 mag (figure 81). Assuming that this is the orbital period, the fractional excesses for positive (stage B) and negative superhumps are 4.2 % and -2.1 %, respectively.

4.5.4. Comparison between Kepler observations and other samples

Kepler obtained highest precision, uninterrupted observations of two SU UMa-type dwarf novae. Some of the features, including substructures in stage A in V1504 Cyg and complex behavior in late stages in V344 Lyr, were new and were outside descriptions derived from our large set of ground-based samples. Apart from them, the $O - C$ behavior of Kepler observations generally fits the descriptions obtained from ground-based samples. The two systems observed by Kepler were either long- P_{orb} or high- \dot{M} , and neither of them were short- P_{orb} and low- \dot{M} systems which show distinct stage A–C and long-persisting superhumps.

Since there were not sufficient ground-based observations for long- P_{orb} or high- \dot{M} systems particularly after

the termination of superoutbursts, it is not clear whether persisting superhumps in V1504 Cyg and V344 Lyr have the origin common to persistent stage C superhumps in short- P_{orb} and low- \dot{M} systems. Future key Kepler observations should include these short- P_{orb} and low- \dot{M} systems.

4.6. Late-Stage Superhumps in WZ Sge Stars

In well-observed WZ Sge-type dwarf novae, late-stage superhumps having periods longer than those observed during the main superoutburst have been reported. Although there was already a suggestion in EG Cnc (Patterson et al. 1998), Kato et al. (2008) established the prevalence of such superhumps in GW Lib, V455 And and WZ Sge. Kato et al. (2009a) further reported further detections in FL Psc (=ASAS J002511+1217.2), ASAS J153616–0839.1, SDSS J0804 and OT J074727.6+065050. In OT J213806.6+261957 (hereafter OT J2138), however, a slightly shorter period was detected (Kato et al. 2010). In this paper, we further detected long-period late-stage superhumps in a new superoutburst of SDSS J0804 and in SDSS J1339. Since the variation in SDSS J1339 looks

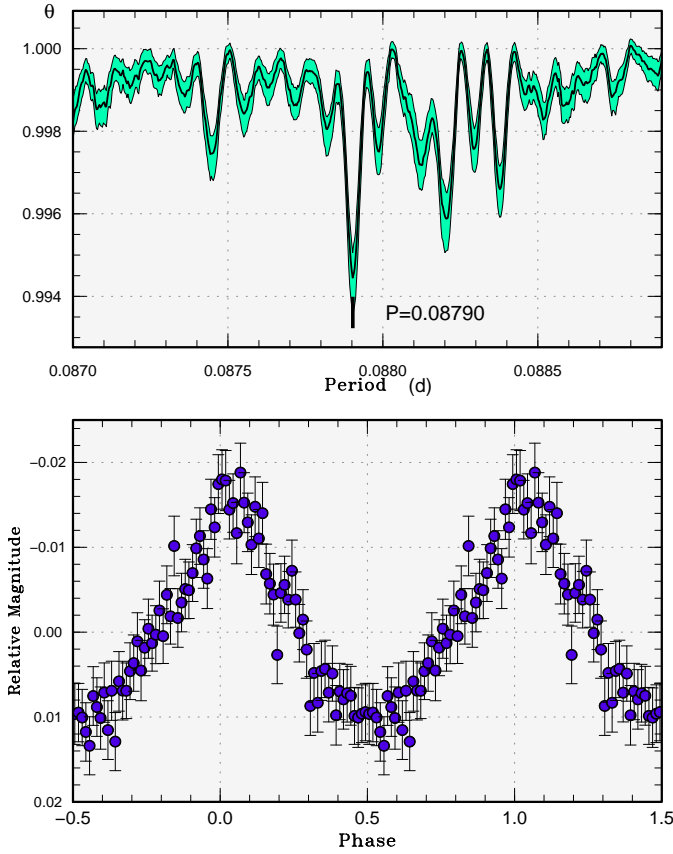


Fig. 81. Period analysis of Kepler V344 Lyr data in quiescence. (Upper): PDM analysis. (Lower): Phase-averaged profile.

somewhat unique, we first examine the phenomenon in this object, and present a survey of the existing data of WZ Sge-type dwarf novae and similar systems for detecting weaker periodicities other than the reported late-stage superhumps.

4.6.1. Late-Stage Superhumps in SDSS J1339

The late-stage superhumps in SDSS J1339 were unique in that they apparently showed a phase reversal, as in “traditional” late superhumps (Schoembs, Vogt 1980; Vogt 1983), despite the fact that most of late-stage superhumps (stage C superhumps) in ordinary SU UMa-type dwarf novae do not show a phase reversal (Kato et al. 2009a). The overall tendency of the $O - C$ diagram, however, resembles those of GW Lib (Kato et al. 2009a) and SDSS J0804 (subsection 3.27), and the $O - C$ variation could be understood without a phase jump if the phase of rapid period decrease immediately following the end of stage B was not observed due to a gap in observation.

In interpreting the structure of these $O - C$ diagrams in Kato et al. (2009a), we did not assume a phase reversal because the phases of superhumps were observationally continuous. Since this continuity may have been superficial and there could have been multiple components or

periods as in V344 Lyr¹⁰, we made an alternative analysis following the method used in V344 Lyr. Since there were sometimes small secondary superhump maxima during the plateau phase, we also measured the times of these secondary maxima (the first eight epochs in table 52). As seen in figure 43, these maxima do not seem to be on a smooth extension of late-stage superhumps unless we assume a discontinuous period change. The situation appears to be different from the case of V344 Lyr.

The long period of persisting superhumps, however, is analogous to that of persistent superhumps in V344 Lyr, and these superhumps are expected to arise from the outermost region of the accretion disk.

As in the case of Kepler observations of V344 Lyr, it would be controversial whether these late-stage superhumps are “traditional” late-superhumps arising from the stream impact point or superhumps arising from varying tidal dissipation. Being a WZ Sge-type dwarf nova, the system parameters, including the mass-transfer rate, are expected to be different from V344 Lyr, and the light from the stream impact point would be expected to be much less in V344 Lyr. Although one might assume an irradiation-induced enhanced mass-transfer, the lack of post-outburst rebrightening suggests that the mass-transfer rate was not sufficient to produce a normal outburst in contrast to V344 Lyr. The situation may be closer to low- \dot{M} systems described in subsection 4.5.3. We might speculate that the (1,0)-mode wave temporarily vanished as the cooling front passed the disk, and the other weaker modes remained and coupled with others to excite the (1,0)-mode, which was by chance formed in the opposite direction to the original (1,0)-mode.

The presence of the beat phenomenon might also provide a clue to the origin of late-stage superhumps. In SDSS J1339, the singly peaked orbital signal was clearly present during the post-superoutburst stage. The actually observed light curve was not explained by a simple addition of the orbital modulation to the superhumps with constant amplitudes, and the amplitudes (subtracted for orbital modulations) of the superhumps cyclically varied with a period of the beat period.¹¹

As a working hypothesis, we propose that these cyclic variations were produced by the cyclically variable eccentricity of the accretion disk precessing with the beat period (cf. Hirose, Osaki 1990): when the disk becomes more circular, the amplitudes become smaller, and when the disk becomes more eccentric, the amplitudes becomes larger. This explanation would apply either to “traditional” late-superhumps-type explanation, assuming the varying release of the gravitational energy, and or to the cyclic variation of the superhump light source itself from varying tidal dissipation.

¹⁰ An attempt to introduce a second component in interpreting the $O - C$ diagram in ER UMa was presented in Kato et al. (2009a).

¹¹ The same phenomenon appears to have been recorded in the SU UMa-type dwarf nova OY Car (Schoembs 1986) during the first two nights of the post-superoutburst state. Since OY Car is an eclipsing system, the condition may be different from the case of SDSS J1339.

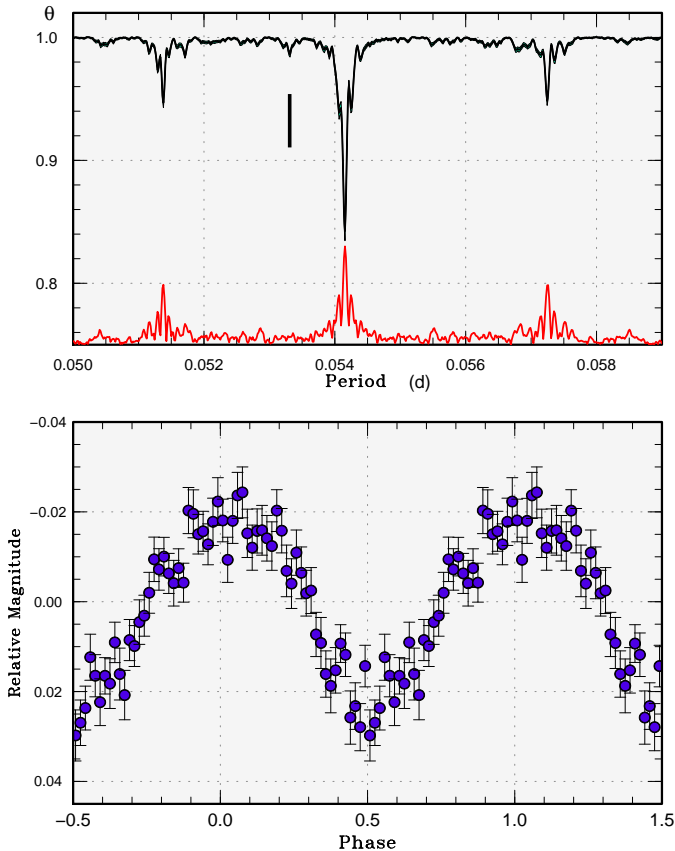


Fig. 82. Post-superoutburst superhumps in GW Lib (2007). (Upper): PDM analysis. The strong signal at 0.054153(8) d is the post-superoutburst superhumps. The signal at 0.053310(2) d is the orbital period. The curve drawn in the bottom of the figure indicates the window function. (Lower): Phase-averaged profile of the orbital modulations.

4.6.2. Late-Stage Superhumps in Other Systems

We have analyzed post-superoutburst observations of GW Lib (Kato et al. 2008). Although it was less striking than in SDSS J1339, GW Lib also showed the orbital signal with an amplitude of 0.045 mag and a period of 0.053310(2) d (figure 82), which is in agreement with the radial-velocity study [0.05332(2) d, Thorstensen et al. 2002]. A beat phenomenon in the superhump amplitudes was also recorded with a smaller degree than in SDSS J1339. The detection of orbital signal is surprising since the inclination of the system is suggested to be very low (11° , Thorstensen et al. 2002), and none of quiescent observations detected orbital modulations (van Zyl et al. 2000; Woudt, Warner 2002; Schwieterman et al. 2010). It appears that GW Lib and SDSS J1339 are very similar in their outburst behavior, evolution of superhumps and the post-superoutburst superhumps and beat phenomenon.

An analysis of post-superoutburst observations of FL Psc (Kato et al. 2009a) yielded a strong periodicity at 0.054210(8) d with a mean amplitude of 0.08 mag (figure 83). The period is too short for an orbital period (5 % shorter than the superhump period during the main

outburst), and is most likely identified as negative superhumps. This is the first indication of negative superhumps during the post-superoutburst stage of WZ Sge-type dwarf novae.

As discussed in subsection 4.5.2, the state with negative superhumps is considered to have a tendency to suppress the disk instability to occur. The appearance of negative superhumps might explain the reason why multiple rebrightenings did not occur. There has been a suggestion that there is a minimum mass-transfer rate to generate a tilt, which has been proposed as the mechanism for negative superhumps (Montgomery, Martin 2010). Although the quiescent mass-transfer rates in WZ Sge-type dwarf novae generally are lower than this limit, the mass-transfer rate may have exceeded this limit in outburst and generated a tilt and negative superhumps. The generation of tilts in WZ Sge-type dwarf novae may affect the dynamics of superoutbursts than had been supposed and requires further investigation. Further systematic, sufficiently long, observations during the post-superoutburst states of WZ Sge-type or SU UMa-type dwarf novae are needed.

We also propose a candidate orbital period of 0.056096(5) d, with a mean amplitude of 0.06 mag. This candidate period is well in agreement with the predicted orbital period of 0.05609 d from stage B superhumps (subsection 4.1). Assuming this orbital period, fractional superhump excesses for positive (stage B) and negative superhumps are 1.8 % and -3.4 %, respectively. It is known that fractional excesses (in absolute values) for positive superhumps are approximately twice larger in long- P_{orb} systems (cf. Patterson et al. 1997; table 2 of Montgomery, Bisikalo 2010), and the larger fractional excess for negative superhumps in FL Psc is unusual. It has been established, however, the fractional excesses (in absolute values) for positive and negative superhumps in ER UMa are almost equal (Ohshima et al. 2011a), and there was a suggestion of a large negative fractional excess for the supposed negative superhumps in V1159 Ori (Patterson et al. 1995). The negative superhumps in very short- P_{orb} systems may have different properties from those in traditional negative superhumps in long- P_{orb} systems.

An analysis of the post-superoutburst observations of OT J2138 (2010, BJD after 2455348) yielded two periodicities (figure 84): persistent superhumps with a period of 0.054853(6) d and an amplitude of 0.11 mag, the orbital period of 0.054523(4) d and an amplitude of 0.05 mag. The other signals were one-day or two-day aliases of the superhumps. The orbital period determined from late-stage observations is consistent with the period of early superhumps. The fractional excess of stage B superhumps has been refined to be 0.91 %.

The origin of orbital signals in these systems during the post-superoutburst stage is unclear, although they were detected in several WZ Sge-type dwarf novae. Although it might have originated from the irradiated secondary by the heated white dwarf, the low inclination in GW Lib would make this interpretation difficult. The asymmetric profile in OT J2138 resembles an combination of a shal-

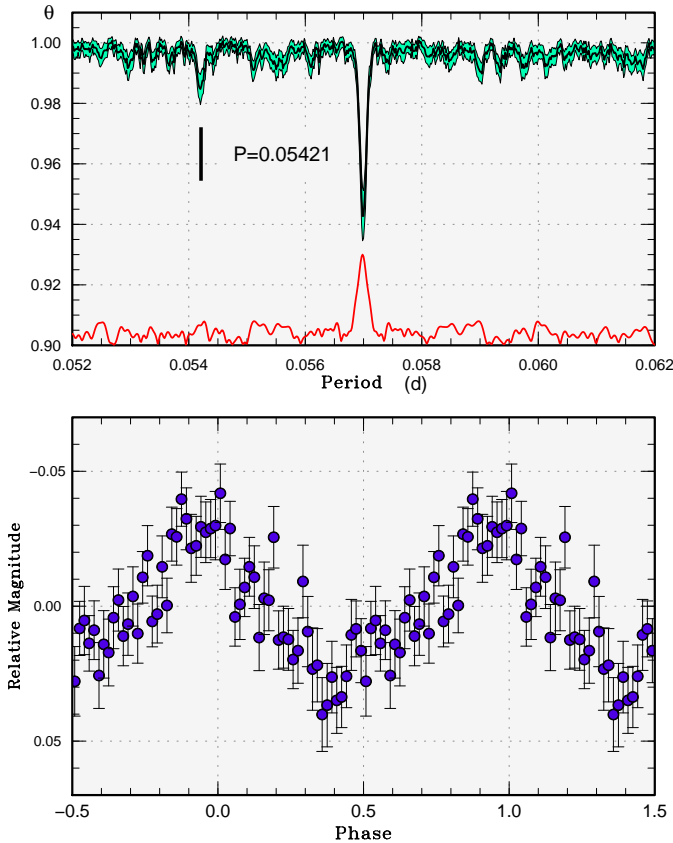


Fig. 83. Post-superoutburst superhumps in FL Psc (2004). (Upper): PDM analysis. The strong signal at 0.05700(3) d is the post-superoutburst (positive) superhumps. The signal at 0.054210(8) d is likely negative superhumps. The curve drawn in the bottom of the figure indicates the window function. The signal at 0.054210 d is not an alias period of the (positive) superhumps. (Lower): Phase-averaged profile by a period of 0.054210 d.

low eclipse and a orbital hump. Although the amplitudes were too small to be regarded as true eclipses, geometrical effect can be responsible for systems with intermediate inclinations.

4.7. Amplitudes of Superhumps

Smak (2010) recently raised a question against the widely believed descriptions about amplitudes of superhumps. Smak (2010) summarized as follows:

1. Superhumps first appear around superoutburst maximum and reach their highest amplitude either at maximum or 1-2 days later.
2. Superhump amplitudes decrease during superoutburst; this effect, however, has been well documented only for relatively few cases.
3. At their full development the superhumps have a range of 0.3-0.4 mag, and are equally prominent in all SU UMa stars independent of inclination (Warner 1995, p.194).
4. There is no strong modulation of the superhump profile at the beat period (Warner 1985, p.372).

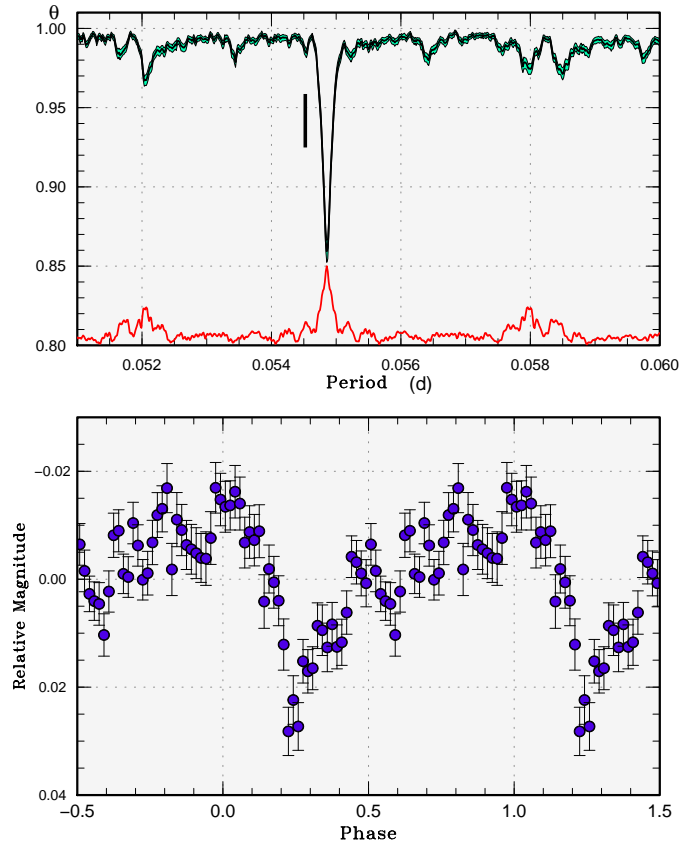


Fig. 84. Post-superoutburst superhumps in OT J2138 (2010). (Upper): PDM analysis. The strong signal at 0.054853(6) d is the post-superoutburst superhumps. The signal at 0.054523(4) d is identified with the orbital period. The curve drawn in the bottom of the figure indicates the window function. (Lower): Phase-averaged profile by a period of 0.054523 d.

The claim by Smak (2010) was that the points 3 and 4 are wrong. These observational findings were, however, derived from observations in the 1970's and 1980's, when most of the knowledges in superhumps came from regularly outbursting bright southern SU UMa-type dwarf novae, i.e. relatively long- P_{orb} objects with higher mass-transfer rates.

Since the modern accumulated data cover much wider range of objects, we first present statistical descriptions of superhump amplitudes, and examine the items individually. Note that we already presented a typical variation of superhump amplitudes in figure 3 of Kato et al. (2009a).

In this paper, we present a statistical analysis and treat only a pilot study of representative objects. We are going to devote ourselves in a separate work to more comprehensive survey of the amplitudes of superhumps as well as detailed data on individual objects.

4.7.1. Amplitudes of Superhumps: Samples and General Behavior in Non-Eclipsing Systems

The samples are observations in Kato et al. (2009a), Kato et al. (2010) and this paper. We restricted analysis to superoutbursts in which the starts of stage B were de-

terminated. Additional criterion for choosing samples was that more than 20 epochs of superhumps maxima were measured. The resultant samples are listed in table 73. The amplitudes of superhumps were measured using the template fitting method described in Kato et al. (2009a), and the derived amplitudes are not literally full minimum-to-maximum amplitudes in usual sense but more reflect a kind of first-order moment. It has become evident that some (less than 1 %) of recorded maxima tabulated in Kato et al. (2009a) were inadequate for measuring amplitudes because they were only observed around superhump maxima. We rejected these maxima in the analysis.

The variation of superhump amplitudes in non-eclipsing systems are shown in figures 85–88. The superhump amplitudes are plotted against cycle numbers after the start of stage B. Since the starts of stage B were measured from $O - C$ variations (shown in tables in Kato et al. 2009a, Kato et al. 2010 and in this paper), they can be different from the maxima of superhump amplitudes. There is also a tendency of 1-d periodicities in the density of data, resulting from uneven distribution of observations against longitudes. There should have been typically this degree (10–15 cycles) of uncertainty in determining the starts of stage B. Since the quality of the data were sometimes low, there are sometimes a number of scattered points in large-amplitude regions. They should be better considered as a result of a selection bias when the errors in the original data were large. Although there must have equally been scattered points in low-amplitude regions, they were not detected either due to poor convergence in numerical fitting or because the resultant amplitudes were negative. Nevertheless, the majority of the measured data are in relatively narrow strips in each figure, and we can regard these strips as typical behavior of amplitude variation. The large increase in the amplitude at late stages (e.g. $E > 130$ in figure 85) corresponds to the final fading of superoutbursts.

Several features can be seen in these figures:

1. The amplitudes of superhumps usually reach a maximum around the stage A–B transition. This means that the time before the system reaches the peak of superhump amplitude is variable between objects or between superoutbursts.
2. Although the amplitudes of superhumps globally decrease with time, secondary peaks of amplitudes are usually seen ~ 50 cycles after the main peak in long- P_{orb} systems (figure 85) and ~ 70 – 80 cycles after the main peak in intermediate- or short- P_{orb} systems (figures 86, 87). In short- P_{orb} systems, the secondary peaks become less evident (figure 88). The epochs of the secondary peaks are close to the epochs of stage B–C transitions. In some cases, the secondary peaks appear later than stage B–C transitions.
3. The amplitude of superhumps are well-correlated with P_{orb} : longer- P_{orb} systems show larger amplitudes. The relation for maximum amplitudes of superhumps is shown in figure 89. Figures for other

Table 73. Superoutbursts used in analyzing superhump amplitudes.

Object*	Year	P_{SH}	Object*	Year	P_{SH}
V455 And	2007	0.0571	WZ Sge	2001	0.0572
V466 And	2008	0.0572	V551 Sgr	2003	0.0676
DH Aql	2002	0.0800	V1212 Tau	2011	0.0701
VY Aqr	2008	0.0647	FL TrA	2005	0.0599
EG Aqr	2006	0.0790	SU UMa	1999	0.0791
BG Ari	2010	0.0849	SW UMa	2000	0.0583
TT Boo	2004	0.0781	SW UMa	2006	0.0582
NN Cam	2009	0.0743	SW UMa	2010	0.0582
HT Cas	2010	0.0763	BC UMa	2003	0.0646
V1040 Cen	2002	0.0622	BZ UMa	2007	0.0702
WX Cet	1998	0.0595	DV UMa	1997	0.0888
GO Com	2003	0.0631	DV UMa	2007	0.0885
V632 Cyg	2008	0.0658	IY UMa	2000	0.0758
V1028 Cyg	1995	0.0617	IY UMa	2006	0.0761
V1504 Cyg	2009b	0.0722	IY UMa	2009	0.0762
HO Del	2008	0.0644	KS UMa	2003	0.0702
KV Dra	2009	0.0601	HV Vir	2002	0.0583
XZ Eri	2007	0.0628	HV Vir	2008	0.0583
XZ Eri	2008	0.0628	1RXS J0423	2008	0.0784
UV Gem	2003	0.0935	1RXS J0423	2010	0.0785
V592 Her	2010	0.0566	ASAS J1025	2006	0.0634
V1108 Her	2004	0.0575	ASAS J1536	2004	0.0646
RU Hor	2008	0.0710	ASAS J1600	2005	0.0650
MM Hya	2011	0.0589	Mis V1443	2011	0.0567
RZ Leo	2000	0.0787	SDSS J0804	2010	0.0596
GW Lib	2007	0.0541	SDSS J0812	2011	0.0779
V344 Lyr	2009	0.0916	SDSS J1146	2011	0.0633
V344 Lyr	2009b	0.0916	SDSS J1227	2007	0.0646
V585 Lyr	2003	0.0604	SDSS J1339	2011	0.0581
DT Oct	2003	0.0748	SDSS J1627	2008	0.1097
V2527 Oph	2004	0.0721	OT J0238	2008	0.0537
UV Per	2000	0.0666	OT J1443	2009	0.0722
UV Per	2003	0.0667	OT J1610	2009	0.0578
UV Per	2007	0.0663	OT J1625	2010	0.0961
QY Per	1999	0.0786	OT J2138	2010	0.0550

*Abbreviations for Kato et al. (2009a) objects:

ASAS J1536: ASAS J153616–0839.1

ASAS J1600: ASAS J160048–4846.2

SDSS J1627: SDSS J162718.39+120435.0

OT J0238: OT J023839.1+355648 = CT Tri

OT J1443: OT J144341.9–175550

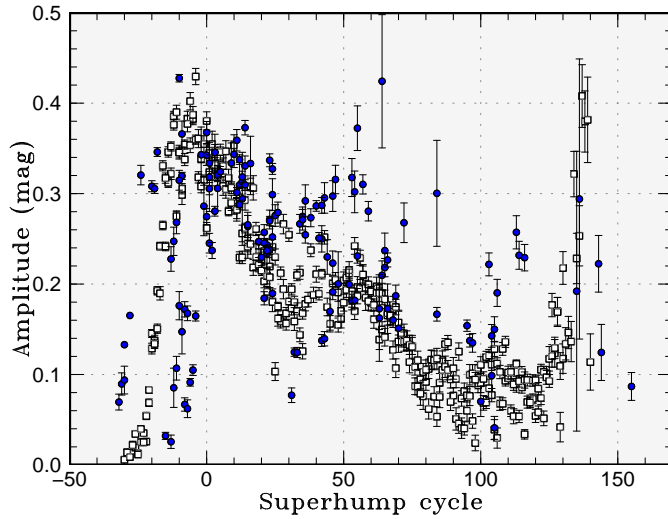


Fig. 85. Variation of superhump amplitudes in systems with P_{orb} longer than 0.08 d. Open squares represent Kepler observations of V344 Lyr.

stages of superoutburst basically show the same trend. Warner’s point 3 (0.3–0.4 mag for maximum amplitudes) apparently came from the long- P_{orb} samples in the older times. The maximum amplitudes seem to decrease for longer- P_{orb} ($P_{\text{orb}} > 0.09$ d) objects.

4. Two systems (RZ Leo and QY Per) show systematically larger amplitudes of superhumps. These systems have long recurrence times similar to WZ Sge-type dwarf novae, but with longer P_{orb} .
5. The amplitudes of superhumps in extreme WZ Sge-type (we refer to systems with recurrence times longer than ~ 10 yr or systems with multiple re-brightenings) are generally smaller than in ordinary SU UMa-type dwarf novae.

4.7.2. Amplitudes of Superhumps: Dependence on Orbital Inclination

We further studied the dependence of superhump amplitudes on orbital inclination (i). As in subsection 4.7.1, we only used epochs $-5 < E < 10$ to illustrate the maximum superhump amplitudes. Due to the strong dependence of superhump amplitudes on P_{orb} , we first removed this effect by using a relation derived in subsection 4.7.1 (curve in figure 89). The normalization was taken so that the average of amplitudes agrees with the pre-normalized value of the sample (0.25 mag). We used i values in the on-line version 7.15 of Ritter, Kolb (2003). As seen in figure 90, the normalized maximum amplitudes do not strongly depend on i for systems with $i < 80^\circ$, including an eclipsing system WZ Sge ($i = 77^\circ$). The right panel of the figure shows the amplitudes for non-eclipsing SU UMa-type dwarf novae without known inclinations. The 90 % of the normalized amplitudes without known inclinations fall in the range of 0.14–0.35 mag, well in agreement with $i < 80^\circ$ samples. This result seems to confirm that Warner’s point 3 is basically valid for non-eclipsing systems. It is worth

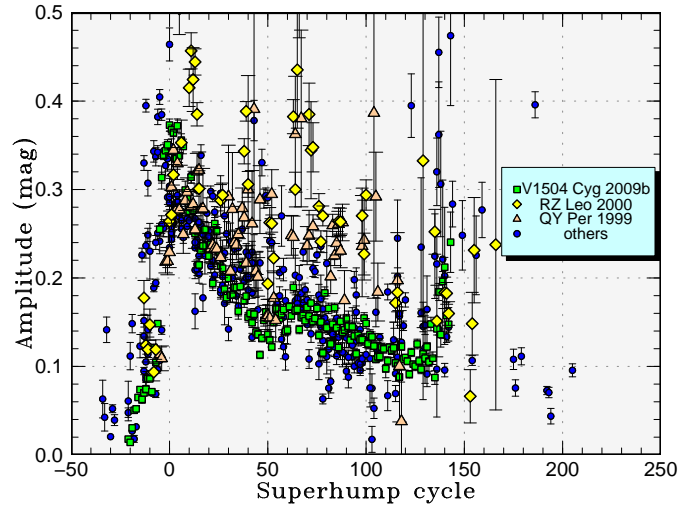


Fig. 86. Variation of superhump amplitudes in systems with $0.07 < P_{\text{orb}}(\text{d}) \leq 0.08$. Filled squares represent Kepler observations of V1504 Cyg. Two objects with large-amplitude superhumps (RZ Leo and QY Per) are shown in different symbols.

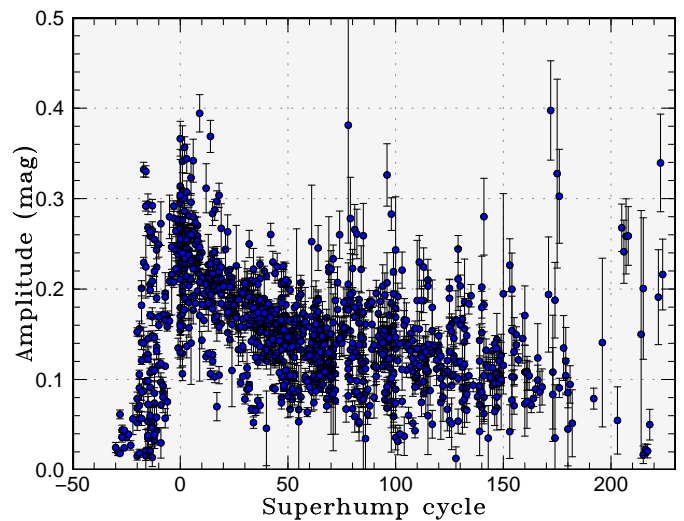


Fig. 87. Variation of superhump amplitudes in systems with $0.06 < P_{\text{orb}}(\text{d}) \leq 0.07$.

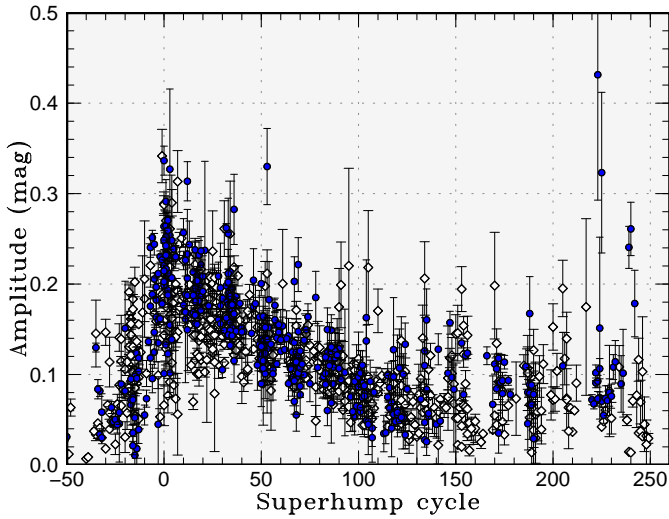


Fig. 88. Variation of superhump amplitudes in systems with $P_{\text{orb}}(d) \leq 0.06$. Filled circles and open diamonds represent ordinary SU UMa-type dwarf novae and extreme WZ Sge-type dwarf novae, respectively.

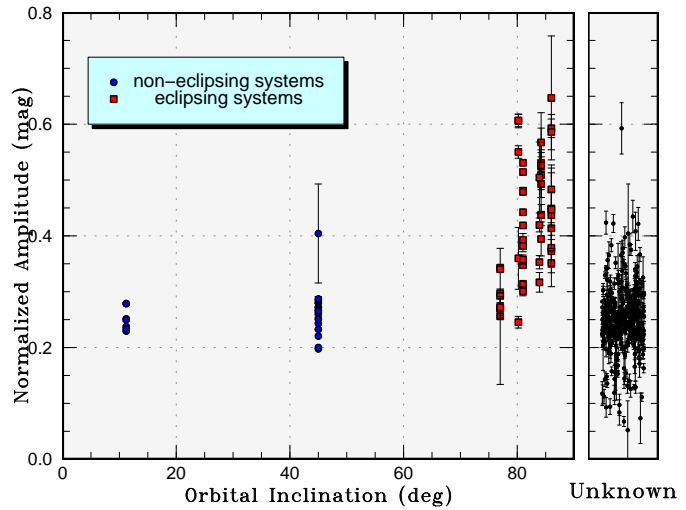


Fig. 90. Dependence of superhump amplitudes on orbital inclination. The superoutburst samples are described in subsection 4.7.1. We selected epochs $-5 < E < 10$ to illustrate the maximum superhump amplitudes. The amplitudes were normalized by using the dependence on superhump periods. The right panel indicates amplitudes for objects without known orbital inclinations.

noting that there is no indication of smaller amplitudes in systems with very low inclinations.

4.7.3. Amplitudes of Superhumps: Beat Phenomenon

As we have already shown, the beat phenomenon in amplitudes of superhumps are clearly present in eclipsing objects (e.g. HT Cas, subsection 3.7 and SDSS J0804 subsection 3.27). While it is not clear what the term “profile” exactly mentioned in Warner’s point 4, the present observations seem to support the presence of a beat phenomenon (at least in amplitudes) in eclipsing systems.

In figure 91, we show variations of superhump amplitudes in IY UMa (2009), which was reported in Kato et al. (2010). Although the beat phenomenon was strongly seen during stage B, it became weaker with time and almost disappeared during stage C. In HT Cas (2010, figure 11), however, the beat phenomenon persisted during its entire plateau phase. It would be worth noting that double-wave modulation in amplitude mentioned in Smak (2010) (A_2 in his designation) is not apparent even in the best observed case of HT Cas.

The beat phenomenon is much weaker in SDSS J0804 (2010, figure 92) than in IY UMa (2009), and became inapparent during the late plateau phase.

Among non-eclipsing systems, RZ Leo, likely a high-inclination system (Mennickent, Tappert 2001; Ishioka et al. 2001) showed the presence of the beat phenomenon [modulations with a 30.6(1)-cycle period is already apparent in figure 86]. The mean amplitude of modulations (A_1 in Smak 2010) was 0.07(2) mag. QY Per, another outlier in figure 86, has a candidate weak beat phenomenon with a period of 28.5(2) cycles and A_1 of 0.02(1) mag. Since the signal was weak and the true orbital period is unknown, this needs to be confirmed by further studies. We could

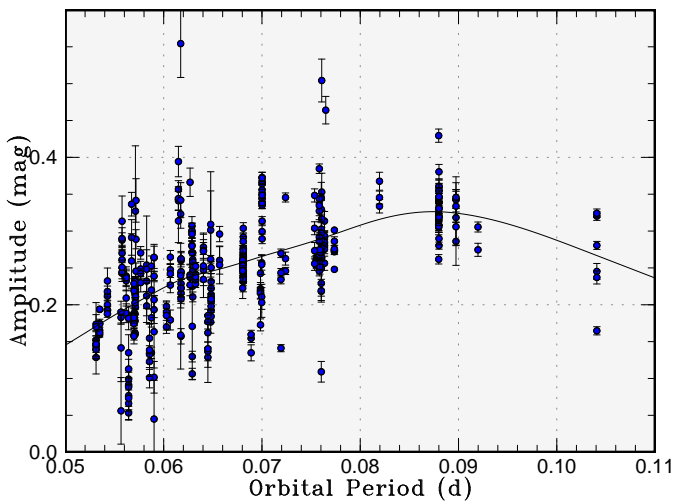


Fig. 89. Dependence of superhump amplitudes on orbital period. The superoutburst samples are described in subsection 4.7.1. We selected epochs $-5 < E < 10$ to illustrate the maximum superhump amplitudes. The curve indicates a spline-smoothed interpolation.

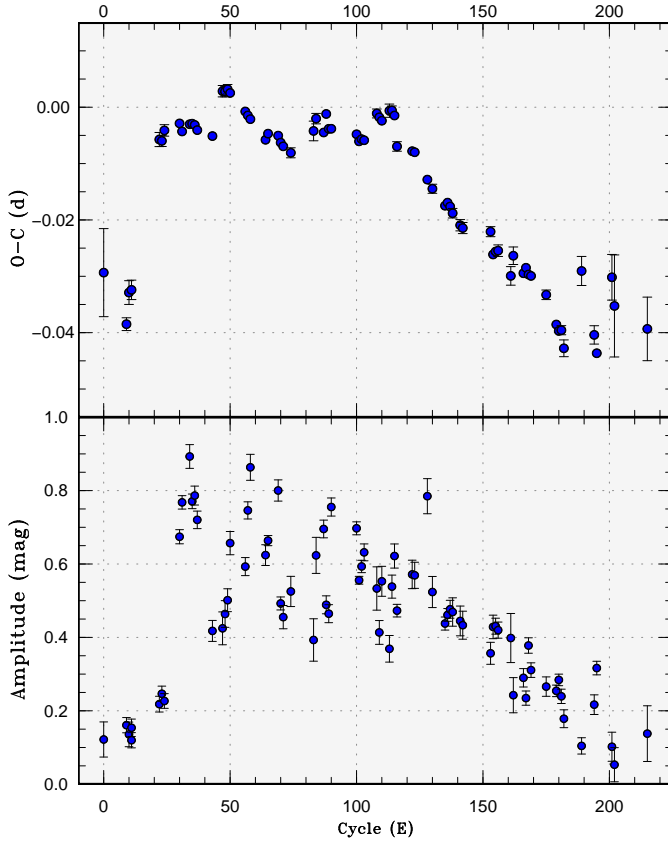


Fig. 91. Beat phenomenon in IY UMa (2009). (Upper): $O - C$ diagram. (Lower): Amplitudes of superhumps. Although the beat phenomenon was strongly seen during stage B, it became weaker during stage C.

not confirm the presence of the beat phenomenon in TT Boo (2004). In KS UMa (2003), we found a weak beat phenomenon with A_1 of 0.02(1) mag whose beat period is consistent with the known P_{orb} .

The degree of the beat phenomenon during the superoutburst plateau appears to be related to the maximum amplitudes of superhumps, and appears to be smaller in WZ Sge-type dwarf novae.

The beat phenomenon in non-eclipsing systems, especially in short- P_{orb} systems, was undetected or close to the detection limit. This finding seems to be consistent with numerical modeling of inclination effect on superhumps (Simpson et al. 1998), in which only systems with i larger than 45–60° show significant orbital modulation of superhumps.

4.7.4. Amplitudes of Superhumps: Discussion

Although Smak (2010) discussed a new interpretation on the origin of superhumps in combination with his earlier findings (e.g. Smak 2009b; Smak 2009a), we restrict our discussion within the traditional framework (cf. Osaki 1989; Hirose, Osaki 1990; Osaki 1996) since we do not have sufficient materials to compare with the analysis by earlier

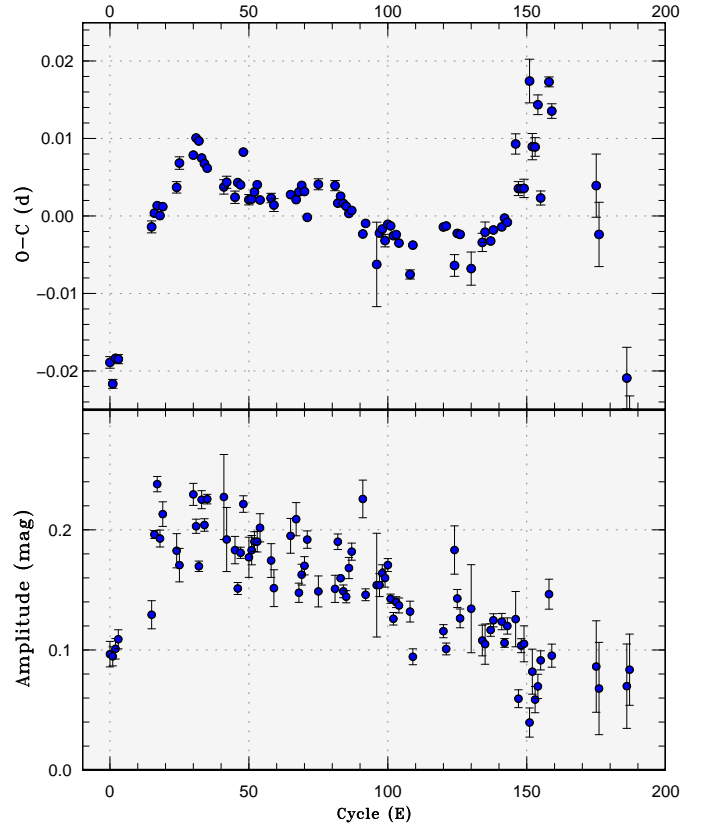


Fig. 92. Beat phenomenon in SDSS J0804 (2010). (Upper): $O - C$ diagram. (Lower): Amplitudes of superhumps. The beat phenomenon is much weaker than in IY UMa (2009), and became inapparent during the late plateau phase.

works by Smak.¹²

In non-eclipsing systems, there is evidence that our normalized amplitudes of superhumps were fairly constant over a wide range of orbital inclinations ($i \leq 80^\circ$).¹³ This can be understood if the superhump light source has al-

¹² This particularly refers to a best-observed southern eclipsing SU UMa-type dwarf novae Z Cha and OY Car, for which we have virtually no new data. The new data in HT Cas, however, seem to provide some degree of negative evidence (subsection 3.7) to Smak's idea. Since the difference in the presence of a hot spot during superoutburst or the irradiated secondary might be dependent on object [for example, in HT Cas, the frequency of outbursts is unusually low, and orbital humps in quiescence is often inapparent (Wood et al. 1992; Feline et al. 2005)]. HT Cas therefore might not be an ideal object representing the entire SU UMa-type population], and we should leave the problem as a future work. Detailed modeling of the eclipse and superhump light curve assuming a vertically extended disk is indispensable for further discussion, which is clearly outside the scope of this paper.

¹³ This way of normalization of amplitudes is different from the one in Smak (2010). We employed a normalization for P_{orb} -dependence while Smak (2010) introduced a concept of normalization to the average luminosity of the disk. This concept by Smak (2010) implicitly assumes that the observed light from the disk suffers from the i -dependent projection and obscuration effects, while the emission from the superhump light source is isotropic, or observable independent of i .

most the same i -dependence as the background disk light. For geometrically thin, and optically thick accretion disks, the projection effect ($\cos i$) plays the strongest role in low-to-intermediate i . This would imply that the i -dependence of the superhump light source can be explained as well, such as in a form of the (superhump phase-dependent) variations of the surface brightness (or the temperature) on a geometrically thin disk. The apparent lack of deviations from this relation up to $i \sim 80^\circ$ suggest that the vertical structure in the superhump light source is smaller than 10° in slope against the remaining disk. This value is not much greater than the flaring angle of $3\text{--}6^\circ$ inferred for a normal outburst of Z Cha (Robinson et al. 1999), and may not require a special mechanism other than additional tidal heating around the superhump light source.

In deeply eclipsing systems, the amplitudes are systematically higher than the above simple assumption of the projection effect. Although this phenomenon can likely be understood as a consequence of the vertical expansion around the superhump light source, even a simple treatment should require numerical estimation of different contribution from a vertically extended and structured disk, self-obscuration and eclipse by the secondary, and will be an elaborate future work.

The dependence of amplitudes on P_{orb} may be a combined effect of the strength of the tidal torque (larger in higher- q systems) and the strength of the 3:1 resonance (which will be expected to be smaller in higher- q systems around the border of the instability condition for tidal instabilities). This would explain a maximum of amplitudes around $P_{\text{orb}} = 0.09$ d. Although not included in our samples, the low ($\sim 0.10\text{--}0.15$ mag) maximum amplitudes in RZ LMi (Nogami et al. 1995; Robertson et al. 1995; Olech et al. 2008) – would be an outlier for a $P_{\text{SH}} = 0.0594$ d object – may be similarly explained by a supposed lower tidal torque than in other SU UMa-type dwarf novae as proposed in Osaki (1995b) and Hellier (2001).

There is an indication that amplitudes of superhumps are higher in systems with longer intervals of outbursts (RZ Leo and QY Per) among long- P_{orb} systems. These systems may have stored larger disk mass, either as a result of a lower quiescent viscosity or by other mechanisms, and the superhump light source or the vertical extent of the disk may be more pronounced at the time of the outburst. The higher vertical extent might also explain the very strong beat phenomenon in HT Cas.

In extreme WZ Sge-type dwarf novae, the superhump amplitudes tend to be lower and the degree of the beat phenomenon is weaker than in other SU UMa-type dwarf novae. This may be explained if the most of the disk mass outside the 3:1 resonance is efficiently accreted during the stage of early superhumps [the development of the 2:1 resonance is expected to suppress the 3:1 resonance (Lubow 1991a; Osaki 1995a)] and there is relatively little amount of mass at the onset of development of ordinary superhumps. Following this interpretation, the maximum amplitudes of superhumps in WZ Sge-type dwarf novae would be a discriminating feature in estimating the strength of the 2:1 resonance prior to the development of ordinary

superhumps.

The relatively weak beat phenomenon in stage C superhumps (subsection 4.7.3) would also deserve attention. The weaker signal of the beat phenomenon would suggest a lower vertical extent for stage C superhumps. An examination whether the lower temperature of the light source of stage C superhumps or its location, can explain the phenomenon could shed light on clarifying the nature of still poorly understood stage C superhumps.

5. Summary

We studied the characteristics of superhumps for 51 SU UMa-type dwarf novae whose superoutbursts were mainly observed during the 2010–2011 season. In addition to the purpose of our previous surveys focusing on systematic variation of superhump periods, we extended our analysis to post-superoutburst variations and a survey of variations of superhump amplitudes for selected objects. We also analyzed public Kepler data for V1504 Cyg and V344 Lyr. Most of the new data for systems with short superhump periods basically confirmed the earlier findings. We recorded early superhumps for four WZ Sge-type dwarf novae (SDSS J0804, SDSS J1339, OT J0120, and likely SDSS J1605). We also refined the ephemerides of eclipsing systems HT Cas, SDSS J0932, SDSS J1227 and OT J0431, and provided firm estimates of fractional superhump excesses for these objects. We have also updated statistics in relations $P_{\text{SH}} - P_{\text{orb}}$ for stage B and C superhumps, $P_{\text{orb}} - P_{\text{dot}}$ and $P_{\text{orb}} - \epsilon$ for stage B superhumps. The traditional Stolz, Schoembs (1984) relation gives systematically longer P_{orb} estimates for stage B superhumps.

In addition to them, we found:

- The spread of period derivative is broader in long- P_{orb} systems. In particular, GX Cas unexpectedly showed a large positive P_{dot} .
- We recorded the long-awaited superoutburst of the eclipsing SU UMa-type dwarf nova HT Cas, and described the full evolution of superhumps during its earliest stage to post-superoutburst stage. A very strong beat phenomenon was recorded particularly when superhumps reached the full amplitudes.
- There was no particularly indication of the reflection effect and conspicuous appearance of the hot spot in HT Cas as judged from the light curves outside the eclipses. These results do not favor an interpretation assuming an irradiation-induced enhanced mass-transfer.
- In SDSS J0804, we for the first time recorded full evolution of early superhumps and ordinary superhumps, as well as persisting superhumps during six rebrightenings.
- Shallow eclipses were detected during the entire course of outbursts in SDSS J0804. The beat phenomenon was also recorded with a smaller degree than in HT Cas.
- Persisting superhumps during the rebrightening phase of SDSS J0804 and WZ Sge (2001) had ampli-

tudes well-correlated with the brightness of the system. The relation can be understood assuming the almost constant luminosity of the superhump light source. The luminosity of the light source showed a decrease just before or around the final rebrightening.

- The $O - C$ diagrams for three WZ Sge-type dwarf novae SDSS J0804, SDSS J1339 and OT J0120 showed a similar pattern to that of GW Lib during the final fading phase. In SDSS J0804, a rapid excursion to a shorter period was recorded. This phase was probably missed in SDSS J1339, and the resultant $O - C$ diagrams even looked like a phase reversal as would be expected for “traditional” late superhumps.
- In SDSS J1339, there was a strong beat phenomenon in the amplitudes of persistent superhumps even during the post-superoutburst phase. We interpret this feature as a manifestation of cyclically variable shape of the eccentric disk with the beat period.
- The overall behavior in OT J0120 was very similar to that of WZ Sge (2001), consisting of a post-outburst “dip” and multiple rebrightenings with short intervals.
- We studied a new superoutburst of the helium dwarf nova V406 Hya and examined its past outburst activities.
- Kepler data for V1504 Cyg and V344 Lyr confirmed the presence of stage A and B superhumps, and the details of stage A evolution, as well as relation to the precursor phenomenon, were described.
- In V344 Lyr, secondary maxima of superhumps appeared during the late stage of superoutbursts, and this signal gradually merged with the primary maxima to form singly-humped superhumps. The initial periods of secondary maxima were longer than those of primary maxima, suggesting that the secondary maxima were formed in the outer part of the disk. These superhumps persisted for at least two cycles of subsequent normal outbursts. We discussed the role of (1,3)-mode wave in manifestation of doubly-humped superhumps.
- In V1504 Cyg, the behavior was different from V344 Lyr in that secondary maxima only transiently appeared.
- In V1504 Cyg, we detected a “failed superoutburst” in which a precursor outburst and a subsequent further rise was recorded. During this outburst, negative superhumps instead of ordinary (positive) superhumps were excited. The appearance of negative superhumps may be related to premature quenching of the superoutburst.
- SDSS J0804 (2010) showed a large P_{dot} for a WZ Sge-type dwarf nova with multiple rebrightenings. This may have been resulted from a rapid increase of the superhump period at the end of the plateau phase. This phenomenon seems to be commonly seen in eclipsing WZ Sge-type dwarf novae.

- We have detected likely negative superhumps during the post-superoutburst stage of FL Psc in 2004, first times recorded among WZ Sge-type dwarf novae. We suggested a possibility that the state with negative superhumps (possibly a state with a tilted disk) can affect the development of the superoutburst itself, particularly the presence of rebrightenings.
- We have detected orbital modulations in a low-inclination WZ Sge-type dwarf nova GW Lib during its post-superoutburst in 2007. We have also identified the orbital period from post-superoutburst observations of OT J2138 in 2010.
- The amplitudes of superhumps usually show complex variations. The amplitudes quickly grow during stage A and reach a maximum around the stage A–B transition. Although the amplitude decay approximately linearly during stage B, many objects show significant regrowth of amplitudes around or after the transition to stage C.
- The amplitudes of superhumps are strongly related to the orbital period. Long-period systems have larger amplitudes.
- After correcting for the dependence on the orbital period, there is little indication of dependence on the system inclination for $i < 80^\circ$.
- In eclipsing systems, the amplitudes of superhumps are larger, and strongly modulated with the beat period.
- The beat phenomenon of superhumps in eclipsing systems decrease with the progress of the superoutburst. The beat phenomenon is significantly reduced in stage C superhumps.
- In WZ Sge-type eclipsing systems, the beat phenomenon is not as striking as ordinary SU UMa-type dwarf novae.
- We interpret that the superhumps in non-eclipsing systems can be approximated by varying surface brightness of the superhump light source on a relatively geometrically thin disk. We interpret the behaviors in eclipsing systems as being a result of vertical extent of the superhump light source. The dependence on the system inclinations suggests that the slope of the vertical extension does not exceed 10° .

This work was supported by the Grant-in-Aid for the Global COE Program “The Next Generation of Physics, Spun from Universality and Emergence” from the Ministry of Education, Culture, Sports, Science and Technology (MEXT) of Japan. The authors are grateful to observers of VSNET Collaboration and VSOLJ observers who supplied vital data. We acknowledge with thanks the variable star observations from the AAVSO International Database contributed by observers worldwide and used in this research. We have been benefited by discussions with Makoto Uemura, Akira Imada and Daisaku Nogami. This work is deeply indebted to outburst detections and announcement by a number of variable star observers worldwide, including participants of

CVNET, BAA VSS alert and AVSON networks. We are grateful to the Catalina Real-time Transient Survey team for making their real-time detection of transient objects available to the public. We thank the Kepler Mission team and the data calibration engineers for making Kepler data available to the public.

Note Added in Proof

The following objects have been named in Kazarovets et al. (2011) during the proofreading period: ASAS J091858–2942.6 = DT Pyx, ASAS J153616–0839.1 = QZ Lib, SDSS J080434.20+510349.2 = EZ Lyn, SDSS J133941.11+484727.5 = V355 UMa, OT J074727.6+065050 = DY CMi.

References

- Antonyuk, O. I., & Pavlenko, E. P. 2005, in ASP Conf. Ser. 330, *The Astrophysics of Cataclysmic Variables and Related Objects*, ed. J.-M. Hameury & J.-P. Lasota (San Francisco: ASP), p. 379
- Baba, H., Kato, T., Nogami, D., Hirata, R., Matsumoto, K., & Sadakane, K. 2000, PASJ, 52, 429
- Baba, H., et al. 2002, PASJ, 54, L7
- Borges, B. W., Baptista, R., Papadimitriou, C., & Giannakis, O. 2008, A&A, 480, 481
- Cannizzo, J. K., Still, M. D., Howell, S. B., Wood, M. A., & Smale, A. P. 2010, ApJ, 725, 1393
- Cleveland, W. S. 1979, *J. Amer. Statist. Assoc.*, 74, 829
- Croom, S. M., Smith, R. J., Boyle, B. J., Shanks, T., Miller, L., Outram, P. J., & Loaring, N. S. 2004, MNRAS, 349, 1397
- Drake, A. J., et al. 2009, ApJ, 696, 870
- Duerbeck, H. W. 1987, *Space Sci. Rev.*, 45, 1
- Feline, W. J., Dhillon, V. S., Marsh, T. R., Watson, C. A., & Littlefair, S. P. 2005, MNRAS, 364, 1158
- Gänsicke, B. T., et al. 2006, MNRAS, 365, 969
- Harvey, D., Skillman, D. R., Patterson, J., & Ringwald, F. A. 1995, *PASP*, 107, 551
- Hellier, C. 2001, *PASP*, 113, 469
- Hessman, F. V., Mantel, K.-H., Barwig, H., & Schoembs, R. 1992, A&A, 263, 147
- Hirose, M., & Osaki, Y. 1990, PASJ, 42, 135
- Homer, L., Szkody, P., Chen, B., Henden, A., Schmidt, G., Anderson, S. F., Silvestri, N. M., & Brinkmann, J. 2006, AJ, 131, 562
- Imada, A., Kubota, K., Kato, T., Nogami, D., Maehara, H., Nakajima, K., Uemura, M., & Ishioka, R. 2006, PASJ, 58, L23
- Ioannou, Z., Naylor, T., Welsh, W. F., Catalán, M. S., Worraker, W. J., & James, N. D. 1999, MNRAS, 310, 398
- Ishioka, R., et al. 2001, PASJ, 53, 905
- Ishioka, R., et al. 2002, A&A, 381, L41
- Kato, T. 2002a, PASJ, 54, L11
- Kato, T. 2002b, PASJ, 54, 87
- Kato, T., Hirata, R., & Mineshige, S. 1992, PASJ, 44, L215
- Kato, T., et al. 2009a, PASJ, 61, S395
- Kato, T., Maehara, H., & Monard, B. 2008, PASJ, 60, L23
- Kato, T., et al. 2010, PASJ, 62, 1525
- Kato, T., Nogami, D., & Masuda, S. 2003a, PASJ, 55, L7
- Kato, T., Nogami, D., Matsumoto, K., & Baba, H. 2004a, PASJ, 56, S109
- Kato, T., Nogami, D., Moilanen, M., & Yamaoka, H. 2003b, PASJ, 55, 989
- Kato, T., et al. 2009b, PASJ, 61, 601
- Kato, T., Poyner, G., & Kinnunen, T. 2002, MNRAS, 330, 53
- Kato, T., Sekine, Y., & Hirata, R. 2001, PASJ, 53, 1191
- Kato, T., & Uemura, M. 2000, IBVS, 4902
- Kato, T., Uemura, M., Ishioka, R., Nogami, D., Kunjaya, C., Baba, H., & Yamaoka, H. 2004b, PASJ, 56, S1
- Kazarovets, E. V., Samus, N. N., Durevich, O. V., Kireeva, N. N., & Pastukhova, E. N. 2011, IBVS, 6008, 1
- Kley, W., Papaloizou, J. C. B., & Ogilvie, G. I. 2008, A&A, 487, 671
- Koch, D. G., et al. 2010, ApJL, 713, L79
- Kwee, K. K., & van Woerden, H. 1956, *Bull. Astron. Inst. Netherlands*, 12, 327
- Lubow, S. H. 1991a, ApJ, 381, 259
- Lubow, S. H. 1991b, ApJ, 381, 268
- Mennickent, R. E., & Tappert, C. 2001, A&A, 372, 563
- Mineshige, S. 1988, ApJ, 335, 881
- Misselt, K. A., & Shafter, A. W. 1995, AJ, 109, 1757
- Montgomery, M. M., & Bisikalo, D. V. 2010, MNRAS, 405, 1397
- Montgomery, M. M., & Martin, E. L. 2010, ApJ, 722, 989
- Murray, J. R. 1998, MNRAS, 297, 323
- Nakano, S., Nishimura, H., Kadota, K., & Yusa, T. 2011, *Cent. Bur. Electron. Telegrams*, 2616
- Neustroev, V. V. 2002, A&A, 382, 974
- Nogami, D., Kato, T., Masuda, S., Hirata, R., Matsumoto, K., Tanabe, K., & Yokoo, T. 1995, PASJ, 47, 897
- Nogami, D., & Masuda, S. 1997, IBVS, 4532
- Nogami, D., Monard, B., Retter, A., Liu, A., Uemura, M., Ishioka, R., Imada, A., & Kato, T. 2004, PASJ, 56, L39
- Ohshima, T., et al. 2011a, PASJ, submitted
- Ohshima, T., et al. 2011b, PASJ, submitted
- Oizumi, S., et al. 2007, PASJ, 59, 643
- Olech, A., et al. 2011, A&A, 532, A64
- Olech, A., Wisniewski, M., Zloczewski, K., Cook, L. M., Mularczyk, K., & Kedzierski, P. 2008, *Acta Astron.*, 58, 131
- Osaki, Y. 1989, PASJ, 41, 1005
- Osaki, Y. 1995a, PASJ, 47, 47
- Osaki, Y. 1995b, PASJ, 47, L25
- Osaki, Y. 1996, *PASP*, 108, 39
- Osaki, Y., & Meyer, F. 2003, A&A, 401, 325
- Parsamyan, E. S., Oganyan, G. B., Kazaryan, E. S., & Yankovich, I. I. 1983, *Astron. Tsirk.*, 1269, 7
- Patterson, J., Jablonski, F., Koen, C., O'Donoghue, D., & Skillman, D. R. 1995, *PASP*, 107, 1183
- Patterson, J., Kemp, J., Saad, J., Skillman, D. R., Harvey, D., Fried, R., Thorstensen, J. R., & Ashley, R. 1997, *PASP*, 109, 468
- Patterson, J., et al. 1998, *PASP*, 110, 1290
- Patterson, J., et al. 2002, *PASP*, 114, 721
- Pavlenko, E., Antoniuk, O., Antoniuk, K., Andreev, M., Samsonov, D., Baklanov, A., & Golovin, A. 2010a, in *AIP Conference Proceedings, 17th European White Dwarf Workshop*, ed. K. Werner & T. Rauch (Maryland: AIP), p. 332
- Pavlenko, E., et al. 2010b, in *AIP Conference Proceedings, 17th European White Dwarf Workshop*, ed. K. Werner & T. Rauch (Maryland: AIP), p. 320
- Pavlenko, E., et al. 2007, in *ASP Conf. Ser. 372, 15th European Workshop on White Dwarfs*, ed. R. Napiwotzki, & M. R. Burleigh (San Francisco: ASP), p. 511

- Pavlenko, E. P. 2009, in ASP Conf. Ser. , (San Francisco: ASP), p. in press (arXiv astro-ph/0812.0791)
- Pavlenko, E. P., Cook, L., Irmambetova, T. R., A., Baklanov, & Dudka, O. 2002, in ASP Conf. Ser. 261, *The Physics of Cataclysmic Variables and Related Objects*, ed. B. T. Gänsicke, K. Beuermann, & K. Reinsch (San Francisco: ASP), p. 523
- Pavlenko, E. P., et al. 2010c, *Astron. Rep.*, 54, 6
- Plaut, L. 1968, *Bull. of the Astron. Institutes of the Netherlands Suppl. Ser.*, 2, 293
- Pojmański, G. 2002, *Acta Astron.*, 52, 397
- Pojmanski, G., Yamaoka, H., Haseda, H., & Itagaki, K. 2005, *IAU Circ.*, 8495
- Qiu, Y.-L., Qiao, Q.-Y., Li, W.-D., Hu, J.-Y., & Esamdin, A. 1997, *IAU Circ.*, 6758, 1
- Rajkov, A. A., & Yushchenko, A. V. 1987, *Astron. Tsirk.*, 1512, 6
- Ramsay, G., et al. 2010, *MNRAS*, 407, 1819
- Ritter, H., & Kolb, U. 2003, *A&A*, 404, 301
- Robertson, J. W., Honeycutt, R. K., & Turner, G. W. 1995, *PASP*, 107, 443
- Robinson, E. L., Wood, J. H., & Wade, R. A. 1999, *ApJ*, 514, 952
- Roelofs, G. H. A., Groot, P. J., Marsh, T. R., Steeghs, D., & Nelemans, G. 2006, *MNRAS*, 365, 1109
- Schoembs, R. 1986, *A&A*, 158, 233
- Schoembs, R., & Vogt, N. 1980, *A&A*, 91, 25
- Schwieterman, E. W., et al. 2010, *J. of the Southeastern Assoc. for Research in Astron.*, 3, 6
- Shears, J., Brady, S., Foote, J., Starkey, D., & Vanmunster, T. 2008, *J. Br. Astron. Assoc.*, 118, 288
- Shears, J., Klingenberg, G., & de Ponthiere, P. 2007, *J. Br. Astron. Assoc.*, 117, 331
- Shears, J., Miller, I., & Sabo, R. 2010a, *J. Br. Astron. Assoc.*, 120, 361
- Shears, J. H., Gänsicke, B. T., Brady, S., Dubovsky, P., Miller, I., & Staels, B. 2010b, *New Astron.*, in press (arXiv astro-ph/1011.1594)
- Simpson, J. C., Wood, M. A., & Burke, C. J. 1998, *Baltic Astron.*, 7, 255
- Smak, J. 2009a, *Acta Astron.*, 59, 121
- Smak, J. 2009b, *Acta Astron.*, 59, 109
- Smak, J. 2010, *Acta Astron.*, 60, 357
- Smak, J. 2011, *Acta Astron.*, 61, 59
- Smith, A. J., Haswell, C. A., Murray, J. R., Truss, M. R., & Foulkes, S. B. 2007, *MNRAS*, 378, 785
- Solheim, J.-E. 2010, *PASP*, 122, 1133
- Stellingwerf, R. F. 1978, *ApJ*, 224, 953
- Still, M., Howell, S. B., Wood, M. A., Cannizzo, J. K., & Smale, A. P. 2010, *ApJL*, 717, L113
- Stolz, B., & Schoembs, R. 1984, *A&A*, 132, 187
- Szkody, P., et al. 2003, *AJ*, 126, 1499
- Szkody, P., et al. 2006, *AJ*, 131, 973
- Szkody, P., et al. 2004, *AJ*, 128, 1882
- Szkody, P., et al. 2007, *AJ*, 134, 185
- Thorstensen, J. R., Patterson, J. O., Kemp, J., & Vennes, S. 2002, *PASP*, 114, 1108
- Tramposch, J., Homer, L., Szkody, P., Henden, A., Silvestri, N. M., Yirak, K., Fraser, O. J., & Brinkmann, J. 2005, *PASP*, 117, 262
- Uemura, M., et al. 2010, *PASJ*, 62, 187
- Uemura, M., et al. 2008, *IBVS*, 5815, 1
- Uemura, M., et al. 2004, *PASJ*, 56, S141
- Uemura, M., et al. 2005, *A&A*, 432, 261
- van Zyl, L., Warner, B., O'Donoghue, D., Sullivan, D., Pritchard, J., & Kemp, J. 2000, *Baltic Astron.*, 9, 231
- Vogt, N. 1983, *A&A*, 118, 95
- Warner, B. 1985, in *Interacting Binaries*, ed. P. P. Eggleton, & J. E. Pringle (Dordrecht: D. Reidel Publishing Company), p. 367
- Warner, B. 1995, *Cataclysmic Variable Stars* (Cambridge: Cambridge University Press)
- Wei, J. Y., Qiu, Y. L., Qiao, Q. Y., & Hu, J. Y. 1998, *IAU Circ.*, 7068, 1
- Wils, P., Gänsicke, B. T., Drake, A. J., & Southworth, J. 2010, *MNRAS*, 402, 436
- Wood, J. H., Horne, K., & Vennes, S. 1992, *ApJ*, 385, 294
- Wood, M. A., Still, M. D., Howell, S. B., Cannizzo, J. K., & Smale, A. P. 2011, *ApJ*, in press (arXiv astro-ph/1108.3083)
- Wood-Vasey, W. M., Aldering, G., Nugent, P., & Li, K. 2003, *IAU Circ.*, 8077
- Woudt, P. A., & Warner, B. 2002, *Ap&SS*, 282, 433
- Woudt, P. A., & Warner, B. 2003, *MNRAS*, 345, 1266
- Yoshida, S., et al. 2011, *Cent. Bur. Electron. Telegrams*, 2633
- Zhang, E.-H., Robinson, E. L., & Nather, R. E. 1986, *ApJ*, 305, 740
- Zharikov, S. V., et al. 2008, *A&A*, 486, 505